Expedition 320/321 summary[1]

Expedition 320/321 Scientists[2]

Chapter contents

Abstract

Integrated Ocean Drilling Program Expedition 320/321, "Pacific Equatorial Age Transect" (Sites U1331–U1338), was designed to recover a continuous Cenozoic record of the equatorial Pacific by coring above the paleoposition of the Equator at successive crustal ages on the Pacific plate. These sediments record the evolution of the equatorial climate system throughout the Cenozoic. As we gained more information about the past movement of plates and when in Earth's history "critical" climate events took place, it became possible to drill an age transect ("flow-line") along the position of the paleoequator in the Pacific, targeting important time slices where the sedimentary archive allows us to reconstruct past climatic and tectonic conditions. The Pacific Equatorial Age Transect (PEAT) program cored eight sites from the sediment surface to basement, with basalt aged between 53 and 18 Ma, covering the time period following maximum Cenozoic warmth, through initial major glaciations, to today. The PEAT program allows the reconstruction of extreme changes of the calcium carbonate compensation depth (CCD) across major geological boundaries during the last 53 m.y. A very shallow CCD during most of the Paleogene makes it difficult to obtain well-preserved carbonate sediments during these stratigraphic intervals, but Expedition 320 recovered a unique sedimentary biogenic sediment archive for time periods just after the Paleocene/Eocene boundary event, the Eocene cooling, the Eocene–Oligocene transition, the "one cold pole" Oligocene, the Oligocene–Miocene transition, and the middle Miocene cooling. Expedition 321, the second part of the PEAT program, recovered sediments from the time period roughly from 25 Ma forward, including sediments crossing the Oligocene/Miocene boundary and two major Neogene equatorial Pacific sediment sections. Together with older Deep Sea Drilling Project and Ocean Drilling Program drilling in the equatorial Pacific, we can delineate the position of the paleoequator and variations in sediment thickness from ~150°W to 110°W longitude.

Scientific objectives, introduction, and background

Scientific objectives

The Pacific Equatorial Age Transect (PEAT) program (Fig. F1) was designed to achieve an age transect of eastern Pacific sediments

deposited within the equatorial region (±2° of the Equator) on the Pacific plate. The age of sediments within the equatorial transect span from the early Eocene through the Pliocene, with Paleocene/Eocene and late Miocene to recent intervals being covered by previous Ocean Drilling Program (ODP) Legs 138 and 199 (Pisias, Mayer, Janecek, Palmer-Julson, and van Andel, 1995; Lyle, Wilson, Janecek, et al., 2002). Drill sites target specific time intervals of interest (Fig. F2) at locations that provide optimum preservation of calcareous sediments (Figs. F3, F4, F5, F6, F7). The overall aim was to obtain a continuous well-preserved equatorial Pacific sediment section that addresses the following primary scientific objectives:

1. To detail the nature and changes of the calcium carbonate compensation depth (CCD) over the Cenozoic in the paleoequatorial Pacific;

2. To determine the evolution of paleoproductivity of the equatorial Pacific over the Cenozoic;

3. To validate and extend the astronomical calibration of the geological timescale for the Cenozoic, using orbitally forced variations in sediment composition known to occur in the equatorial Pacific, and to provide a fully integrated and astronomically calibrated bio-, chemo-, and magnetostratigraphy at the Equator;

4. To determine temperatures (sea surface and bottom water), nutrient profiles, and upper water column gradients;

5. To better constrain Pacific plate tectonic motion and better locate the Cenozoic equatorial region in plate reconstructions, primarily using paleomagnetic methods; and

6. To make use of the high level of correlation between tropical sedimentary sections and existing seismic stratigraphy to develop a more complete model of equatorial circulation and sedimentation.

Additional objectives included:

7. To provide information about rapid biological evolution and turnover rates during times of climatic stress;

8. To improve our knowledge of the reorganization of water masses as a function of depth and time, as our strategy also implies a paleodepth transect (Fig. F3);

9. To develop a limited north–south transect across the paleoequator, caused by the northward offset of the proposed sites by Pacific plate motion, providing additional information about north–south hydrographic and biogeochemical gradients; and

10. To obtain a transect of mid-ocean-ridge basalt (MORB) samples from a fixed location in the absolute mantle reference frame and to use a transect of basalt samples along the "flow-line" that have been erupted in similar formation-water environments to study low-temperature alteration processes by seawater circulation.

Introduction

As the world's largest ocean, the Pacific Ocean is intricately linked to major changes in the global climate system that took place during the Cenozoic. Throughout the Cenozoic the Pacific plate motion has had a northward component. The Pacific is unique in that the thick sediment bulge of biogenic-rich deposits from the currently narrow equatorial upwelling zone is slowly moving away from the Equator. Hence, older sections are not deeply buried and can be recovered by drilling without extensive diagenesis. Previous Legs 138 and 199 were remarkably successful in giving us new insights into the workings of the climate and carbon system, productivity changes across the zone of divergence, time-dependent calcium carbonate dissolution, an integrated astronomically age-calibrated bio- and magnetostratigraphy, the location of the intertropical convergence zone (ITCZ), and evolutionary patterns for times of climatic change and upheaval. Together with older Deep Sea Drilling Project (DSDP) drilling in the eastern equatorial Pacific (Legs 8, 9, 16, and 85), ODP drilling also helped to delineate the paleoequatorial position on the Pacific plate and variations in sediment thickness from ~150°W to 110°W longitude.

Legs 138 and 199 were designed as latitudinal transects across the paleoequator in order to study the changing patterns of sediment deposition across equatorial regions at critical time intervals. As we have gained more information about the past movement of plates and when in Earth's history "critical" climate events took place it became possible to drill an age transect (flow-line) along the track of the equatorial region on the Pacific plate, targeting important time slices where calcareous sediments have been preserved best and the sedimentary archive in general allows us the reconstruction of past climatic and tectonic conditions. Consequentially, the PEAT program will sharpen our understanding of extreme changes of the CCD across major geological boundaries during the last 53 m.y.

During most of the Paleogene the CCD was between 500 and 1300 m shallower than today. Thus, a very shallow CCD makes it difficult to obtain well-preserved sediments during these stratigraphic intervals because initial thermal subsidence of the ridge crest is rapid (Fig. F3). Nevertheless, the careful coring and site location strategy of Expedition 320/321 allowed us to drill the most promising sites and to obtain a unique sedimentary biogenic sediment archive for time periods just after the Paleocene/Eocene boundary event, the Eocene cooling, the Eocene–Oligocene tran-

sition, the "one cold pole" Oligocene, the Oligocene–Miocene transition, and the Miocene. These new cores and data will significantly contribute to the objectives of the Integrated Ocean Drilling Program (IODP) Extreme Climates Initiative and are a new archive for detailed paleoceanographic study of the equatorial Pacific.

Background

The circulation of the equatorial surface ocean is inescapably linked to the trade wind system. The equatorial Pacific is the classic "world ocean" example of this linkage. It is dominated by wind-driven circulation and is largely unfettered by ocean boundaries. Here, the Equator itself is characterized by a narrow zone of divergence that results from the change in the sign of the Coriolis effect and that gives rise to a band of high biologic productivity (Fig. F6). The strength of the equatorial circulation and of this divergence is linked to the strength of the trade winds, which are in turn strongly tied to the global climate system. Variations in global climate, interhemispheric differences in temperature gradients, and marked changes in the ocean boundaries are all imprinted on the biogenic-rich sediments that are accumulating in the equatorial zone. The PEAT program was designed to provide an understanding of equatorial Pacific circulation, carbonate production, deposition, and dissolution for the last ~53 m.y. at a scale where orbital forcing can be resolved. Combined with seismic reflection data (Lyle et al., 2006, 2002) following in the vein of Mitchell et al. (2003) and synthesized with earlier drilling (e.g., Moore et al., 2002, 2004, 2008b; Lyle et al., 2005) we can reconstruct equatorial Pacific history with high confidence and substantially improve upon work from the early stages of DSDP and more recent ODP legs.

Deciphering the sedimentary history of the equatorial Pacific has been greatly simplified by favorable motion of the Pacific plate. Throughout the Cenozoic, the movement of the Pacific plate has had a northward latitudinal component of ~0.25°/m.y. This northward movement transports the equatorial sediments gradually out from under the zone of highest sediment delivery, resulting in a broad mound of biogenic sediments (Fig. F8). This transport prevents older equatorial sections from being buried deeply beneath younger sections as the crust moves northward. The diminished overburden resulting from this transport also allows relatively good preservation of biogenic sediments and minimizes burial diagenesis. In addition, it allows us to core nearly all sediment sections using the advanced piston corer (APC). The northward tectonic displacement, however, is not so large that a traverse of the

equatorial zone (within 2° latitude of the Equator) was too rapid to record a reasonable period of equatorial ocean history. Typically drill sites remain within the equatorial zone for 10–20 m.y. before passing beyond the northern edge of high-biogenic sedimentation. Older equatorial sections are thus buried beneath a thin veneer of younger sediments as the crust moves northwestward.

In their summary of DSDP results in the equatorial Pacific, van Andel et al. (1975) gave a general view of the development of the equatorial mound of sediments in the Pacific Ocean, based mostly upon three early DSDP legs (5, 8, and 16). Van Andel et al. (1975) showed how both temporal and spatial variation in sediment accumulation rates resulted from plate movement, varying biologic productivity at the equatorial divergence, and carbonate preservation. The buildup of the Pacific equatorial mound of sediment has been more recently documented and discussed by Mitchell (1998) and Mitchell et al. (2003) (Fig. F8).

Drilling across the Pacific equatorial mound was addressed again some 20 y after the van Andel et al. (1975) compilation when an equatorial latitudinal transect along 10 Ma crust was drilled during ODP Leg 138 (Pisias, Mayer, Janecek, Palmer-Julson, and van Andel, 1995), and then again 10 y later when a similar transect along 56 Ma aged crust was conducted during Leg 199 (Lyle, Wilson, Janecek, et al., 2002). The newer drilling, coupled with major advances in geochronology, has documented the remarkable correlation of paleoceanographic events over thousands of kilometers in the equatorial Pacific, caused by the large scale of Pacific equatorial circulation (Fig. F9). It was thus possible during the PEAT program, coherent with the addition of a relatively small number of new sites, to build detailed reconstructions of equatorial Pacific circulation throughout the Cenozoic.

Earlier drilling missed most of this detail because of the lack of important drilling technologies such as extended core barrel (XCB) and APC coring, which allow the collection of relatively undisturbed sediments; multisensor track correlation; core-log integration; the rebuilding of a continuous sediment column from individual cores; and correlation to seismic reflection data. Together with an improved knowledge of the plate tectonic regime, these advances allow us to locate the areas of enhanced depositional rates associated with paleoequatorial positions. Combining multiple sites along the Equator, as in the PEAT drilling plan, will result in a detailed sediment record from the Pleistocene to the Paleocene. These records will also be invaluable for the continued development of the Cenozoic timescale as well as for the paleoceanographic information they contain.

Excellent sections were recovered during Legs 138 and 199, on which detailed orbital tuning of the geologic timescale has been carried out. These sections give a much clearer picture of variations in sedimentation rates, isotopic evolution of the oceans, biologic evolution and zoological provenance, variations in carbonate preservation, and variations in geochemical fluxes that result from paleoceanographic and paleoclimate changes. Parts of the Cenozoic timescale still require further refinement and verification of the proposed orbital tuning. The timescale older than the late Eocene has not been calibrated sufficiently, even though there is evidence of orbital frequencies in parts of the records recovered from this older interval (e.g., Norris and Röhl, 1999; Röhl et al., 2001).

To develop a detailed history of the Pacific equatorial current system, the strategy pursued during Legs 138 and 199 was to drill along a line of equal oceanic crustal age, thus obtaining an approximate north–south transect across the major east–west currents during time intervals of particular interest.

During the Paleocene and Eocene, the shallow CCD prevents deposition of carbonate except at shallow ocean crust. Drilling near the paleoposition of the ridge crest at the critical time interval allows the recovery of the shallowest sections available in the pelagic oceans and thereby assures the best possible preservation of the carbonate sediments recovered. As the crust cools and sinks, the seafloor on which the sediments are deposited approaches the lysocline and CCD. Thus, the best preserved part of the sections recovered in such "time line" transects is restricted by the depth at which carbonate dissolution significantly increases, as well as by the northward movement of sediment sections out of the region of high equatorial productivity. This limitation was exemplified by the results from Leg 199, during which only limited amounts of carbonate prior to the Eocene/Oligocene boundary were recovered (e.g., at ODP Site 1218 on 42 Ma crust).

For the PEAT program, we planned to overcome this limitation of the time line strategy by pursuing an equatorial age transect, or flow-line strategy (Figs. F1, F4), to collect well-preserved equatorial sections through the Cenozoic while also making use of the Pacific plate motion to add an oblique latitudinal transect across all time slices.

We drilled a series of sites on the paleoequator at key intervals in the evolution of the Cenozoic climate. These intervals span the extremely warm times of the early Eocene, the cooling of the late Eocene through Oligocene, the early Miocene time of relatively warm climates (or low ice volume), and sections deposited during the development of the major Southern and Northern Hemisphere ice sheets (Fig. F2). There are very few previous drill sites that match our site selection criteria. Each site is selected to be close to the geographic paleoequator and on crust aged slightly older than the age intervals of particular interest.

In this way we were able to track the paleoceanographic conditions at the paleoequator in the best preserved sediments obtainable. We can also make use of the high level of correlation between tropical sediment sections and seismic stratigraphy to develop a more complete model of equatorial productivity and sedimentation.

Understanding the interplay between the CCD, CaCO$_3$ dissolution, and productivity

The Pacific Ocean, specifically the equatorial upwelling zone, is the largest oceanic source of CO$_2$ to the atmosphere and controls atmospheric CO$_2$ levels (Dore et al., 2003). The release and uptake of CO$_2$ is the direct consequence of calcium carbonate deposition and the interplay between nutrient supply, carbonate dissolution, surface water productivity, and export of biogenic carbonate from the surface waters to the sediment pile. Distinguishing between the effects of carbonate dissolution and productivity has been a field of intense study in the past. An important objective of the PEAT program is to address the detailed workings of depth-dependent carbonate dissolution, which is intricately linked to the climate system and paleoceanography. In the standard model for carbonate dissolution, accumulation rates locally decrease linearly from a lysocline down to a CCD, reflecting a linearly increasing rate of dissolution. The depth of both of these mappable surfaces varies spatially and in time as a result of climatic and physical processes. The equatorial Pacific is one of the classic areas where the lysocline-CCD model was first developed, but little subsequent effort has been made to test it—a necessary step, considering that the functional form of dissolution is now known to depend in a more complex way on organic carbon burial and water mass properties. The age transect will provide the necessary additional data with which to test the carbonate paradigm and recover previously unavailable carbonate material from important Paleogene time slices in the Pacific.

Specifically, the recovery of shallowly buried carbonate sediments from near the paleoequatorial upwelling zone would contribute significantly toward separating the various processes that affect carbonate deposition and preservation and reduce some of the processes that affect climatic proxy records, such as diagenetic recrystallization (Pearson et al., 2001a). Neogene productivity has been strongly oriented parallel to

the Equator, so differences in carbonate thicknesses at a common latitude but differing depth permit the effect of dissolution to be isolated (Lyle, 2003; Mitchell et al., 2003; Mitchell and Lyle, 2005). In addition, the strategy adopted in this program provided new data throughout the Cenozoic with which it will be possible to map the spatial evolution of the equatorial CCD with time (see "Results and highlights"). This is because the northward component of the Pacific plate movement results in the multiple recovery of the same time slice at different sites but with a slightly different paleolatitude (Fig. F3).

Recovering more detailed records from the best possible material will also allow a better understanding of physical processes that might affect or hinder our interpretation of carbonate proxy records, such as the "carbonate ion effect"—an observed and modeled influence of carbonate ion concentration on stable isotope fractionation in carbonate (Spero et al., 1997; Zeebe and Wolf-Gladrow, 2001; Lear et al., 2008).

Preliminary work with seismic data (Mitchell et al., 2003) has revealed a surprising lack of correlation between dissolution and depth in the westerly region of this study area. Our aim is to develop a more extensive three-dimensional model for the stratigraphy of the equatorial Pacific deposits that links all existing core data using a grid of high-resolution seismic reflection profiles, including more recent data from the PEAT site survey AMAT03 (Lyle et al., 2006). A numerical stratigraphic model will then be used to assess carbonate dissolution and, in particular, the spatial pattern of sharp changes in dissolution, such as the extremely abrupt change in the CCD at the Oligocene/Eocene boundary, which has been linked to a possible abrupt onset of continental weathering. The sediment archive recovered during the PEAT program will allow the application of the substantial array of carbonate-based proxies with which the wider regional seismic study can be constrained and calibrated.

Reconstructing paleoceanographic properties and sea-surface temperature

A large number of paleoceanographic interpretations rely on obtaining proxy data such as stable isotope measurements, element ratios such as Mg/Ca, sea-surface temperature (SST) estimates from faunal distributions and isotope data, alkenone proxies, TEX86, geochemical productivity, and so on. In turn, a very large number of these measurements rely on the presence of biogenic calcium carbonate. For the Pacific Ocean, the PEAT drilling strategy was designed to recover this important material with the best possible preservation and the least amount of

diagenetic effects for long intervals throughout the Cenozoic.

Spatial range considerations

The age transect siting strategy results in a restricted north–south transect and recovery of sediments from different paleolatitudes (separated by several degrees) at identical times in the past (Fig. F5). However, we note that the regional seismic study to be developed as part of our site survey work gives us the opportunity to integrate data from older drill sites with the new drilling. The site survey linked the new sites to key drill sites from DSDP Legs 9 and 85 and ODP Legs 138 and 199. Combining data from these expeditions and surveys will allow us to construct a site-to-site correlation and, finally, a Pacific "megasplice" of high-resolution data spliced together to cover most of the Cenozoic.

Paleomagnetic objectives

One important aspect of the PEAT program is the recovery of high-quality paleomagnetic data so that efforts to improve existing geologic timescales (Gradstein et al., 2004) can be extended further back in time. Results from Leg 199 demonstrate that these records can be recovered from near-equatorial carbonate sediments (e.g., Lanci et al., 2004, 2005). Almost all magnetic reversals from the Paleogene to the present were recovered during Leg 199. However, neither biogenic carbonate sediments through most of the Eocene nor for ages younger than the lower Miocene were recovered during Leg 199. Thus, although the paleomagnetic record during these times was of high quality, global stratigraphic correlation is hindered by the lower mass accumulation rate, the absence of a detailed isotope stratigraphy, and sparser biostratigraphic control. In order to facilitate the development of an integrated magneto- and biostratigraphic framework with a stable isotope stratigraphy (necessary to enable global correlation), recovery of magnetic reversals within carbonate sediment is desirable. In addition, further detailed paleomagnetic, magnetostratigraphic, and magnetic rock fabric data, most importantly from the Eocene, will help to resolve the suggestion that the geographic Equator, as determined from the biogenic sediment bulge, might not coincide with the paleoequator position backtracked with a fixed-hotspot reference frame (Moore et al., 2004; Tarduno, 2003; Parés and Moore, 2005).

Ancillary benefits (MORB, basement)

Our drilling aimed to recover basement samples at all sites. A transect of MORB samples from a fixed location in the absolute mantle reference frame is a

unique sample suite for mantle geochemists. A transect of basalt samples along the flow-line that have erupted in similar environments will be of interest for low-temperature alteration studies (see, e.g., Elderfield and Schultz, 1996).

Site selection strategy and site targets

Time slices drilled during the PEAT program were chosen to cover the overall climatic history of the Cenozoic and to target particular times of marked changes in the climatic regime. The spacing of the sites was determined by what we knew of the Cenozoic evolution of the lysocline from previous drilling. When the CCD is particularly shallow, the difference in time of age transect sites must be closer than when the CCD is deep (Fig. F3). As a guide, Site 1218 was drilled on 42 Ma crust during times when the CCD was near 3.3 km. Nannofossil oozes were deposited at this location to ~37 Ma before the crust at this site sank below the CCD. An age separation between drill sites of 2–5 m.y. is a maximum for the shallow CCD of the Eocene; for good preservation of foraminifers an even closer spacing should be used. The results of our paleoequator reconstruction and drill site locations are shown in Figure F4.

Site location strategy

In pursuing the history of the equatorial Pacific Ocean through both time line and flow-line transects we have two major advantages over the efforts that took place in the earlier days of scientific ocean drilling. Although previous drill sites have targeted the general area, they mostly do not fulfill all of our criteria in terms of (1) a sufficient number of holes to obtain a continuous record, (2) modern coring technology to obtain undisturbed sediments, (3) location inside the paleoequatorial zone, or (4) location on the right crustal age to ensure the presence of calcium carbonate at the targeted time slice. We positioned Sites U1331–U1338 somewhat south of the estimated paleoequatorial position at their target ages (Fig. F6) to maximize the time that drill sites remain within the equatorial zone (i.e., ±2° of the Equator), to allow for some error in positions (evidence suggests a southward bias of the equatorial sediment mound relative to the hotspot frame of reference [Knappenberger, 2000]), and to place the interval of maximum interest above the basal hydrothermal sediments.

To determine the site and site survey location, we used the digital age grid of seafloor ages from Müller et al. (1997), heavily modified and improved with additional magnetic anomaly picks from Petronotis (1991) and Petronotis et al. (1994), as well as DSDP/ODP basement ages. For this grid, each point is back-rotated in time to zero age using the fixed-hotspot stage-poles from Koppers et al. (2001) and Engebretson et al. (1985) and the paleopole data from Sager and Pringle (1988). From the backtracked latitudes for each grid point, we obtained the paleoequator at the crustal age by contouring all backrotated latitudinal positions.

Eocene (Sites U1331–U1334)

The Eocene was a time of extremely warm climates that reached a global temperature maximum near 52 Ma, a period around the Early Eocene Climatic Optimum (EECO) (Fig. F2) (Zachos et al., 2001a; Shipboard Scientific Party, 2004 [ODP Leg 208]). From this maximum there was a gradual climatic cooling through the Eocene to the Eocene/Oligocene boundary. There appears to have been a slight reversal to this trend in the middle Eocene near 43 Ma and in the late Eocene at 34–36 Ma, just prior to the pronounced drop in oxygen isotopes that marks the Eocene/Oligocene boundary and one of the most dramatic changes of the CCD (Fig. F3).

Throughout the Eocene, the CCD lay near a depth of 3.2–3.3 km, albeit with potentially significant short-term fluctuations (Lyle et al., 2005). Thus, recovering well-preserved carbonate sediments from the equatorial region is a substantial challenge but not impossible if the depth of the East Pacific Rise lay near the global average of ~2.7 km. We presently lack calcareous sediments from the region of the equatorial circulation system during this time of maximum Cenozoic warmth (Zachos et al., 2001a), elevated atmospheric pCO_2 concentrations (Lowenstein and Demicco, 2007), and a shallow early Eocene CCD estimated between 3200 and 3300 meters below sea level (mbsl) (Lyle, Wilson, Janecek, et al., 2002; Lyle et al., 2005; Rea and Lyle, 2005). The Eocene equatorial upwelling system appears to differ from the modern equatorial upwelling regime by having strong secondary upwelling lobes ~10° in latitude away from the primary equatorial region (Figs. F10, F11). These lobes produce a much broader region of (relatively) high productivity than is present today.

Early and middle Eocene (Sites U1331 and U1332; ~53 Ma and 50 Ma crust)

During Leg 199, a north–south transect across the equatorial region was drilled on ~56 Ma oceanic crust. Sites on this transect had generally drifted below the CCD by 52–53 Ma. Thus, we have yet to recover calcareous sediments from the equatorial Pacific during the time of maximum Cenozoic warmth. Site U1331 is on crust with an estimated age

of ~53 Ma in order to intercept the interval between 53 and 50 Ma in basal carbonate sediments above the shallow early Eocene CCD (4.2–4.3 km), whereas Site U1332 is located on 50 Ma crust to collect a carbonate interval from ~50–48 Ma.

Average (noncarbonate) accumulation rates in the early Eocene were moderate, showing only slight increases in some of the more northern sites on the Leg 199 transect (ODP Sites 1215 and 1220). What is particularly interesting in the records of Leg 199 is that the very shallow CCD of this early Eocene time appears to deepen to the north, perhaps suggesting a northern source for the bottom waters. Sites targeting this time interval would ideally give us sediments with sufficient carbonate material to better constrain the isotopic and biotic characteristics of the near-surface equatorial waters.

During the early Eocene, a very shallow CCD and typical rapid tectonic plate subsidence of young crust near the shallow ridge crest conspire to make the time window above the CCD short (~2–5 Ma). Thus, although good records of pelagic carbonates during and just after the Paleocene/Eocene Thermal Maximum (PETM) were recovered during Leg 199 (Lyle, Wilson, Janecek, et al., 2002; Nuñes and Norris, 2006; Raffi et al., 2005), the time period of the EECO (Zachos et al., 2001a) is not well sampled.

Sites U1331 (53 Ma crust) and U1332 (50 Ma crust) aim to provide the sedimentary archive to address several important questions that relate to causes and responses of the true Cenozoic "Greenhouse" world: the Eocene was a time of extremely warm climates that reached a maximum in temperatures near 52 Ma (Zachos et al., 2001a). From this maximum there was a gradual climatic cooling to the Eocene/Oligocene boundary. Good paleomagnetic stratigraphy from Leg 199 sites allowed a much improved calibration of nannofossil and radiolarian biostratigraphic datums throughout the Eocene. A north–south transect across the equatorial region at ~56 Ma was drilled during Leg 199. Although good records of pelagic carbonates during and just after the PETM were recovered at Leg 199 sites (Lyle, Wilson, Janecek, et al., 2002; Raffi et al., 2005; Nuñes and Norris, 2006), the time period of the EECO (Zachos et al., 2001a) and the shallowest CCD is not well sampled.

Middle and late Eocene (Site U1333; 46 Ma crust)

Good paleomagnetic stratigraphy from Leg 199 sites allowed a much improved calibration of nannofossil and radiolarian biostratigraphic datums (Pälike et al., 2005, 2006b; Raffi et al., 2005, 2006; Moore et al., 2004). From the combined information a more detailed picture emerged of temporal variations in sediment accumulation through the middle and upper Eocene of the tropical Pacific. These data showed an increase of a factor of up to 2–3 in accumulation rates of siliceous ooze in the middle Eocene (41–45 Ma).

There are also several notable periods of highly fluctuating CCD associated with intervals in which carbonate is preserved as deep as 4000 mbsl, or ~700 m deeper than the average Eocene CCD (Lyle, Wilson, Janecek, et al., 2002; Lyle et al., 2005; Rea and Lyle, 2005; Bohaty et al., 2009). These fluctuations occur immediately prior to the Middle Eocene Climatic Optimum (MECO), which is associated with CCD shoaling (Bohaty and Zachos, 2003; Bohaty et al., 2009). Such fluctuations in the CCD are similar in magnitude to those at the Eocene/Oligocene boundary (Coxall et al., 2005). High siliceous sedimentation rates occur near an apparent short reversal in the middle Eocene cooling interval. It is difficult to interpret the cause of such a substantial change in silica flux during a very warm climatic regime.

The primary objective of coring at Site U1333 is to recover a complete sequence of carbonate sediments spanning the middle Eocene to Oligocene so we can evaluate changes in the temperature and structure of the near-surface ocean, bottom water temperatures, and the evolution of the CCD.

One of the additional objectives of the PEAT program is to provide a depth transect for several Cenozoic key horizons, such as the Eocene–Oligocene transition (Coxall et al., 2005) targeted at Sites U1331–U1334. Site U1333 forms the third deepest paleodepth constraint, with an estimated crustal paleodepth of <4 km and a paleolatitude of ~3° north of the paleoequator during the Eocene–Oligocene transition.

Eocene/Oligocene boundary (Site U1334; 38 Ma crust)

Site U1334 sediments are estimated to have been deposited on top of late middle Eocene ~38 Ma crust, and this site targets the events bracketing the Eocene–Oligocene transition with the specific aim to recover carbonate-bearing sediments of latest Eocene age prior to a large deepening of the CCD that occurred during this greenhouse to icehouse transition (Kennett and Shackleton, 1976; Miller et al., 1991; Zachos et al., 1996; Coxall et al., 2005). The Eocene–Oligocene transition experienced the most dramatic deepening of the Pacific CCD during the Paleogene (van Andel, 1975), which has been shown by Coxall et al. (2005) to coincide with a rapid step-wise increase in benthic oxygen stable isotope ratios interpreted to reflect a combination of growth of the Antarctic ice sheet and decrease in deepwater temperatures (DeConto et al., 2008; Liu et al., 2009).

Prior to the PEAT expedition, the most complete Eocene/Oligocene boundary section recovered from the equatorial Pacific was Site 1218 on 42 Ma crust; however, it is far from pristine. Carbonate percentages drop markedly below the boundary and reach zero near 34 Ma during a time of apparent global shoaling of the CCD just prior to the Eocene–Oligocene transition and CCD deepening (Bohaty et al., 2008). This prevented the recovery of information about paleoceanographic conditions prior to the Eocene–Oligocene transition and also has implications for the interpretation of paleotemperature proxies such as Mg/Ca ratios in foraminifer shells that were bathed in waters with very low carbonate ion concentrations (Lear et al., 2008; Elderfield et al., 2006). The integrated stratigraphy from Site 1218 has been correlated to the planktonic foraminifer marker extinction of the genus *Hantkenina* in exceptionally well preserved, shallow clay-rich sediments from Tanzania by Pearson et al. (2008), who demonstrated that the Eocene/Oligocene boundary falls within the middle plateau of the stable isotope double-step described by Coxall et al. (2005) just prior to the base of Chron C13n.

Data from Site 1218 allowed the astronomical time calibration of the entire Oligocene (Coxall et al., 2005; Wade and Pälike, 2004; Pälike et al., 2006b), but the lack of carbonate in the uppermost Eocene at this site made the detailed time control now available for the Oligocene much less certain for the late Eocene. Site U1334 is on crustal basement with an age of ~38 Ma and crossed the paleoequator shortly thereafter. It was located to provide the missing information about the crucial chain of events prior to and during the Eocene–Oligocene transition.

Oligocene (Site U1336, ~32 Ma crust)

Site U1336 targets the Oligocene and is on early Oligocene crust. This interval of time is noted for its markedly heavy benthic oxygen isotopes (Fig. F2) and its relatively deep CCD (Fig. F3). There was probably ice on Antarctica during this interval, but not the large ice sheets to be found there later in the middle Miocene. Compelling evidence does not exist for ice sheets in the Northern Hemisphere during the Oligocene and early Miocene. Thus, a time of low global ice volume, cold bottom waters, a cold South Pole, and a relatively warm North Pole apparently existed. This scenario of a "one cold pole" world has given rise to speculation on the impact of interhemispheric temperature imbalance on pole to Equator temperature gradients and on the symmetry of the global wind systems. The extent to which such an imbalance may have affected the trade winds, the

position of the ITCZ, and the seasonal shifts in this zone should be seen in the wind-driven currents of the equatorial region.

The older low-resolution DSDP data indicate relatively high but variable sediment accumulation rates during this interval and better carbonate preservation south of the Equator (van Andel, 1975). In the Leg 199 equatorial transect, the highest accumulation rates encountered (>15 m/m.y.) occurred in the lower part of the Oligocene, but these were at sites north of the Oligocene Equator or on relatively old (and therefore deep) crust. Thus we expected a better preserved, thicker carbonate section at the Oligocene Equator. Studies of Oligocene sections from Leg 199 and other ODP sites (e.g., Paul et al., 2000; Zachos et al., 2001a; Billups et al., 2004; Pälike et al., 2006a) indicate the presence of strong eccentricity and obliquity cycles in carbonate preservation and suggest a strong (southern) high-latitude influence on the carbonate record. These cycles led to the development of an orbitally tuned timescale that reaches back to the base of the Oligocene (Pälike et al., 2006b). Such a timescale makes it possible to develop a very detailed picture of equatorial geochemical fluxes and of the degree of variability in the equatorial system of the Oligocene.

Latest Oligocene–earliest Miocene (Site U1335; 26 Ma crust)

Site U1335 was designed to focus on the paleoceanographic events in the late Oligocene and into the early and middle Miocene, including the climatically significant Oligocene–Miocene transition and its recovery. In conjunction with Sites U1336 and U1337, Site U1335 was also designed to provide a latitudinal transect for early Miocene age slices. A significant several million year long rise in the oxygen isotope record (Lear et al., 2004; Pälike et al., 2006b) at the end of the Oligocene is closely followed by a relatively short, sharp increase in oxygen isotope values. This increase has been interpreted as a major glacial episode (Mi-1) (Fig. F2) (Paul et al., 2000; Zachos et al., 1997, 2001a, 2001b; Pälike et al., 2006a) and correlated to a pronounced drop in sea level (Miller et al., 1991). The Mi-1 event is very close to the Oligocene/Miocene boundary and has now been astronomically age calibrated in several ocean basins (Shackleton et al., 2000; Billups et al., 2004). Although there are clear periodic isotopic signals indicating major changes in ice volume, ocean temperatures, and/or ocean structure, this biostratigraphic boundary has always been somewhat of an enigma. Unlike the major changes in the isotopic stratigraphy, the biostratigraphies of the planktonic microfossils show very little change across this boundary. In fact it is

one of the most difficult epoch boundaries to pick using only microfossil biostratigraphy.

At Leg 199 Sites 1218 and 1219 this interval was well recovered; however, carbonate preservation still presented a problem for foraminifer stratigraphy. Both sites were deep and well within the lysocline, making the application of temperature proxies such as Mg/Ca ratios in foraminifer tests more difficult (Lear et al., 2008). At the time Miocene–Oligocene sediments were deposited, Site 1218 already resided on ~18 m.y. old crust and was ~4100 m deep. Site 1219 was on ~32 m.y. old crust and was ~4500 m deep. There was a relative increase in the large diatoms near this boundary in the siliceous coarse fraction, suggesting increased productivity; however, detailed high-resolution flux rates across this interval have yet to be determined. A well-recovered section on the latest Oligocene Equator near the late Oligocene ridge crest was targeted by Site U1335 and should provide both the resolution and the preservation required to better describe the changes in the equatorial ocean taking place at this time.

Miocene (Site U1337; 24 Ma crust)

Site U1337 was proposed for drilling to focus on the paleoceanographic events in the early and middle Miocene. The latest Oligocene through the middle Miocene appears to have been a time of relative warmth comparable to the latest Eocene. However, the variability in the isotopic record of the early to middle Miocene is larger than that of the Eocene and may indicate more variability in climate and global ice volume. The climatic "optimum" at ~15 Ma comes just before the major development of ice sheets on Antarctica and the marked increase in ice-rafted debris in circum-Antarctic sediments. The early Miocene also marks a major evolutionary change from the relatively static Oligocene planktonic foraminifer biota. In the equatorial Pacific, the early Miocene also marks the beginning of abundant diatoms in the stratigraphic record (J. Barron, pers. comm., 2003) and thus may represent a major change in carbon cycling as well.

The only major ocean boundary change proposed for the time near the Oligocene/Miocene boundary was the opening of the Drake Passage to deep flow; however, there is some debate as to the exact timing of this event (Barker, 2001; Lawver and Gahagan, 2003; Scher and Martin, 2006; Lyle et al., 2007) and its direct impact on the tropical ocean is uncertain. It may be that, as in the Eocene/Oligocene boundary section, the link lies in the shallow intermediate waters that provide nutrients to lower latitude upwelling regions. For the equatorial region, an even more pertinent question is "What changes were occurring in the Miocene tropical ocean that led to this burst of Miocene evolution?"

Early and middle Miocene (Site U1338; ~18 Ma crust)

In principle, the age transect strategy of Expedition 320/321 would not be complete without data from the Pliocene–Pleistocene. However, in addition to logistical reasons of cruise length, near-paleoequatorial records have already been targeted by ODP Legs 138 (Pisias, Mayer, Janecek, Palmer-Julson, and van Andel, 1995) and 202 (Mix, Tiedemann, Blum, et al., 2003), which provided information about the development of Northern Hemisphere glaciation. Our last site (U1338) focuses instead on the events across and after a middle Miocene maximum in deposition (van Andel et al., 1975).

Site U1338 was proposed for drilling to focus on the paleoceanographic events following a middle Miocene maximum in deposition (van Andel et al., 1975). In addition, large changes in the glaciation state and frequency have been described in the late early and middle Miocene (Holbourn et al., 2005; Abels et al., 2005; Raffi et al., 2006), in the interval following ~14 Ma. There is a wide latitude range of $CaCO_3$ deposition during the earliest Neogene, with a relatively sharp transition to a narrower $CaCO_3$ belt after 20 Ma (Lyle, 2003). $CaCO_3$ mass accumulation rates in the central equatorial Pacific recovered from the 18–19 Ma "famine" and in the period between 14 and 16 Ma reached a second maximum in carbonate deposition, which is also evident in the seismic stratigraphy of the equatorial sediment bulge (Knappenberger, 2000; Mitchell et al., 2003).

Results and highlights

During Expedition 320, 16 holes at 6 sites (Holes U1331A–U1331C, U1332A–U1332C, U1333A–U1333C, U1334A–U1334C, U1335A and U1335B, and U1336A and U1336B) (Table T1) were cored as part of the PEAT program. During Expedition 321, two major Neogene equatorial Pacific sediment sections were recovered by drilling seven holes at two sites (Holes U1337A–U1337D and Holes U1338A–U1338C) (Table T2). One additional hole (U1338D) was drilled at Site U1338 to provide sediment cores for laboratory training conducted during IODP Expedition 323. By drilling a series of sites that follow the position of the paleoequator and a limited latitudinal and depth transect, as outlined below, we recovered cores that allow us to address the combined PEAT objectives (see **"Scientific objectives"**).

Lithologies recovered and stratigraphic summary

Figure F12 summarizes the lithostratigraphy of the northwest–southeast transect of sites drilled during Expedition 320/321 together with the sedimentary sequence from Site 1218, which is included in the PEAT flow-line strategy (see "Scientific objectives, introduction, and background"). In this figure, the Eocene sequence (green shading) thins from north to south, pinching out before Site U1336 where the basement is of early Oligocene age. The Miocene sequence (yellow shading) thins substantially from south to north, whereas the Oligocene sequence (blue shading) is thickest in the middle of the transect (Sites U1334 and U1335) and thins both north and south. Sediments of early Eocene age are only present at Site U1331, and sediments of Pliocene–Pleistocene age are present at Sites U1331, U1334, U1335, U1337, and U1338. The thickness of sediments from different parts of the age transect is compatible with that expected from our drilling strategy (see "Site selection strategy and site targets").

Six main lithologies are present in these sites:

- Surface clays,
- Nannofossil oozes and chalks,
- Radiolarian ooze and radiolarite,
- Diatom ooze and diatom nannofossil ooze,
- Porcellanite and chert, and
- Basal chalks, limestones, and clay.

Surface clays are present at Sites U1331–U1335. These sediments are affected by intense dissolution, which has removed most of the siliceous and calcareous biogenic components, and only the clay components remain. This pattern reflects the northward motion of the Pacific plate, which transports the sites out of the equatorial upwelling zone of high production as the underlying crust subsides with age.

Nannofossil oozes and chalks are the main lithology of the Oligocene in the PEAT transect. To the south, at the sites near the paleoequator, nannofossil ooze is also the main lithology in strata of early and middle Miocene age. At the older sites nannofossil ooze is also present but in decreasing importance moving northwestward as basement age becomes progressively older and water depth increases. At the northernmost end of the transect (Site U1331), nannofossil ooze is primarily restricted to an interval of early and middle Eocene and Oligocene age. The middle Eocene interval is broadly correlative to carbonate accumulation event (CAE) 3 (Lyle et al., 2005).

Radiolarian ooze is present at Sites U1331–U1336 (Fig. F12), but it is a far more abundant lithology in the north (Sites U1331 and U1332), where it is the main lithology of the Eocene, than in the south (Sites U1334–U1336).

Porcellanite is a major lithology in sediments of early and early middle Eocene age toward the northern end of the Expedition 320/321 transect (especially at Sites U1331 and U1332), where it is associated with thin clay horizons that are interbedded with radiolarian ooze. Chert is a major lithology in sediments of early and early late Oligocene age at Site U1336, where it proved a major impediment to recovery of a complete section. One stratigraphically equivalent chert/porcellanite layer was found in middle Miocene sediments at Sites U1337 and U1338.

At nearly all sites drilled on the PEAT transect, the recovered basal sediments overlying basalt are calcareous in lithology, indicating that, at the onset of sediment accumulation at these sites, the seafloor lay above the local CCD. This result is in keeping with the Expedition 320/321 rationale of drilling a flow-line of sites on crust of increasing age (southeast to northwest) to recover stratigraphic "windows" of calcareous sediments overlying contemporaneously young crust prior to its subsidence below the CCD. The only site on the PEAT transect where calcareous sediments were not found overlying basement is Site U1332. The basal sediment unit is primarily zeolite clay of middle Eocene age, although calcareous nannofossils were common in several samples. This result indicates that the crust at Site U1332 lay below the CCD, even at the point of its formation (~50 Ma), pointing to a very shallow CCD (<2700 m) at this time (see "Cenozoic CCD in the equatorial Pacific").

The combined results of Leg 199 and the PEAT program (Figs. F13, F14, F15) will allow us to decipher paleoceanographic and paleoclimatic changes within a latitudinal and depth transect in the equatorial Pacific Ocean. Intervals of interest include the EECO (Zachos et al., 2001a; Lyle, Wilson, Janecek, et al., 2002), the MECO (Bohaty and Zachos, 2003; Bohaty et al., 2009), the middle through late Eocene CAE events (Lyle et al., 2005), the Eocene–Oligocene transition (Coxall et al., 2005), late Oligocene warming (see supplementary material in Pälike et al., 2006b), the Oligocene–Miocene transition (Zachos et al., 2001b; Pälike et al., 2006a), the middle Miocene glaciation intensification event (Holbourn et al., 2005), and late Miocene–Pleistocene cooling.

Sediments of early Eocene age in the Pacific equatorial age transect are characterized by clay, cherts, and porcellanite. In general, sediments of middle Eocene age from the equatorial Pacific transect are dominated by radiolarian ooze, radiolarite, and clay, but carbonate-rich intervals also occur and appear correlative between Expedition 320 sites and Sites 1218 and 1219, where the CAE events were originally de-

fined. Sediments of middle Eocene age at Site U1333 are carbonate rich compared to those at Site 1218, an observation that cannot be explained by their assumed relative paleodepths during this interval. The Eocene–Oligocene transition is characterized by a major lithologic change from Eocene radiolarian oozes to Oligocene nannofossil oozes at ODP Sites 1218–1221 and Sites U1331–U1333. At Site U1334, sediments of latest Eocene age are more carbonate rich than in any of the other Eocene intervals.

The Oligocene–Miocene transition occurs within a succession of pale and dark nannofossil ooze cycles at all sites where it was recovered except for Site 1220, where it is characterized by a transition from Oligocene radiolarian ooze to Miocene clay. Clay- and diatom-rich sediments characterize the middle to late Miocene interval at Sites U1331–U1335.

Within the PEAT program, only Sites U1337 and U1338 recovered sedimentary sections of late Miocene–Holocene age with relatively high sedimentation rates and preserved carbonate (~15 m/m.y.) (Fig. F14). Site U1335 recovered this interval, but sedimentation rates are ~6 m/m.y. Sites further west and north on older crust (Sites U1331–U1336) suffer from low sedimentations rates or hiatuses in the younger section because they are far from the modern equatorial productivity zone and on deeper (older) ocean crust where depth-dependent carbonate dissolution has become strong. Of the older sites, U1334–U1336 had the highest sedimentation rates in the interval from middle Miocene through late Oligocene.

Both Sites U1337 and U1338 recovered continuous, essentially complete Neogene sedimentary sections, Site U1338 from 0 to >17 Ma and Site U1337 from 0 to >23 Ma, just beyond the Oligocene/Miocene boundary. These represent the only complete Neogene sections in the equatorial Pacific, possibly for all the tropics, that have high enough sedimentation rates to resolve orbitally forced sediment cycles. Coring during Legs 8, 9, and 16 was accomplished with the rotary core barrel, and the sediments were highly disturbed. During Leg 85 at Site 574, the middle Miocene to present was double APC cored, but sedimentation rates were slow from 0 to 10 Ma (~5 m/m.y.) and the middle Miocene section was never spliced (Mayer et al., 1985). Below the middle Miocene, only one hole was drilled. Similarly, Site 572 had only a single hole drilled through the upper and middle Miocene interval (Mayer et al., 1985). Most Leg 138 sites were drilled on 10 Ma crust and did not contain significant middle and lower Miocene sediments (Mayer, Pisias, Janecek, et al., 1992). Site 846 was drilled on 17 Ma crust on the Nazca plate but experienced poor recovery below 12 Ma. In addition, Site

845 in the Guatemala Basin has a spliced sediment section to only ~12 Ma (Mayer, Pisias, Janecek, et al., 1992), even though it was located on 17 Ma crust. Even in the tropical Atlantic on the Ceara Rise, the middle and early Miocene were discontinuously cored and longer records were spliced between different sites (Shipboard Scientific Party, 1995; Raffi et al., 2006).

Cenozoic CCD in the equatorial Pacific

One of the primary objectives of the PEAT program was to detail the nature and changes of the CCD throughout the Cenozoic in the paleoequatorial Pacific (Objective 1 in "Scientific objectives"), with potential links to organic matter deposition (Olivarez Lyle and Lyle, 2005). The choice of drilling locations, targeting positions on the paleoequator to track carbonate preservation during crustal subsidence throughout time (Figs. F13, F16), followed the initial work on DSDP sites by van Andel (1975). This first reconstruction of the Cenozoic CCD was augmented by additional results from Leg 199 (Lyle, Wilson, Janecek, et al., 2002; Rea and Lyle, 2005). One of the significant contributions of Leg 199 drilling was the latitudinal mapping of CCD variations with time. During the Eocene, the CCD appeared to be deeper outside the zone ±4° from the Equator, opposite to the pattern established during the Neogene (Lyle, 2003). The PEAT cores will allow us to refine our knowledge of temporal and spatial variation in sediment accumulation rates resulting from plate movement, varying biologic productivity at the equatorial divergence, and carbonate preservation (Fig. F13). The shipboard sampling program allowed for >1000 determinations of $CaCO_3$ concentrations, approximately one every section from one hole of each site. Shipboard results reveal the carbonate accumulation events of Lyle et al. (2005) as sharp carbonate concentration fluctuations at ~44, 41, 39, and 36 Ma across Sites U1331–U1334 and 1218, followed by a sharp transition into much higher carbonate accumulation rates from the Eocene into the Oligocene. Results from the PEAT expeditions reveal a complex latitudinal pattern where Sites U1331, U1332, and U1334 track the equatorial CCD that matches well with the signal observed from Site 1218. However, Site U1333, which is slightly north of the equatorial zone during the Eocene–Oligocene transition, shows significantly more carbonate accumulation than expected at this latitude and paleodepth.

The early middle Eocene equatorial CCD is much shallower than previously thought, as shown by results from Site U1332, where we recovered little or no carbonate in the basal sediment section above

basement, in contrast to Site U1331, which is only ~2 m.y. older. Our estimated CCD at ~49 Ma is only ~3000 m deep. Surprisingly, Expedition 320 results also show a shallower CCD than previously known during the late Oligocene, perhaps 300 m shallower in the time interval between 23 and 27 Ma. This shallower CCD, at a paleodepth of ~4.5 km, and associated reduced carbonate fluxes to the seafloor could be linked to the gradual late Oligocene cooling, first fully documented at Site 1218 (supplementary fig. 3 in Pälike et al., 2006b). The design of our drilling locations in combination with existing data will allow us to generate a 3-D view of CCD evolution during the Cenozoic during postcruise research.

Late Miocene carbonate crash and middle Miocene glaciation

Sites U1337 and U1338 recovered a full suite of Pleistocene to earliest Miocene calcareous and siliceous microfossils. All groups exhibit prominent downcore variations in preservation and abundance that appear related to major changes in primary production, export flux, and water-column and seafloor dissolution, thus reflecting fundamental changes in global climate. The carbonate crash, an extended period of low carbonate deposition widely recorded throughout the eastern Pacific Ocean at ~9–11 Ma (Lyle et al., 1995; Farrell et al., 1995), is strikingly expressed at Sites U1337 and U1338 by sharp decreases or the disappearance of planktonic foraminifers, high benthic to planktonic foraminifer ratios, and generally impoverished benthic foraminifer assemblages (Fig. **F17**). Calcareous and siliceous microfossils indicate that this prominent dissolution event was less intense and of shorter duration at Site U1338 than at Site U1337 (Fig. **F16, F17**), probably because it is located on younger oceanic crust and in closer proximity to the Equator during this time window. Site U1338 was ~200 m shallower than Site U1337 and essentially at the Equator during the carbonate crash interval.

During episodic expansion of the Antarctic ice sheet at ~14–15 Ma, calcareous microfossils exhibit overall good preservation and relatively high diversity, suggesting a vigorous Pacific Ocean circulation and deep CCD. In contrast, the preceding prolonged period of global warmth, often referred to as the Middle Miocene Climate Optimum (MMCO), appears marked by transient changes in CCD. Postcruise studies and integration of paleontological data will provide an opportunity to further investigate temporal and spatial variations in microfossil distribution across the equatorial Pacific Ocean and to unravel links with global climatic and oceanographic events during the Neogene (Objectives 1 and 9 in **"Scientific objectives"**).

Biostratigraphy and preservation

Biostratigraphic integration

A virtually complete composite section with biogenic sediments spanning 52 m.y. from the upper Pleistocene to the lower Eocene was recovered during Expedition 320/321 (Objectives 2, 3, 4, and 7 in **"Scientific objectives"**). The youngest record of the last 12 m.y. (late middle Miocene to Holocene) was well preserved at Sites U1335, U1337, and U1338 but elsewhere is only present as a thin (5–10 m) section of noncalcareous brown clay. Biostratigraphic records spanning the middle Miocene through lower Eocene are composed of nannofossil and radiolarian oozes as two major biogenic components. At Sites U1331 and U1335 turbidite beds containing reworked microfossils were present, with mixing most obvious at Site U1331. At the shipboard biostratigraphic resolution, all drilled sites contribute apparently continuous successions to this composite section and stratigraphic highlights include multiple recoveries of Eocene–Oligocene transitions at Sites U1331–U1334 and Oligocene/Miocene boundaries at Sites U1332–U1337. These sections provide excellent records of biotic response to rapid environmental change in the principal phyto- and zooplankton groups as well as benthic foraminifers.

For Expedition 321, one of the highlights was the recovery of well-preserved and diverse assemblages of siliceous radiolarians and diatoms and calcareous planktonic foraminifers and nannofossils for the Neogene. Although the zonation and calibrations of each of these groups have been established and refined over the last 50 y, there are very few locations with both well-preserved and abundant siliceous and calcareous microfossils. Leg 199 established a well-defined radiolarian stratigraphy and calibration for the equatorial Pacific Ocean (Nigrini et al., 2006); unfortunately only for the Oligocene were the planktonic foraminifers and calcareous nannofossils sufficiently preserved to provide robust calibrations (Pälike et al., 2006b; Wade et al., 2007).

In spite of a well-defined Neogene diatom stratigraphy and calibration for the low-latitude Pacific (Baldauf and Iwai, 1995; Barron, 1985), it is clear from the initial results that the presence of some of the diatoms used in the diatom stratigraphy is discontinuous in the expanded Miocene section. This has been noticed in sediments recovered during Leg 138 (Baldauf and Iwai, 1995). The discontinuous occurrences may reflect large variations in the abundances of these species with time and changing ecologic conditions (Objective 7 in **"Scientific objectives"**).

The diatom, radiolarian, calcareous nannofossil, and planktonic foraminifer stratigraphies at all sites gen-

erally agree, with some minor discrepancies. The fully integrated biostratigraphies coupled with the cyclostratigraphy and paleomagnetostratigraphy will lead to an integrated magneto-, astro-, and biochronology of all four microfossil groups for the equatorial Pacific Ocean (Objective 3 in **"Scientific objectives"**).

Dissolution and microfossil preservation

The preservation of carbonate microfossils varies dramatically throughout the succession as a result of biotic production and export rates, water-column and seafloor dissolution, and other processes. The strength of dissolution reflects the depths of the drilling sites, which are all presently bathed at >4.3 km water depth, whereas the amount of dissolution strongly depends on the paleodepth (subsidence) history at each site and fluctuations of the CCD on a regional and basin-wide scale. The dissolution effect is greatest in the oldest successions at Sites U1331–U1333 (Figs. **F13, F18**). The Eocene equatorial CCD has been estimated at a depth shallower than ~3.5 km (Lyle et al., 2005), with short-term CCD fluctuations occurring during the middle to late Eocene based on preservation of calcareous microfossils and calcium carbonate records at Sites U1331–U1334. The most striking CCD change has been recorded close to the Eocene–Oligocene transition where the sediments change from radiolarian-dominated Eocene sediments to Oligocene nannofossil oozes. The depth transect of these sites indicates a deepening of at least 1 km over this short time interval. The recovery of carbonate-rich Oligocene successions at all sites that penetrated an Oligocene sediment section is evidence for a considerably deeper CCD (>4.5 km water depth) throughout this interval (see Fig. **F13**).

A compilation of semiquantitative estimates of preservation and abundance of calcareous microfossils reveals a strong coupling of the fossil records with paleodepth history and the CCD at these drilling sites. The carbonate dissolution effect is strikingly different between microfossil groups (Fig. **F18**). Planktonic foraminifers are the most sensitive to dissolution, and well-preserved specimens were found in sediments if carbonate contents exceeded at least 60–70 wt%. At the deepest Site U1331, planktonic foraminifers are only present during carbonate maxima in the Oligocene, middle Eocene, and early Eocene sediments. At Site U1332 they were present only in the carbonate-rich Oligocene nannofossil oozes (Fig. **F18**). At Sites U1334 and U1335 high-carbonate sediments (80–90 wt%) contain abundant and well-preserved planktonic foraminifers.

Calcareous nannofossils and benthic foraminifers are less susceptible to dissolution than planktonic fora-

minifers and closely track the presence or absence of carbonates in the sediments. The preservation of both groups varies with carbonate content, but the preservation of calcareous nannofossils varies even in sediments with low carbonate content that are barren of planktonic foraminifers. Poor preservation of specimens is observed in sediments of 5–25 wt% carbonate contents, moderate preservation in sediments of 30–70 wt%, and good benthic foraminifer and moderate to good nannofossil preservation in sediments with >75 wt% $CaCO_3$.

Within the nannofossil assemblages, however, certain taxa are never present in these sediments, such as holococcoliths. The relatively robust holococcolith *Zygrhablithus bijugatus* was only recorded in one or two samples from Sites U1335 and U1336, and other taxa show distributions that are more similar to those of planktonic foraminifers, such as the long-ranging heterococcolith genus *Helicosphaera* (Fig. **F18**).

Biotic response to climatic change, Neogene Sites U1337 and U1338

Phytoplankton, zooplankton, and benthic foraminifers provide an excellent opportunity to document the biotic response to intervals of rapid climatic change in both the surface and deep ocean, addressing PEAT Objectives 1, 2, 4, and 7 (see **"Scientific objectives"**).

Planktonic foraminifer assemblages are generally well preserved at Sites U1337 and U1338. As with other microfossil groups, distinct changes in assemblage composition reflect preservational and evolutionary changes, fluctuations in the water-column structure, and the position of each site relative to the paleoequator (Fig. **F19**). Globoquadrinids and dentoglobigerinids dominate the assemblages from the Oligocene to middle–late Miocene. This interval is also associated with extremely abundant and diverse paragloborotaliids. These taxa are considered to occupy the thermocline and prefer nutrient-rich environments (Wade et al., 2007). The decrease in globoquadrinids and dentoglobigerinids is associated with an increase in *Globigerinoides*, which increases in abundance from the middle Miocene. Keeled globorotaliids dominate the Pleistocene assemblages. Peak abundances of *Globigerinoides* spp. occur within the late Miocene.

There appears to be a relationship between the diversity in the planktonic foraminifers and climatic change. At Site U1338, a high diversity of planktonic foraminifers is recorded in Zone M5, with many microperforate taxa (*Globigerinita, Globigerinatella, Mutabella,* and *Tenuitella*). The diversity of this group is particularly high through the early middle Miocene.

These taxa occupied the warmer mixed layer (Pearson et al., 2001b; Majewski, 2003), and the high diversity may be related to higher SSTs and increased stratification associated with the MMCO.

Planktonic foraminifers, because they dissolve more easily than benthic foraminifers or nannofossils, are useful to evaluate the degree of dissolution in calcareous biogenic sediments (Objective 1 in "Scientific objectives") (Fig. F17). Intervals of enhanced dissolution have been detected at Sites U1337 and U1338 and are associated with laminated diatom oozes between 11.5 and 9 Ma, the "carbonate crash" interval. Another short interval is barren of planktonic foraminifers and marked by a high benthic/planktonic foraminifer ratio at ~17 Ma at Site U1337.

Much like the planktonic foraminifers, calcareous nannofossil assemblages reflect global and regional oceanographic changes. Neogene placolith diversity peaks in the early to middle Miocene, during the MMCO. At ~14 Ma, nannofossil assemblages begin to fluctuate, indicating changes in productivity. At Site U1338 there are several instances when assemblages are dominated by very small (<3 µm) *Dictyococcites* species. These events are also less frequently present at Site U1337. These dominance intervals may reflect greater surface water productivity and perhaps suggest a more intense upwelling regime at the MMCO. Another indication that Site U1338 records a higher productivity signal is the exclusion of certain taxa, such as the marker species *Helicosphaera ampliaperta* and *Catinaster coalitus*, both of which are present but rare at Site U1337.

Lower bathyal to abyssal benthic foraminifers occur throughout the early Miocene to Pleistocene at Sites U1337 and U1338 and show relatively good preservation. Marked variations in downcore abundance and assemblage composition may relate to fundamental changes in global climate, major ice-volume fluctuations, and reorganizations in oceanic circulation during the Neogene. Organic flux–sensitive taxa track substantial changes in equatorial Pacific Ocean surface productivity throughout the latest Miocene to Pleistocene. Impoverished assemblages and high benthic/planktonic ratios prominently mark the late Miocene carbonate crash (Fig. F17), whereas diversified assemblages, including high numbers of epifaunal or near surface dwellers such as *Cibicidoides*, signal a marked improvement in deep ocean ventilation following middle Miocene high-latitude ice sheet expansion. Early to early middle Miocene assemblages exhibit significant fluctuations in abundance and diversity, hinting at major changes in upper ocean structure and deepwater ventilation at the onset of and during the MMCO.

Basal carbonates

Eocene basal carbonate sediments were confirmed on top of basaltic basement at all PEAT sites apart from U1332 and U1336 (Fig. F20). At Site U1332, several samples immediately on top of basement basalt contained relatively common calcareous nannofossils. The existence of carbonates suggests that paleodepths were above the shallow Eocene CCD during the early to middle Eocene. At Sites U1331 and U1333–U1335, these carbonate intervals are thin and their lower parts are lithified to limestones, probably because of the combined influence of hydrothermal fluids and overburden. These sediments contain slightly diagenetically modified calcareous microfossils and are barren of siliceous microfossils. The sites where Eocene sediments were recovered were located within 2° latitude of the paleoequator at the time of first sediment accumulation, so evidence of equatorial upwelling might be expected to have influenced the assemblages (see below). The absence of siliceous microfossils is likely a result of dissolution associated with hydrothermal flow of the crust (Moore, 2008a).

Productivity indicators

Shipboard analyses of quantitative microfossil faunal assemblages allow only preliminary speculation on potential microfossil-based productivity indicators; quantitative work will be required to follow up on these initial observations and fully address Objective 2 of the PEAT program (see "Scientific objectives"). Calcareous nannofossil assemblages at these lowest stratigraphic levels are not strikingly different from younger examples. At several sites, however, the common presence of taxa that are considered to be higher productivity (or cooler water) indicators is suggestive of an upwelling signal (e.g., common *Chiasmolithus* and small reticulofenestrids [*Reticulofenestra minuta*] at Sites U1333 and U1334). At all sites sphenoliths are also common at these levels, and although some representatives of this group are considered to be oligotrophs (e.g., Gibbs et al., 2004), certain species clearly display more opportunistic behavior, which may explain their abundant presence here (e.g., Wade and Bown, 2006; Dunkley Jones et al., 2008).

The absence or relative rarity of the warm-water oligotrophic discoasters in the lowest parts of Sites U1331, U1333, and U1334 is also suggestive of higher productivity surface waters, at least for the sediments immediately overlying basement. Discoasters are actually common in the lowest sediments at Site U1331, and this either represents selective concentration due to the dissolution of less robust taxa or indicates that these species (*Discoaster*

deflandrei and *Discoaster lodoensis*) were adapted to more eutrophic paleoenvironments. Planktonic foraminifer assemblages in the basal carbonates at Sites U1333 and U1334 are dominated by relatively robust taxa: subbotinids, parasubbotinids, and paragloborotalids. These genera are thought to occupy a (sub)thermocline habitat (Wade et al., 2007; Sexton et al., 2006) and are often associated with high-productivity environments (Wade et al., 2007), an association consistent with both sites being situated in the equatorial upwelling region. However, planktonic foraminifer assemblages at Sites U1333 and U1334 may also be biased toward these more robust taxa by the effects of dissolution. Detailed assemblage study is required to elucidate the relative contributions of calcium carbonate dissolution and the true paleoecological signal.

Radiolarian stratigraphy

The radiolarian stratigraphy in sediments recovered during Expedition 320 (Table **T3**) spans Zones RN14 (lower Pleistocene) to RP10 (lower middle Eocene) and provides the highest shipboard biostratigraphic resolution for most sections within the Eocene. The preservation of assemblages is generally good with only a few scattered intervals of moderate to poor preservation. Nigrini et al. (2006) took a comprehensive approach toward establishing ages for all radiolarian datums recovered at Leg 199 sites. In so doing, they produced age estimates for >300 radiolarian datums, greatly enhancing our ability to date the Cenozoic section in the tropical Pacific. However, several of these calibrations need to be checked and/or refined. In addition, some of the datums appear to be more reliable than others, and this needs to be further evaluated. Results from Sites U1331–U1334 will allow recalibration of radiolarian datums near the Eocene/Oligocene boundary.

In some cases, variation in the levels of first and last appearances of species may be caused by variation in taxonomic interpretation, but more often these variations are due either to real differences in the ranges of species at different locations in the tropical Pacific or to the extremely low abundance of certain species in samples from a given site. Thus, taxonomic difficulty, abundance, and preservation all figure into how well a species serves as a stratigraphic marker.

A few levels were not adequately covered by Leg 199 sites. For the upper Miocene we have relied on the radiolarian studies of Leg 138 in the far eastern tropical Pacific (Moore, 1995). In their studies of Leg 199 sites, Kamikuri et al. (2005) and Funakawa et al. (2006) added substantially to our understanding of the radiolarian assemblage transitions at the Oligocene/Miocene and Eocene/Oligocene boundaries.

However, these studies focused on the statistical changes in the faunal assemblages as a whole and made no wholesale attempt to recalibrate first and last appearance datums. During Expedition 320 we were able to add to the stratigraphic control in the lower part of the middle Eocene collected at Site U1331 and test the usefulness of individual datums at the sites drilled. The full integrated biostratigraphies will address Objective 3 (see **"Scientific objectives"**).

Diatoms

The diatom stratigraphy in sediments recovered during Expedition 320/321 represent the Pleistocene *Fragilariopsis doliolus* through the lower Oligocene *Coscinodiscus excavatus* Zones. Not all zones are represented at all sites given variability in the state of diatom preservation and the age of the sedimentary sections recovered.

The species observed are typical of the low-latitude eastern equatorial Pacific Ocean (Barron, 1985; Baldauf and Iwai, 1995). Primary biostratigraphic markers are typically applicable. Noted exceptions include the often inconsistent occurrences of *Coscinodiscus gigas* var. *diorama*, *Actinocyclus moronenesis*, and *Cestodiscus peplum*. When necessary, secondary stratigraphic indicators were used for zonal assignments.

Diatoms are most common in the Holocene through upper lower Miocene sediments (0–18 Ma) (Fig. **F21**). This interval is best represented at Sites U1335, U1337, and U1338. Distinct within this interval is the occurrence of thick sequences of laminated diatom oozes (diatom mats) at Site U1337 (Fig. **F22**). These diatom intervals are mainly composed of the needle-shaped diatom *Thalassiothrix* and are deposits that record unusual oceanographic conditions that repeated several times in the eastern equatorial Pacific region during the middle to late Miocene and early Pliocene (Fig. **F23**) (Kemp and Baldauf, 1993). One of the unresolved questions of these expeditions is why the diatom mats are prominent at Site U1337, whereas at Site U1338 the same time intervals contain diatom rich sediment, but only rarely laminated diatom intervals.

Kemp and Baldauf (1993) proposed that the diatom mats record high open-ocean sedimentation rates and may represent vast sinks of silica and carbon. However, a change in sedimentation rates across these intervals was not observed based on the coarse shipboard biostratigraphic resolution. The alternation between *Thalassiothrix* and mixed sediment laminae could reflect the periodic movement of the frontal zone in the eastern equatorial Pacific Ocean. An improved understanding of these diatom mats

will be an important prerequisite for enhancing the understanding of the marine biogeochemical cycling and for assessing the impacts of rapid climate change on export production in the low-latitude eastern Pacific Ocean) Objectives 1, 2, 4, and 7 in **"Scientific objectives"**).

Diatoms are less common in the lowermost Miocene through uppermost Oligocene sediments than those from the upper Neogene. The lower diatom numbers in part reflect a deterioration, but variability, in diatom preservation. Diatom abundance and preservation improves for the lowermost upper Oligocene and lower Oligocene and typically allow identification of the *Bogorrovia veniamini* through *Coscinodiscus excavatus* Zones. These zones are best represented at Sites U1333 and U1334. The base of the *C. excavatus* Zone approximates the Oligocene/Eocene boundary. Diatom preservation and therefore abundance deteriorates at or immediately below this boundary, with diatoms typically not observed in the majority of samples examined from the Eocene.

Paleomagnetism

Paleomagnetism and magnetostratigraphic studies are important observations needed to fulfill the expedition objectives of obtaining a well-intercalibrated Cenozoic megasplice and constraining Pacific plate tectonic motion (Objectives 3 and 5 in **"Scientific objectives"**). Results obtained so far indicate that the sediments recovered will provide the needed archive to address these objectives in a comprehensive fashion. For example, during Expedition 320, shipboard paleomagnetic results were obtained from 56,222 intervals measured along ~2000 split-core sections and from detailed progressive alternating-field (AF) and thermal demagnetization of 411 small discrete samples (Figs. **F24, F25**) These data indicate that a useful magnetic signal (characteristic remanent magnetization [ChRM]) is preserved in APC cores after removal of the drilling-induced overprint by partial AF demagnetization at 20 mT except for intervals affected by reduction diagenesis. Cleaned paleomagnetic data were characterized by shallow inclinations, consistent with the sites being near the paleoequator, and by 180° alternations in declinations downhole, reflecting magnetic polarity zones (magnetozones). These qualities, along with demagnetization results from discrete samples, indicate that the ChRM is the primary depositional remanent magnetization. Magnetostratigraphy at each site is constructed by correlating the distinct declination alternations with the geomagnetic polarity timescale (GPTS) (Fig. **F24**).

The magnetic polarity stratigraphy of the entire middle Eocene to Quaternary interval was resolved at the eight sites occupied during Expedition 320/321. The middle Eocene and Oligocene intervals were well documented at Sites U1332 and U1333. At Site U1332, mean sedimentation rates in this interval range from 3 to 8 m/m.y., and at Site U1333 the mean sedimentation rates reach ~12 m/m.y. in the lower Oligocene. At Site U1334 the upper Oligocene and lower Miocene magnetic stratigraphy was well resolved with mean sedimentation rates of 12 m/m.y. in the lower part of the interval and 4 m/m.y. in the upper part. At Site U1335, the upper Miocene and Quaternary magnetic stratigraphy was well resolved at sedimentation rates of ~6 m/m.y., and below these sediments lies an interval of upper middle Miocene where the magnetic stratigraphy is not resolved because of weak magnetization intensities. This ~20 m long unresolved interval is underlain by sediments that carry a magnetic stratigraphy of part of the middle and lower Miocene, although the interval is interspersed with turbidites and evidence of reworking. At Site U1336, the magnetic stratigraphy of part of the middle and lower Miocene is resolved in the 0–80 m CSF interval at mean sedimentation rates of ~10 m/m.y.; however, below ~80 m CSF magnetization intensities are too low for resolvable magnetization directions. At Site U1337, although the magnetic polarity stratigraphy is interpretable for the late Miocene to Quaternary, data quality is not high for the upper Miocene. At Site U1338, the magnetic stratigraphy is resolvable in three intervals: part of the Pliocene–Pleistocene (0–4 Ma), part of the late Miocene (8.7–11 Ma), and part of the middle Miocene (12.7–16 Ma). These three intervals at Site U1338 are separated by intervals of low magnetization intensities where the magnetostratigraphy was not resolvable.

In total, the magnetostratigraphies from Expedition 320/321 yield 868 dates ranging from 51.743 Ma (base of Chron 23n.2n at Site U1331) to the present. In addition, 83 short polarity intervals were observed that might correspond to cryptochrons or geomagnetic excursions. At these short events and at the geomagnetic reversals, magnetization intensities are low, as would be expected if the sediments are accurately recording the past paleomagnetic field intensity. Analysis of paleomagnetic directions over stable polarity intervals (full chrons) indicates the long-term record provides paleolatitude information that will aid in refining the Pacific apparent polar wander path and directional dispersion information for studying geomagnetic secular variation (Objective 5 in **"Scientific objectives"**). Thus, besides providing ages for the eight sites, the high-quality paleomagnetic records have the potential to resolve long- and short-term geomagnetic field variability and provide important plate kinematic constraints.

Cenozoic megasplice and stratigraphic correlation

One of the major shipboard scientific efforts for every paleoceanographic drilling cruise is to place the depth column into a time framework. For the PEAT program a prime objective was a detailed intercalibration of bio-, magneto-, and chemostratigraphic records for the Cenozoic from the early Eocene to the present within an astronomically age-calibrated framework (Objective 3 in "Scientific objectives"). During Expedition 320/321 we depended on shipboard biostratigraphy and magnetostratigraphy for the basic time framework. Shipboard biochronostratigraphy is based upon the PEAT timescale (see "Reconstruction of geologic age during Expedition 320/321" in the "Methods" chapter) developed before the PEAT expeditions and to be refined postcruise. Depth positions of recognized biostratigraphic zones and microfossil datum levels will be listed in each of the site summaries.

The PEAT program was designed to incorporate results from Leg 138 for the younger Neogene part and Leg 199 for time intervals in the Eocene (Pälike et al., 2008) (Fig. F2). Expedition 320/321 shipboard results indicate that we can achieve this objective, based on the observation that even decimeter-scale features in the sedimentary record from the drilled sites can be correlated over large distances across the Pacific seafloor (Fig. F9) (Pälike et al., 2005). The PEAT program will leave a long-lasting legacy for the detailed intercalibration of all major fossil groups, a detailed magnetostratigraphy with 870 identified dated reversals, and sedimentary cycles that can be calibrated across large distances in the Pacific Ocean. Figure F26 demonstrates that a Cenozoic megasplice can be constructed from the material recovered and spliced onto previous Leg 138 and 199 sites. Physical property data that proxy calcium carbonate oscillations at Sites U1331 and U1332 show a remarkable match with those from Site 1220, which also has an excellent magnetostratigraphy. Similarly, Sites U1333 and U1334 can be spliced to Site 1218, providing a coherent and integrated record of large-scale Pacific sedimentation patterns of biogenic material from the Eocene through the Miocene and younger (Fig. F27, F28). Such stratigraphic correlation makes possible the study of sedimentation patterns and mass accumulation rates at orbital resolution. The material recovered will also allow us to verify existing calibrations (e.g., Pälike et al., 2006b) and further extend these up into the Miocene and down into the Eocene.

We can exemplify the approach toward the Cenozoic by constructing a preliminary multisite splice of gamma ray attenuation (GRA) bulk density (Fig. F29). This record of GRA bulk density from tropical Pacific sediments encompasses a major part of the Cenozoic, stretching from the upper Eocene to the recent, using data from Legs 138 and 199 and the PEAT program.

Sedimentation rates

A study of paleoceanographic processes and variations of mass accumulation rates across the PEAT latitudinal transect and its evolution over time depends on a detailed knowledge of sedimentation rates (Fig. F14). The integrated bio- and magnetostratigraphies obtained for all Expedition 320/321 sites will allow us to fully exploit and understand the complex interplay of productivity, dissolution, and spatial biogenic sedimentation patterns, which leave their imprint in the sedimentation rates recorded at different drill sites. Depending on the crustal subsidence and age for each site, sedimentation rates vary from site to site over time (Figs. F14, F30).

Our results reveal the change in linear sedimentation rates (LSRs) in both the latitudinal and age transect components of the PEAT program. LSRs of the middle Eocene are extremely high, frequently >10 m/m.y., with a maximum of 18 m/m.y. at Site U1331. Rates at Sites U1332 and U1333 are similar (8–6 m/m.y.). LSRs of the late Eocene decrease to 3.5–6 m/m.y. at Sites U1331–U1333. The highest LSR peaks (>20 m/m.y.) exist in the early to late Oligocene section at Sites U1333 and 1334 and in the early Miocene for Sites U1336 and U1335. Middle to late Miocene sedimentation rates are in the range of 20–30 m/m.y. at Sites U1337 and U1338. LSRs also increase from the west (Site U1331) to the east (Site U1336), reflecting the relative age, depth, and latitudinal position of the sites. LSRs frequently show high rates >20 m/m.y in the east (Sites U1334–U1338) but rarely exceed 15 m/m.y. in the western sites. The LSRs of Sites 1218 and 1219 are also reflected at Site U1334 but show slightly lower values during the early Miocene (15–20 m.y.). By combining the available data from Legs 138 and 199 and Expeditions 320 and 321, we will obtain a continuous history of sedimentation rates in the equatorial Pacific region for the past 56 m.y.

Middle Eocene Climatic Optimum

A complete downhole transition of the MECO event was recovered at Sites U1331–U1333 (Bohaty and Zachos, 2003; Bohaty et al., 2009) (Fig. F31). Based on bio- and magnetostratigraphic datums, the MECO event (40–41 Ma) occurs between magnetic Chrons C18n.1n and C18r and falls into the radiolarian Zone RP15 to lowermost RP16. Bohaty et al. (2009) revised the position of peak middle Eocene warming to 40.0 Ma in Chron C18n.2n. At Site U1333 the lithostratigraphy of the MECO event is characterized by an alternating sequence of nannofossil ooze and

radiolarian nannofossil ooze interrupted by an interval of radiolarian clay as thick as 4.2 m (Fig. F31). The MECO event at Site U1332 is marked by an alternating sequence of nannofossil ooze, radiolarian nannofossil ooze, radiolarian ooze, and clayey radiolarian ooze. Site U1331 lithostratigraphy also shows an alternating sequence of nannofossil radiolarian ooze, radiolarian nannofossil ooze, and nannofossil ooze. However, at Site U1331 the interval is interrupted by coarse-grained gravity flows. These lithostratigraphic results for the MECO event are similar to those obtained from ODP Sites 1218–1221; at Site 1222 the interval is dominated by clay (Lyle, Wilson, Janecek, et al., 2002).

Eocene–Oligocene transition

Lithology

An Eocene–Oligocene transition was recovered at four sites drilled during Expedition 320 (Sites U1331–U1334). The Eocene/Oligocene boundary as formally defined cannot be identified at these sites because of the absence of the planktonic foraminifer biostratigraphic marker *Hantkenina*. Magnetostratigraphy from APC-cored intervals and biostratigraphy (radiolarians and nannofossils) provide excellent age control, however, with the Eocene/Oligocene boundary falling just below the Magnetochron C13n/C13r reversal, near the middle of nannofossil Biozone NP21, and just above the radiolarian Biozone RP20/RP19 boundary. (Fig. F32).

Sites U1331–U1334 capture the lithostratigraphy of the Eocene–Oligocene transition in the equatorial Pacific Ocean in a depth transect from ~3600 to 4300 m paleowater depth (~34 Ma) (Fig. F32). At each site, a downhole transition takes place from white to pale brown nannofossil ooze of earliest Oligocene age to much darker brown sediments of Eocene age. At the deep end of the depth transect where the Eocene–Oligocene transition is thinnest (Site U1331), the transition is sharp (over a ~5 cm thick interval) from carbonates into homogeneous dark brown clayey radiolarian ooze. At the shallow end of the transect (Site U1334), where the correlative section is much more expanded, it is less sharp and takes place through dark clayey nannofossil chalk to alternations of dark nannofossil chalk and even darker clayey nannofossil chalk. At Site U1332 the lithologic transition is through radiolarian nannofossil ooze to radiolarian ooze with clay; at Site U1333 the transition is through radiolarian ooze to alternations of radiolarian nannofossil ooze with clay and clayey radiolarian ooze. At Sites U1332–U1334 prominent ~50–100 cm thick beds of particularly dark clays or radiolarian clays are noticeable (Fig. F32). At all sites,

the line-scan core images reveal stepwise downhole transitions in sediment color (Fig. F32). Associated pronounced downhole stepwise increases occur in magnetic susceptibility, a*, and b*, together with pronounced downhole deceases in GRA bulk density, L*, and $CaCO_3$ content (see **"Lithostratigraphy"** in the "Site U1331" chapter, **"Lithostratigraphy"** in the "Site U1332" chapter, **"Lithostratigraphy"** in the "Site U1333" chapter, and **"Lithostratigraphy"** in the "Site U1334" chapter).

The lithostratigraphy of the Eocene–Oligocene transition from Expedition 320 sites is remarkably consistent with both the expedition rationale for drilling these sites and Leg 199 results and will allow the study of the early history of Cenozoic glaciation and CCD behavior (see Coxall et al., 2005; Pälike et al., 2006b) across a depth transect. Two major lithostratigraphic results from the Eocene–Oligocene transition from Expedition 320 are unexpected and also demand evaluation:

1. The discovery that the section at Site U1333 (paleowater depth = ~34 Ma; ~4000 m) is more carbonate rich than Site 1218 (paleowater depth = ~34 Ma; ~3850 m), which perhaps reflects a paleolatitudinal signal given that this site is at the northern edge of the latitudinal transect of PEAT sites during the Eocene–Oligocene; and

2. Recovery in the most expanded section (Site U1334) of darker and more clay rich and yet more calcareous lithologies than at either Site U1333 or Site 1218 (Figs. F32, F33).

The datums throughout a major part of the Cenozoic section provided by the Nigrini et al. (2006) radiolarian calibration offsets any taxonomic, abundance, or preservation problems that were encountered with a few of the species. One interval, however, has proven to be particularly troublesome: the Eocene/Oligocene boundary. This interval not only shows substantial turnover in the radiolarian fauna (Fig. F34) (Funakawa et al., 2006), it is often represented by a hiatus and is associated with reworked older Eocene radiolarians being deposited in uppermost Eocene and lower Oligocene sediments. Thus, the upper appearance limit of many Eocene species is problematic. A further complication in establishing the true age of first and last appearances of these lower Oligocene and upper Eocene species arises from the impact of missing sections on establishing a paleomagnetic stratigraphy. With part of the section missing, chron boundaries can be truncated, giving an inaccurate estimate of the age of the sediment marking that boundary. Finally, the sharp change in the CCD across the Eocene/Oligocene boundary often makes it difficult to correlate the sec-

tion recovered at one site to that of another site in the same region (Fig. F35). Of all the means of making regional correlations across the Eocene/Oligocene boundary, paleomagnetic chron boundaries appear to be the most reliable (Fig. F35).

Through the many studies on the material collected during Leg 199, we have come to appreciate more fully the true stratigraphic nature of the Eocene/ Oligocene boundary. From the study and comparison of these sections we have been able to identify those sites that appear to have the most complete record across this boundary. From Leg 199, Site 1218 appears to provide the most complete stratigraphic record. From this expedition, a complete boundary section appears to have been recovered at Sites U1333 and U1334; however, only Site U1333 has paleomagnetic control.

In an effort to make a detailed correlation of these three sites, we compared their magnetic susceptibility records and, where available, the paleomagnetic stratigraphy (Fig. F35). This comparison is revealing in many ways. Although Site 1218 and U1334 magnetic susceptibility records look quite similar superficially, when compared in detail they are substantially different. The two-step change in magnetic susceptibility (as well as in other geochemical variables) at the base of Chron C13n is common to Sites 1218 and U1334, as well as to Site U1333. This is one of the first indications that the Eocene/Oligocene boundary section at a site is relatively complete (e.g., Coxall et al., 2005). By simple "peak counting," the maximum in magnetic susceptibility at the top of Chron 15n is also fairly easily identifiable at Site U1334 (as well as at Site U1333). However, the broad, major peak in magnetic susceptibility seen at Site 1218 is only partially represented at Site U1334, with only the younger part of this broad maximum seen at Site U1334. It is not seen at all at Site U1333. A sharp minimum in magnetic susceptibility just below the top of Chron C17n.1n at Site 1218 can also be seen, along with similar minima at Sites U1334 and U1333. Finally, the minimum in magnetic susceptibility just below the broad maximum near the top of Chron 18n.1n is associated with the first appearance of *Calocyclas turris* at Site 1218, as well as at Sites U1334 and U1333.

The magnetic susceptibility record from Site U1333 looks very dissimilar to those of the two sites drilled on younger basement (Fig. F35). It looks more similar to those records from Sites 1219 and 1220 that were drilled on 56 Ma crust (Fig. F36). These differences and similarities exist even though Site U1334 has fairly good preservation of calcium carbonate in the upper Eocene section, whereas at Site 1218 car-

bonate preservation is relatively poor, and at Sites 1219, 1220, and U1333 carbonate is only occasionally present. Thus, it appears that the high-amplitude excursions in magnetic susceptibility records near the top of Chron 16n.1n are found only in sections deposited on crust that is only a few million years older than this chron (~35.5 Ma).

One would hope that the biostratigraphic record of the Eocene/Oligocene boundary region at the more complete sites would reveal a consistent record of faunal turnover. This may be true for the first appearances of species in the lower Oligocene; however, the position of the last occurrences of Eocene species within the uppermost Eocene seem to indicate that the reworking of older fossils into younger sections is common, even if there are no apparent breaks in the sections. For example, the position of the last occurrence of the radiolarian *Cryptocarpium azyx* at Site 1218 is considerably higher in the section than at Sites U1333 and U1334 (Fig. F35). The first appearance of species in these sections is somewhat more reliable (Fig. F35), but it is the very nature of such large faunal turnovers as seen near the Eocene/Oligocene boundary that most of the biostratigraphic datums involve extinctions. Only a very detailed sampling of the section and a more quantitative analysis of the fauna can reveal when the presence of a species in a sample is likely to indicate reworking of older sediments.

Just as the rapid extinction of many Eocene species is a dramatic illustration of the impact of climate change on the planktonic fauna, the recovery from this event is also of interest. A few radiolarian species survived the transition from the warm Eocene to the cooler Oligocene (Funakawa et al., 2006), but the rapid appearance of new species did not occur until several hundred thousand years after the Eocene/ Oligocene boundary at 33.7 Ma. Two lower Oligocene radiolarian marker species (*Lithocyclia crux* and *Theocyrtis tuberosa*) first appear near 33.4 Ma (recalibrated age), followed by *Dorcadospyris pseudopapilio, Dorcadospyris quadripes,* and *Centroboytris gravida* near 33.0 Ma (recalibrated age) (Fig. F34). Abundant diatoms are found in the coarse fraction slides alongside the radiolarians starting in the uppermost Eocene at the same level as the first (older) step in the magnetic susceptibility record (Fig. F34), and the species makeup of this flora changes rapidly upsection. Thus, it appears that there is an increase in the productivity of larger diatoms associated with the Eocene–Oligocene transition (Fig. F21) and that the changeover of the species makeup of the flora occurs quickly in the diatoms relative to the radiolarians. Radiolarians allow the correlation of Eocene/Oligocene boundary sections between different sites without relying directly on the lithostratigraphy (Fig. F37).

Oligocene–Miocene transition

At the end of the Oligocene a significant multimillion year–long rise in the oxygen isotope record (Lear et al., 2004) is closely followed by a relatively short, sharp increase in oxygen isotope values that has been interpreted as a major glacial episode (Mi-1) (Zachos et al., 1997, 2001a, 2001b; Pälike et al., 2006a, 2006b) and correlated to a pronounced drop in sea level (Miller et al., 1991). This event is very close to the Oligocene/Miocene boundary and has now been astronomically age calibrated in several ocean basins (Shackleton et al., 2000; Billups et al., 2004; Pälike et al., 2006a). Although there are clear periodic isotopic signals indicating major changes in ice volume, ocean temperatures, and/or ocean structure, this biostratigraphic boundary has always been somewhat of an enigma. Unlike the major changes in the isotopic stratigraphy, the biostratigraphies of the planktonic microfossils show very little change across this boundary. In fact, it is one of the most difficult epoch boundaries to pick using solely microfossil biostratigraphies.

At Sites 1218 and 1219 this interval was well recovered; however, carbonate preservation still presented a problem for foraminifer stratigraphy. Both sites were deep and well within the lysocline, making the application of temperature proxies such as Mg/Ca ratios in foraminifer tests more difficult (Lear et al., 2008). At the time Miocene–Oligocene sediments were deposited, Site 1218 already resided on 18 Ma old crust and was ~4.1 km deep. Site 1219 was on ~34 Ma crust and was ~4.5 km deep (Lyle, Wilson, Janecek et al., 2002). A relative increase in large diatoms near this boundary in the siliceous coarse fraction suggests increased productivity; however, detailed, high-resolution flux rates across this interval have yet to be determined.

Complete sequences to the biozone and magnetochron level of the Oligocene–Miocene transition were recovered at Sites U1332–U1336 and at the very base of Site U1337 (Fig. **F38**), providing an excellent integrated stratigraphy. Sites U1332–U1334 display unambiguous magnetostratigraphy coherent with biostratigraphy and a distinct record of alternations in sediment constituents and physical properties. Because of Fe reduction, late Oligocene and early Miocene sediments from Sites U1335 and U1336 do not retain a sufficiently strong remanent intensity to allow retrieval of a reliable shipboard magnetostratigraphy, but good biostratigraphic control is available. The northwesternmost Site U1331 (Fig. **F1**) does not record the Oligocene–Miocene transition. The Oligocene/Miocene boundary is approximated by the first occurrence of the planktonic foraminifer *Paragloborotalia kugleri* (23.0 Ma) and the total range

of the short-lived (~100 k.y.) calcareous nannofossil *Sphenolithus delphix* (23.1–23.2 Ma) just below Chron C6Cn.2n. The Oligocene–Miocene transition in Expedition 320 sediments is characterized by alternations of nannofossil- and radiolarian/clay-dominated intervals upsection of the Oligocene/Miocene boundary at Sites U1332 and U1333 and by subtle light–dark color alternations of nannofossil ooze at Sites U1334, U1336 (Fig. **F38**), and U1337.

Miocene

Carbonate-bearing Miocene sediments were recovered primarily at Sites U1335–U1338. At Site U1335, U1337, and U1338, the early and middle Miocene sections are expanded and sedimentation rates are as high as 20–30 m/m.y., allowing us to achieve our Miocene specific objectives (see **"Latest Oligocene– earliest Miocene [Site U1335; 26 Ma crust],"** **"Miocene [Site U1337; 24 Ma crust],"** and **"Early and middle Miocene [Site U1338; ~18 Ma crust]"**). The Miocene and younger periods form the prime focus for Expedition 321.

Neogene biogenic events and cycles

The Neogene saw significant changes in temperature, glaciation, plankton community, and carbon cycle, including a significant warm interval at ~15–16 Ma, and multiple glaciations first in Antarctica and then in the Northern Hemisphere (Zachos et al., 2001a). There were also important changes in the CCD. Changes in isotope composition and SST proxies can only be monitored by shore-based geochemical studies. However, shipboard monitoring of changes in plankton composition and relative abundance indicate that dissolution has taken place in the Neogene equatorial Pacific (Figs. **F17, F19**), achieving parts of Objectives 2, 3, 4, and 7 listed in **"Scientific objectives."**

The eastern equatorial Pacific has times of known change in CCD at ~18 and ~10 Ma (Lyle et al., 1995; Lyle, 2003). There are also important intervals where biogenic fluxes have changed significantly (Farrell et al., 1995) and important time intervals of high diatom flux (Kemp and Baldauf, 1993). We were able to identify these intervals at Sites U1337 and U1338 (Fig. **F23**) and expect that further work will identify new intervals, thereby achieving Objective 1 listed in **"Scientific objectives."**

Equatorial productivity and redox-related color changes

White nannofossil oozes are the backdrop for the vivid color changes observed midsection at Sites U1334–U1336 (Oligocene–Miocene but independent

of section age). Sediment color shifts from brown/ very pale brown to light greenish gray and white. At each of the three sites, the shift in color is illustrated by a steplike drop in b* reflectance (yellow-blue) and a near complete loss of magnetic susceptibility (Fig. **F39**). Dissolved Fe concentrations in pore fluids increase at least sixfold in the zone of greenish gray sediments. Dissolved Mn concentrations increase at least fivefold in peaks just shallower than the dissolved Fe peaks, consistent with remobilization of Mn under less reducing suboxic diagenesis. The link between sediment color and suboxic diagenesis is clearest at Site U1335, where the light greenish gray color is interrupted by a small interval of very pale brown before returning to greenish gray again (~180 m CSF; lower Miocene). That very pale brown interval corresponds to a pronounced dip in dissolved Fe and a small increase in dissolved Mn. Together with the reduced remanent intensity and magnetic susceptibility, increases in dissolved Fe concentrations and changes in sediment color indicate intensified microbial Fe reduction, perhaps fueled by higher organic carbon accumulation rates across this interval. The intensification of suboxia at depth is largely controlled by site location with respect to the core of the equatorial upwelling system (Figs. **F6, F39B**). The greenish gray coloration is restricted to the time interval when each site was located south of 3°N. This pattern of geographic control on organic matter deposition and sediment diagenesis is supported by sediment color change observations in three additional DSDP sites (78, 79, and 574) (Fig. **F39B**). Further postcruise research will establish to what extent geochemical proxies of organic matter productivity, burial, and degradation contribute to the observed patterns, following Olivarez Lyle and Lyle (2005).

While Expedition 320 scientific party noted a relationship among magnetic susceptibility, brown-green color change, and Mn and Fe contents in interstitial waters at Sites U1334–U1336, the results are not as clear-cut at Sites U1337 and U1338 (Fig. **F39**). All sites have significant dissolved manganese peaks in the upper sediment column. The low-latitude younger sites (U1335, U1337, and U1338) have the Mn peak very near the sediment/water interface, whereas the dissolved manganese peak in the older, more northerly sites is found tens of meters into the sediment column. The dissolved Mn peaks in Site U1337 and U1338 sediments are about a factor of 30 higher than those found in the other sites, however, perhaps because of higher water-column scavenging of Mn to the sediments. The dissolved Fe peak does not clearly match the green intervals, especially at Site U1338. Although not plotted on the paleolatitude graph, green sediments at Sites U1337 and

U1338 are associated with intervals when they were near or within the equatorial zone, showing an apparent sedimentary "memory" of the equatorial productivity zone.

Geochemistry

Bulk sediment geochemistry: sedimentary organic carbon and carbonate burial

A high-priority objective of the PEAT program is to reveal the history of CCD fluctuations during the Cenozoic. The findings resulting from >1000 coulometric carbonate measurements (Figs. **F16, F40**) are described in **"Cenozoic CCD in the equatorial Pacific"** (Fig. **F13**). Calcium carbonate, inorganic carbon (IC), and total carbon (TC) concentrations were determined on sediment samples from one hole at every site.

We measured TC and total organic carbon (TOC) at a similar sample resolution and determined very low TOC concentrations, as previously found during Leg 199 (Lyle, Wilson, Janecek, et al., 2002; Olivarez Lyle and Lyle, 2005). TOC concentrations were determined separately by a difference method and by an acidification method for Site U1331. However, we concluded that the TOC concentrations determined by the normal difference method were overestimates in high-weight percent $CaCO_3$ and very low weight percent TOC sediments because they were determined as a small difference between two numbers comparable in magnitude. Therefore, TOC analyses were performed only by the acidification method, in which TOC was determined by using carbonate-free sediments after treatment by acidification for the remaining sites. Using this acidification technique, we reduced the detection limit for TOC measurements to 0.03 wt%. TOC concentrations in sediments determined by this method are very low throughout the sediment column and near or below the detection limit for samples from Sites U1331–U1335 (Figs. **F40, F41**). TOC concentrations tend to be slightly higher at those depths where $CaCO_3$ concentrations are low at Sites U1332–U1335. The maximum TOC value determined is 0.18 wt% in surface sediments from Site U1332. Despite the very low TOC values across the PEAT sediments recovered, postcruise research will be able to measure biomarkers and alkenones from some of the more organic rich sediments, addressing Objectives 2, 4, and 9 (see **"Scientific objectives"**). For Sites U1337 and U1338, TOC increases from low levels at the base of the sedimentary section to levels ~0.2 wt% in the youngest sediments upcore. Postcruise research will focus upon measuring alkenones, other biomarkers, and productivity proxies to better understand the variations in TOC and productivity (Objectives 2, 4, and 9 in **"Scientific objectives"**).

Figure F16 shows the TOC and carbonate profiles versus age at Sites U1336–U1338. None of these sites were ever below the CCD, although Site U1337 briefly approached zero carbonate levels during the 9–11 Ma carbonate crash interval. We can date other carbonate minima between 16 and 18 Ma and 3 and 4 Ma. The 16–18 Ma minimum correlates with the early Miocene carbonate flux minimum identified by Lyle (2003) but is much better defined at Site U1337. It reaches its minimum at 17.2 Ma. The 3–4 Ma carbonate minimum is not well identified in Leg 138 sediments, perhaps because these sites are on younger, shallower crust.

TOC profiles identify a trend from lower to higher TOC from the base of the cores and small intervals of high TOC that were not resolved well at the very coarse shipboard sample interval. High TOC was found in high-biosiliceous intervals at levels as high as 0.7 wt%. The distribution of high TOC deserves more study postcruise to determine how these short events have affected TOC burial fluxes. The base of each site had TOC contents of ~0.1 wt% or below, whereas younger sediments have values of 0.2 wt% or higher. Site U1336, which has a hiatus at 12 Ma, has low TOC values to the surface of the core. Earlier drilling did not find trends in TOC because the standard technique to measure TOC on ODP and DSDP legs (assigning the difference between total carbon and carbonate carbon to TOC) has very high errors in carbonate-rich sediments.

The longer TOC trend could be the result of age and long-term degradation or the strength of early diagenetic degradation, or it could result from changes in TOC particulate rain ("productivity") through time. Distinguishing between these alternatives will require postcruise study of mass accumulation rates and abundances of different biomarkers.

Interstitial water profiles: Sr and Li

Interstitial water geochemistry profiles of the different sites drilled during Expedition 320 show considerable differences in respect to dissolved Sr^{2+} concentrations (Fig. F42). Whereas Sites U1331 and U1332 show little variability with depth, Sites U1333–U1338 reveal increasing variability of Sr^{2+} concentrations. At Sites U1331 and U1332, Sr^{2+} shows mainly concentrations around seawater values; Sr^{2+} increases at Sites U1333 and U1334 up to ~110 μM, at Site U1335 up to 250 μM, Site U1336 up to 430 μM, and Site U1338 up to 400 μm. Sites U1335 and U1338 are characterized by a pronounced increase in Sr^{2+} with depth followed by a strong decrease toward basement to seawater-like concentrations. A similar pattern is revealed for Sites U1333 and U1334, but it is considerably less pro-

nounced and developed. This pattern indicates the influence of carbonate diagenesis and recrystallization, releasing Sr^{2+} to the pore fluid at intermediate depth, and the flow of relatively unaltered seawater through basement and diffusion between end-members. Limited variability of Sr^{2+} at Sites U1331 and U1332 might be related to the relatively thin sediment thickness preventing the establishment of large gradients. At Site U1337 a rapid change in Sr^{2+} occurred at the "baby chert" layer, showing that it acts as a diffusional barrier in the sediments.

Similar to Sr^{2+}, Li^+ shows considerable differences between the different sites of Expedition 320, with the least variability at Sites U1331–U1333 and increasing depletion of Li^+ in the pore fluid at Sites U1334 (down to 15 μM), U1336 (down to 7 μM), and U1335 and U1338 (down to 4 μM) at intermediate depth (Fig. F43). Near basement, Li^+ increases again toward seawater-like values. The Site U1337 Li^+ profile also shows a major offset at the baby chert layer, like Sr^{2+}. Profiles of Li^+ in the pore fluid indicate diagenetic reactions in the sediments consuming Li, possibly low-temperature clay alteration. Li^+ concentrations similar to seawater values are compatible with observations of Sr^{2+}, suggesting the flow of relatively unaltered seawater through the oceanic crust.

Seismic stratigraphy and integration, physical properties, site correlation and orbital cycles

The equatorial Pacific is a classic "binary" sediment system, with variable amounts of biogenic calcium carbonate and biosiliceous sediment components but very little clay. It is also well known that carbonate contents of equatorial Pacific sediments can be estimated from the bulk density because the carbonates have lower porosity and higher grain density than biosiliceous sediments (Mayer, 1991). Consequently, physical property records contain meter-scale cyclicity that will ultimately be useful for orbital-tuning timescales (Objective 3 in "Scientific objectives").

On longer depth scales, physical property records are useful to correlate among sites. Figure F28 shows the two high-resolution density logs at Sites U1337 and U1338 and illustrates the high degree of correlation between the two sites that are separated by ~600 km. Lines on the figure represent equivalent nannofossil biostratigraphic datum levels. The two records are aligned such that the top peaks line up. The depth scale for Site U1338 is compressed so that the bottom event also lines up. Density variations can easily be correlated between the sites even though they are separated by ~600 km.

Mayer et al. (1985) developed a seismic stratigraphy for the central Pacific at Site 574 during Leg 85. They noted that major seismic horizons were caused by density variations associated with low-carbonate intervals. They proposed that these intervals were chronostratigraphic because they were caused by paleoceanographic changes in deposition and/or dissolution of calcium carbonate.

Unfortunately, Mayer et al. (1985) did not have logs to measure in situ velocities. One of the important experiments of Expedition 321 was to use logging as well as cores to check this conclusion and to better constrain the age of the equatorial Pacific seismic horizons. For this reason, we planned a vertical seismic profile (VSP) experiment at one of the Neogene PEAT sites (Objective 6 in "Scientific objectives"). We were able to run the VSP log at both Site U1337 (Fig. F44) and U1338. Figure F44 is an initial comparison between the Site 574 seismic stratigraphy of Mayer et al. (1985) and the initial results for Site U1337. The events appear to correlate in age, as would be predicted by Mayer et al. (1985). Site 574 is at essentially the same latitude as Site U1337 but >1000 km to the west. The length scale of the correlatable seismic horizons across the Pacific helps to define the length scale of the paleoceanographic events with which they are associated. Postcruise studies will focus on better defining the seismic stratigraphy at both Sites U1337 and U1338, allowing new tie points for the seismic stratigraphic study of the equatorial Pacific sediment bulge (Mitchell et al., 2003).

Objective 6 of the PEAT program (see "Scientific objectives") is to establish the age and lithologic origin of the seismic reflections previously identified in the eastern equatorial Pacific and make use of the high level of correlation between tropical sedimentary sections and existing seismic stratigraphy to develop a more complete model of equatorial circulation and sedimentation (Lyle et al., 2002, 2006). We achieved this objective by calculating synthetic seismograms made from bulk density and sonic velocity data from core material and downhole logs for the Paleogene Site U1331 (Fig. F45).

The known depths and two-way traveltimes (TWTs) to the seafloor and basement provided an initial depth to TWT model and average sonic velocity for the sediment cover. The depth to TWT model was then adjusted to bring the reflectors in the synthetic seismogram into line with the corresponding reflectors in the seismic section. Typically, only a small number of adjustments were needed to give a good match.

Downhole logging data at two sites discriminate between radiolarian and nannofossil ooze using density, conductivity, and magnetic susceptibility, which are more useful in understanding the lithology in the poor recovery intervals composed of chert and porcellanite. In addition, a hard lithified limestone altered by hydrothermal activity occurred 10–20 m above basement at most drilling sites. Correlation between seismic profiles and drilling is important in understanding an estimation of basement age and thickness of sedimentary sequences. At Site U1335 the thickness is was originally estimated to be 361 m, but 420 m of sediment was recovered above the basement. Thus, our results contribute to the drilling strategy for future drilling in the equatorial Pacific.

MORB age transect

An age transect of sediments on top of basaltic basement in the equatorial Pacific region was recovered during Expedition 320/321. Basement ages decrease eastward from Site U1333 to Site U1338 (Fig. F20). Basement basalts are covered by hard lithified limestones spanning from early Eocene through early Miocene age except at Site U1332, where zeolitic clays were recovered above basalt. These clays yielded poorly preserved calcareous nannofossils, and the position of the clays may be due to hydrothermal alteration. At Site U1331, however, a typical calcareous ooze with high carbonate contents containing abundant planktonic foraminifers and calcareous nannofossils was recovered as observed at Site 1221. Basement basalts are highly altered with a spherulitic texture, whereas ferromagnesian minerals (mainly clinopyroxene) are replaced by chlorite. Thin section analysis indicates a sparsely phyric basalt mainly composed of phenocryst plagioclase.

Chert and porcellanite occurrence

Sites U1331–U1333 and U1336 recovered chert and porcellanite (Fig. F46). Cherts are characterized by their hardness and highly silicified matrix in which sediments are cemented with microcrystalline quartz. Primary pore spaces (e.g., within chambers of foraminifers and radiolarians) are sometimes filled with chalcedony. Porcellanites are silicified to a lesser extent and are richer in clay minerals than the cherts. Porcellanite is much more abundant than chert at Sites U1331–U1333, which is interbedded with radiolarian ooze and nannofossil ooze in the early middle Eocene interval at Sites U1332 and U1333 (Fig. F46). In stratigraphic intervals from the early Eocene through earliest middle Eocene at Sites U1331 and U1332, the presence and original structures of porcellanite are not clear because of poor core recovery. Site U1336 contains mostly chert. Porcellanite-bearing intervals at Sites U1331–U1333 correspond to a time interval between early Eocene

and early middle Eocene (~42 Ma), roughly coincident with the chert-rich intervals at Sites 1220–1222 recovered during Leg 199 (Fig. F46). At Sites U1331 and U1332, porcellanite layers are associated with thin clay horizons interbedded with radiolarian ooze. Oligocene chert layers from Site U1336 are interbedded with nannofossil ooze and chalk and show various colors such as greenish gray, dark gray, pink, and black and contain abundant foraminifers that are occasionally replaced with microcrystalline quartz and pyrite.

At the base of the sections recovered there was always an interval in which all biogenic silica had been dissolved and which was barren of radiolarians. This "silica free zone" (SFZ) is usually not thick—only 7 to 16 m at most of the sites drilled (Table T3). This is well within the usual 1–40 m thickness of the SFZ described by Moore (2008a) for Pacific open-ocean sections recovered by scientific ocean drilling. Moore (2008a) associated this dissolution zone with the circulation of hydrothermal waters in the upper oceanic crust and related the silica removed by this process to the ultimate formation of cherts. Thus, Site U1336 stands out as very unusual. It has a SFZ almost 130 m thick from ~170 m CSF to the base of the drilled section at 298 m CSF, with abundant chert stringers. The extensive alteration suggests that hydrothermal waters may actually invade well up into the section near this site, possibly along more permeable, small-offset faults.

Within the Neogene sediments recovered, chert/porcellanite intervals were found at Sites U1336–U1338. At Site U1336, a chert interval was found in unlithified early Miocene sediments at ~130 m CSF. The section below 200 m CSF also had significant numbers of chert intervals and the carbonates had turned to limestone, suggesting significant higher temperature diagenesis.

At Sites U1337 and U1338, only one cherty interval was found—what we referred to as the baby chert interval. At both sites the cherty interval hampered core recovery around it, but it was easily penetrated by drilling. Interestingly, its position appears to be chronostratigraphic, at ~11 Ma in the late middle Miocene (~240 m CSF at Site U1337 and ~282 m CSF at Site U1338). This baby chert interval was located in a diatom mat interval at Site U1337 and a diatom-rich interval at Site U1338. The interval was well-imaged by Formation MicroScanner (FMS) logging and shows that the chert interval is 40 cm thick at Site U1337 and about one-quarter of the way up from the base of the low-resistivity diatom-rich interval (Fig. F47). At Site U1338 the chert interval was only 16 cm thick but also about one-quarter of the way through the low-resistivity interval from the base

upward. The logs allowed us to estimate the amount of disturbed and missing section in the cored sediments—there is only a small loss of material (<1 m) around the chert.

At Site U1337 it was clear from interstitial water profiles that the chert interval is a barrier to diffusion. There were offsets in Li, Sr, and SO_4 in interstitial waters immediately below and above the baby chert interval (Fig. F43, F45). It is unclear why the chert formed in this interval alone at both sites because there was nothing unique about it. There were additional diatom-rich intervals below the baby chert that were unaffected. The more extensive chert layer at Site U1337 is actually formed ~30 m shallower (250 m CSF) than the interval at Site U1338 (280 m CSF). Postcruise research focused on diagenesis and fluid flow may provide insight into chert formation within these diatom-rich intervals.

Heat flow measurements

Geothermal gradient and heat flow values were determined at Sites U1331–U1338 from in situ temperature measurements made using the advanced piston corer temperature tool (APCT-3) and the sediment temperature tool (SET). At least four APCT-3 deployments were made per site to a maximum depth of 316 m. Bottom water temperature was also determined for each site, with values ranging from 1.44° to 1.65°C. Linear geothermal gradients obtained from these data ranged widely from 7.5°C/km at Site U1335 to 75.0°C/km at Site U1332.

Heat flow was calculated according to the Bullard method, to be consistent with the Leg 199 analyses and the synthesis of ODP heat flow data by Pribnow et al. (2000). Similar to the geothermal gradients, Site U1335 had the lowest heat flow, 7.0 mW/m², and Site U1332 the highest, 70.7 mW/m² (Fig. F48). These heat flows are within the range of values in the eastern equatorial Pacific heat flow data set maintained by the International Heat Flow Commission (Pollack et al., 1993).

The wide range of values emphasizes the possibility that local crustal hydrothermal circulation is strongly influencing heat flow values. Results from the PEAT expeditions will also provide heat flow information in an area of the Pacific Ocean that has only a sparse existing heat flow data set.

Gravity flow deposits

Throughout the sedimentary section drilled at Sites U1331 and U1335, sharp irregular contacts are present between lithologies (Fig. F49) (see "Lithostratigraphy" in the "Site U1331" chapter and "Lithostratigraphy" in the "Site U1335" chapter). Many are

recognizable by distinct changes in color. Sharp contacts, occasionally associated with an erosional basis, are often overlain by coarser grained, more carbonate rich (including planktonic and benthic foraminifers), and/or opaque-coated sediments than those below the contact. At Site U1335 angular basalt fragments, pyritized foraminifers and/or radiolarians, and fish teeth are often present at the base of the gravity flows. The overlying sediments fine uphole and in some cases show cross or parallel laminations in the middle of the bed. These features indicate that the erosional contacts and their overlying coarse sediments at both Sites U1331 and U1335 are the product of mass flow events, typically turbidity currents. Commonly, turbidite thickness is between 2 and 25 cm, with the maximum thickness of 176 cm found at Site U1335. The total thickness of the identified turbidites at Site U1335 occupies at least 2% of the recovered sediment. The provenance of the inferred turbidites observed at Site U1331 is unknown, but their typically calcareous composition points to a source that lay above the CCD at the time that the reworked sediments were originally deposited, possibly a seamount lying a few kilometers south of the drilled location. A similar provenance of turbidites is proposed for Site U1335, where two seamounts lie ~15–20 km northeast and southeast of the drilled location.

New capabilities on the *JOIDES Resolution*

The shipboard laboratories have new capabilities that greatly improve the ability of shipboard scientists and later researchers to study the sediment column and that complement excellent core recovery achieved during the PEAT expeditions (Fig. F50). One important capability is a much better capacity to integrate line-scan core images into descriptions and analyses. Figure F51 shows color images from different holes at Site U1337 and how they were joined into the Site U1337 splice. The color images are particularly useful to resolve color banding and cyclic behavior in the multicolored sediment intervals. In the upper parts of all the sites, it is common to find oxidized brown sediments that become green when Fe within the sediments is reduced (Lyle, 1983). Typically, this feature has been described in the upper meter of the sediment column. Further west, where the PEAT sites are located, brown colors extend downward for tens of meters. Not all of the color information is stratigraphically useful—redox state and other diagenetic processes can overprint other sediment information. For example, the color change from green to yellow at the base of the Site U1338 sedimentary section cuts across stratigraphic correlations between different holes.

Dark–light color banding, whatever shade of color, is indicative of carbonate content in the equatorial Pacific. Darker layers usually have lower carbonate contents, higher magnetic susceptibility, higher natural gamma activity, and lower bulk density. Different scales of carbonate cycles are found in the core images. Because many of the low-carbonate events are chronostratigraphic, they can be used to correlate between cores. At the larger scale, the dark–light color banding can be used to correlate between sites.

Another new instrument on the *JOIDES Resolution* is the Natural Gamma Radiation Logger (NGRL). The instrument is much more sensitive than the ODP NGR and can be used as part of the normal core-flow measurements. Biogenic sediments of the equatorial Pacific are not ideal for natural gamma activity studies—they only have low levels of natural radioactivity. Nevertheless, the NGRL was able to reliably detect natural gamma ray activity variations of <1 counts per second (cps). Small natural gamma activity highs correlated with dark sediment layers. One of the objectives for the natural gamma ray measurement on cores is to produce a record that can be correlated with the wireline logging measurements. Unfortunately, the low natural gamma ray activity levels resulted in only a few peaks that could be consistently correlated between core and logs.

The seafloor was one interval that consistently had high natural gamma ray activity (Fig. F52). Whereas counts at a distance from the seafloor were <5 cps, seafloor natural radioactivity levels were as high as 160 cps within 1 m of the top of the sediments. Natural gamma ray activity dropped to the typical low count a few meters below the surface. Spectral studies using hour-long counts on the surface cores revealed that natural gamma ray activity at the surface is being produced by high uranium levels, not thorium or potassium. It is not clear yet why uranium is concentrated only near the sediment/water interface. Because the near-surface sediments have low organic carbon contents, uranium has not been concentrated by reduction and precipitation from seawater. Kunzendorf et al. (1983) instead argues that enrichments of uranium in tropical Pacific sediments result from coprecipitation of seawater uranium with Fe oxides. This solution still begs the question as to why the level of Fe oxides might be higher at the surface of the sediments.

Site summaries
Site U1331

Three holes were cored at Site U1331 (12°04.088′N, 142°09.708′W; 5116 mbsl), which is the northwesternmost site drilled during the PEAT program (Fig.

F53; see Table T1 in the "Site U1331" chapter). In Hole U1331A, seafloor basalt is overlain by 187.02 m of pelagic sediment, containing radiolarian and nannofossil ooze with varying amounts of clay. The oldest sediment is of early Eocene age. For detailed coring activities, see "Operations" in the "Site U1331" chapter.

The sediment column at Site U1331 has a strong resemblance to that of Site 1220 (Fig. F54) (Lyle, Wilson, Janecek, et al., 2002), but with noteworthy sharp erosive contacts concentrated within the upper two-thirds of the section (Fig. F55). A total of 7 m of Pleistocene–Pliocene clay overlies lower Oligocene to lower Eocene alternations of nannofossil ooze, radiolarian nannofossil ooze, and radiolarian oozes of varying clay and calcium carbonate content (see "Lithostratigraphy" in the "Site U1331" chapter), with a sharp lithologic change at the Eocene–Oligocene transition (~26 m core depth below seafloor [CSF]). The lowermost target interval in Hole U1331C is characterized by a ~20 m thick radiolarian ooze and porcellanite layer from 157 to 177 m CSF overlying a dominantly clayey radiolarian ooze and zeolitic clay with hydrothermal red staining from 177 to 187.5 m CSF deposited on top of a thin (187.6–188.5 m CSF in Hole U1331C) layer of calcareous ooze and zeolitic clay above the basalt. Some fine-grained basaltic fragments show fresh glassy chilled margins.

Carbonate content approaches 80 wt% in the Oligocene nannofossil oozes in the upper part of the site and cycles between 0 and 40 wt% in the middle Eocene section (see "Geochemistry" in the "Site U1331" chapter). A concentration of sharp erosive contacts occurs in the interval between 80 and 120 m CSF, with calcareous material dominating the basal portion of these contacts and then fining upward in grain size into radiolarian oozes. Rarely, the sediment above a sharp contact contains well-rounded clasts up to 1 cm in diameter (interval 320-U1331B-10H-6, 117–130 cm). The lithologic and stratigraphic characteristics of these sediments have been interpreted as gravity-driven deposits, possibly from nearby seamounts ~10 km to the south (Fig. F53B). Between ~177 and 187.2 m CSF, Cores 320-U1331A-22X, 320-U1331C-16H, and 17H achieved our site objective of recovering carbonate-bearing material from the time interval just following 52 Ma.

All major microfossil groups were found in sediments from Site U1331, and they provide a consistent and coherent biostratigraphic succession from basement to below the surficial clay layer. Nannofossils are common in the Oligocene and lower Eocene but sporadic in sediments from the upper Eocene because of dissolution. Middle Eocene sediments com-

monly contain calcareous nannofossils punctuated by several barren intervals, notably below Zone NP21 (radiolarian Zone RP19 equivalent), below Zone NP17, and between Zones NP15 and NP13 (radiolarian Zones RP12–RP8 equivalent). Radiolarians are common to abundant throughout the section. Radiolarian and nannofossil datums and their age determinations agree and range from nannofossil Zone NP12 in the basal sediment section (~51–53 m.y. before present) to Zones NP23/NP24 and radiolarian Zones RP8 just above basement through RP21 (late Oligocene, older than 25 Ma) in the uppermost section, below the Pleistocene clays. Both radiolarian and nannofossil assemblages contain reworked older components (deeper than ~50 m CSF) but within a coherent and ordered stratigraphy. Planktonic foraminifers are generally absent, except for sporadic occurrences often associated with sediment just above sharp lithologic contacts and also in the basal carbonate section (Zones E4/E5). Benthic foraminifers are generally rare and indicate lower bathyal to upper abyssal paleodepths. They are frequently found in the graded coarse sediment above the base of sharp contacts but indicate there is no apparent difference in the depth habitat between benthic foraminifers from just above sharp contacts and other parts of the section.

Apparent sedimentation rates, as implied by the biostratigraphic age determinations and aided by magnetostratigraphic polarity interpretations, vary throughout the section. The radiolarian-rich section between ~80 m CSF and basement was deposited at an average rate of 10 m/m.y., whereas the late middle Eocene to Oligocene section was deposited at a rate of ~4 m/m.y., with an apparent inflection between 60–80 m CSF. Porcellanite is located in an interval that spans a time of ~2–3 m.y. The presence of all major fossil groups as well as a detailed magnetostratigraphy will allow us to achieve one of the main PEAT objectives to arrive at an integrated Cenozoic stratigraphy and age calibration (e.g., Pälike et al., 2006b).

A full physical property program was run on cores from all three holes, including Whole-Round Multisensor Logger (WRMSL) measurements of magnetic susceptibility, bulk density, P-wave velocity, and noncontact resistivity, along with natural gamma radiation (NGR), followed by discrete measurements of color reflectance, index moisture and density properties, sound velocities, and thermal conductivity. Bulk density measurements increase markedly in the carbonate-rich Oligocene section. Magnetic susceptibility measurements are variable throughout the section, allowing detailed correlation between different holes and picking of sharp contacts and

clay layers by increased susceptibilities. NGR measurements are elevated by an order of magnitude in the surficial clay layer and reach 130 cps at the seafloor, dropping to <5 cps deeper than 30 m CSF. Porosity values are generally high in radiolarian-rich sediments (80%) and decrease within the Oligocene carbonate section. Carbonate content is positively correlated with thermal conductivity. Discrete physical property measurements will prove useful to calibrate WRMSL velocity and density estimates and generally agree with WRMSL estimates, once appropriate correction factors are included for the core liner. Discrete velocities are significantly higher (50–100 m/s) than track measurements in the direction perpendicular to the split plane of the core section (*x*-axis), which is likely an artifact.

Using whole-round magnetic susceptibility measurements, Holes U1331A–U1331C can be spliced to form a continuous section to at least 140 m CSF or 150 m core composite depth (CCSF-A) (see **"Core composite depth scale"** in the "Methods" chapter), with no apparent gaps. Core expansion is ~15%. It is possible that Hole U1331C cores can provide an additional spliced section to the top of the porcellanite interval at ~157 m CSF. Below 149 m CCSF-A, it was only possible to tentatively correlate features in the track data down to Core 320-U1331A-17X for a total composite section to ~172 m CCSF-A.

A full range of paleomagnetic analyses was conducted on cores and samples from Site U1331. Our aims are to determine the magnetostratigraphy and study geomagnetic field behavior, environmental magnetism, and Pacific plate paleogeography. Shipboard analyses conducted suggest that a useful magnetic signal is preserved in almost all APC-cored intervals. Preliminary comparison of biostratigraphic data and changes in magnetic paleodeclinations suggest the recovery of Oligocene magnetochrons to the base of the middle Eocene (Chron C21n; ~47 Ma). Paleomagnetic directions from discrete samples agree well with those from split-core results.

A standard shipboard suite of geochemical analyses of pore water and organic and inorganic sediment properties was conducted on samples from Site U1331, including a pilot study of high-resolution "Rhizon" pore water sampling, which does not require the cutting of whole rounds for squeezing. Carbonate coulometry yielded carbonate concentrations of ~80 wt% in the Oligocene nannofossil ooze and sporadic horizons with up to 40 wt% $CaCO_3$ in the middle Eocene radiolarian-rich oozes. Preliminary calcium carbonate determinations from the white, hydrothermally stained sediments just above basement (whole-round Sample 320-U1331C-17H-4, 83–84 cm) yielded low values of only 2–3 wt% $CaCO_3$.

Alkalinity values range between 2.5 and 3 mM throughout the section. Additional ephemeral samples were taken for shore-based microbiology and permeability studies.

Wireline logging provided valuable information to constrain the interval of porcellanite formation within the borehole, and further analysis will aid in interpretations of carbonate content and lithologies. Integration with the seismic data will allow further improvements with the regional seismic interpretations. Data from Site U1331 indicate that the top of seismic Horizon P2 (Lyle et al., 2002) correlates with the top of the chert section. Downhole temperature measurements with the APCT-3 tool, when combined with the thermal conductivity values obtained from the cores, indicate that Site U1331 had a thermal gradient of 13.4°C/km and a heat flow of 10.3 mW/m². This is within the range of lower values in the global heat flow data set for the eastern Pacific but significantly lower than values obtained for Sites 1218 and 1219.

Highlights

Carbonate ooze in basal section

At Site U1331 we recovered a 1.2 m thick interval (lithologic Unit IV) of calcareous ooze with concretions and reddish color streaks, achieving one of the objectives for this site. The nannofossil ooze recovered in Sample 320-U1331A-22X-CC contains a moderately to poorly preserved assemblage of early Eocene planktonic foraminifers (planktonic foraminifer Zone E5). This moderately preserved assemblage was also observed in the basal section of Hole U1331C.

Stratigraphic integration

One of the primary objectives of the PEAT science program is the integration of different stratigraphic methodologies and tools. Site U1331 contains almost all major fossil groups (nannofossils, radiolarians, foraminifers, and diatoms), as well as an excellent magnetostratigraphy. The possibility of a cycle-by-cycle match between Sites U1331 and 1220 has been demonstrated using magnetic susceptibility and bulk density data, providing additional stratigraphic tie points and verification of the completeness of the stratigraphic section on a regional scale. Thus, Site U1331 will help us to achieve an integrated stratigraphy for the Cenozoic Pacific Ocean.

Eocene–Oligocene transition and depth transect

Site U1331 forms the oldest and deepest component of the PEAT depth transect component, which will allow the study of critical intervals (such as the

Eocene–Oligocene transition; see Coxall et al., 2005) and variations of the equatorial CCD. Site U1331 is estimated to have been ~4.2 km deep during the Eocene–Oligocene transition, ~800 m shallower than today. Sediments rapidly change from radiolarian ooze below the Eocene–Oligocene transition to nannofossil oozes above and will provide a tie point for calcium carbonate burial at ~5° paleolatitude.

Variations in the CCD

Site U1331 will provide important constraints for variations and depth of the CCD from the early Eocene to the late Oligocene. This site shows increased carbonate content and much increased mass accumulation rates approximately from the middle of Chron C18r to the base of Chron C19r during the middle Eocene and can be correlated to an interval of enhanced carbonate burial that was previously documented by Lyle et al. (2005) in Leg 199 cores.

Age transect of seafloor basalt

At Site U1331 we recovered what appear to be fresh fragments of seafloor basalt, aged between 52 and 53 Ma as estimated from biostratigraphic results. This material will, when combined with other PEAT basalt samples, prove to be important for the study of, for example, seawater alteration of basalt, as well as paleomagnetic studies.

Site U1332

Three holes were cored at Site U1332 (11°54.722′N, 141°02.743′W; 4924 mbsl) (Fig. F56; see Table T1 in the "Site U1332" chapter), which is the second northwesternmost site drilled during the PEAT program. At Site U1332, seafloor basalt is overlain by ~150 m of pelagic sediment, containing radiolarian and nannofossil ooze with varying amounts of clay and zeolitic clay. The oldest sediment is of earliest middle Eocene age. Hole U1332A provided high-quality and high-recovery APC-cored sediments from the mudline to 125.9 m CSF (Core 320-U1332A-14H), where we encountered porcellanite and chert and switched to the XCB cutting shoe. XCB coring advanced to 152.4 m drilling depth below seafloor (DSF) through a ~10 m thick porcellanite-rich interval with reduced recovery. In the basal section, we recovered a short, ~3.8 m long interval of barren very dense and stiff clay above basalt, ~10 m shallower than predicted from the seismic profile, in Core 320-U1332A-18X. Basement was reached at 152.4 m CSF. For detailed coring activities, see "Operations" in the "Site U1332" chapter.

The uppermost 17.7 m consists of upper Miocene to Pleistocene–Pliocene clay, with varying amounts of radiolarians and zeolite minerals, overlying ~130 m of Oligocene to middle Eocene nannofossil and radiolarian ooze with porcellanite deep in the section. A thin ~3 m thick unit of middle Eocene zeolite clay bearing small porcellanite and chert nodules was recovered at the base of the sedimentary sequence, above basaltic basement. The sedimentary sequence at Site U1332 was divided into five major lithologies (Fig. F57).

The upper stratigraphy at Site U1332 has a strong resemblance to that of Site U1331 but without the sharp erosive contacts described at Site U1331. Several meters of white to beige-colored Pleistocene–Pliocene clay (lithologic Unit I) overlie lower Miocene to lowermost Oligocene nannofossil ooze (Units II and III). There is a sharp lithologic change at the Eocene–Oligocene transition to alternating radiolarian ooze with nannofossils and nannofossil ooze (Subunit IVa). The lithology gradationally changes downhole into a dominance of radiolarian nannofossil ooze and nannofossil radiolarian ooze (Subunit IVb) and then into an interval of alternating radiolarian ooze, radiolarian nannofossil ooze, and nannofossil radiolarian ooze with porcellanite layers (Subunit IVc). Lithologic Unit V is composed of very dark grayish brown to black clay, very dark grayish brown to black zeolite clay, and chert. The sediments directly above basaltic basement are partially lithified. Basalt is designated as lithologic Unit VI, at ~150 m CSF.

Carbonate content approaches 85 wt% in Unit III within the Oligocene nannofossil oozes and cycles between 0 and 40–60 wt% in the middle Eocene section (Unit IV) (Fig. F58). All major microfossil groups were found in sediments from Site U1332 and provide a consistent, coherent, and high-resolution biostratigraphic succession from basement to the top of Unit II. Calcareous nannofossils are abundant and moderately well preserved in the Oligocene and poor to moderately well preserved in the Miocene and Eocene. Most middle Eocene sediments commonly contain nannofossils; however, there are several barren intervals. Radiolarians are common to abundant throughout most of the section, apart from the lowermost sediment section above basalt, and are well preserved, particularly in the Eocene and in the early Oligocene. Radiolarian and nannofossil datums and zonal determinations agree, ranging from nannofossil Zones NP13/NP14 in the basal dark clay section (~48.4–50.7 Ma) to Zone NN1 and radiolarian Zones RP13 above basement through RN1 (lowermost Miocene, ~22.3 Ma) below the upper Pliocene–Pleistocene clay cover in Core 320-U1332A-3H (Fig. F58). Planktonic foraminifers are generally rare throughout the Oligocene but are absent in the Miocene and Eocene. Benthic foraminifers are present

through most of the section but are rare in Miocene and Eocene sediments. They indicate lower bathyal to abyssal paleodepths. Sedimentation rates, as implied by biostratigraphic age determinations, vary throughout the section and are ~5 m/m.y. in the Eocene section and ~2.5 m/m.y. in the Oligocene, with two prominent hiatuses in the Miocene and between the Miocene and younger sediments. The presence of all major fossil groups as well as a detailed and well-resolved magnetostratigraphy will allow us to achieve one of the main PEAT objectives, to arrive at an integrated Cenozoic stratigraphy and age calibration (e.g., Pälike et al., 2006b) for major parts of the Oligocene and Eocene.

Magnetostratigraphic studies as well as high-resolution biostratigraphy and stratigraphic correlation determined that a 4 m interval from the base of Core 320-U1332A-8H was repeated in the top of Core 9H, which comprises Chron C13n and the lowermost Oligocene. This repetition also occurs in Cores 320-U1332B-8H and 9H and within Core 320-U1332C-9H. The lithologic succession from the lower occurrence of Chron C13n downhole as well as from the upper occurrence of Chron C13n uphole both appear complete and continuous; hence Site U1332 achieved the fortuitous feat of recovering the complete Eocene–Oligocene transition four times and the upper part of Chron C13n five times at a triple-cored site. A likely explanation for this is the widespread occurrence of a slumped interval.

A full physical property program was run on cores from all three holes, including WRMSL measurements of magnetic susceptibility, bulk density, P-wave velocity, and noncontact resistivity, along with NGR, followed by discrete measurements of color reflectance, index moisture and density properties, sound velocities, and thermal conductivity. Bulk density measurements show a marked increase in the carbonate-rich Oligocene section, as well as in carbonate-bearing horizons in the Eocene (CAE cycles; Lyle et al., 2005). Magnetic susceptibility is variable throughout the section, allowing a detailed correlation among holes. NGR measurements are elevated by an order of magnitude in the surficial clay layer. Porosity values are generally high in the radiolarian-rich sediments (85%) and decrease in the Oligocene and Eocene carbonate section, which also shows higher thermal conductivity values of ~0.9 to 1.2 W/(m·K), compared with ~0.8 W/(m·K) in the radiolarian oozes and surficial clay.

Stratigraphic correlation allowed us to obtain a complete section to ~125.5 m CSF near the top of the porcellanite interval in Hole U1332A, equivalent to a composite depth of ~140 m CCSF-A. The overall core expansion (growth factor), which is calculated by the ratio between the CCSF-A and CSF (formerly meters composite depth [mcd] and meters below seafloor [mbsf]) depth scales, is ~10%. The tops of APC cores were often affected by ~3 m heave that occurred during operations at Site U1332. Stratigraphic correlation supports the biostratigraphic, paleomagnetic, and sedimentologic description of a repeated sequence, possibly due to slumping, spanning the Eocene–Oligocene transition.

A full range of paleomagnetic analyses was conducted on cores and samples from Site U1332 and resulted in a well-resolved magnetostratigraphy. Shipboard analyses suggest that a useful magnetic signal is preserved in all APC-cored intervals and that it was possible to remove the drilling-induced steep inclination overprint by AF demagnetization. Comparison of biostratigraphic data and changes in magnetic paleodeclinations suggests the recovery of magnetic reversals Chrons C1n/C1r.1r to C2An.3n/C2Ar above a hiatus and then a continuous sequence of magnetic reversals from Chrons C5En/C5Er (18.52 Ma) in the Miocene at ~12.95 m CSF (interval 320-U1332C-2H-4, 95 cm) to C19r/C20n (42.54 Ma) at interval 320-U1332A-14H-5, 80 cm. Magnetostratigraphic interpretation supports the presence of a slump through multiple recovery (five times) of parts of Chron C13n in a triple-cored sequence. Paleomagnetic directions from discrete samples agree well with those from split-core results.

A standard shipboard suite of geochemical analyses of pore water and organic and inorganic sediment properties was conducted on samples from Site U1332. Alkalinity values increase from ~2.2 to 3.4 mM downsection, and Sr^{2+} increases from ~80 to ~110 μM. H_4SiO_4 remains relatively stable between 400 and 600 μM above 90 m depth in the Oligocene nannofossil oozes but increases to 800–1000 μM in the Eocene silica-rich radiolarian oozes. Carbonate coulometry yielded carbonate contents of ~85 wt% in the Oligocene nannofossil ooze and horizons with up to 60 wt% $CaCO_3$ in the middle Eocene radiolarian-rich oozes. TOC contents were measured both by difference between TC and total IC as well as by using an acidification method. Using the acidification method, TOC values were <0.3 wt% for all measured samples. The top ~5 m shows values of 0.18–0.17 wt% TOC. Between ~40 and 70 m CSF the measurements indicate TOC below the detection limit of 0.03 wt%, and downhole from this, values are generally low. We conducted a high-resolution Rhizon pore water experiment across an alkalinity trough around 40 m CSF, which highlighted comparisons between squeezed and Rhizon-sampled pore waters. Additional ephemeral samples were taken for shore-based microbiology and permeability studies.

Wireline logging provided valuable information to constrain the interval of porcellanite and chert formation within the borehole. Downhole NGR, density, and magnetic susceptibility logs provide important constraints on the poorly recovered lithologies below and between porcellanite-bearing horizons. The logging data document the presence of two thin porcellanite horizons at ~126 and 130 m wireline log depth below seafloor (WSF) and an ~14 m thick interval of increased magnetic susceptibility, reduced conductivity, and enhanced density and photoelectric factor that appears to be the dark and dense clays and zeolitic clays above basement, rather than carbonate. Integration with the seismic data will allow further improvements with the regional seismic interpretations. Data from Site U1332 indicate that the top of seismic Horizon P2 (Lyle et al., 2002) correlates with the top of the porcellanite section, just as it did for Site U1331. No FMS data were collected, as it was not possible to retrieve the "paleo-" triple-combination (triple combo) tool string back into the bottom-hole assembly (BHA). Eight downhole temperature measurements were conducted in Holes U1332B and U1332C with the APCT-3 tool. Three of these yielded good data; the other measurements were impaired by strong, sometimes >3 m heave during operations in Hole U1332B.

Downhole temperature measurements, when combined with the thermal conductivity values obtained from the cores, indicate that Site U1332 has a heat flow of 70.7 mW/m² and a thermal gradient of 75.0°C/km. This is significantly higher than the values obtained for Site U1331 but comparable to values obtained for Sites 1218 and 1219.

Highlights

Shallow early Eocene CCD

Coring at Site U1332 was designed to capture a very short period of time (~2 m.y.) at ~50 Ma during which this site was thought to be located above the very shallow Eocene CCD (~3.3 km) (Lyle, Wilson, Janecek, et al., 2002; Rea and Lyle, 2005) just after the EECO (Zachos et al., 2001a). Unlike Site U1331, at Site U1332 we cored a ~10 m thick section of dense and dark brown clays, zeolite clays, and chert above basement, although relatively common nannofossils were present in the lowermost samples from Hole U1332B. This finding will provide important new constraints on the depth of the CCD at ~48–50 Ma at the paleoequator, indicating that the CCD was shallower than previously thought.

Stratigraphic integration

One of the primary objectives of the PEAT science program is the integration of different stratigraphic

methodologies and tools. Site U1332 contains all major fossil groups (nannofossils, radiolarians, foraminifers, and diatoms), as well as an excellent magnetostratigraphy and composite depth correlation, which can be tied to nearby Leg 199 sites (e.g., Site 1220) by way of physical property variations. The possibility of a cycle-by-cycle match between Sites U1332 and 1220 has been demonstrated using magnetic susceptibility and bulk density data, providing additional stratigraphic tie points and a verification of the completeness of the stratigraphic section on a regional scale. Thus, Site U1332 will help us to achieve an integrated stratigraphy for the Cenozoic Pacific Ocean, ranging from the Miocene to the middle Eocene.

Eocene–Oligocene and Oligocene–Miocene transitions and depth transects

Site U1332 forms the second oldest and deepest component of the PEAT depth transect, which will allow the study of critical intervals (such as the Eocene–Oligocene transition; see Coxall et al., 2005) and variations of the equatorial CCD. Site U1332 is estimated to have been ~4 km deep during the Eocene–Oligocene transition, ~1 km shallower than today and 200 m shallower at that time than Site U1331. Sediments rapidly change from radiolarian ooze below the transition into nannofossil oozes above, and unlike Site U1331, Site U1332 also contains carbonate-bearing sediments across the Oligocene–Miocene transition. For the Eocene–Oligocene transition, Site U1332 will provide a tie point for calcium carbonate burial at ~4° to 5° paleolatitude.

Variations in the CCD

Site U1332 has provided important constraints for variations and depth of the CCD from the early Eocene to the late Miocene. This site shows increased carbonate content and much increased mass accumulation rates approaching 200 mg $CaCO_3$/cm²/k.y. around the middle of Chron C18r to the base of Chron C19r during the middle Eocene, which can be correlated to an interval of enhanced carbonate burial that was previously documented by Lyle et al. (2005) in Leg 199 cores. The early Oligocene high $CaCO_3$ concentrations decrease significantly in sediments younger than ~27 Ma. By ~22 Ma, in the early Miocene, carbonate was no longer preserved. This is presumably related to Site U1332 sinking below the prevalent CCD and coincides with a CCD shoaling event between ~20 and 15.5 Ma described by Lyle (2003).

Formation of porcellanite and chert

Together with Site U1331, Site U1332 provides important new information on the formation of porcel-

lanite and chert. Coring has shown that the top of the porcellanite-rich interval is mapped by seismic Horizon P2 (Lyle et al., 2002). In lithologic Subunit IVc, layers and pebbles of very dark brown partially to well-lithified mudstones, often layered or even laminated, are observed within alternating sequences of nannofossil ooze and radiolarian ooze of late to late middle Eocene age. In hand specimen, the partially lithified mudstones are particularly rich in clay and show evidence of partial secondary silicification. Pieces of porcellanite contain clay minerals, microcrystalline quartz, opaques, and calcite, as well as biogenic shells and fragments from radiolarians and foraminifers. Sediments from Sites U1331 and U1332 appear to document the silicification process in clay-rich horizons near basement, which will likely extend the findings of Moore (2008a, 2008b).

Age transect of seafloor basalt

At Site U1332 we recovered what appear to be fresh fragments of seafloor basalt, aged between 49 and 50 Ma as estimated from biostratigraphic results. This material will, when combined with other PEAT basalt samples, provide important sample material for the study of seawater alteration of basalt.

Site U1333

Three holes were cored at Site U1333 (10°30.996′N, 138°25.159′W; 4853 mbsl) (Fig. F59; see Table T1 in the "Site U1333" chapter). At Site U1333, seafloor basalt is overlain by ~183 m of pelagic sediment, dominated by nannofossil and radiolarian ooze with varying amounts of clay (Fig. F60). The oldest sediment is of early middle Eocene age.

In Hole U1333A, APC-cored sediments were recovered from ~3 m below the mudline (~4850 mbsl) to 95 m CSF (Core 320-U1333A-10H). XCB coring advanced to 184.1 m DSF through an ~60 m thick sequence of lowermost Oligocene carbonate oozes and nannofossil-bearing Eocene sediments. Near the basal section, we recovered a 30 cm long interval of lithified carbonate in Core 320-U1333A-20X. The following Core 21X contained a limestone basalt breccia. A 6 cm piece of basalt was recovered in Core 22X.

Coring in Hole U1333B started 5 m shallower than in Hole U1333A to recover the mudline and to span the core gaps from the first hole. A total of 7.73 m of carbonate-bearing ooze overlain by a few meters of clay were recovered in Core 320-U1333B-1H. Although the cores recovered from Hole U1333A showed significant porcellanite layers, we used the APC drillover strategy in Hole U1333B to obtain APC cores across and below the Eocene–Oligocene transi-

tion to 162.7 m CSF. We then XCB cored to basement and a total depth of 180.3 m CSF.

Hole U1333C was designed to provide stratigraphic overlap and confirm stratigraphic correlations made between Holes U1333A and U1333B. APC coring in Hole U1333C started 2.75 m shallower than in Hole U1333B and reached 163.2 m CSF before we had to switch to XCB coring. No downhole logging was conducted at Site U1333.

The sediment column at Site U1333 has a strong resemblance to that of Site 1218 (Lyle, Wilson, Janecek, et al., 2002) but with notably more carbonate-bearing sediments in the Eocene portion. The ~183 m of pelagic sediments has been divided into four major lithologic units (Fig. F61; see Table T2 in the "Site U1333" chapter). Unit I is ~7 m thick and contains an alternating sequence of clay, clayey radiolarian ooze, radiolarian clay, clayey nannofossil ooze, and nannofossil ooze of early Miocene age. Unit II is ~112 m thick and composed of alternating very pale brown nannofossil ooze and yellowish brown nannofossil ooze with radiolarians of early Miocene to latest Eocene age. Unit III is ~60 m thick and composed of Eocene biogenic sediments comprising clayey nannofossil ooze, nannofossil radiolarian ooze, nannofossil ooze, radiolarian nannofossil ooze, and porcellanite of latest Eocene to middle Eocene age (Unit III). Unit III is divided into two subunits, based on the absence (Subunit IIIa) or presence (Subunit IIIb) of porcellanite, which occurs between ~168 and 174 m CSF. Unit IV is a thin unit (~3.3 m) of lithified carbonate (partly limestone) and nannofossil ooze, overlying basalt (Unit V).

All major microfossil groups were found in sediments from Site U1333 and provide a consistent, coherent, and high-resolution biostratigraphic succession from basement to the top of lithologic Unit II. Shipboard biostratigraphy indicates that sediments recovered at Site U1333 span a near-continuous succession from around the lower Miocene boundary to the middle Eocene. Radiolarians are common and well preserved in the Eocene succession but less well preserved in the Oligocene sediments. A complete sequence of radiolarian zones from RN2 to RP14 (middle Eocene) was described. Initial assessment of the radiolarian assemblages across the Eocene/Oligocene boundary interval indicates a significant loss of diversity through this apparently complete succession. Although a few species from the Eocene carry through to the Oligocene, only one stratigraphic marker species (*Lithocyclia angusta*) first appears near the Eocene/Oligocene boundary. Calcareous nannofossils are present and moderately to well preserved through most of the succession, although there are some short barren intervals in the middle to upper

Eocene. The succession spans a complete sequence of nannofossil zones from lower Miocene Zone NN1 to middle Eocene Zone NP15. The Oligocene/Miocene boundary is bracketed by the base of *Sphenolithus disbelemnos* in Sample 320-U1333A-2H-5, 70 cm (16.20 m CSF), and the presence of rare *Sphenolithus delphix* in Sample 320-U1332A-2H-CC (9.57 m CSF). Discoasters are very rare in basal assemblages, indicative of a eutrophic environment and consistent with the paleolatitude of this site in the early middle Eocene within the equatorial upwelling zone. Planktonic foraminifers are relatively abundant and well preserved from the lowest part of the Miocene to the lower Oligocene. Oligocene fauna is characterized by the common presence of *Catapsydrax* spp., *Dentoglobigerina* spp., and *Paragloborotalia* spp. In contrast, upper Eocene sediments contain poorly preserved specimens or are barren of planktonic foraminifers. Preservation and abundance slightly increased in some intervals of the middle Eocene, which is recognized by the presence of acarininids and clavigerinellids. The absence of the genera *Globigerinatheka* and *Morozovella* makes precise age determination of individual samples problematic. High abundances of *Clavigerinella* spp. have been linked to high-productivity environments, consistent with the paleogeographic location of this site (Coxall et al., 2007). Benthic foraminifers were almost continuously present and indicate lower bathyal to abyssal depths. Oligocene fauna is characterized by calcareous hyaline forms, such as *Nuttallides umbonifer, Oridorsalis umbonatus,* and *Cibicidoides mundulus. Nuttallides truempyi* and *O. umbonatus* often dominate the Eocene fauna. Benthic foraminifers are present through most of the section apart from an interval in the middle Eocene equivalent to radiolarian Zone RP16. They indicate lower bathyal to abyssal paleodepths.

Sedimentation rates at Site U1333 are ~6 m/m.y. in the upper sediment column from the early Miocene to the late Oligocene. In the early Oligocene, linear sedimentation rates increase to ~12 m/m.y. Between ~31 and 39 Ma (early Oligocene to early late Eocene), sedimentation rates are ~4 m/m.y. but increase slightly to ~5 m/m.y. in the interval from ~39 to 45 Ma (middle Eocene).

Paleomagnetic results from measurements made along split-core sections and on discrete samples from Site U1333 provide a well-resolved magnetostratigraphy. Shipboard analyses suggest that a useful magnetic signal is preserved in most APC-cored intervals after removal of the drilling-induced overprint by partial AF demagnetization at 20 mT. The overprint was nearly absent in those cores collected in nonmagnetic core barrels at Site U1333, whereas it was quite prominent for cores recovered in standard steel core barrels. Paleomagnetic directions from discrete samples agree well with those from split cores, confirming that AF demagnetization at 20 mT is generally sufficient to resolve the primary paleomagnetic direction regardless of which type of core barrel was used. Cleaned paleomagnetic data provide a series of distinct ~180° alternations in declination and subtle changes in inclination, which, when combined with biostratigraphic age constraints, allow a continuous magnetostratigraphy to be constructed that correlates well with the geomagnetic polarity timescale. The magnetostratigraphic record extends from the base of Chron C6n (19.722 Ma) at 1.7 m CSF in Hole U1333C to the top of Chron C20r (43.789 Ma) at 161.6 m CSF in Hole U1333C. Highlights include very high quality paleomagnetic data across Chrons C13r and C13n, which span the latest Eocene and earliest Oligocene, and a newly recognized cryptochron within Chron 18n.1n.

Geochemistry results indicate that samples from the upper part of Site U1333 have modest $CaCO_3$ contents of 26–69 wt% between 0 and 4 m and have frequent variations between 58 and up to 93 wt% in the interval between 4 and 35 m CSF. Calcium carbonate contents are consistently high (75.5–96 wt%) from 35 to 111 m CSF, whereas in the Eocene (between 111 and 171 m CSF) $CaCO_3$ contents vary abruptly between <1 and 74 wt%. The lowermost lithified carbonate rocks between 173 and 180 m CSF have high $CaCO_3$ contents between 76 and 90 wt%. TOC content, as determined by the acidification method, is generally very low. Pore water alkalinity values are never elevated, but alkalinity and dissolved strontium values are somewhat higher near the Eocene–Oligocene transition; these are generally consistent with carbonate dissolution or recrystallization processes. Dissolved silica increases with depth, with values always <1000 µM.

A full physical property program was run on cores from Holes U1333A–U1333C comprising WRMSL measurements of magnetic susceptibility, bulk density, and *P*-wave velocity; NGR; and measurements of color reflectance, followed by discrete measurements of moisture and density properties, sound velocities, and thermal conductivity on Hole U1333A cores only. All track data show variability throughout the section, allowing a detailed correlation among holes primarily using magnetic susceptibility and density (magnetic susceptibility varies around 24×10^{-5} SI in radiolarian ooze–dominated sections and ~3×10^{-5} SI in more carbonate rich intervals). Magnetic susceptibility values gradually increase uphole. NGR measurements are elevated by an order of magnitude in the uppermost clays and increase near the lower

Oligocene at ~115 m CSF (from 5 to 8 cps). *P*-wave velocity gradually increases downhole as we move from carbonate- to radiolarian-dominated successions. *P*-wave velocity generally varies between 1490 and 1560 m/s depending on lithology, with lower velocities corresponding more to carbonate-rich sections. Bulk density and grain density show a marked decrease at ~112 m CSF (~1.70 to 1.31 g/cm³ in bulk density), where carbonate content decreases rapidly. Porosity values are generally high in the radiolarian-rich sediments (80%) and decrease in the carbonate-rich section (~60%). Thermal conductivity measurements are increased in carbonate-rich intervals and range from ~0.8 W/(m·K) in lithologic Unit I to 1.2–1.3 W/(m·K) in lithologic Unit II.

Stratigraphic correlation indicated that a complete section was recovered to ~130 m CSF in the upper Eocene, equivalent to a composite depth of ~150 m CCSF-A. For Site U1333, a growth factor of 15% is estimated from the ratio between the CCSF-A and CSF depth scales. Stratigraphic correlation with Site 1218 suggests a complete stratigraphic section in the Oligocene to uppermost Eocene interval.

Five formation temperature measurements were conducted in Hole U1333B with the APCT-3. These temperature measurements, when combined with thermal conductivity values obtained from the cores, indicate that Site U1333 has a heat flow of 42.3 mW/m² and a thermal gradient of 37.9°C/km.

Highlights

High carbonate fluctuations in middle Eocene sediments

Coring at Site U1333 was designed to capture a time interval when the CCD was slightly deeper within the middle Eocene interval that showed prominent fluctuations of carbonate content (Lyle et al., 2005). This interval occurs during the cooling that took place after the EECO (Zachos et al., 2001a) and before the Eocene–Oligocene transition (e.g., Coxall et al., 2005). Unlike Site 1218, Site U1333 sediments show carbonate contents >75 wt% in this interval at a deeper water depth and apparently coeval with the CCD cycles described by Lyle et al. (2005). Basal lithologic Unit IV recovered partially lithified carbonates.

MECO, Eocene–Oligocene and Oligocene–Miocene transitions, and depth transects

Site U1333 forms the third oldest and deepest component of the PEAT depth transect component and can be directly compared with Site 1218, which will allow the study of critical intervals (such as the Eocene–Oligocene transition; see Coxall et al., 2005) and variations of the equatorial CCD. Site U1333 is estimated to have been ~3.8 km deep during the

Eocene–Oligocene transition, ~1 km shallower than today and 200 m shallower at that time than Site U1332. Carbonate content in these sediments does not change as rapidly as at the deeper and older Sites U1332 and U1333. Some of these sediments appear to be Eocene–Oligocene transition sediments that are suitable for paleoceanographic studies using carbonate-based geochemical proxies and thus are an improvement over Site 1218. Of note, Site U1333 also contains high carbonate content–bearing sediments around the MECO event (Bohaty and Zachos, 2003; Bohaty et al., 2009), allowing a detailed study of the sequence of events linking carbonate preservation cycles (Lyle et al., 2005) with climatic oscillations.

Carbonate-bearing sediments across the Oligocene–Miocene transition were also recovered at Site U1333, adding important data to the study of this time interval in the context of the PEAT Oligocene/Miocene depth transect.

Age transect of seafloor basalt

At Site U1333 we recovered what appear to be fresh fragments of seafloor basalt overlain by sediments aged 45 to 46 Ma as estimated from biostratigraphic results. This material will, when combined with other PEAT basalt samples, provide important sample material for the study of seawater alteration of basalt.

Site U1334

Three holes were cored at Site U1334 (7°59.998′N, 131°58.408′W; 4799 mbsl) (Fig. **F62;** see Table **T1** in the "Site U1334" chapter), targeting the events bracketing the Eocene–Oligocene transition as part of an investigation of the wider Cenozoic climatic evolution (e.g., Zachos et al., 2001a) and providing data toward a depth transect across the Oligocene (see **"Eocene/Oligocene Boundary [Site U1334; 38 Ma crust]"**) that will allow exploitation and verification of a previous astronomical age calibration from Site 1218 (Pälike et al., 2006a).

Site U1334 is in the center of the PEAT program transect, ~100 km north of the Clipperton Fracture Zone and ~380 km southeast of the previously drilled Site 1218. At Site U1334, seafloor basalt is overlain by ~285 m of pelagic sediment. The oldest sediment is of late middle Eocene age (38 Ma).

The topmost ~47 m thick lithologic Unit I contains a 15 m thick interval of brown radiolarian clay overlying ~32 m of alternating radiolarian clay and nannofossil ooze. The uppermost section (320-U1334A-1H-CC) is of late Miocene age (radiolarian Zone RN7; ~8.5 Ma). Below, Unit II comprises a ~200 m thick succession of upper Miocene to Oligocene nannofossil ooze and

chalk above a ~35 m thick sequence of upper Eocene nannofossil chalk, radiolarite, and claystone (Unit III). Basal lithologic Unit IV (~1 m thick; 285 m CSF) consists of middle Eocene intercalated micritic chalk and limestone on basalt (Figs. F63, F64).

Holes U1334A–U1334C provided high-quality APC-cored sediments from the mudline to ~210 m CSF (Cores 320-U1334A-22H, 320-U1334B-22H, and 320-U1334C-22H). Below this depth we encountered increasingly stiffer and harder sediment, after which we switched to the XCB cutting shoe. XCB coring advanced to 288.5 m DSF through lower Oligocene and Eocene sediments with high recovery. At the base of the holes, an intercalated unit of basalt and hard micritic chalk and limestone occurs below a 10–20 m thick section of nannofossil ooze and chalk. For detailed coring activities, see "Operations" in the "Site U1334" chapter.

Carbonate content exceeds 92 wt% in the upper lower Miocene below Section 320-U1334A-5H-3 and remains high throughout the Oligocene. Eocene sediments still contain considerable amounts of carbonate, and nannofossil ooze and chalk are dominant lithologies apart from several short less carbonate rich intervals (e.g., Section 320-U1334A-28X-3). In the middle Eocene, carbonate content cycles between ~40 and 85 wt% (see "Geochemistry" in the "Site U1334" chapter) (Fig. F65), with higher values encountered toward the basal part of the Eocene section. Two short intervals in the upper Eocene (~249 to ~257 m CSF) exhibit carbonate content of <20 wt%.

A series of middle Oligocene cores (Cores 320-U1334A-16H through 21H) were recovered that had very distinct colors ranging from light grayish green to light blue (see "Lithostratigraphy" in the "Site U1334" chapter). These uniquely colored carbonate oozes exhibit extremely low magnetic susceptibilities that complicated stratigraphic correlation. These oozes have lost almost their entire magnetic susceptibility signal from ~145 to ~215 m CSF (Figs. F64, F66). Similar colored cores have previously been described for Sites 78 and 79 (Hays et al., 1972).

The Eocene–Oligocene transition at Site U1334 is much more expanded than at IODP Sites U1331–U1333 and even Site 1218. The transition was encountered at ~250 m CSF and fully recovered in Cores 320-U1334A-27X and 320-U1334B-26X; Hole U1334C was used to fill small stratigraphic gaps. The Oligocene–Miocene transition was fully recovered in all three holes in Cores 320-U1334A-10H (based on magnetostratigraphy, the boundary is at Sample 320-U1334A-10H-6, 98 cm), 320-U1334B-10H (top of Section 2), and 320-U1334C-10H.

All major microfossil groups occur in sediments from Site U1334 and provide a consistent, coherent, and high-resolution biostratigraphic succession spanning a near-continuous sequence from the middle Miocene to the uppermost middle Eocene. The uppermost 12 m of radiolarian clay is barren of calcareous microfossils but contains radiolarians of middle Miocene age, similar to the site survey piston Core RR0306-08JC (Lyle et al., 2006). Nannofossil ooze and radiolarian clays are present in the Miocene and Eocene parts of the section, with nannofossil ooze dominant in the thick Oligocene section. Radiolarians are present through most of the section, apart from the lowermost cores, and are well preserved in the Eocene. They provide a coherent high-resolution biochronology and indicate a complete sequence of radiolarian zones from RN7 (upper Miocene) to RP17 (uppermost middle Eocene). Calcareous nannofossils are present and moderately to well preserved through most of the succession, and there appears to be a complete sequence of nannofossil zones from NN6 (middle Miocene) to NP17 (uppermost middle Eocene), providing a minimum age estimate for basaltic basement of 38 Ma. In the Eocene, the base of *Chiasmolithus oamaruensis* is determined in Sample 320-U1334A-30X-1, 66 cm, and the top of *Chiasmolithus grandis* in Sample 320-U1334A-30X-2, 74 cm. Intriguingly, both species are mid- to high-latitude taxa (Wei and Wise, 1989) and are present only rarely and sporadically at Site U1334. Planktonic foraminifers are present through most of the succession and are relatively abundant and well preserved from the lower Miocene to the lower Oligocene. The lower Miocene is characterized by the presence of *Dentoglobigerina* spp., *Paragloborotalia siakensis–mayeri, Paragloborotalia kugleri,* and *Paragloborotalia pseudokugleri.* Oligocene sediments contain *Catapsydrax* spp., *Paragloborotalia opima-nana,* and characteristic *Dentoglobigerina* spp. Preservation and abundance of planktonic foraminifers is more variable in the middle Miocene and upper Eocene/lowermost Oligocene. No Eocene/Oligocene boundary marker hantkeninids were identified. Benthic foraminifers are present through most of the section and indicate lower bathyal to abyssal paleodepths.

Sedimentation rates, as derived from magneto- and biostratigraphic age determinations, vary throughout the section and are ~4 m/m.y. in the topmost sediment cover, vary between ~12 and 14 m/m.y. in the lower Miocene through upper lower Oligocene section, increase to ~24 m/m.y. in the lower Oligocene, and are ~8 m/m.y. in the upper Eocene. There is no obvious hiatus in the shipboard biostratigraphic sequence. The presence of all major fossil groups as well as a detailed and well-resolved magnetostratigraphy will allow us to achieve one of the main PEAT objectives of arriving at an integrated

Cenozoic stratigraphy and age calibration for major parts of the Miocene, Oligocene, and Eocene.

A full physical property program was run on cores from Site U1334. This program comprises WRMSL measurements of magnetic susceptibility, bulk density, and *P*-wave velocity, along with NGR and measurements of color reflectance, followed by discrete measurements of moisture and density (MAD) properties, sound velocities, and thermal conductivity in Hole U1334A. All track data are variable throughout the section, allowing a detailed correlation between different holes, with the exception of a very low magnetic susceptibility signal within an interval extending slightly above and below the light greenish gray tinted cores of Unit II (see "Lithostratigraphy" in the "Site U1334" chapter for exact color definitions), between ~140 and 205 m CSF. Magnetic susceptibility varies between 10×10^{-5} and 40×10^{-5} SI in Unit I, oscillates around 5×10^{-5} to 10×10^{-5} SI above the colored sediments, and then drops to near zero and negative values, returning to values around 10×10^{-5} SI in the lower part of Unit II and Subunit IIIa. NGR increases slightly at the Eocene/Oligocene boundary at ~246 m CSF (from 4 to 7 cps). *P*-wave velocity remains uniform through the upper 150 m of sediment (varying around 1500 m/s) but increases rapidly below the ooze/chalk boundary to ~1600 m/s. This explains the slightly thicker sediment section than was expected from seismic data prior to coring (~20 m thicker). For Hole U1334B, no *P*-wave velocity WRMSL data were collected between ~125 and 240 m CSF to allow for a more timely stratigraphic correlation of cores within the iron reduction–dominated colored cores with the GRA instrument. Bulk density and grain density increase gradually with carbonate content to ~204 m CSF to a maximum of ~1.8 g/cm³ and then show stepped decreases in the lower part of this succession. Ephemeral whole-round samples were collected at ~50 and ~165 m for shore-based studies of sediment permeability.

WRMSL data were used to achieve stratigraphic correlation among holes at Site U1334. Magnetic susceptibility was initially the main parameter used for real-time correlation, as a second loop of the susceptibility meter is mounted on the Special Task Multisensor Logger (STMSL); the second bulk density instrument on this track was not working. In the very low (sometimes negative) magnetic susceptibility interval between ~140 and ~205 m CSF (Cores 320-U1334A-16H through 21H), the signal was not useful for correlation, and we measured the corresponding cores from Hole U1334B out of sequence to establish the amount of core overlap using bulk density. The coring effort in Hole U1334C was successful at covering gaps between cores at this site to ~111 m CCSF-A,

as well as from 250 to 335 m CCSF-A, almost to the bottom of the section. The correlation was challenging between the three holes at Site U1334 in the greenish–light gray interval (Cores 320-U1334A-15H through 22H, 320-U1334B-14B through 22H, and 320-U1334C-14H through 22H) and in the bottom 80 m of the section, where XCB coring compromised the GRA density variations that would otherwise help stratigraphic correlation. Visual inspection, comparison with core imagery, and biostratigraphic datums were used to establish and verify hole to hole correlation where track data lacked clearly identifiable features. Stratigraphic correlation between individual holes indicates a growth factor (ratio between the CCSF-A and CSF depth scales) of ~16%. Stratigraphic correlation resulted in a complete splice through the Eocene–Oligocene transition almost to basement (~38 Ma).

A full range of paleomagnetic analyses was conducted on 66 APC cores and 188 discrete samples from Site U1334 for the APC-cored section of Site U1334 (upper ~209 m). Unlike Sites U1331 and U1332, the drilling overprint was generally weak for Site U1334 cores, but only for those collected with nonmagnetic core barrels (Cores 320-U1334A-1H through 16H, 320-U1334B-1H through 15H, and 320-U1334C-1H through 15H). In contrast, those cores collected with steel core barrels are highly overprinted. The overprint is so severe that even demagnetization at 20 mT only partially removes it. This extreme overprint notably degrades the paleomagnetic declination data, as can be noted by their higher variability, which makes polarity determination much more difficult in the intervals collected with steel core barrels. The problem is exacerbated by the decay in the intensity (and magnetic susceptibility) that occurs at ~135 m CSF in all three holes as a result of reduction diagenesis. Even within the highly reduced interval, an interpretable signal was present prior to switching to steel core barrels. Magnetic susceptibility in the upper 45 m of Hole U1334A averages $\sim18 \times 10^{-5}$ SI (volume normalized) and decreases to a mean of 6×10^{-5} SI from 45 to 135 m CSF. A notable low occurs from ~140 to 204 m CSF, where the average susceptibility is 0.6×10^{-5} SI. This low interval is associated with a change in sediment color from yellowish tan to very light green, blue, and gray at ~143 m CSF and another abrupt change to reddish brown tones at ~192 m CSF, which corresponds to middle early Oligocene (~30 Ma). Just below 205 m, magnetic susceptibility steps up to an average of 5×10^{-5} SI and then increases again across the Eocene/Oligocene boundary (~245 m) to an average of 18×10^{-5} SI. The magnetostratigraphy in Hole U1334A has been interpreted from the top of Chron

11r (29.957 Ma), which occurs ~55 cm below the top of Section 320-U1334C-21H-4 (~195 m CSF) through the base of Chron C3n.4n (5.235 Ma) in Core 320-U1334A-1H (~4 m CSF). The youngest sediments recovered are in the upper ~2 m of Core 320-U1334A-1H, which record Chrons C1n through C2r.1r.

A standard shipboard suite of geochemical analyses of pore water and organic and inorganic sediment properties was undertaken on samples from Site U1334. We also conducted a high-resolution (one per section) Rhizon pore water investigation across the interval's middle Oligocene cores (320-U1334C-16H through 21H) that exhibited colored sediments. Site U1334A is marked by alkalinities between 3 and 4 mM throughout. The most striking features in the interstitial water geochemistry are a dissolved manganese peak from ~20 to ~240 m CSF with a maximum of ~6 µM at ~110 m CSF and a dissolved iron peak as high as >15 µM centered at 165 m CSF. The depth range of the dissolved iron peak, indicative of iron oxide reduction, coincides with the colorful interval seen in the lithology and with the interval of low magnetic susceptibilities (~140–205 m CSF). Sulfate results indicate limited sulfate reduction. Calcium carbonate contents are low in the uppermost ~35 m of Site U1334, and calcium carbonate contents are generally high (~80 wt%) below the uppermost clay layer.

Wireline logging was attempted in Hole U1334C with a redesigned tool string configuration after the loss of equipment at Site U1332. However, this attempt had to be abandoned after the logging winch failed when the tool was on its way down the drill pipe.

Five downhole temperature measurements were conducted in Hole U1334B with the APCT-3 tool and reveal a thermal gradient of 33°C/km. Seafloor temperature is ~1.5°C. Temperature data combined with whole-round core temperature conductivity measurements indicate the heat flow is 31.6 mW/m² at this site. This is somewhat lower than values obtained for the nearest site (1218).

Highlights

Eocene–Oligocene and Oligocene–Miocene transitions and depth transects

Site U1334 was planned as the youngest and shallowest component of the PEAT Eocene–Oligocene depth transect component, which will allow the study of critical intervals (such as the Eocene–Oligocene transition; see Coxall et al., 2005) and variations of the equatorial CCD. Site U1334 is estimated to have been ~3.5 km deep during the Eocene–Oligocene transition, ~1.3 km shallower than today and 800 m

shallower at that time than Site U1333. Unlike previously drilled sites, the dominant lithology below the Eocene–Oligocene transition is still nannofossil ooze and chalk, with significant amounts of carbonate present. These carbonate amounts will allow us to achieve the prime objective for this site. The Eocene–Oligocene transition, which was cored multiple times at Site U1334, has higher sedimentation rates than previously cored examples. The overlying Oligocene is also much more expanded than at Site 1218, with better preservation of planktonic foraminifers over a longer time interval, permitting a more detailed study of the Oligocene climate system. Site U1334 contains carbonate-bearing sediments across the Oligocene–Miocene transition. Physical property data from Site U1334 can be correlated cycle by cycle to Site 1218, allowing correlation to a previously astronomically calibrated site for the Oligocene.

Geochemical front

At Site U1334 we recovered a ~50 m thick interval of light greenish gray carbonates that show a distinct peak in dissolved Fe concentrations, characteristic of a geochemical alteration front. A similar but much thicker alteration zone is also observed at IODP Site U1335 and provides the opportunity to study organic matter degradation while these sites migrate from south to north through the equatorial belts of high productivity.

Age transect of seafloor basalt

At Site U1334 we recovered what appear to be fresh fragments of seafloor basalt, aged ~38 Ma as estimated from biostratigraphic results. This material will, when combined with other PEAT basalt samples, provide important sample material for the study of seawater alteration of basalt.

Site U1335

Two holes were cored at Site U1335 (5°18.735′N, 126°17.002′W; 4327.5 mbsl) (Fig. F67; see Table T1 in the "Site U1335" chapter), targeting paleoceanographic events in the late Oligocene and into the early and middle Miocene, including and focusing on the climatically significant Oligocene–Miocene transition and the recovery from the Mi-1 glaciation event (Zachos et al., 2001b; Pälike et al., 2006a) and the expansion of the East Antarctic cryosphere (Holbourn et al., 2005). Site U1335 also provides data toward a depth transect across the latest Oligocene and Miocene (see "Latest Oligocene–earliest Miocene [Site U1335; 26 Ma crust]") that will allow exploitation and verification of a previous astronomical age calibration from Site 1218 (Pälike et al., 2006b).

Site U1335 (~26 Ma crust) is situated halfway between Site U1336 ~340 km toward the northwest and Site U1337 ~390 km toward the southeast, ~250 km south of the Clipperton Fracture Zone (Lyle et al., 2006). At Site U1335, seafloor basalt is overlain by ~414 m of pelagic sediment. The oldest sediment is of late Oligocene age (26 Ma).

The sedimentary sequence at Site U1335 is divided into two major lithologic units (see "Lithostratigraphy" in the "Site U1335" chapter). The topmost ~64 m thick lithologic Unit I comprises an alternating sequence of earliest late Miocene to Pleistocene calcareous nannofossil, diatom, radiolarian, and foraminifer oozes. The topmost sediment of Unit I is younger than the Pleistocene/Pliocene boundary (see "Biostratigraphy" in the "Site U1335" chapter) as recognized by the top of planktonic foraminifer *Globigerinoides fistulosus* (between Samples 320-U1335A-1H-CC and 2H-2, 104–106 cm) and then follows a continuous biostratigraphic succession to the early late Miocene. Below, lithologic Unit II comprises a ~350 m thick succession of late Miocene to late Oligocene (calcareous nannofossil Zone NP25) nannofossil ooze and chalk overlying basalt (lithologic Unit III) (Figs. F68, F69). One of the prominent features of Unit II is the presence of at least 49 described beds (2–176 cm thick) of nannofossil foraminifer ooze that have sharp basal boundaries, many of which are irregular and some of which are inclined. These beds are interpreted as gravity flow deposits from the nearby seamounts and represent ~2% of the total sediment recovered.

Holes U1335A and U1335B provided high-quality APC-cored sediments from the mudline to ~341 and 378 m CSF, respectively (Cores 320-U1335A-36H and 320-U1335B-41H). At the time it was recovered, the APC-cored interval from Hole U1335B represented the second deepest APC-cored depth in ODP and IODP history. Below this depth we encountered stiffer and harder sediment, after which we switched to the XCB cutting shoe. XCB coring advanced to ~420 m DSF through lower Miocene and upper Oligocene sediments with high recovery. In the basal section, Core 320-U1335B-46X recovered pieces of basalt up to 10 cm in length with a glassy rim and overlain by nannofossil chalks of Unit II. For detailed coring activities, see "Operations" in the "Site U1335" chapter.

The sediment column at Site U1335 represents the youngest end-member drilled during Expedition 320 and provides one of the most stratigraphically complete and expanded lower Miocene sections from the equatorial Pacific to date (~320 m cored depth from the lowermost to uppermost Miocene).

At Site U1335, carbonate content fluctuates between 12 and 87 wt% within Unit I (see "Geochemistry" in the "Site U1335" chapter) (Fig. F70), presumably reflecting the close proximity of the seafloor to the lysocline. With the exception of the depth interval from 140 to 220 m CSF, the remainder of Unit II exhibits uniformly high calcium carbonate content between 80 and 90 wt%. From ~150 to 210 m CSF (approximately equivalent to Cores 320-U1335A-16H through 22H), carbonate content cycles between ~50 and 90 wt% and corresponds to a change in dominant sediment color from light greenish gray to tan, displaying higher magnetic susceptibility values up to 25×10^{-5} SI.

A series of upper Oligocene through upper middle Miocene cores (320-U1335A-8H through 40X) were recovered with distinct colors ranging from light grayish green to light blue (see "Lithostratigraphy" in the "Site U1335" chapter), similar but much thicker in total stratigraphic thickness (~70–170 and ~200–350 m) than those observed at Site U1334 (see the "Site U1334" chapter). The colored carbonate oozes have extremely low magnetic susceptibilities that complicated a confident stratigraphic correlation. These colored oozes have lost almost their entire magnetic susceptibility signal from ~70 to ~105 m CSF and below ~210 m CSF (Figs. F69, F71, F72). Similar colored cores have previously been described for Sites 78 and 79 (Hays et al., 1972).

All major microfossil groups occur in sediments from Site U1335, representing a complete biostratigraphic succession at the shipboard sample resolution level of Pleistocene to uppermost Oligocene sediments, including a thick sequence of lower Miocene nannofossil ooze and chalk (see "Biostratigraphy" in the "Site U1335" chapter). Radiolarians are present through most of the section apart from the basal 3 m of nannofossil chalk. They provide a coherent high-resolution biochronology through a complete sequence of radiolarian zones from RN14 (Pleistocene) to RP21 (upper Oligocene). Calcareous nannofossils are present and moderately to well preserved through most of the succession, representing the complete sequence from Zone NP25 (upper Oligocene) above basaltic basement through Zone NN20 (Pleistocene). Planktonic foraminifers are present throughout the succession and are moderately to well preserved. Recognized planktonic foraminifer zones range from Zone PT1a (Pleistocene) to Zone O6 (upper Oligocene). Nannofossil, radiolarian, and planktonic foraminifer datums are in good agreement. Benthic foraminifers are present through most of the section and indicate lower bathyal to abyssal paleodepths. The Oligocene–Miocene transition at Site U1335 was encountered at ~350 m and was fully re-

covered in Cores 320-U1335A-37X and 320-U1335B-38H as approximated by the planktonic foraminifer datum base of *Paragloborotalia kugleri* between Samples 320-U1335A-37X-4, 136–138 cm, and 37X-CC (midpoint = 348.6 m CSF), in good agreement with the calcareous nannofossil event top of *Sphenolithus delphix* at 349.7 m CSF between Samples 320-U1335A-37X-6, 50 cm, and 37X-CC. The oldest sediment overlying seafloor basalt has been assigned to calcareous nannofossil Zone NP25 (24.4–26.8 Ma).

Sedimentation rates, as derived from the magneto- and biostratigraphic age determinations (see **"Stratigraphic correlation and composite section"** in the "Site U1335" chapter), vary throughout the section and are ~6 m/m.y. in the late to middle Miocene to recent sediment cover, ~17 m/m.y. in the middle early Miocene and as high as ~25 m/m.y. throughout the late Oligocene and early Miocene. There is no obvious hiatus at the shipboard biostratigraphic resolution, although some condensed horizons exist (e.g., near the early/middle Miocene boundary and in the early late Miocene; see **"Biostratigraphy"** in the "Site U1335" chapter). The presence of all major fossil groups as well as a detailed and partly well resolved magnetostratigraphy will allow us to achieve one of the main PEAT objectives of arriving at an integrated Cenozoic stratigraphy and age calibration for the Miocene and late Oligocene.

A full physical property program was run on cores from Site U1335. This program comprises WRMSL measurements of magnetic susceptibility, bulk density, and *P*-wave velocity; NGR; and measurements of color reflectance, followed by discrete measurements of MAD properties, sound velocities, and thermal conductivity in Hole U1335A. All track data vary throughout the section, allowing a detailed correlation among holes, with the exception of a low magnetic susceptibility signal within an interval extending slightly above and below the light greenish gray tinted cores of Unit II (see **"Lithostratigraphy"** in the "Site U1335" chapter for exact color definitions), between ~70 and 110 and ~210 and ~380 m CSF. Magnetic susceptibility varies between 5×10^{-5} and 20×10^{-5} SI in the upper parts of Unit I and then increases to ~25×10^{-5} SI toward the lower part of Unit I, coinciding with the presence of clayey radiolarian ooze within the major lithology of nannofossil ooze. Magnetic susceptibility values decrease at the top of Unit II (~64 m CSF) and then fall to values around -1×10^{-5} SI near 70 m CSF. Between ~110 and 150 m CSF, magnetic susceptibility values increase slightly and become highly variable (0 to 10×10^{-5} SI). Magnetic susceptibility values are higher in the interval from 160 to 200 m CSF, coinciding with an observed decrease in Fe reduction (see **"Lithostratigraphy"** in

the "Site U1335" chapter). Below 200 m CSF, the magnetic susceptibility signature is dominantly diamagnetic, with values close to zero. Magnetic susceptibility values slightly increase again in the basal 20 m of Unit II (below ~400 m CSF). NGR is elevated at the surface sediment (~73 cps) but low throughout the rest of the sedimentary column. *P*-wave velocities from the WRMSL agree with discrete velocity measurements and reflect key lithologic transitions, particularly the ooze to chalk transition near ~220 m CSF. *P*-wave velocities are between 1460 and 1490 m/s in Unit I and the upper part of Unit II and then increase to >1500 m/s. Slightly below the ooze–chalk transition near 345 m CSF, velocities increase significantly, reaching 1600–1750 m/s at the bottom of Unit II. This partly explains the thicker sediment section than was expected from seismic data prior to coring (~60 m thicker). Bulk density and grain density increase with depth, with an increase in wet bulk density from 1.2 to 1.6 g/cm³ in Unit I to ~1.7 g/cm³ at the top of Unit II and ~1.8 g/cm³ in the basal part of the section. Sediment porosity ranges from 70% to 90% in Unit I to 50%–60% at ~300 m CSF in Unit II. Ephemeral whole-round samples were collected at ~96, ~196, and ~305 m CSF for shore-based studies of sediment permeability.

The coring effort in Holes U1335A and U1335B was successful at covering stratigraphic gaps between cores at this site from the surface throughout most of the APC-cored section (see **"Stratigraphic correlation and composite section"** in the "Site U1335" chapter), with the exception of a gap (~1 m) at the bottom of Core 320-U1335A-16H due to flow-in (~146.40–151.46 m CSF). Features in magnetic susceptibility and GRA density are well aligned down to a depth of 337 m CSF (Hole 1335A) and 344 m CSF (Hole U1335B), corresponding to ~398 m CCSF-A. Between ~230 and ~398 m CCSF-A, GRA density data allowed confident alignment of cores despite very low magnetic susceptibility values. The section below ~398 m CCSF-A was mostly XCB cores, lacked clearly identifiable features, and therefore had to be appended to the splice. A single spliced record was assembled for the aligned cores down to Section 320-U1335B-37H-6 (343.76 m CSF; 398.15 m CCSF-A). Stratigraphic correlation between individual holes indicates a growth factor (ratio between the CCSF-A and CSF depth scales) of ~16%. Stratigraphic correlation resulted in a complete splice through the Eocene–Oligocene transition almost to basement (~38 Ma).

A full range of paleomagnetic analyses was conducted on 78 archive halves and 257 discrete samples from Site U1335 for the APC-cored section (upper ~378 m). The most prominent feature of the records is the

magnetic intensity and susceptibility low that occurs between ~70 and 110 m CSF and below ~210 m CSF. We could not obtain any reliable paleomagnetic directions from this interval because the magnetic intensity after 20 mT AF demagnetization is on the order of 10^{-5} A/m, which is comparable to the noise level of the superconducting rock magnetometer (see "Paleomagnetism" in the "Site U1335" chapter). The drilling overprint was generally weak when non-magnetic core barrels were used (Cores 320-U1335A-1H through 16H and 320-U1335B-1H through 19H). In contrast, cores collected with the steel core barrels are highly overprinted. Except for the low magnetic intensity interval, the cleaned paleomagnetic data provide a series of distinct ~180° alternations in declination. When combined with biostratigraphic age constraints (see "Biostratigraphy" in the "Site U1335" chapter), the data allow a continuous magnetostratigraphy from Chrons C1n (0–0.781 Ma) to C5n.2n (9.987–11.040 Ma) from 0 to 65.95 m CSF in Hole U1335A and from Chrons C1n to C5r.1n (11.118–11.154 Ma) from 0 to 66.225 m CSF in Hole U1335B. Below the bottom of the first magnetic low zone (~70–110 m CSF), magnetostratigraphy is again interpretable downhole: from Chrons C5Br (15.160–15.974 Ma) to C6n (18.748–19.722 Ma) from 155.35 to 208.40 m CSF in Hole U1335A and from Chrons C5AAn (13.015–13.183 Ma) to C5Er (18.524–18.748 Ma) from 107.95 to 202.60 m CSF in Hole U1335B. The highlights of the magnetostratigraphy at Site U1335 are the identifications of (1) a previously observed cryptochron (C5Dr-1n) in two holes and (2) 40 potential geomagnetic excursions (10 of which are recorded in both holes).

A standard shipboard suite of geochemical analyses of pore water and organic and inorganic sediment properties was undertaken on samples from Site U1335. Site U1335 is marked by alkalinities between 2.5 and 4.3 mM throughout, sulfate concentrations between 23 and 28 mM, and dissolved phosphate concentrations of ~2 µM in the shallowest sample, decreasing to ~0.5 µM in the uppermost ~50 m. The most striking features in the interstitial water geochemistry are three dissolved manganese peaks with concentrations of up to 44, 13, and 5 µM at ~0–40, 50–80, and 150–210 m CSF, respectively. Dissolved iron also shows three peaks, with concentrations up to 6 µM at ~6 m CSF, between 90 and 170 m CSF, and between 190 and 370 m CSF. Minima in dissolved Fe correspond to elevated Mn concentrations. The alternating pattern of dissolved Mn and Fe correspond well to apparent color changes in the sediment column (see "Lithostratigraphy" in the "Site U1335" chapter). Lithium concentrations decrease from ~26 µM at the sediment surface to 5 µM at ~300 m CSF, below which Li concentrations increase strongly

to ~32 µM. The Sr concentration profile mirrors that of Li, with concentrations ranging between 82 and 250 µM. Sr values increase from the top to 200 m CSF, followed by a decrease toward basement. Calcium carbonate, IC, and TC contents were determined on sediment samples from Hole U1335A (Fig. F70). $CaCO_3$ contents ranged between 13 and 96 wt%. In the uppermost ~67 m, carbonate contents range from 12 to 87 wt%, and concentrations are then consistently high (~72–96 wt%) between 67 and 157 m CSF and below 222 m CSF. Carbonate contents vary more widely (between 37 and 89 wt%) from 157 to 222 m CSF. TOC concentrations were determined by acidification and are generally low.

Wireline logging was not conducted at Site U1335. Five downhole temperature measurements were conducted in Hole U1335B with the APCT-3 and reveal a thermal gradient of 7.5°C/km. Temperature data combined with whole-round core temperature conductivity measurements indicate the heat flow is 7 mW/m² at this site. This is much lower than values obtained for any of the other Expedition 320 sites and would suggest recirculation of seawater through basement, consistent with some of the interstitial pore water results (see "Geochemistry" in the "Site U1335" chapter).

Highlights

Highly expanded Miocene sedimentary section

One of the highlights from Site U1335 is the recovery of a thick Miocene carbonate-dominated section from the central equatorial Pacific, one of the high-priority objectives of the PEAT program. The early Miocene (7.1 m.y. duration) is captured in ~190 m of sediment, corresponding to a sedimentation rate of 27 m/m.y. The middle Miocene (4.4 m.y. duration) is recovered in ~95 m sediment, with a sedimentation rate of ~21 m/m.y. The sedimentation rate from the late Oligocene into the Miocene is just under 20 m/m.y. These high sedimentation rates will facilitate the study of paleoceanographic processes at unprecedented resolution for the equatorial Pacific.

Oligocene–Miocene transition and depth transects

Site U1335 was planned as the youngest and shallowest component of the PEAT Oligocene–Miocene depth transect component, which will allow the study of critical intervals (such as the Mi-1 glacial inception; see Zachos et al., 2001b; Pälike et al., 2006a) and variations of the equatorial CCD throughout this transition and during the latest Oligocene and early Miocene. Site U1335 is estimated to have been ~3.3 km deep during the Oligocene–Miocene transition, ~1.5 km shallower than today. The dominant lithologies are nannofossil ooze and chalk, with bet-

ter preservation of calcareous microfossils than any other site drilled during Expedition 320, which will allow us to achieve the prime objective for this site. Physical property data from Site U1335 provide an important contribution toward the Cenozoic megasplice, connecting with younger sediments from ODP Leg 138 (e.g., Site 850) and older sediments from Leg 199 (Site 1218), allowing the generation of astronomically calibrated datums and isotope stratigraphies from the Miocene into the Eocene.

Geochemical front

At Site U1335 we recovered an interval of light greenish gray carbonates that show a distinct peak in dissolved Fe concentrations, characteristic of a geochemical alteration front. At Site U1335, this zone is similar to but much thicker in total stratigraphic thickness (~70–170 and ~200–350 m CSF) than that observed at Site U1334 (~50 m; see the "Site U1334" chapter). Although the paleomagnetic signal was lost in most parts of this section, sediments recovered will provide the opportunity to study organic matter degradation while these sites migrated from south to north through the equatorial belts of high productivity. Paleolatitudinal reconstructions show that these characteristic geochemical alteration fronts can be mapped to similar equatorial positions between Sites U1334 and U1335, roughly between the Equator and ~2°N. One feature of interest at Site U1335 is the observation that the multicolored interval of sediments is interrupted between ~170 and 200 m CSF (Cores 320-U1335A-18H through 20H), again showing higher magnetic susceptibility values. It remains to be established whether this interruption in the geochemical alteration front is related to the shape and position of the equatorial high-productivity zone or instead is the result of reduced sedimentation rates during this time (late early Miocene). Interstitial pore water profiles provide additional important information about the redox chemical processes operating in this zone (see "Geochemistry" in the "Site U1335" chapter), which have also been observed at Sites 78, 79, and 574 (e.g., Hays et al., 1972).

Gravity flow deposits

One of the prominent features of Unit II is the presence of at least 49 described beds (2–176 cm thick) of nannofossil foraminifer ooze that have sharp basal boundaries, many of which are irregular and some of which are inclined. These beds are interpreted as gravity flow deposits from the nearby seamounts and represent ~2% of the total sediment recovered. Their grain size fines upward from medium sand to silt, and they are often darker colored than immediately overlying deposits and instantly recognizable

by their coarser texture. Angular basalt fragments (<1 mm), fish teeth, and pyritized foraminifers and radiolarians were also found within the basal parts of these beds, of which at least three show parallel or cross-laminations in their upper or middle part. These beds, interpreted as gravity flow deposits, are present with an approximate frequency of one or two beds per core. The abundance and thickness of these beds is highest within Cores 320-U1335-21H through 37X (189.4–350.1 m CSF). No gravity flow deposits were observed in Cores 320-U1335A-3H through 8H. The provenance of these deposits, as indicated by the observed basalt fragments, is inferred to be the nearby seamounts (Fig. F67B) situated ~15–20 km northeast and southeast of Site U1335, with present summit water depths that are 400–600 m shallower than Site U1335. Initial indications are that these gravity flow deposits, unlike those observed at Site U1331, might not be very erosive and therefore essentially add to the sediment column rather than removing large sections of geological time. The high sedimentation rates at Site U1335 will allow paleoceanographic studies to avoid the generally thin layers of gravity flows.

Age transect of seafloor basalt

At Site U1335 we recovered what appear to be fresh fragments of seafloor basalt with an age of ~26 Ma, as inferred by the oldest biostratigraphic datums from the sediment above. This material will, when combined with other PEAT basalt samples, provide important sample material for the study of seawater alteration of basalt.

Site U1336

Two holes were cored at Site U1336 (proposed Site PEAT-5C; 7°42.067′N, 128°15.253′W; 4286 mbsl) (Fig. F73; see Table T1 in the "Site U1336" chapter) targeting paleoceanographic events in the late Oligocene and into the Miocene, including a focus on the Oligocene–Miocene transition and the recovery of the Mi-1 glaciation event (Zachos et al., 2001b; Pälike et al., 2006b). In conjunction with Sites U1335 and U1337, Site U1336 was also designed to provide a latitudinal transect for early Miocene age slices. Site U1336 provides data toward a depth transect across the late Oligocene and Miocene that allow us to verify and apply a previous astronomical age calibration from Site 1218 (Pälike et al., 2006a).

At Site U1336, APC cores were taken from the seafloor to 184.8 m (Cores 320-U1336A-1H through 21H) and 173.6 m (Cores 320-U1336B-1H through 20H). Nonmagnetic core barrels were used for Cores 320-U1336A-1H through 16H and Cores 320-U1336B-1H through 16H and steel barrels were used

for all other cores. Two hard layers, one at ~121 m CSF (Cores 320-U1336A-14H and 320-U1336B-14H) and one at ~135 m CSF (Core 320-U1336B-16H) caused core loss and prevented the development of a continuous sediment section. XCB cores (320-U1336A-22X through 35X) were taken from 184.8 to 302.9 m CSF in Hole U1336A. We stopped coring before reaching the basement objective because of decreasing rates of penetration, relatively low recovery, and the possibility of obtaining a stratigraphically complete Miocene section by allocating the remaining operational time during Expedition 320 to Hole U1336B.

At Site U1336, ~300 m of pelagic sediments are divided into three major lithologic units (Fig. F74). The sediments are composed mainly of nannofossil oozes, nannofossil chalks, and chert. The lower to middle Miocene sedimentary sequence of Unit I (0–74.54 m CSF) contains more radiolarians, clay, foraminifers, and diatoms relative to the lower Miocene to lower Oligocene sediments below ~70 m CSF. Subtle changes in the relative proportions of these minor components produce meter-scale dark–light color cycles and two diatom-rich layers. Numerous rounded fragments of pumice occur throughout this unit.

Unit II (74.50–189.50 m CSF) is dominated by nannofossil ooze. Sediment color changes downhole from pale yellow to light greenish gray at 92 m CSF. Below this boundary, the color of Unit II alternates between light greenish gray and white to 184.80 m CSF. Oxidation-reduction reactions are responsible for the observed vivid colors and pore water chemistry changes, likely fueled by varied availability of organic carbon. Occasional thin chert layers were encountered below 120 m CSF in Unit II. Mainly broken chert fragments were recovered, except for a small in situ chert fragment at 159.6 m CSF in Section 320-U1336B-18H-4, 106 cm. More abundant chert layers are common in the lower third of the recovered sequence.

Unit III (189.5–299.6 m CSF) was only recovered in Hole U1336A. The dominant lithologies of this unit are light greenish gray and white nannofossil chalk with light greenish gray millimeter-scale color banding and chert layers. The chert shows many different colors including black, dark greenish gray, very dark greenish gray, dark gray, olive-yellow, dark brown, and pink. The Unit II–III transition is identified by the uppermost common occurrence of chert. Below 289 m CSF, nannofossil chalk contains increasing amounts of micrite and the cherts vary in color. The lowermost cherts are olive-yellow, then pink, and, finally, dark brown at the base. The chalk changes color to white below 298.54 m CSF. CaCO$_3$

contents remain >88 wt% in the chalk layers. Igneous basement was not recovered at Site U1336.

All major microfossil groups were found in sediments from Site U1336, representing a complete biostratigraphic succession at the shipboard sample resolution level of middle Miocene to lower Oligocene sediments. They provide a coherent, high-resolution biochronology through a complete sequence (Fig. F74). Calcareous nannofossils are moderately to poorly preserved throughout the succession. There appears to be a complete sequence of nannofossil zones from Zone NN6 (middle Miocene) through NP22 (lower Oligocene), except for Zone NN3, which could not be resolved. Planktonic foraminifers are present throughout the succession ranging from Zones N12 through O1. They are moderately well preserved in the Miocene and less well preserved in the Oligocene.

Benthic foraminifers are present throughout the section, although abundances are overall quite low. The preservation of tests is moderate in the upper part of Site U1336 (Samples 320-U1336A-1H-CC through 19H-CC, 8.22–170.63 m CSF, and 320-U1336B-1H-CC through 20H-CC, 1.68–174.01 m CSF) but deteriorates below this level. The Oligocene to middle Miocene benthic foraminifer assemblage is relatively diverse and indicates oligotrophic lower bathyal to abyssal paleodepths.

The Oligocene/Miocene boundary is placed between the first occurrence of *Paragloborotalia kugleri* (23.0 Ma) and the extinction of *Sphenolithus delphix* (23.1 Ma). The former occurs between Samples 320-U1336A-16H-CC and 17H-2, 38–40 cm (142.96 m CSF) and Samples 320-U1336B-16H-1, 52–54 cm, and 17H-3, 80–82 cm (137.72 m CSF). The top of *S. delphix* is recognized between Samples 320-U1336A-17X-2, 90 cm, and 17X-4, 90 cm (145.9 m CSF), and between Samples 320-U1336B-16H-CC and 17H-1, 150 cm (137.56 m CSF).

The radiolarian stratigraphy at Site U1336 spans the interval from just above the Zone RN6/RN5 boundary (middle Miocene) to the upper part of Zone RP22 (upper Oligocene) at ~170 m CSF. Below this level the sediments are barren of radiolarians. Above this level the assemblages tend to have good to moderate preservation with intermittent intervals of good preservation in Zones RN3 and RN4 (lower to middle Miocene). The downsection decrease in preservation and ultimate disappearance of the radiolarians below Core 320-U1336A-19H appears to be associated with dissolution and reprecipitation of the biogenic silica as intergranular cement and as chert.

Diatom stratigraphy in Hole U1336B spans the interval from just above the *Cestodiscus peplum* zone (middle Miocene) in Core 320-U1336B-1H to the

lowermost part of the *Crucidenticula nicobarica* zone (upper lower Miocene) in Core 320-U1336B-7H. Below Sample 320-U1336B-7H-CC, the sediments are barren of diatoms. Above this level the valves tend to be mostly poorly preserved. Sample 320-U1336B-1H-CC contains the highest diversity with *Cestodiscus pulchellus* as dominant component, accompanied by *Synedra jouseana* and *Thalassiosira yabei*. Fragments of the large centric diatom *Ethmodiscus* are present in the upper part of Hole U1336B.

Paleomagnetic measurements were conducted on archive-half sections of 21 APC cores from Hole U1336A and 20 APC cores from Hole U1336B. Measurements of natural remanent magnetization (NRM) above ~80 m CSF in Holes U1336A and U1336B indicate moderate magnetization intensities (~1×10^{-3} A/m) with a patchy but generally weak viscous remanent magnetization (VRM) or isothermal remanent magnetization (IRM) drilling overprint. Polarity reversal sequences are clearly recognized (Fig. **F74**). Demagnetization data from discrete samples above ~80 m CSF indicate that the characteristic remanent magnetization of the sediments is identified at the 10–20 mT demagnetization steps. The reversals pattern can be correlated with the GPTS from the base of Chrons C5r to C6n (~12 to 19 Ma).

Below ~80 m CSF, a zone of diagenetic alteration involving dissolution of remanence carriers reduces remanence intensities after AF demagnetization of 20 mT to values close to magnetometer noise level in the shipboard environment (~1×10^{-5} A/m). In this zone, sediment magnetizations have been partly or entirely overprinted during the coring process and remanence inclinations are sometimes steep after AF demagnetization at peak fields of 20 mT. At ~130–140 m CSF (Cores 320-U1336A-15H through 16H and 320-U1336B-15H) and below ~160 m CSF (Cores 320-U1336A-19H through 21H and 320-U1336B-18H through 20H), polarity reversals are apparently present but the inclinations are steep (as much as 80°), indicating that the drilling overprint has not been effectively removed during shipboard demagnetization.

A complete physical property program was conducted on whole cores, split cores, and discrete samples comprising WRMSL measurements of magnetic susceptibility, bulk density, and *P*-wave velocity; NGR; and measurements of color reflectance, followed by discrete measurements of moisture and density properties, sound velocities, and thermal conductivity. Physical properties measurements on whole-round sections and samples from split cores reflect the differences among lithologies drilled at Site U1336 (Fig. **F74**). Nannofossil ooze with varying amounts of clay, radiolarians, and diatoms makes up

lithologic Unit I and is characterized by high-amplitude and high-frequency variations in bulk density, magnetic susceptibility, NGR, and color reflectance. Magnetic susceptibility is highest in Unit I, with values ranging from 5×10^{-5} to 30×10^{-5} SI. NGR is also high in this unit, with values to 56 cps near the seafloor. Wet bulk densities are lowest in Unit I, with values ranging from 1.4 to 1.7 g/cm³. Porosity is highest in this interval, ranging from 65% to 80%. The grain density of most of the sediments of Unit I, as well as Units II and III, ranges from 2.6 to 2.9 g/cm³, reflecting the dominance of carbonate constituents at Site U1336. The sediment velocity in Unit I is low, averaging 1500 m/s. The color reflectance of Unit I is marked by luminance (L*) values that are slightly lower and more variable than values determined for sediments in Units II and III.

Below Unit I, a more uniform increase in wet bulk density and decrease in porosity in Units II and III reflects the increasing compaction of the sediments. A slight step increase in wet bulk density marks the transition between Units II and III. In Unit III wet bulk density and porosity average 1.9 g/cm³ and 51%, respectively. Magnetic susceptibility and NGR are low and nearly uniform in Units II and III. Magnetic susceptibility is typically below 5×10^{-5} SI, and NGR is ~2 cps. Lower clay abundance in Unit II is marked by an increase in L* at the boundary between Units I and II. At 92 m CSF, within Unit II, sharp decreases in the a* and b* reflectance parameters mark the change in sediment color from pale yellow to greenish gray. One of the most pronounced changes in physical properties at Site U1336 is the sharp increase in velocity that accompanies the change from nannofossil ooze to nannofossil chalk at the boundary between Units II and III. The velocity at the base of Unit II is ~1700 m/s. Below 190 m CSF, in Unit III, the rate at which velocity increases with depth increases, ultimately reaching ~2200 m/s at 290 m CSF, near the base of Hole U1336A.

STMSL data were collected at 5 cm intervals from Hole U1336B and compared to the WRMSL data obtained at 2.5 cm resolution from Hole U1336A during Expedition 320. Features in the magnetic susceptibility and gamma ray attenuation density are well aligned between Holes U1336A and U1336B to a depth of ~94 m CCSF-A. Below 94 m CCSF-A, the magnetic susceptibility signal drops to very low values but the density data are good enough to sustain a correlation to interval 320-U1334B-14H-4, 122 cm. At this point (138.50 m CCSF-A) sediments recovered in both holes are disturbed.

Paleomagnetic reversals were used to calculate the average LSR for the upper 74 m of the section at Site

U1336 on the corrected core composite depth below seafloor (CCSF-B; see **"Corrected core composite depth scale"** in the "Methods" chapter) depth scale. Below 74 m CSF only biostratigraphic datums were used to calculate the average LSR. The LSR at Site U1336 decreases from 15 m/m.y. in the upper Oligocene to 12 m/m.y. in the lower Miocene and stays relatively constant at 9 m/m.y. in the remainder of the section.

Standard geochemical analyses of pore water and organic and inorganic sediment properties were undertaken on Site U1336 samples. Alkalinity is relatively constant at values >2.5 mM in the upper 110 m CSF, with a pronounced decline to 1 mM by 170 m CSF. Sulfate concentrations decrease with depth to values as low as 22 mM. Dissolved manganese has a broad peak in the depth range from ~25 to 120 m CSF, and dissolved iron appears then peaks below 100 m CSF. The increase of dissolved iron occurs where Mn decreases downhole. Concentrations of dissolved silicate increase with depth from <400 to 800 µM.

Highlights

Miocene sedimentary section and cyclic sedimentation

One of the highlights from Site U1336 is the recovery of a thick Miocene carbonate section from the central equatorial Pacific, one of the high-priority objectives of the PEAT program. We recovered the complete early Miocene sequence (7.1 m.y. duration) in a ~110 m thick section, with a sedimentation rate of 12 m/m.y. and the middle Miocene sequence (4.4 m.y. duration) in a ~45 m thick interval with a sedimentation rate of ~21 m/m.y. These high sedimentation rates will facilitate the study of paleoceanographic processes at unprecedented resolution for the equatorial Pacific.

The obvious variations of both color and biogenic composition within nannofossil oozes represent cyclic fluctuations of CCD and upwelling intensity during the middle Miocene through early Miocene. The variable lithology also results in the variations of many petrophysical signals of physical properties including L*, b*, magnetic susceptibility, NGR, and GRA bulk density.

Oligocene–Miocene transition and depth transects

Site U1336 was planned as part of a latitudinal transect for early Miocene age slices and the PEAT Oligocene–Miocene depth transect compound in conjunction with Sites U1335 and U1337. The Miocene sequence at these sites includes the critical intervals of the Mi-1 glaciation and middle Miocene ice sheet expansion (Holbourn et al., 2005; Zachos et al., 2001b; Pälike et al., 2006b). The dominant lithologies of nannofossil ooze and chalk at Sites U1336 and U1335, with good preservation of calcareous microfossils, will allow us to achieve the prime objective for this site.

The Oligocene–Miocene transition in Hole U1336A occurs in homogeneous nannofossil ooze within the alternations of white and light greenish gray ooze. The same alternating sequence is observed above the Oligocene–Miocene transition at Site U1334. Biostratigraphy reveals that the Oligocene/Miocene boundary exists between 142.96 and 145.9 m CSF at Site U1336; this will allow the high-resolution study of this critical interval.

Geochemical front

Site U1336 recovered an interval of greenish gray carbonates that exhibit a distinct peak in dissolved Fe concentrations in pore water with similar characteristics as geochemical alteration fronts at Sites U1334 and U1335. At Site U1336, this zone is ~200 m thick. The remanent magnetization intensity is very weak in most parts of this section (80–180 m CSF). High dissolved Fe and Mn concentrations in pore water are caused by changes in the oxidation state of the sediments. The oxidation-reduction reactions are likely fueled by variable availability of organic carbon in the sediments. This site may provide the opportunity to study organic matter degradation.

Site U1336 migrated from south to north through the equatorial belt of high productivity. Based on paleolatitude reconstructions these geochemical alteration fronts can be mapped to similar equatorial positions between Sites U1334 and U1335, roughly between the Equator and ~4°N.

Chert formation in the early Oligocene

The sequence at Site U1336 includes barren intervals of radiolarian fossils and many thin intercalated chert layers and fragments. The radiolarians decrease in preservation downsection and disappear below Core 320-U1336A-19H. Instead, the sediments contain several chert fragments. Some inferred chert layers occur at ~120–140 m CSF and blocked APC penetration. Below ~190 m CSF, various colored chert layers and fragments occurred within the cores. The chert frequently contains foraminifer tests, reflecting diagenetic process of dissolution and reprecipitation of the biogenic silica.

The dissolution of biogenic silica is the source of porcellanite and chert and, on crust younger than 65 Ma, almost all cherts in the Pacific Ocean lie <150 m above basement. Although we did not recover basement rocks at this site, the sediments became hard, lithified limestones and the drilled section is probably close to basement. The dissolution of silica in the

basal sedimentary section is likely associated with the circulation of warm hydrothermal waters in the upper oceanic crust that extend into the lower sediments where they are cut by fractures and faults (Moore, 2008a, 2008b). This site will provide information on chert formation in the equatorial Pacific regions.

Site U1337

The latest Oligocene through the middle Miocene appears to have been a time of relative warmth comparable to the latest Eocene. However, variability in the isotopic record of the early to middle Miocene is larger than that of the Eocene and may indicate more variability in climate and global ice volume. Site U1337 (proposed Site PEAT-7C; 3°50.009′N, 123°12.352′W; 4463 mbsl) (Fig. F75; see Table T1 in the "Site U1337" chapter) was targeted to collect an early middle Miocene segment of the PEAT equatorial megasplice on ~24 Ma crust between the Galapagos and Clipperton Fracture Zones, ~390 km southeast of Site U1335. In conjunction with Sites U1335 and U1336, it was also designed to provide a latitudinal transect for early Miocene age slices. The recovered sediment column at Site U1337 represents a nearly complete and continuous Neogene sedimentary section.

Operations

Four holes were cored at Site U1337. In Hole U1337A, APC cores were taken from the seafloor to 195.5 m DSF (Cores 321-U1337A-1H through 21H). Nonmagnetic core barrels were used for all APC cores except for Core 321-U1337A-21H. FlexIt core orientation was conducted for all cores except Core 321-U1337A-1H. In addition, five successful APCT-3 temperature measurements were taken with Cores 321-U1337A-5H, 7H, 9H, 11H, and 13H. XCB coring continued with Cores 321-U1337A-22X through 48X. The sediment/basement contact was recovered at the base of Core 321-U1337A-48X. Three logging strings (triple combo, FMS-sonic, and Versatile Seismic Imager [VSI]) were deployed in Hole U1337A.

In Hole U1337B, APC cores were taken from the seafloor to 245.2 m DSF (Cores 321-U1337B-1H through 27H). Nonmagnetic core barrels were used through Core 321-U1337B-20H. The FlexIt core orientation tool was deployed successfully for all but two APC cores (321-U1337B-17H and 18H). FlexIt and steel core barrels were used through Core 321-U1337B-27H. APCT-3 measurements were obtained with Cores 321-U1337B-15H, 17H, and 19H. Coring continued with a single XCB core (321-U1337B-28X) to 251.9 m DSF; however, this barrel could not be recovered and Hole U1337B was abandoned prematurely.

Hole U1337C was cored to recover sections that were missing from Holes U1337A and U1337B. APC cores were taken from the seafloor to 11.4 m DSF (Cores 321-U1337C-1H through 2H) using nonmagnetic core barrels and the FlexIt core orientation tool. A wash barrel (Core 321-U1337C-3W) was then deployed, and the hole was washed to 169.4 m DSF. APC coring resumed at that depth and continued through Core 321-U1337C-9H to 221.3 m DSF and then switched to steel core barrels. Coring with the XCB system continued with Cores 321-U1337C-10X through 33X. Basement was recovered in Core 321-U1337C-33X.

Hole U1337D was planned to target the few remaining areas that had yet to be fully recovered and to duplicate recovery through those sections of the formation already recovered to provide additional sample material. The most troublesome material encountered in the previous holes was the large diatom mats located directly above and below a hard ~0.4 m thick porcellanite layer. In Hole U1337D, APC cores were taken from the seafloor to 237.7 m DSF (Cores 321-U1337D-1H to 26H). Nonmagnetic core barrels were used through Core 321-U1337D-20H. The first XCB core (321-U1337D-27X) was designed to only core through the hard ~0.4 m thick porcellanite layer. The APC was once again deployed and cored to 267.0 m DSF (Cores 321-U1337D-28H through 30H). At this point the XCB coring system was once again deployed for Cores 321-U1337D-31X through 49X to a total depth of 442.9 m DSF. The FlexIt core orientation tool was deployed successfully with all APC cores. The SET was deployed for the first time from the *JOIDES Resolution* after Core 321-U1337D-17X at 298.1 m DSF.

Lithostratigraphy

At Site U1337, latest Oligocene seafloor basalt is overlain by ~450 m of nannofossil and biosiliceous oozes and nannofossil chalks that are divided into four lithologic units (Fig. F76). The Pleistocene through uppermost Miocene sediments of lithologic Unit I are characterized by multicolored (various hues of white, brown, green, and gray) nannofossil oozes, diatom oozes, and radiolarian oozes that alternate on meter scales with a general downsection increase in siliceous microfossils relative to nannofossils. The uppermost Miocene to middle Miocene lithologic Unit II is dominated by meter-scale interbeds of greenish gray biosiliceous sediments with white to light greenish gray nannofossil ooze. Within the unit are numerous diatom mat deposits. Meter-scale color alternations in Units I and II are associated with variations in lithology and physical properties. However, similar to the common millimeter- and

centimeter-scale color banding that do not mark compositional changes, they are likely associated with sediment redox conditions. White, pale yellow, and pale green nannofossil oozes and chalks dominate the sediments of middle Miocene to latest Oligocene age, although diatoms and radiolarians remain present in low abundances. Seafloor basalt (lithologic Unit IV) was recovered at the base of the sedimentary section, dated as latest Oligocene.

Biostratigraphy

All major microfossil groups occur in the sediments recovered at Site U1337. Planktonic foraminifers at Site U1337 are rare to abundant with poor to good preservation throughout most of the succession but are absent or extremely rare in some intervals of the upper Miocene and lower Miocene. Biozones PT1b to O6 are recognized, with the exception of Zones PL4, M12, and M3 (Fig. F76). Calcareous nannofossils at Site U1337 are moderately to poorly preserved and some samples with high silica content are barren. Nannofossil Zones NN1 to NN21 are present, indicating an apparently complete sequence. The radiolarian stratigraphy at Site U1337 spans the interval from the uppermost part of Zones RN16–RN17 (upper Pleistocene) to RN1 (lower Miocene). The radiolarian assemblages of Pleistocene to upper Miocene age tend to have good preservation, whereas middle to lower Miocene assemblages show moderate preservation. In the lowermost part of the section, above the basement, sediments are barren of radiolarians. The high-resolution diatom stratigraphy at Site U1337 spans the interval from the *Fragilariopsis* (*Pseudoeunotia*) *doliolus* Zone (upper Pleistocene) to the lowermost part of the *Craspedodiscus elegans* Zone (lower Miocene). The diatom assemblage is generally well to moderately preserved throughout the recovered section; however, in several intervals valve preservation becomes moderate to poor. The base of the sediment column is barren of diatoms. The nannofossil, foraminifer, radiolarian, and diatom datums and zonal schemes generally agree, though some discrepancies occur in the lowest part of the core. Benthic foraminifers occur continuously throughout the succession recovered in Hole U1337A and show good to moderate preservation. The overall assemblage composition indicates lower bathyal to abyssal paleodepths.

Stratigraphic correlation

Stratigraphic correlation provided a complete spliced record to ~220 m CCSF-A. Several gaps were encountered over the next 50 m CCSF-A. Comparison of GRA density records with well logging density data suggest that no more than 1 m of section was lost in any of the gaps. Correlation between the holes was broken again several times between 440 m CCSF-A and basement at 490 m CCSF-A. Growth factor for the correlation was 1.12. The linear sedimentation rate decreases from ~21 m/m.y. in the middle Miocene to 17 m/m.y. in the late Miocene.

Paleomagnetism

Paleomagnetic measurements were conducted on archive-half sections of 20 APC cores and 14 XCB cores from Hole U1337A, 27 APC cores from Hole U1337B, 8 APC cores from Hole U1337C, and 30 APC cores from Hole U1337D. The FlexIt core orientation tool was deployed in conjunction with all APC cores, and we conclude that the FlexIt orientation data are generally reliable. Measurements of NRM above ~93 m CSF indicate moderate magnetization intensities (on the order of 10^{-3} A/m) with a patchy but generally weak VRM or IRM drilling overprint, and polarity reversal sequences from Chrons C1n to C3r (0 to ~6 Ma) are recognized. Below ~93 m CSF, remanent intensities after AF demagnetization of 20 mT are reduced to values close to magnetometer noise level in the shipboard environment (~2×10^{-5} A/m). In this zone, sediment magnetizations have been partly overprinted during the coring process, and remanent inclinations are occasionally steep after AF demagnetization at a peak field of 20 mT. Nonetheless, polarity reversals are apparently recorded to ~200 m CSF and are provisionally correlated to the GPTS from Chrons C3An to C5n (~6–11 Ma) (Fig. F76). Magnetic polarity interpretation was impossible for APC cores taken with steel core barrels and XCB cores because of severe magnetic overprint during coring.

Physical properties

Physical property measurements comprised WRMSL measurements of magnetic susceptibility, bulk density, and *P*-wave velocity; NGR; and measurements of color reflectance, followed by discrete measurements of moisture and density properties, sound velocities, and thermal conductivity. Physical property measurements on whole-round sections and samples from split cores display a strong lithology-dependent variation at Site U1337 (Fig. F76). Variations in the abundances of nannofossils, radiolarians, diatoms, and clay in lithologic Unit I account for high-amplitude, high-frequency variations of all physical properties. Intervals enriched in biogenic silica and clay generally display lower grain density and bulk density and higher porosity, magnetic susceptibility, and NGR. Velocity is generally directly related to bulk density; however, it is commonly higher in low-density siliceous-rich sediments than it is in more calcareous intervals. Wet bulk density is low in Unit I, ranging

from 1.12 to 1.46 g/cm³. Porosity is as high as 92% in this unit. Velocity also is low, averaging 1525 m/s. The natural gamma record, as at previous sites, is marked by an anomalously high near-surface peak (~65 cps). Magnetic susceptibility varies between 4×10^{-5} and 18×10^{-5} SI. The color of Unit I is characterized by the lowest L* and high and variable a* and b* values. Lithologic Unit II is characterized by a continued high variability in grain density. Together, the grain density in Units I and II averages 2.51 g/cm³ and ranges from 2.17 to 2.85 g/cm³. All other physical properties display less variability in Unit II than in Unit I, reflecting a less variable lithology. Wet bulk density increases and porosity decreases with depth in Unit II; however, in Units II and III these trends are interrupted by low-density high-porosity diatom- and radiolarian-rich intervals. Unit II is slightly lighter colored (lower L*) and distinctly more blue (lower a*) and green (lower b*) than Unit I. Unit III is characterized by more uniform physical properties that accompany the high and uniform carbonate composition of the unit. The nannofossil oozes and chalks of this unit are characterized by a uniform grain density that averages 2.67 g/cm³. The bulk density and porosity trends of Unit II continue in Unit III. The transition from ooze to chalk is marked by a change in gradient of these properties to a more rapid decrease in wet bulk density and an increase in porosity with depth. Wet bulk density and porosity at the base of the sediment section are 1.95 g/cm³ and 47%, respectively. The increase in velocity with depth also changes to a higher gradient in Unit III, with values increasing from 1510 m/s at ~340 m CSF to ~1800 m/s near the base of the hole. Magnetic susceptibility and NGR values remain low in Unit III but do vary in response to small changes in lithology. The sharp color change from greenish gray to pale yellow at ~410 m CSF is marked by a sharp increase in a* and b*. The change in color to pale brown chalk immediately above basement is marked by an increase in both a* and b* and a decrease in L*.

Downhole logging

Three downhole logging tool strings were deployed in Hole U1337A. Two tool strings took measurements of NGR radioactivity, bulk density, electrical resistivity, elastic wave velocity, and borehole resistivity images in the 77–442 m WSF depth interval. The third tool string measured seismic waveforms in a VSP experiment in the 214–439 m WSF depth interval. Measurement depths were adjusted to match across different logging runs, obtaining a wireline log matched depth below seafloor (WMSF) depth scale. The downhole log measurements were used to define three logging units. Unit 1 (77–212 m WMSF)

and Unit 2 (212–339 m WMSF) have average densities of ~1.3 and ~1.6 g/cm³, respectively, that do not show any trend with depth, whereas Unit III (339–442 m WMSF) density increases with depth, reaching 1.85 g/cm³ at the base of the hole (Fig. F77). Resistivity and *P*-wave velocity follow a pattern similar to that of density, suggesting that the major control on these physical properties are variations in sediment porosity. NGR measurements are low throughout the logged interval (~5 gAPI), except for two pronounced peaks caused by uranium, one at the seafloor and the other at 240 m WMSF. The gamma ray peak at 240 m WMSF corresponds to the ~40 cm thick pocellanite layer that has only been recovered as rubble in the cores but can be clearly identified in the downhole logs and borehole images as an interval of high density and resistivity. VSP logging measured arrival time of the seismic pulse from the sea surface at 16 stations. Together with the traveltime to the seafloor, VSP measurements are the basis for a traveltime-depth conversion that allows seismic reflectors to be correlated to stratigraphic events. Downhole temperature measurements and thermal conductivities of core samples were combined to estimate a geothermal gradient of 32.4°C/km and a heat flow of 28.4 mW/m² at Site U1337.

Geochemistry

A total of 85 interstitial water samples were collected from Hole U1337A, 49 using the whole-round squeezing approach across the entire hole and 36 in the upper 100 m by Rhizon sampling. Alkalinity increases slightly downhole from ~2.7 mM in the upper 100 m to values scattered around 3.8 mM below 300 m CSF. Sulfate concentrations vary between 26 and 29 mM, with slightly decreasing values with depth. A dissolved manganese peak of ~150 µM at 13 m CSF is captured by the high-resolution interstitial water sampling. Dissolved iron is sporadically detectable in the upper 200 m and then increases to a peak of ~5 µM between 275 and 300 m CSF before becoming undetectable again below 400 m CSF. These variations in manganese and iron reflect changes in redox chemistry that also manifest as changes in sediment color. Calcium carbonate and inorganic carbon concentrations were determined on 283 and 28 sediment samples from Holes U1337A and U1337B, respectively. Calcium carbonate contents vary greatly in the upper two lithologic units, ranging from 30 to 90 wt% (Fig. F76). In lithologic Unit III calcium carbonate contents are generally high, scattered around 80 wt%, but a distinctive decrease is observed between 350 and 400 m CCSF-A. In the upper 235 m CCSF-A, TOC content ranges between 0.10 and 0.34 wt% except for the high value of

0.72 wt% in the uppermost sample. TOC content increases at 44.00 m CCSF-A and in the interval from 87.28 to 108.59 m CCSF-A. Below 235 m CCSF-A, TOC values are generally <0.10 wt%.

Shipboard geochemical analyses of interstitial water and bulk sediment samples reflect large variations in sediment composition resulting from shifts in carbonate versus opal production. The large-scale redox state and diagenetic processes of the sediment column are related to overall changes in sediment composition. Interstitial water chemistry is also influenced by the porcellanite layer forming a barrier to diffusion at ~240 m CSF and by seawater circulation in the basement. The basement itself appears to exert little influence on the geochemistry of sediments and interstitial waters.

Highlights

Diatom mat deposition

Lithologic Unit II at Site U1337 is mostly composed of biosiliceous lithologies, notably diatoms. The abundance of diatoms in the middle and upper Miocene section at Site U1337 is much higher than encountered in any interval at Sites U1331–U1336. Several decimeter- to meter-scale intervals of diatom ooze are laminated, and smear slide analyses indicate that the diatom assemblage is composed primarily of pennate taxa, with abundant "needlelike" *Thalassiothrix* spp., indicating diatom mat deposition. The lowermost laminated diatom mat is in the upper portion of Unit III at ~15 Ma. Much thicker intervals are present in Unit II at roughly 10 Ma and shorter intervals at ~4.5 Ma. Ages of laminated diatom mats at this site are similar to those found at Leg 138 sites farther to the east (Mayer, Pisias, Janecek, et al., 1992), which have been interpreted to reflect regional bursts of silica export in the eastern equatorial Pacific (Kemp and Baldauf, 1993). No laminated diatom oozes were recorded during Expedition 320 at drill sites farther to the northwest.

Oligocene–Miocene transition

The Oligocene/Miocene boundary was recovered in Holes U1337A, U1337C, and U1337D. In Hole U1337A, the Oligocene/Miocene boundary is estimated to fall between Samples 321-U1337A-48X-2, 85–87 cm, and 48X-3, 55 cm (445.56–446.75 m CSF; 490.92–492.11 m CCSF-A). It occurs in white (2.5Y 8/1) nannofossil chalk with foraminifers, interbedded and heavily mottled with pale yellow (2.5Y 7/4) to very pale brown (10YR 7/4) nannofossil chalk. Abundant millimeter-scale dendritic manganese oxide grains occur throughout this interval. The lower 15 cm of the core catcher of Core 321-U1337A-48X is basaltic basement. No prominent change in lithology, GRA

bulk density, reflectance, or magnetic susceptibility is seen through the Oligocene–Miocene transition.

Neogene carbonate dissolution

The CCD of the Neogene is much more stable than that of the Eocene, but there are intervals of lower carbonate deposition at Site U1337 that probably represent significant changes of the Neogene CCD. In the early Miocene, a significant carbonate low reaches its minimum at ~17 Ma (340 m CSF in Hole U1337A), when the site was at a depth of ~3500 meters below sea level. This early Miocene interval marks a strong minimum at Site U1334 as well, on crust with a depth of ~4000 m at that time. Highly variable carbonate is also characteristic of the late/middle Miocene boundary interval, but the role of carbonate dissolution versus elevated deposition of biosilica needs to be determined.

Site U1338

Site U1338 (proposed Site PEAT-8D; 2°30.469'N, 117°58.178'W; 4200 mbsl) (Figure **F78;** see Table **T1** in the "Site U1338" chapter) was sited to collect a 3–18 Ma segment of the PEAT equatorial megasplice and is located on ~18 Ma crust just north of the Galapagos Fracture Zone, 324 nmi (600 km) southeast of Site U1337 (Fig. **F78**). A seamount (3.7 km water depth) with surrounding moat is found ~25 km north-northwest of Site U1338 at the downslope end of the survey area. Originally a site was chosen ~10 km from the seamount (proposed Site PEAT-8C). However, the alternate proposed site was selected and drilled uphill and further away from the seamount to avoid possible turbidites, as were found near seamounts during drilling of Expedition 320 Sites U1331 and U1335. The recovered sediment column at Site U1338 represents a nearly complete and continuous lower Miocene to Holocene sedimentary section.

Operations

Four holes were cored at Site U1338. From Hole U1338A, APC cores were taken from the seafloor to 221.2 m DSF (Cores 321-U1338A-1H through 24H) using nonmagnetic core barrels and the FlexIt core orientation tool installed. FlexIt and steel core barrels were used for Cores 321-U1338A-25H and 26H. In addition, five successful APCT-3 temperature measurements were taken with Cores 321-U1338A-5H, 7H, 9H, 11H, and 13H. XCB coring continued with Cores 321-U1338A-27X through 44X. A small piece of basement was recovered in the core catcher of Core 321-U1338A-44X.

From Hole U1338B, APC cores were taken from the seafloor to 188.1 m DSF (Cores 321-U1338B-1H

through 20H) except for a short drilled interval of 2.5 m from 235.6 to 238.1 m DSF to adjust the core breaks. Nonmagnetic core barrels and the FlexIt core orientation tool were used through Core 321-U1338B-20H. FlexIt and steel core barrels continued through Core 321-U1338B-42H to 387.4 m DSF. Coring continued with three XCB cores (321-U1338B-43X through 45X) to 416.1 m DSF. Basement contact was recovered in Core 321-U1338B-45X. Three logging strings (triple combo, FMS-Sonic, and VSI) were deployed in Hole U1338B.

Hole U1338C was cored to recover sections that were missing from Holes U1338A and U1338B. APC cores were taken from the seafloor to 189.8 m DSF (Cores 321-U1338C-1H through 21H) using nonmagnetic core barrels and the FlexIt core orientation tool. FlexIt and steel core barrels were used through Core 321-U1338C-44H to 396.9 m DSF. Coring continued through Core 321-U1338C-47H to a total depth of 414.4 m DSF, which, at the time, set a new all time depth record for the APC.

Hole U1338D was primarily planned to recover a few "instructional" cores to be used during Expedition 323. Three APC cores were cut to 23.9 m DSF.

Lithostratigraphy

At Site U1338, ~415 m of nannofossil ooze and chalk with varying concentrations of diatoms and radiolarians overlie the seafloor basalt and are divided into three lithologic units (Fig. F79). Pleistocene through middle Pliocene sediments of Unit I are characterized by multicolored (various hues of white, brown, green, and gray) nannofossil ooze, diatom nannofossil ooze, and radiolarian nannofossil ooze that alternate on a decimeter to meter scale. Light green and light gray nannofossil ooze with occasional darker intervals with abundant siliceous microfossils, notably diatoms, comprise the upper Miocene to middle Pliocene Unit II. Decimeter-, meter- and tens of meters–scale color alternations in Units I and II are associated with variations in lithology and physical properties. Some of these color changes, as well as common millimeter- and centimeter-scale color banding, are not associated with compositional changes and likely reflect variations in sediment redox state. White, pale yellow, light greenish gray, and very pale brown nannofossil oozes and chalks dominate Unit III of the lower to upper Miocene, although slightly darker green and gray intervals with larger amounts of siliceous microfossils remain present. Seafloor basalt (Unit IV) was recovered at the base of the sedimentary section, overlain by lower Miocene sediments.

Biostratigraphy

All major microfossil groups have been found in the ~415 m thick succession of Holocene to lower Miocene sediment bulge recovered from Site U1338. Calcareous nannofossils at Site U1338 are in general moderately preserved, but there are some intervals in which the preservation is good or poor. Nannofossil Zones NN4 to NN21 are present, indicating an apparently complete sequence. Planktonic foraminifers vary from rare to abundant, with moderate to good preservation throughout most of the succession, but are absent or rare in a short interval in the upper Miocene. Planktonic foraminifer Zones PT1b (upper Pleistocene) to M2 (lower Miocene) are documented, with the exception of Zones PL4, M12, and M6. The radiolarian stratigraphy spans the interval from the uppermost part of Zones RN16–RN17 (upper Pleistocene) to the uppermost part of Zone RN3 (lower Miocene). Radiolarian assemblages show good to moderate preservation except in the lowermost portion (lower Miocene), which is barren of radiolarians. The high resolution diatom stratigraphy spans the interval from the *Fragilariopsis (Pseudoeunotia) doliolus* Zone (upper Pleistocene) to the lowermost part of the *Craspedodiscus elegans* Zone (lower Miocene). The diatom assemblage is generally well to moderately preserved throughout the recovered section; however, there are several intervals in which valve preservation becomes moderate to poor. The nannofossil, foraminifer, radiolarian, and diatom datums and zonal schemes generally agree, with some inconsistencies (Fig. F79). Benthic foraminifers occur continuously throughout the succession recovered in Hole U1338A and show generally good preservation. The overall assemblage composition indicates lower bathyal to abyssal paleodepths.

Stratigraphic correlation

Stratigraphic correlation provided a complete spliced record to a depth of ~260 m CCSF-A. Several gaps were seen between 280 and 360 m CCSF-A. Comparison of GRA density records with well logging density data suggests that no more than 1 m of section was lost in any of the gaps. Correlation between the holes became difficult again several times between 435 m CCSF-A and basement at 460 m CCSF-A. The growth factor for the correlation was 1.11. The linear sedimentation rate decreases from ~29 m/m.y. in the Miocene to 13 m/m.y. in the Pliocene–Pleistocene.

Paleomagnetism

Paleomagnetic measurements were conducted on archive-half sections of 26 APC cores from Hole U1338A, 42 APC cores from Hole U1338B, and 47 APC cores from Hole U1338C. The FlexIt core orien-

tation tool was deployed in conjunction with all APC cores except for the deepest three cores of Hole U1338C, and we conclude that the FlexIt orientation data are generally reliable. NRM measurements indicate moderate magnetization intensities (on the order of 10^{-3} A/m) for depth intervals 0–50, 280–225, and 295–395 m CSF. Polarity reversal sequences of these intervals are provisionally correlated to Chrons C1n to C2Ar (0 to ~4 Ma), Chrons C4An to C5n (~9–11 Ma), and Chrons C5r to C5Br (~12–16 Ma) of the GPTS, respectively (Fig. F79). Except for these intervals, remanent magnetic intensities after AF demagnetization of 20 mT are reduced to values close to magnetometer noise level in the shipboard environment (~2 × 10^{-5} A/m). Magnetization directions are dispersed and not interpretable there.

Physical properties

Physical property measurements comprised WRMSL measurements of magnetic susceptibility, bulk density, and *P*-wave velocity; NGR; and measurements of color reflectance, followed by discrete measurements of moisture and density properties, sound velocities, and thermal conductivity. Physical property measurements on whole-round sections and samples from split cores display a variation strongly dependent on the relative abundance of biosiliceous and calcareous sediment components at Site U1338. As at Site U1337, intervals enriched in siliceous microfossils and clay generally display darker colors, lower grain density and bulk density, and higher porosity, magnetic susceptibility, and NGR. The variation of velocity is more complex in that it is dependent on both the wet bulk density and the sediment rigidity. These parameters vary independently with the variation in abundance of biosiliceous and calcareous components. The physical properties at Site U1338 also display cyclicity on multiple scales, a decimeter to meter scale and a scale with a spacing on the order of tens of meters.

Lithologic Unit I at Site U1338 is characterized by low wet bulk density that decreases from 1.4 g/cm³ near the seafloor to 1.2 g/cm³ at the base of the unit as a result of an increasing abundance of radiolarians and diatoms with depth. The grain density in Units I and II displays a greater variability than is found deeper at the site as a result of the greater variability in the abundance of biosiliceous and calcareous components. The average grain density for Units I and II is relatively low, at 2.59 g/cm³. The NGR signal at Site U1338 is characterized by a near-seafloor peak that is somewhat lower than those recorded at the other PEAT drill sites but extends deeper and is marked by a double peak. Spectral reflectance measurements show that Unit I is characterized by lower

L* and higher a* and b* values in the upper 25 m of Unit I (Fig. F79). Below 25 m CSF, the sediment becomes lighter colored (L* increases) and more bluish green (a* and b* decrease).

Unit II is characterized by increasing wet bulk density with depth to ~175 m CSF. Below this depth, an increase in the abundance of siliceous microfossils produces a broad density minimum. Magnetic susceptibility and NGR signals are low in Unit II to the depth at which the biosiliceous material increases in abundance. The interval of the broad density minimum is characterized by higher magnetic susceptibility values that are roughly equal to those in the upper 25 m of Unit I. Unit II is lighter colored than Unit I (higher L*) and more blue (lower b*).

Unit III at Site U1338 is characterized by a higher and more uniform carbonate content and, as a result, more uniform physical properties. Wet bulk density increases from ~1.5 g/cm³ at the top of Unit III to 1.7 g/cm³ at the base of the unit. Grain density varies over a narrower range in Unit III than it does in Units I and II and displays an average (2.64 g/cm³) nearer to that of calcite. Velocity, which through much of Units I and II is close to the velocity of water, displays a regular increase in Unit III, from ~1620 m/s at the top to ~1820 m/s near the base of the unit. Velocity gradient increases near the base of Unit III accompanying the transition from nannofossil ooze to chalk. Magnetic susceptibility is low from the boundary between Units II and III, at ~245 m CSF, to 300 m CSF. Below 300 m CSF, susceptibility again increases to values comparable to those in the upper part of Unit I. NGR variability is lower in Unit III than in Unit II and remains uniformly low throughout the unit. Overall, Unit III is the lightest colored (highest L* values) unit at Site U1338. The transition from greenish gray to pale yellow is marked at ~385 m CSF by a shift to higher values of both a* and b*.

Downhole logging

Three downhole logging tool strings were deployed in Hole U1338B: a modified triple combo (that did not include a neutron porosity measurement), an FMS-sonic combination, and a VSI seismic tool with a Scintillation Gamma Ray (SGT-N) sonde. The modified triple combo and FMS-sonic tool strings took downhole measurements of natural gamma ray radioactivity, bulk density, electrical resistivity, elastic wave velocity, and borehole resistivity images in the 125–413 m WSF depth interval. The VSI seismic tool string measured seismic waveforms in a VSP experiment that covered the 189.5–414.5 m WSF depth interval. Measurement depths were adjusted to match across different logging runs, obtaining the WMSF depth scale.

Downhole log measurements were used to define three logging units: Unit I (139–244 m WMSF) and Unit II (244–380 m WMSF) have average densities of ~1.45 and ~1.6 g/cm³, respectively, that do not show any trend with depth, whereas in Unit III (from 380 m WMSF) density increases with depth, reaching 1.7 g/cm³ at the base of the hole (Fig. **F80**). Resistivity and *P*-wave velocity follow a pattern similar to that of density throughout the logged interval, suggesting that the major control on these physical properties are variations in sediment porosity. Both resistivity and density measurements show a small-scale peak at 280 m WMSF. This peak at 280 m WMSF is clearly visible in the borehole resistivity images as a high-resistivity layer 16 cm thick, and it corresponds to a chert layer that has only been recovered as rubble in the cores. Natural gamma ray measurements are low throughout (~4 gAPI) but do show a pronounced high at the seafloor caused by a local increase in uranium concentration.

In the VSP experiment, the arrival time of a seismic pulse was measured from the sea surface at 14 stations. Together with the traveltime to the seafloor, the VSP measurements are the basis for a traveltime-depth conversion that allows seismic reflectors to be correlated to stratigraphic events. Downhole temperature measurements and thermal conductivities of core samples were combined to estimate a geothermal gradient of 34.4°C/km and a heat flow of 33.6 mW/m² at Site U1338.

Geochemistry

A standard shipboard suite of geochemical analyses of pore water and organic and inorganic sediment properties was undertaken on samples from Site U1338. Alkalinity increases slightly downhole from ~2.7 mM at the sediment/water interface to peak slightly above 4 mM at 140 m CSF. A large dissolved manganese peak of 150 mM at 10 m CSF is captured by the high-resolution interstitial water sampling and is remarkably similar to that observed at Site U1337. These peaks are >10 times larger than the highest dissolved manganese concentrations encountered during Expedition 320. Lithium concentrations decrease from ~26 µM at the surface to a minimum of ~3 µM at ~250 m CSF before increasing sharply with depth to seawater values at the base of the section. The interstitial water strontium profile is a mirror image to that of lithium except the decrease from the peak of 400 µM at 200 m CSF is punctuated by a sharp drop of >100 µM between ~260 and 290 m CSF. The lithium and strontium profiles indicate seawater circulation in the basement as their values tend toward seawater values near the basement.

Calcium carbonate contents range between 26 and 88 wt% with substantial variability in the upper 273.31 m CCSF-A, corresponding to the alternation between calcite and opal production in the upper two lithologic units. Below 273.31 m CCSF-A (lithologic Unit III), calcium carbonate contents become relatively high and stable between 66 and 91 wt% compared with the upper part of the stratigraphic column (Fig. **F79**). In the upper ~230 m CCSF-A, TOC content is generally high and variable ranging between 0.09 and 0.46 wt%, whereas below ~230 m CCSF-A, TOC content is <0.09 wt%. Downhole TOC variability is most likely related to lithologic changes, with higher TOC being found in the more biosiliceous intervals.

Interstitial water and bulk sediment geochemistry reflect large variations in sediment composition resulting from shifts between carbonate and opal dominance. The large-scale redox state and diagenetic processes of the sediment column are related to overall changes in sediment composition. Interstitial water chemistry points to seawater circulation in the basement, although the basement itself appears to exert little influence on the geochemistry of the sediments and interstitial waters.

Highlights

Color changes, lithology, and redox state

Smear slide analyses and visual core descriptions show that many of the decimeter-, meter-, and tens of meters–scale color variations in lithologic Units I and II to some extent relate to changes in lithology (e.g., Fig. **F79**). We suspect, however, that some of these color variations, notably the transitions between pale green and pale yellow lithologies, are controlled by sediment redox state, similar to those recorded at Sites U1331–U1337 and earlier work in the equatorial Pacific Ocean (e.g., Lyle, 1983).

Magnetic susceptibility is moderately low in the light gray and light brown intervals in Unit I (Fig. **F79**). A significant decrease in magnetic susceptibility in Unit II suggests dissolution of magnetite resulting from intensified microbial Fe reduction. In the lower part of Unit III, a sharp downcore transition from green to yellow is not associated with any other lithologic change, does not occur at the same stratigraphic level between holes, and thus should not be considered as an equivalent time horizon. Pore water Fe concentrations reach 6 to 7 µM in the green interval, and Fe is absent below the transition to yellow and brown. Although some of this signal may be affected by seawater contamination during XCB drilling, all available information suggests that the lowermost color change represents a redox front.

Occurrence of diatom-rich layers

Lithologic Unit II at Site U1338 is mainly composed of nannofossil ooze with relatively high abundances of biosiliceous components, notably diatoms (Fig. **F79**). The relative abundance of diatoms is lower than that at Site U1337, and the record lacks laminated diatom ooze intervals (diatom mats) such as those observed at Site U1337. However, centimeter to sometimes 1–2 m thick diatom nannofossil ooze layers containing abundant specimens of *Thalassiothrix* spp. are occasionally interbedded with nannofossil ooze (e.g., ~126.2–127.1 and ~231.8–234.3 m CSF in Hole U1338A and ~127.3–128.0 and ~233.8–234.8 m CSF in Hole U1338C). Units II and III also contain significant amounts of pyrite, particularly in diatom-rich intervals in Unit II (e.g., Cores 321-U1338B-14H, 19H through 21H, 26H, 28H, 29H, and 32H through 41H). In addition, the middle part of Unit III contains thin intervals of abundant pyrite-filled siliceous microfossils (e.g., intervals 321-U1338B-33H-4, 58–66 cm, and 35H-5, 76–82 cm). These diatom-rich layers, pyrite nodule occurrences, and pyrite-rich siliceous microfossil layers in Units II and III are associated with high TOC content, suggesting a relation between the abundance of diatoms in the sediments, sediment redox state, and the export or preservation of organic carbon.

References

Abels, H.A., Hilgen, F.J., Krijgsman, W., Kruk, R.W., Raffi, I., Turco, E., and Zachariasse, W.J., 2005. Long-period orbital control on middle Miocene global cooling: integrated stratigraphy and astronomical tuning of the Blue Clay Formation on Malta. *Paleoceanography,* 20(4):PA4012. **doi:10.1029/2004PA001129**

Amante, C., and Eakins, B.W., 2008. *ETOPO1 1 Arc-Minute Global Relief Model: Procedures, Data Sources and Analysis:* Washington, DC (DOC/NOAA/NESDIS/NGDC).

Baldauf, J.G., and Iwai, M., 1995. Neogene diatom biostratigraphy for the eastern equatorial Pacific Ocean, Leg 138. *In* Pisias, N.G., Mayer, L.A., Janecek, T.R., Palmer-Julson, A., and van Andel, T.H. (Eds.), *Proc. ODP, Sci. Results,* 138: College Station, TX (Ocean Drilling Program), 105–128. **doi:10.2973/odp.proc.sr.138.107.1995**

Barker, P.F., 2001. Scotia Sea regional tectonic evolution: implications for mantle flow and palaeocirculation. *Earth-Sci. Rev.,* 55(1–2):1–39. **doi:10.1016/S0012-8252(01)00055-1**

Barron, J.A., 1985. Late Eocene to Holocene diatom biostratigraphy of the equatorial Pacific Ocean, Deep Sea Drilling Project Leg 85. *In* Mayer, L., Theyer, F., Thomas, E., et al., *Init. Repts. DSDP,* 85: Washington, DC (U.S. Govt. Printing Office), 413–456. **doi:10.2973/dsdp.proc.85.108.1985**

Billups, K., Pälike, H., Channell, J.E.T., Zachos, J.C., and Shackleton, N.J., 2004. Astronomic calibration of the late Oligocene through early Miocene geomagnetic polarity time scale. *Earth Planet. Sci. Lett.,* 224(1–2):33–44. **doi:10.1016/j.epsl.2004.05.004**

Bohaty, S.M., Pälike, H., Ridgwell, A., Zachos, J.C., and Lear, C.H., 2008. Timing and significance of a global deep-sea dissolution event during the Eocene–Oligocene transition. *Eos, Trans. Am. Geophys. Union,* 89(53)(Suppl.):PP41D-1487. (Abstract) **http://www.agu.org/meetings/fm08/waisfm08.html**

Bohaty, S.M., and Zachos, J.C., 2003. Significant Southern Ocean warming event in the late middle Eocene. *Geology,* 31(11):1017–1020. **doi:10.1130/G19800.1**

Bohaty, S.M., Zachos, J.C., Florindo, F., and Delaney, M.L., 2009. Coupled greenhouse warming and deep-sea acidification in the middle Eocene. *Paleoceanography,* 24(2):PA2207. **doi:10.1029/2008PA001676**

Coxall, H.K., Wilson, P.A., Pälike, H., Lear, C.H., and Backman, J., 2005. Rapid stepwise onset of Antarctic glaciation and deeper calcite compensation in the Pacific Ocean. *Nature (London, U. K.),* 433(7021):53–57. **doi:10.1038/nature03135**

Coxall, H.K., Wilson, P.A., Pearson, P.N., and Sexton, P.F., 2007. Iterative evolution of digital planktonic foraminifera. *Paleobiology,* 33(4):495–516. **doi:10.1666/06034.1**

DeConto, R.M., Pollard, D., Wilson, P.A., Palike, H., Lear, C.H., and Pagani, M., 2008. Thresholds for Cenozoic bipolar glaciation. *Nature (London, U. K.),* 455(7213):652–656. **doi:10.1038/nature07337**

Dore, J.E., Lukas, R., Sadler, D.W., and Karl, D.M., 2003. Climate-driven changes to the atmospheric CO_2 sink in the subtropical North Pacific Ocean. *Nature (London, U. K.),* 424(6950):754–757. **doi:10.1038/nature01885**

Dunkley Jones, T., Bown, P.R., Pearson, P.N., Wade, B.S., Coxall, H.K., and Lear, C.H. 2008. Major shifts in calcareous phytoplankton assemblages through the Eocene–Oligocene transition of Tanzania and their implications for low-latitude primary production. *Paleoceanography,* 23(4):PA4204. **doi:10.1029/2008PA001640**

Elderfield, H., and Schultz, A., 1996. Mid-ocean ridge hydrothermal fluxes and the chemical composition of the ocean. *Annu. Rev. Earth Planet. Sci.,* 24(1):191–224. **doi:10.1146/annurev.earth.24.1.191**

Elderfield, H., Yu, J., Anand, P., Kiefer, T., and Nyland, B., 2006. Calibrations for benthic foraminiferal Mg/Ca paleothermometry and the carbonate ion hypothesis. *Earth Planet. Sci. Lett.,* 250(3–4):633–649. **doi:10.1016/j.epsl.2006.07.041**

Engebretson, D.C., Cox, A., and Gordon, R.G., 1985. *Relative Motions between Oceanic and Continental Plates in the Pacific Basin.* Spec. Pap.—Geol. Soc. Am., 206.

Farrell, J.W., Raffi, I., Janecek, T.R., Murray, D.W., Levitan, M., Dadey, K.A., Emeis, K.-C., Lyle, M., Flores, J.-A., and Hovan, S., 1995. Late Neogene sedimentation patterns in the eastern equatorial Pacific Ocean. *In* Pisias, N.G., Mayer, L.A., Janecek, T.R., Palmer-Julson, A., and van Andel, T.H. (Eds.), *Proc. ODP, Sci. Results,* 138: College Station, TX (Ocean Drilling Program), 717–756. **doi:10.2973/odp.proc.sr.138.143.1995**

Funakawa, S., Nishi, H., Moore, T.C., and Nigrini, C.A., 2006. Radiolarian faunal turnover and paleoceanographic change around Eocene/Oligocene boundary in the central equatorial Pacific, ODP Leg 199, Holes 1218A, 1219A, and 1220A. *Palaeogeogr., Palaeoclimatol., Palaeoecol.,* 230(3–4):183–203. doi:10.1016/j.palaeo.2005.07.014

Gibbs, S., Shackleton, N.J., and Young, J., 2004. Orbitally forced climate signals in mid-Pliocene nannofossil assemblages. *Mar. Micropaleontol.,* 51(1–2):39–56. doi:10.1016/j.marmicro.2003.09.002

Gradstein, F.M., Ogg, J.G., and Smith, A. (Eds.), 2004. *A Geologic Time Scale 2004:* Cambridge (Cambridge Univ. Press). http://stratigraphy.science.purdue.edu/

Hays, J.D., et al., 1972. *Init. Repts. DSDP,* 9: Washington, DC (U.S. Govt. Printing Office). doi:10.2973/dsdp.proc.9.1972

Holbourn, A., Kuhnt, W., Schulz, M., and Erlenkeuser, H., 2005. Impacts of orbital forcing and atmospheric carbon dioxide on Miocene ice-sheet expansion. *Nature (London, U. K.),* 438(7067):483–487. doi:10.1038/nature04123

Huber, M., 2002. Straw man 1: a preliminary view of the tropical Pacific from a global coupled climate model simulation of the early Paleogene. *In* Lyle, M., Wilson, P.A., Janecek, T.R., et al., *Proc. ODP, Init. Repts.,* 199: College Station, TX (Ocean Drilling Program), 1–30. doi:10.2973/odp.proc.ir.199.103.2002

Kamikuri, S., Nishi, H., Moore, T.C., Nigrini, C.A., and Motoyama, I., 2005. Radiolarian faunal turnover across the Oligocene/Miocene boundary in the equatorial Pacific Ocean. *Mar. Micropaleontol.,* 57(3–4):74–96. doi:10.1016/j.marmicro.2005.07.004

Kemp, A.E.S., and Baldauf, J.G., 1993. Vast Neogene laminated diatom mat deposits from the eastern equatorial Pacific Ocean. *Nature (London, U. K.),* 362(6416):141–144. doi:10.1038/362141a0

Kennett, J.P., and Shackleton, N.J., 1976. Oxygen isotopic evidence for the development of the psychrosphere 38 Myr ago. *Nature (London, U. K.),* 260(5551):513–515. doi:10.1038/260513a0

Knappenberger, M., 2000. Sedimentation rates and Pacific plate motion calculated using seismic cross sections of the Neogene equatorial sediment bulge [M.Sc. thesis]. Boise State Univ., Idaho.

Koppers, A.A.P., Phipps Morgan, J., Morgan, J.W., and Staudigel, H., 2001. Testing the fixed hotspot hypothesis using $^{40}Ar/^{39}Ar$ age progressions along seamount trails. *Earth Planet. Sci. Lett.,* 185(3–4):237–252. doi:10.1016/S0012-821X(00)00387-3

Kunzendorf, H., Pflüger, W.L., and Friedrich, G.H., 1983. Uranium in Pacific deep-sea sediments and manganese nodules. *J. Geochem. Explor.,* 19(1–3):147–162. doi:10.1016/0375-6742(83)90014-6

Lanci, L., Parés, J.M., Channell, J.E.T., and Kent, D.V., 2004. Miocene magnetostratigraphy from equatorial Pacific sediments (ODP Site 1218, Leg 199). *Earth Planet. Sci. Lett.,* 226(1–2):207–224. doi:10.1016/j.epsl.2004.07.025

Lanci, L., Parés, J.M., Channell, J.E.T., and Kent, D.V., 2005. Oligocene magnetostratigraphy from equatorial Pacific sediments (ODP Sites 1218 and 1219, Leg 199). *Earth Planet. Sci. Lett.,* 237(3–4):617–634. doi:10.1016/j.epsl.2005.07.004

Lawver, L.A., and Gahagan, L.M., 2003. Evolution of Cenozoic seaways in the circum-Antarctic region. *Palaeogeogr., Palaeoclimatol., Palaeoecol.,* 198(1–2):11–37. doi:10.1016/S0031-0182(03)00392-4

Lear, C.H., Bailey, T.R., Pearson, P.N., Coxall, H.K., and Rosenthal, Y., 2008. Cooling and ice growth across the Eocene–Oligocene transition. *Geology,* 36(3):251–254. doi:10.1130/G24584A.1

Lear, C.H., Rosenthal, Y., Coxall, H.K., and Wilson, P.A., 2004. Late Eocene to early Miocene ice sheet dynamics and the global carbon cycle. *Paleoceanography,* 19(4):PA4015. doi:10.1029/2004PA001039

Liu, Z., Pagani, M., Zinniker, D., DeConto, R., Huber, M., Brinkhuis, H., Shah, S.R., Leckie, R.M., and Pearson, A., 2009. Global cooling during the Eocene–Oligocene climate transition. *Science,* 323(5918):1187–1190. doi:10.1126/science.1166368

Lowenstein, T.K., and Demicco, R.V., 2007. Elevated Eocene atmospheric CO_2 and subsequent decline. *Science,* 313(5795):1928. doi:10.1126/science.1129555

Lyle, M., 1983. The brown-green color transition in marine sediments: a marker of the Fe(III)-Fe(II) redox boundary. *Limnol. Oceanogr.,* 28:1026–1033.

Lyle, M., 2003. Neogene carbonate burial in the Pacific Ocean. *Paleoceanography,* 18(3):1059. doi:10.1029/2002PA000777

Lyle, M., Dadey, K.A., and Farrell, J.W., 1995. The late Miocene (11–8 Ma) eastern Pacific carbonate crash: evidence for reorganization of deep-water circulation by the closure of the Panama gateway. *In* Pisias, N.G., Mayer, L.A., Janecek, T.R., Palmer-Julson, A., and van Andel, T.H. (Eds.), *Proc. ODP, Sci. Results,* 138: College Station, TX (Ocean Drilling Program), 821–838. doi:10.2973/odp.proc.sr.138.157.1995

Lyle, M., Gibbs, S., Moore, T.C., Jr., and Rea, D.K., 2007. Late Oligocene initiation of the Antarctic Circumpolar Current: evidence from the South Pacific. *Geology,* 35:691–694.

Lyle, M., Liberty, L., Moore, T.C., Jr., and Rea, D.K., 2002. Development of a seismic stratigraphy for the Paleogene sedimentary section, central tropical Pacific Ocean. *In* Lyle, M., Wilson, P.A., Janecek, T.R., et al., *Proc. ODP, Init. Repts.,* 199: College Station, TX (Ocean Drilling Program), 1–21. doi:10.2973/odp.proc.ir.199.104.2002

Lyle, M., Olivarez Lyle, A., Backman, J., and Tripati, A., 2005. Biogenic sedimentation in the Eocene equatorial Pacific—the stuttering greenhouse and Eocene carbonate compensation depth. *In* Lyle, M., Wilson, P.A., Janecek, T.R., et al., *Proc. ODP, Init. Repts.,* 199: College Station, TX (Ocean Drilling Program), 1–35. doi:10.2973/odp.proc.sr.199.219.2005

Lyle, M.W., Pälike, H., Moore, T.C., Mitchell, N., and Backman, J., 2006. *Summary Report of R/V Roger Revelle Site Survey AMAT03 to the IODP Environmental Protection and*

Safety Panel (EPSP) in Support for Proposal IODP626: Southampton, U.K. (Univ. Southampton). http://eprints.soton.ac.uk/45921/

Lyle, M., Wilson, P.A., Janecek, T.R., et al., 2002. *Proc. ODP, Init. Repts.,* 199: College Station, TX (Ocean Drilling Program). doi:10.2973/odp.proc.ir.199.2002

Majewski, W., 2003. Water-depth distribution of Miocene planktonic foraminifera from ODP Site 744, southern Indian Ocean. *J. Foraminiferal Res.,* 33(2):144–154. doi:10.2113/0330144

Mayer, L., Pisias, N., Janecek, T., et al., 1992. *Proc. ODP, Init. Repts.,* 138: College Station, TX (Ocean Drilling Program). doi:10.2973/odp.proc.ir.138.1992

Mayer, L.A., 1991. Extraction of high-resolution carbonate data for palaeoclimate reconstruction. *Nature (London, U. K.),* 352(6331):148–150. doi:10.1038/352148a0

Mayer, L.A., Shipley, T.H., Theyer, F., Wilkens, R.H., and Winterer, E.L., 1985. Seismic modeling and paleoceanography at Deep Sea Drilling Project Site 574. *In* Mayer, L., Theyer, F., Thomas, E., et al., *Init. Repts. DSDP,* 85: Washington, DC (U.S. Govt. Printing Office), 947–970. doi:10.2973/dsdp.proc.85.132.1985

Miller, K.G., Wright, J.D., and Fairbanks, R.G., 1991. Unlocking the ice house: Oligocene–Miocene oxygen isotopes, eustasy, and margin erosion. *J. Geophys. Res.,* 96(B4):6829–6848. doi:10.1029/90JB02015

Mitchell, N.C., 1998. Modeling Cenozoic sedimentation in the central equatorial Pacific and implications for true polar wander. *J. Geophys. Res., [Solid Earth],* 103(B8):17749–17766. doi:10.1029/98JB01577

Mitchell, N.C., and Lyle, M.W., 2005. Patchy deposits of Cenozoic pelagic sediments in the central Pacific. *Geology,* 33(1):49–52. doi:10.1130/G21134.1

Mitchell, N.C., Lyle, M.W., Knappenberger, M.B., and Liberty, L.M., 2003. Lower Miocene to present stratigraphy of the equatorial Pacific sediment bulge and carbonate dissolution anomalies. *Paleoceanography,* 18(2):1038. doi:10.1029/2002PA000828

Mix, A.C., Tiedemann, R., Blum, P., et al., 2003. *Proc. ODP, Init. Repts.,* 202: College Station, TX (Ocean Drilling Program). doi:10.2973/odp.proc.ir.202.2003

Moore, T.C., Rea, D.K., Lyle, M., and Liberty, L.M., 2002. Equatorial ocean circulation in an extreme warm climate. *Paleoceanography,* 17(1):1005. doi:10.1029/2000PA000566

Moore, T.C., Jr., 1995. Radiolarian stratigraphy, Leg 138. *In* Pisias, N.G., Mayer, L.A., Janecek, T.R., Palmer-Julson, A., and van Andel, T.H. (Eds.), *Proc. ODP, Sci. Results,* 138: College Station, TX (Ocean Drilling Program), 191–232. doi:10.2973/odp.proc.sr.138.111.1995

Moore, T.C., Jr., 2008a. Biogenic silica and chert in the Pacific Ocean. *Geology,* 36(12):975–978. doi:10.1130/G25057A.1

Moore, T.C., Jr., 2008b. Chert in the Pacific: biogenic silica and hydrothermal circulation. *Palaeogeogr., Palaeoclimatol., Palaeoecol.,* 261(1–2):87–99. doi:10.1016/j.palaeo.2008.01.009

Moore, T.C., Jr., Backman, J., Raffi, I., Nigrini, C., Sanfilippo, A., Pälike, H., and Lyle, M., 2004. Paleogene tropical Pacific: clues to circulation, productivity, and plate motion. *Paleoceanography,* 19(3):PA3013. doi:10.1029/2003PA000998

Müller, R.D., Roest, W.R., Royer, J.-Y., Gahagan, L.M., and Sclater, J.G., 1997. Digital isochrons of the world's ocean floor. *J. Geophys. Res.,* 102(B2):3211–3214. doi:10.1029/96JB01781

Nigrini, C., Sanfilippo, A., and Moore, T.C., Jr., 2006. Cenozoic radiolarian biostratigraphy: a magnetobiostratigraphic chronology of Cenozoic sequences from ODP Sites 1218, 1219, and 1220, equatorial Pacific. *In* Wilson, P.A., Lyle, M., and Firth, J.V. (Eds.), *Proc. ODP, Sci. Results,* 199: College Station, TX (Ocean Drilling Program), 1–76. doi:10.2973/odp.proc.sr.199.225.2006

Norris, R.D., and Röhl, U., 1999. Carbon cycling and chronology of climate warming during the Palaeocene/Eocene transition. *Nature (London, U. K.),* 401(6755):775–778. doi:10.1038/44545

Nuñes, F., and Norris, R.D., 2006. Abrupt reversal in ocean overturning during the Palaeocene/Eocene warm period. *Nature (London, U. K.),* 439(7072):60–63. doi:10.1038/nature04386

Olivarez Lyle, A., and Lyle, M., 2005. Organic carbon and barium in Eocene sediments: possible controls on nutrient recycling in the Eocene equatorial Pacific Ocean. *In* Wilson, P.A., Lyle, M., and Firth, J.V. (Eds.), *Proc. ODP, Sci. Results,* 199: College Station, TX (Ocean Drilling Program), 1–33. doi:10.2973/odp.proc.sr.199.222.2005

Paillard, D., Labeyrie, L., and Yiou, P., 1996. Macintosh program performs time-series analysis. *Eos, Trans. Am. Geophys. Union,* 77(39):379. doi:10.1029/96EO002590

Pälike, H., Frazier, J., and Zachos, J.C., 2006a. Extended orbitally forced palaeoclimatic records from the equatorial Atlantic Ceara Rise. *Quat. Sci. Rev.,* 25(23–24):3138–3149. doi:10.1016/j.quascirev.2006.02.011

Pälike, H., Lyle, M.W., Ahagon, N., Raffi, I., Gamage, K., and Zarikian, C.A., 2008. Pacific equatorial age transect. *IODP Sci. Prosp.,* 320/321. doi:10.2204/iodp.sp.320321.2008

Pälike, H., Moore, T., Backman, J., Raffi, I., Lanci, L., Parés, J.M., and Janecek, T., 2005. Integrated stratigraphic correlation and improved composite depth scales for ODP Sites 1218 and 1219. *In* Wilson, P.A., Lyle, M., and Firth, J.V. (Eds.), *Proc. ODP, Sci. Results,* 199: College Station, TX (Ocean Drilling Program), 1–41. doi:10.2973/odp.proc.sr.199.213.2005

Pälike, H., Norris, R.D., Herrle, J.O., Wilson, P.A., Coxall, H.K., Lear, C.H., Shackleton, N.J., Tripati, A.K., and Wade, B.S., 2006b. The heartbeat of the Oligocene climate system. *Science,* 314(5807):1894–1898. doi:10.1126/science.1133822

Parés, J.M., and Moore, T.C., 2005. New evidence for the Hawaiian hotspot plume motion since the Eocene. *Earth Planet. Sci. Lett.,* 237(3–4):951–959. doi:10.1016/j.epsl.2005.06.012

Paul, H.A., Zachos, J.C., Flower, B.P., and Tripati, A., 2000. Orbitally induced climate and geochemical variability across the Oligocene/Miocene boundary. *Paleoceanography,* 15(5):471–485. doi:10.1029/1999PA000443

Pearson, P.N., Ditchfield, P.W., Singano, J., Harcourt-Brown, K.G., Nicholas, C.J., Olsson, R.K., Shackleton, N.J., and Hall, M.A., 2001a. Warm tropical sea surface temperatures in the Late Cretaceous and Eocene epochs. *Nature (London, U. K.),* 413(6855):481–487. **doi:10.1038/35097000**

Pearson, P.N., McMillan, I.K., Wade, B.S., Dunkley Jones, T., Coxall, H.K., Bown, P.R., and Lear, C.H., 2008. Extinction and environmental change across the Eocene–Oligocene boundary in Tanzania. *Geology,* 36(2):179–182. **doi:10.1130/G24308A.1**

Pearson, P.N., Norris, R.D., and Empson, A.J., 2001b. *Mutabella mirabilis* gen. et sp. nov., a Miocene microperforate planktonic foraminifer with an extreme level of intraspecific variability. *J. Foraminiferal Res.,* 31(2):120–132. **doi:10.2113/0310120**

Petronotis, K.E., 1991. Paleomagnetic studies of the skewness of Pacific plate marine magnetic anomalies 25–32R: implications for Anomalous skewness and the motion of the Pacific plate and hotspots [Ph.D. thesis]. Northwestern Univ., Evanston, IL.

Petronotis, K.E., Gordon, R.G., and Acton, G.D., 1994. A 57 Ma Pacific plate paleomagnetic pole determined from a skewness Analysis of crossings of marine magnetic anomaly 25r. *Geophys. J. Int.,* 118(3):529–554. **doi:10.1111/j.1365-246X.1994.tb03983.x**

Pisias, N.G., Mayer, L.A., Janecek, T.R., Palmer-Julson, A., and van Andel, T.H. (Eds.), 1995. *Proc. ODP, Sci Results,* 138: College Station, TX (Ocean Drilling Program). **doi:10.2973/odp.proc.sr.138.1995**

Pollack, H.N., Hurter, S.J., and Johnson, J.R., 1993. Heat flow from the earth's interior: analysis of the global data set. *Rev. Geophys.,* 31(3):267–280. **doi:10.1029/93RG01249**

Pribnow, D.F.C., Kinoshita, M., and Stein, C.A., 2000. *Thermal Data Collection and Heat Flow Recalculations for ODP Legs 101–180:* Hanover, Germany (Inst. Joint Geosci. Res., Inst. Geowiss. Gemeinschaftsauf. [GGA]). **http://www-odp.tamu.edu/publications/heatflow/ODPReprt.pdf**

Raffi, I., Backman, J., Fornaciari, E., Pälike, H., Rio, D., Lourens, L., and Hilgen, F., 2006. A review of calcareous nannofossil astrobiochronology encompassing the past 25 million years. *Quat. Sci. Rev.,* 25(23–24):3113–3137. **doi:10.1016/j.quascirev.2006.07.007**

Raffi, I., Backman, J., and Pälike, H., 2005. Changes in calcareous nannofossil assemblages across the Paleocene/Eocene transition from the paleo-equatorial Pacific Ocean. *Palaeogeogr., Palaeoclimatol., Palaeoecol.,* 226(1–2):93–126. **doi:10.1016/j.palaeo.2005.05.006**

Rea, D.K., and Lyle, M.W., 2005. Paleogene calcite compensation depth in the eastern subtropical Pacific: answers and questions. *Paleoceanography,* 20(1):PA1012. **doi:10.1029/2004PA001064**

Röhl, U., Ogg, J.G., Geib, T.L., and Wefer, G., 2001. Astronomical calibration of the Danian time scale. *In* Kroon, D., Norris, R.D., and Klaus, A. (Eds.), *Western North Atlantic Paleogene and Cretaceous Paleoceanography.* Geol. Soc. Spec. Publ., 183:163–184.

Sager, W.W., and Pringle, M.S., 1988. Mid-Cretaceous to early Tertiary apparent polar wander path of the Pacific plate. *J. Geophys. Res., [Solid Earth],* 93(B10):11753–11771. **doi:10.1029/JB093iB10p11753**

Scher, H.D., and Martin, E.E., 2006. Timing and climatic consequences of the opening of Drake Passage. *Science,* 312(5772):428–430. **doi:10.1126/science.1120044**

Sexton, P.F., Wilson, P.A., and Pearson, P.N., 2006. Palaeoecology of late middle Eocene planktic foraminifera and evolutionary implications. *Mar. Micropaleontol.,* 60(1):1–6. **doi:10.1016/j.marmicro.2006.02.006**

Shackleton, N.J., Hall, M.A., Raffi, I., Tauxe, L., and Zachos, J., 2000. Astronomical calibration age for the Oligocene–Miocene boundary. *Geology,* 28(5):447–450. **doi:10.1130/0091-7613(2000)28<447:ACAFTO>2.0.CO;2**

Shipboard Scientific Party, 1995. Leg 154 synthesis. *In* Curry, W.B., Shackleton, N.J., Richter, C., et al., *Proc. ODP, Init. Repts.,* 154: College Station, TX (Ocean Drilling Program), 421–442. **doi:10.2973/odp.proc.ir.154.109.1995**

Shipboard Scientific Party, 2002. Leg 199 summary. *In* Lyle, M., Wilson, P.A., Janecek, T.R., et al., *Proc. ODP, Init. Repts.,* 199: College Station, TX (Ocean Drilling Program), 1–87. **doi:10.2973/odp.proc.ir.199.101.2002**

Shipboard Scientific Party, 2004. Leg 208 summary. *In* Zachos, J.C., Kroon, D., Blum, P., et al., *Proc. ODP, Init. Repts.,* 208: College Station, TX (Ocean Drilling Program), 1–112. **doi:10.2973/odp.proc.ir.208.101.2004**

Spero, H.J., Bijma, J., Lea, D.W., and Bemis, B.E., 1997. Effect of seawater carbonate concentration on foraminiferal carbon and oxygen isotopes. *Nature (London, U. K.),* 390(6659):497–500. **doi:10.1038/37333**

Steiger, T.H., 2006. Biogenic sedimentology of radiolarian assemblages in a middle Eocene diatom-rich unit from the eastern equatorial Pacific: ODP Leg 199, Site 1219. *In* Wilson, P.A., Lyle, M., and Firth, J.V. (Eds.), *Proc. ODP, Sci. Results,* 199: College Station, TX (Ocean Drilling Program), 1–19. **doi:10.2973/odp.proc.sr.199.217.2006**

Tarduno, J.A., Duncan, R.A., Scholl, D.W., Cottrell, R.D., Steinberger, B., Thordarson, T., Kerr, B.C., Neal, C.R., Frey, F.A., Torii, M., and Carvallo, C., 2003. The Emperor Seamounts: southward motion of the Hawaiian hotspot plume in Earth's mantle. *Science,* 301(5636):1064–1069. **doi:10.1126/science.1086442**

van Andel, T.H., 1975. Mesozoic/Cenozoic calcite compensation depth and the global distribution of calcareous sediments. *Earth Planet. Sci. Lett.,* 26(2):187–194. **doi:10.1016/0012-821X(75)90086-2**

van Andel, T.H., Heath, G.R., and Moore, T.C., Jr., 1975. *Cenozoic History and Paleoceanography of the Central Equatorial Pacific Ocean.* Geol. Soc. Am. Mem., 143.

Wade, B.S., Berggren, W.A., and Olsson, R.K., 2007. The biostratigraphy and paleobiology of Oligocene planktonic foraminifera from the equatorial Pacific Ocean (ODP Site 1218). *Mar. Micropaleontol.,* 62(3):167–179. **doi:10.1016/j.marmicro.2006.08.005**

Wade, B.S., and Bown, P.R., 2006. Calcareous nannofossils in extreme environments: the Messinian salinity crisis,

Polemi Basin, Cyprus. *Palaeogeogr., Palaeoclimatol., Palaeoecol.,* 233(3–4):271–286. doi:10.1016/j.palaeo.2005.10.007

Wade, B.S., and Pälike, H., 2004. Oligocene climate dynamics. *Paleoceanography,* 19(4)PA4019. doi:10.1029/2004PA001042

Wei, W., and Wise, S.W., Jr., 1989. Paleogene calcareous nannofossil magnetobiochronology: results from South Atlantic DSDP Site 516. *Mar. Micropaleontol.,* 14(1–3):119–152. doi:10.1016/0377-8398(89)90034-0

Zachos, J.C., Dickens, G.R., and Zeebe, R.E., 2008. An early Cenozoic perspective on greenhouse warming and carbon-cycle dynamics. *Nature (London, U. K.),* 451(7176):279–283. doi:10.1038/nature06588

Zachos, J.C., Flower, B.P., and Paul, H., 1997. Orbitally paced climate oscillations across the Oligocene/Miocene boundary. *Nature (London, U. K.),* 388(6642):567–570. doi:10.1038/41528

Zachos, J.C., Pagani, M., Sloan, L., Thomas, E., and Billups, K., 2001a. Trends, rhythms, and aberrations in global climate 65 Ma to present. *Science,* 292(5517):686–693. doi:10.1126/science.1059412

Zachos, J.C., Quinn, T.M., and Salamy, K.A., 1996. High-resolution (10^4 years) deep-sea foraminiferal stable isotope records of the Eocene–Oligocene climate transition. *Paleoceanography,* 11(3):251–266. doi:10.1029/96PA00571

Zachos, J.C., Shackleton, N.J., Revenaugh, J.S., Pälike, H., and Flower, B.P., 2001b. Climate response to orbital forcing across the Oligocene–Miocene boundary. *Science,* 292(5515):274–278. doi:10.1126/science.1058288

Zeebe, R.E., and Wolf-Gladrow, D.A., 2001. *CO_2 in Seawater: Equilibrium, Kinetics, Isotopes:* Amsterdam (Elsevier).

Figure F1. Location map of sites drilled during Expedition 320/321. Red stars = sites drilled during Expedition 320, red circles = sites drilled during Expedition 321, black circles = previous DSDP and ODP sites. F.Z. = fracture zone. The positions of Honolulu and Papeete are indicated for orientation.
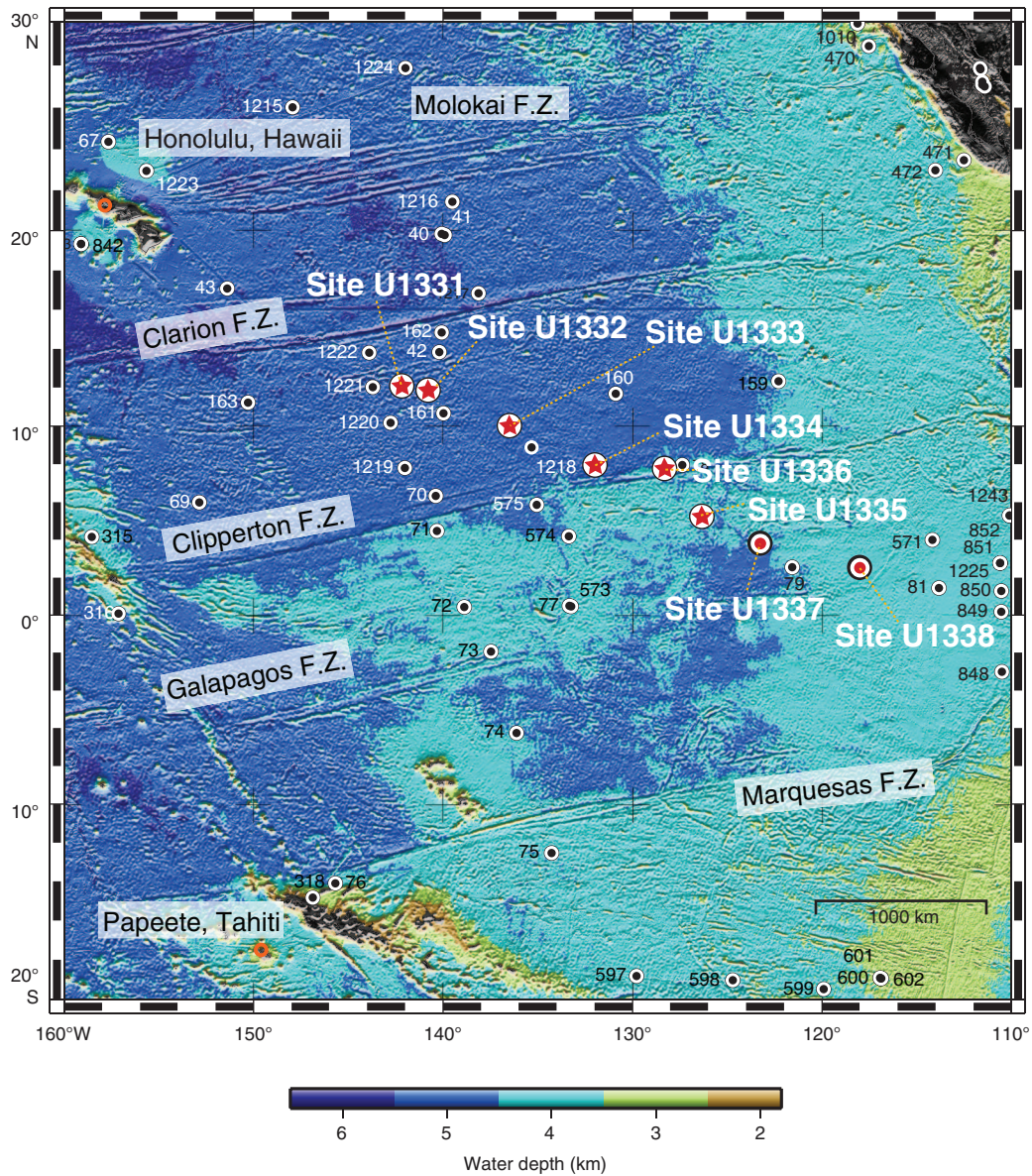
Figure F2. Evolution of oxygen stable isotopes ($\delta^{18}O$) through the Cenozoic and related major phases of climate change (modified from Zachos et al., 2001b, 2008). Yellow boxes = time slices of interest for the PEAT program, green and blue boxes = ODP legs and sites previously drilled in the equatorial Pacific region; these additional sites will be used with the PEAT sites to obtain a nearly continuous Cenozoic record of the equatorial Pacific region. VPDB = Vienna Peedee belemnite. Oi-1 = Oligocene isotopic Event 1, Mi-1 = Miocene isotopic Event 1 (described in Miller et al., 1991). ETM2 = Eocene thermal maximum 2.
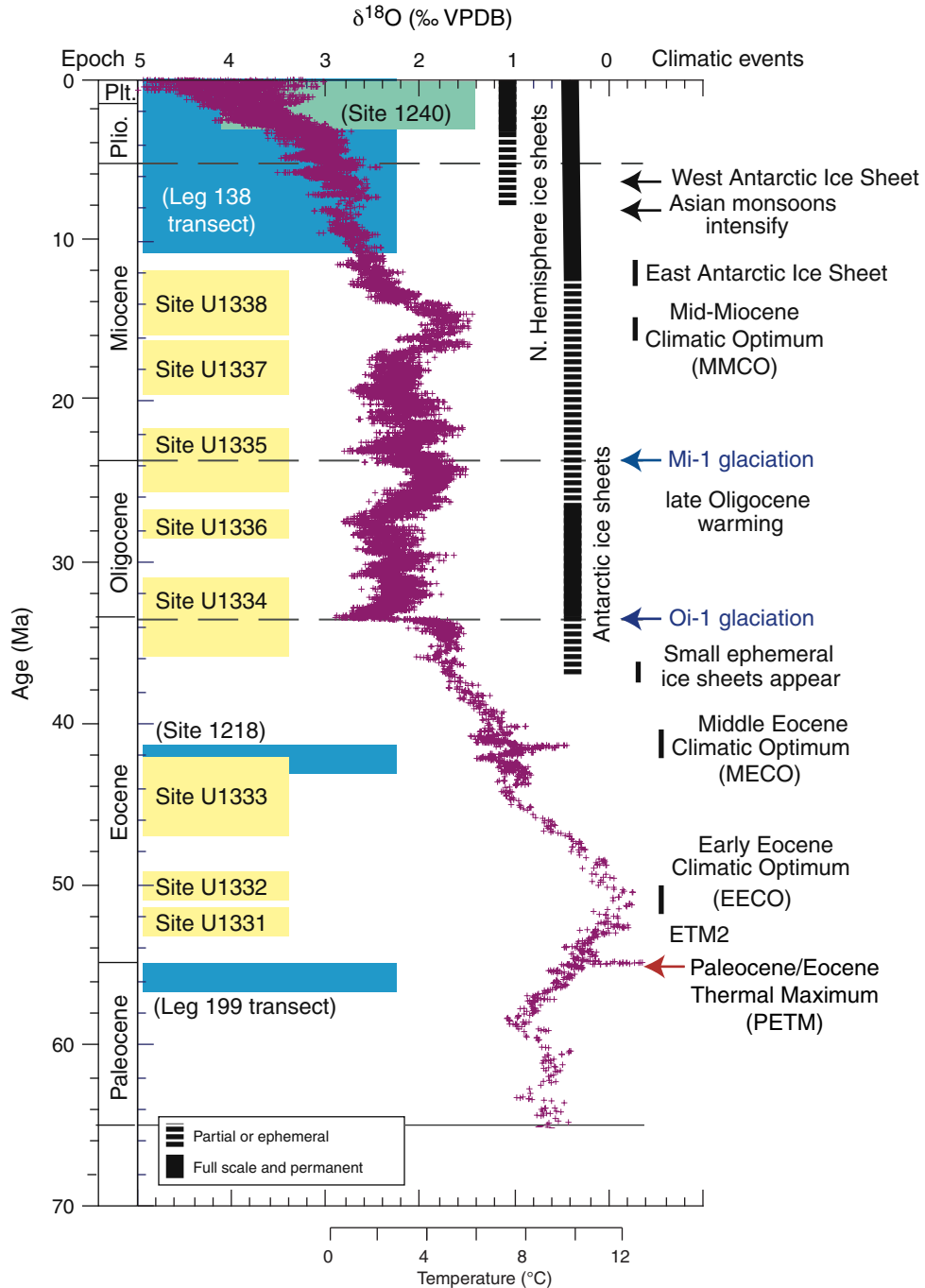
Figure F3. Targeting drill sites based on calcium carbonate compensation depth (CCD) history (van Andel, 1975), with new data from Leg 199 prior to coring. Colored boxes = critical time interval targeted for each site. Colored subsidence lines = time intervals when we expected carbonate to be deposited (i.e., when site is above CCD). Subsidence curves use a subsidence parameter calculated from estimated basement age of PEAT sites and their present-day depth (k = ~0.35). Additional subsidence due to sediment loading was not modeled.
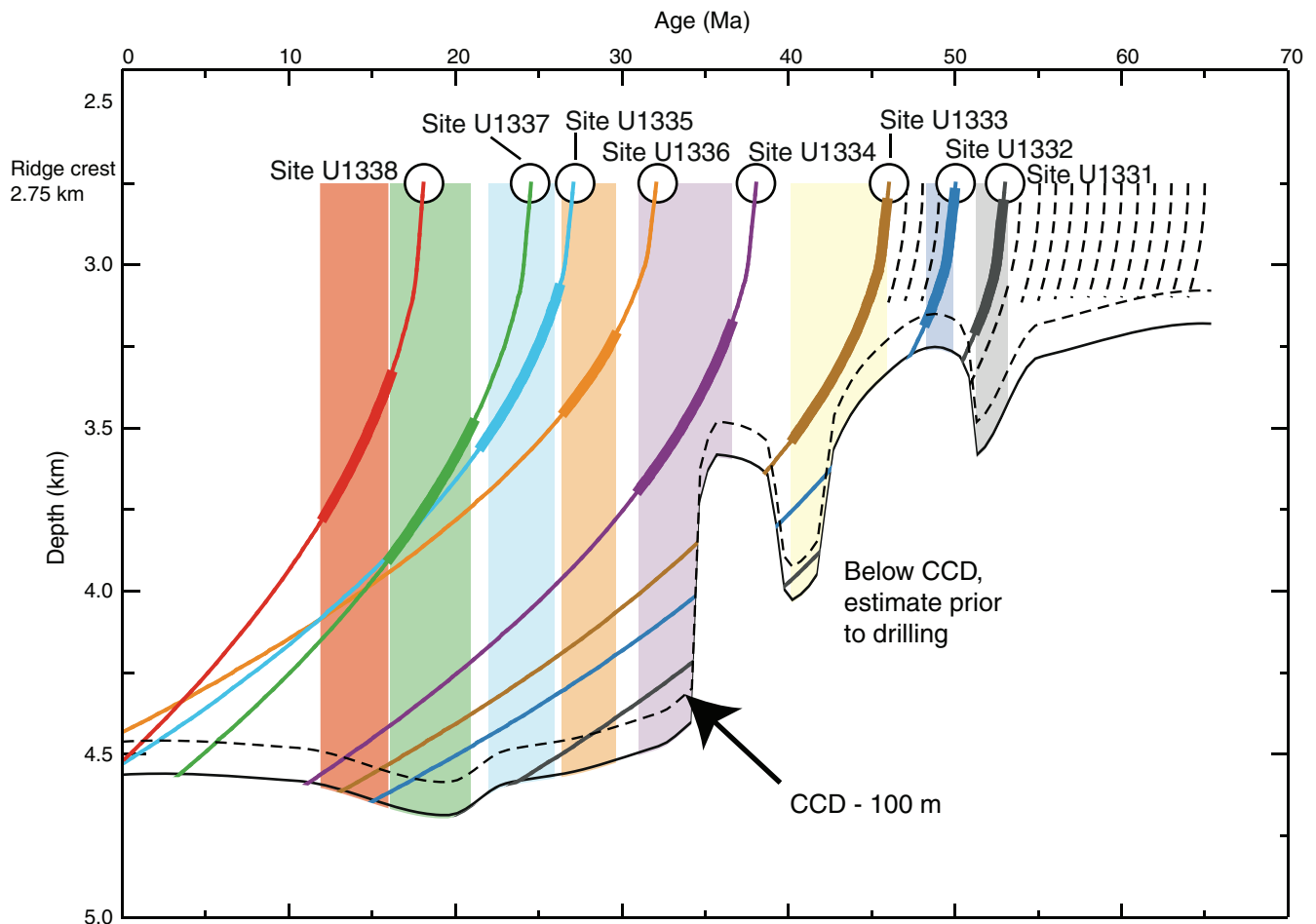
Figure F4. Location map of drill sites with backtracked position of paleoequator, corresponding to time slices targeted. Gray scale = present-day bathymetry (darker = deeper), thin yellow lines = revised magnetic anomaly isochrons (modified with new points from Petronotis, 1991, and Petronotis et al., 1994). Paleoequator position at crustal age obtained by backtracking, using fixed-hotspot stage poles from Koppers et al. (2001; pink) and Engebretson et al. (1985; orange) and paleomagnetic poles from Sager and Pringle (1988; purple). Shaded band lies within 1° north and south of the paleoequator (averaged from fixed-hotspot rotation models). Colored areas = time intervals of interest obtained by intersecting white paleoequator area with younger end of the time interval of interest, which was then backrotated to the older boundary of the time slice. Method requires correction if backtracking occurs across fracture zones. Positions of PEAT sites as plotted are slightly different to final positions. Locations of previous DSDP and ODP sites are also shown.
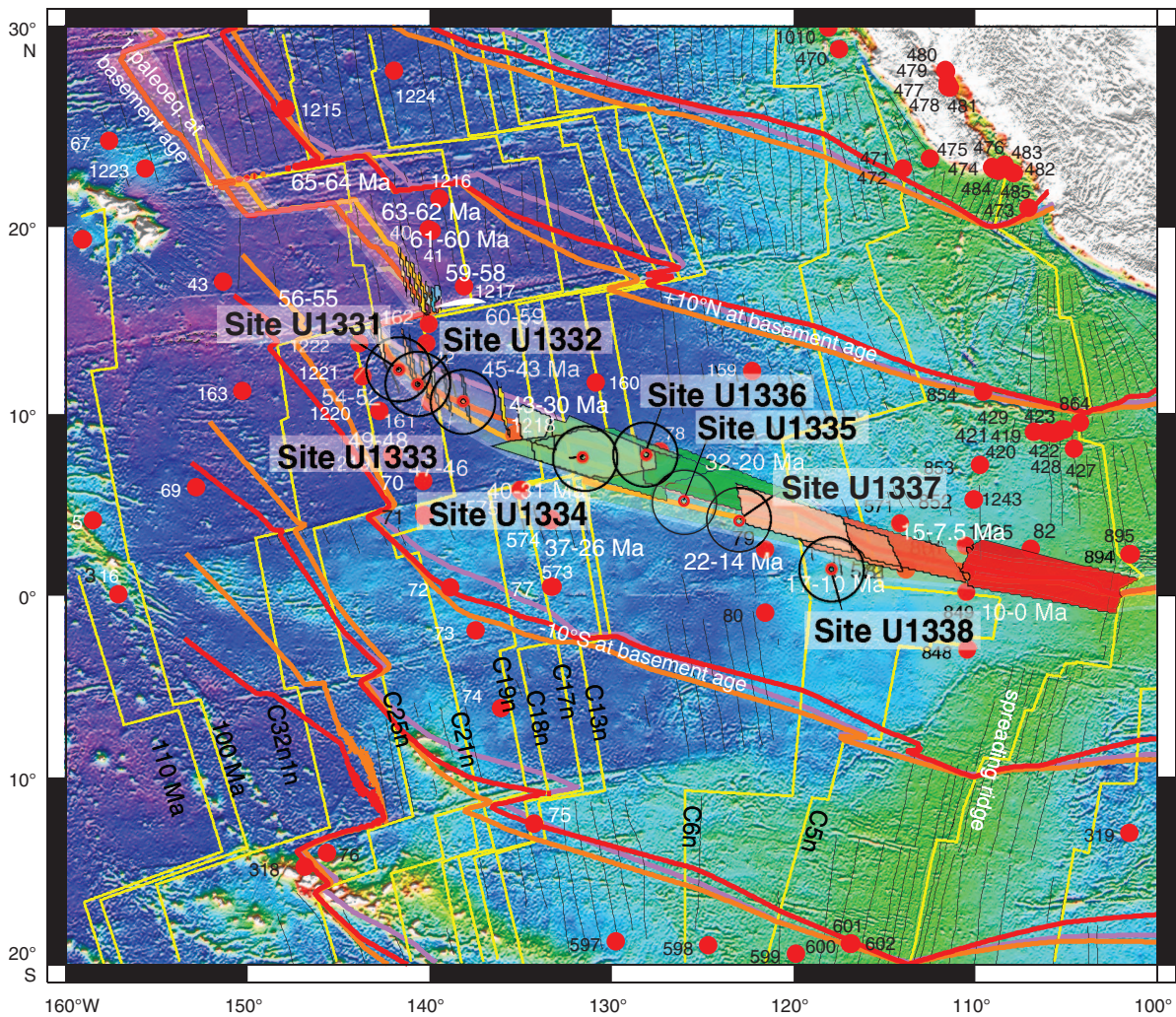
Figure F5. Backtracked latitudinal positions for PEAT sites and ODP Sites 1218 and 1220 vs. geological age. Sites were backrotated along the flow-line using stage poles from Koppers et al. (2001).
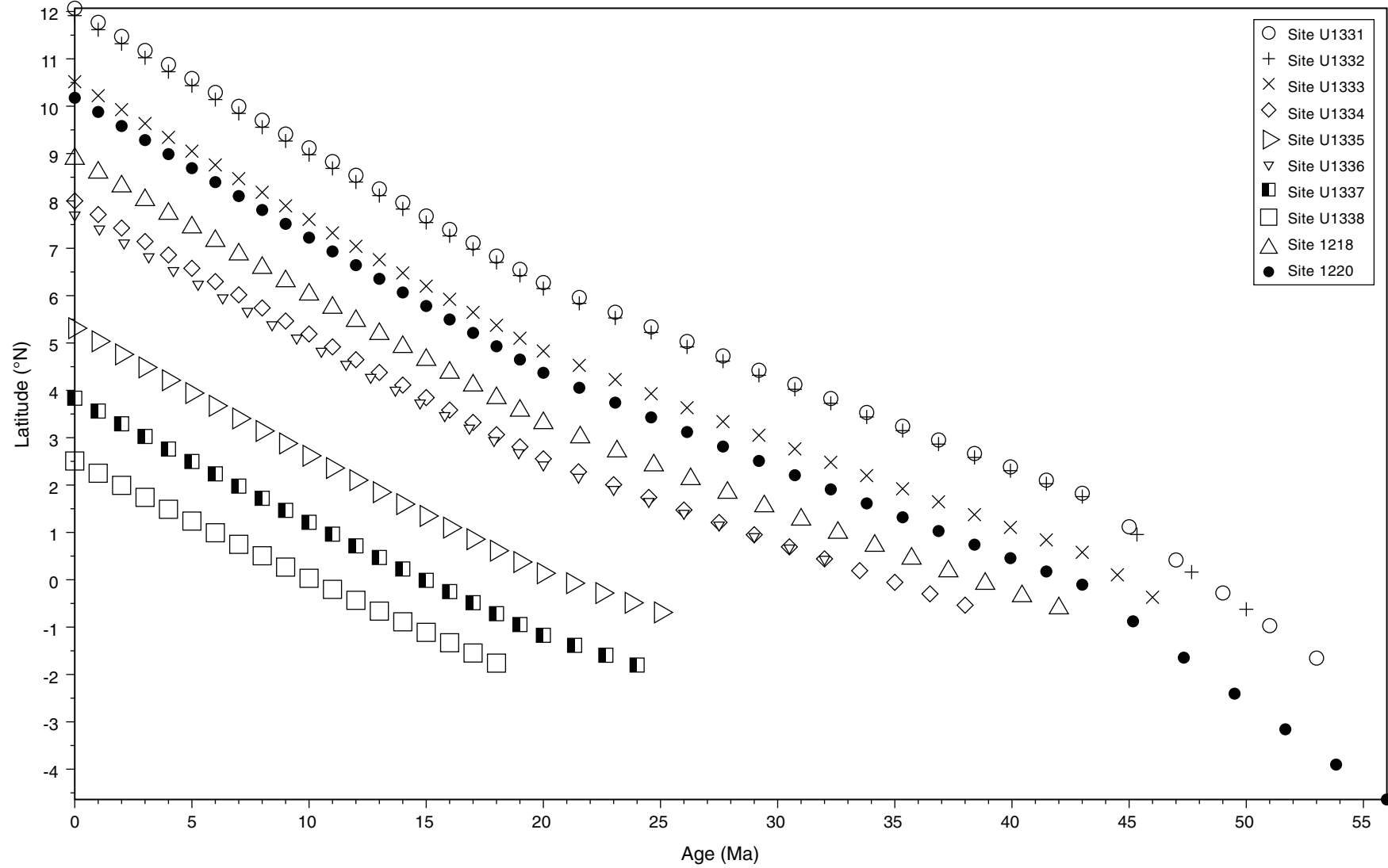
Figure F6. A. Backtracked positions for PEAT sites (red circles), using stage poles from Koppers et al. (2001) superimposed on a satellite-derived (GlobColour) map of present ocean chlorophyl-a concentrations (December 2005 mean monthly). Red = high productivity, blue = low productivity. Solid circles = previous DSDP and ODP sites. **B.** Backtracked positions for PEAT sites, with annotated positions every 10 m.y. back from present. Estimated basement ages for each site while situated at paleo–ridge crest are noted.
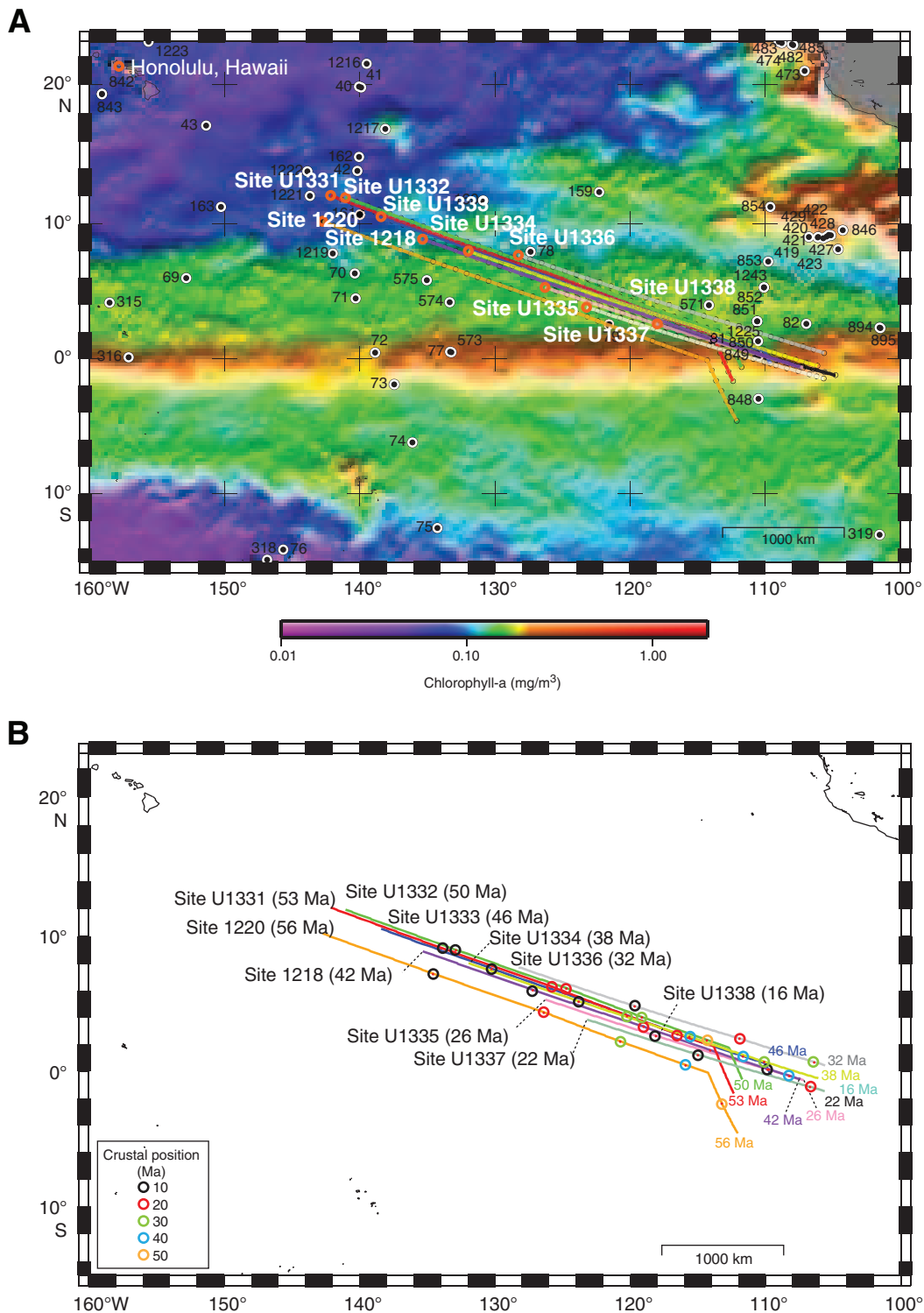
Figure F7. Times when PEAT sites (U1331–U1338) and selected DSDP and ODP sites (574, 572, 849, 851, and 1218) were positioned within paleoequatorial band. Equatorial band is defined as being within 2° latitude of Equator. Lighter shading = calcium compensation depth (CCD) (estimated prior to drilling for PEAT sites). Paleopositions were calculated with a fixed-hotspot model.
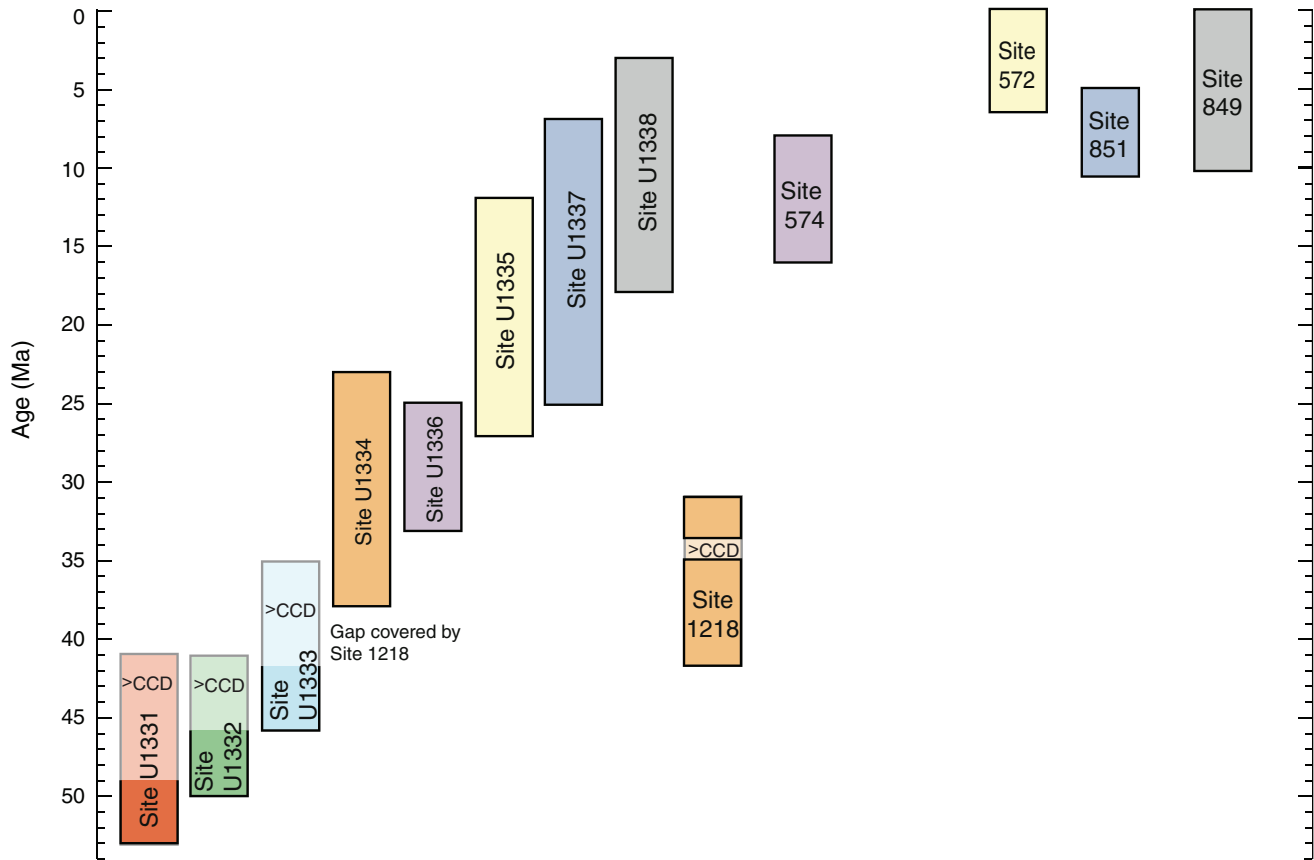
Figure F8. A. Model cross-section of equatorial sediment mound taking into account northward drift of Pacific plate. **B.** Mapped thickness of Pacific equatorial sediment mound. Color code = thickness of mound. (Both modified from Mitchell, 1998; Mitchell et al., 2003.)
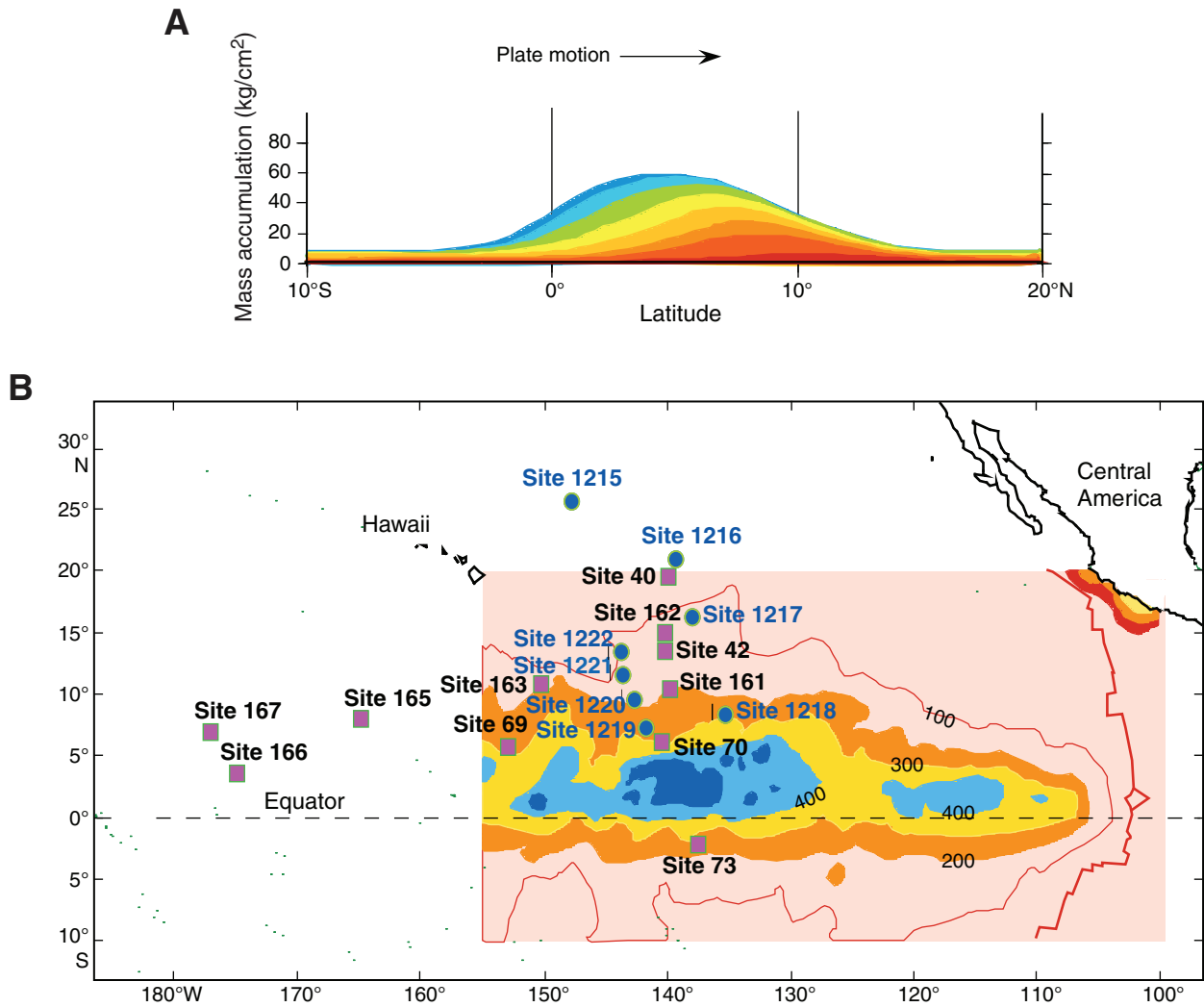
Figure F9. Coherence of sediment properties between widely separated drill sites in the equatorial Pacific is very high, allowing correlation of sediment properties over hundreds of kilometers. Figure shows Sites 1218 and 1219 (Shipboard Scientific Party, 2002), two sites >740 km apart. VGP = virtual geomagnetic pole, GRA = gamma ray attenuation, L* = lightness reflectance value of sediment as defined in the LAB color model. GRA and magnetic susceptibility measurements were completed on board. (**Figure shown on next page.**)

Figure F9 (continued). (Caption shown on previous page.)
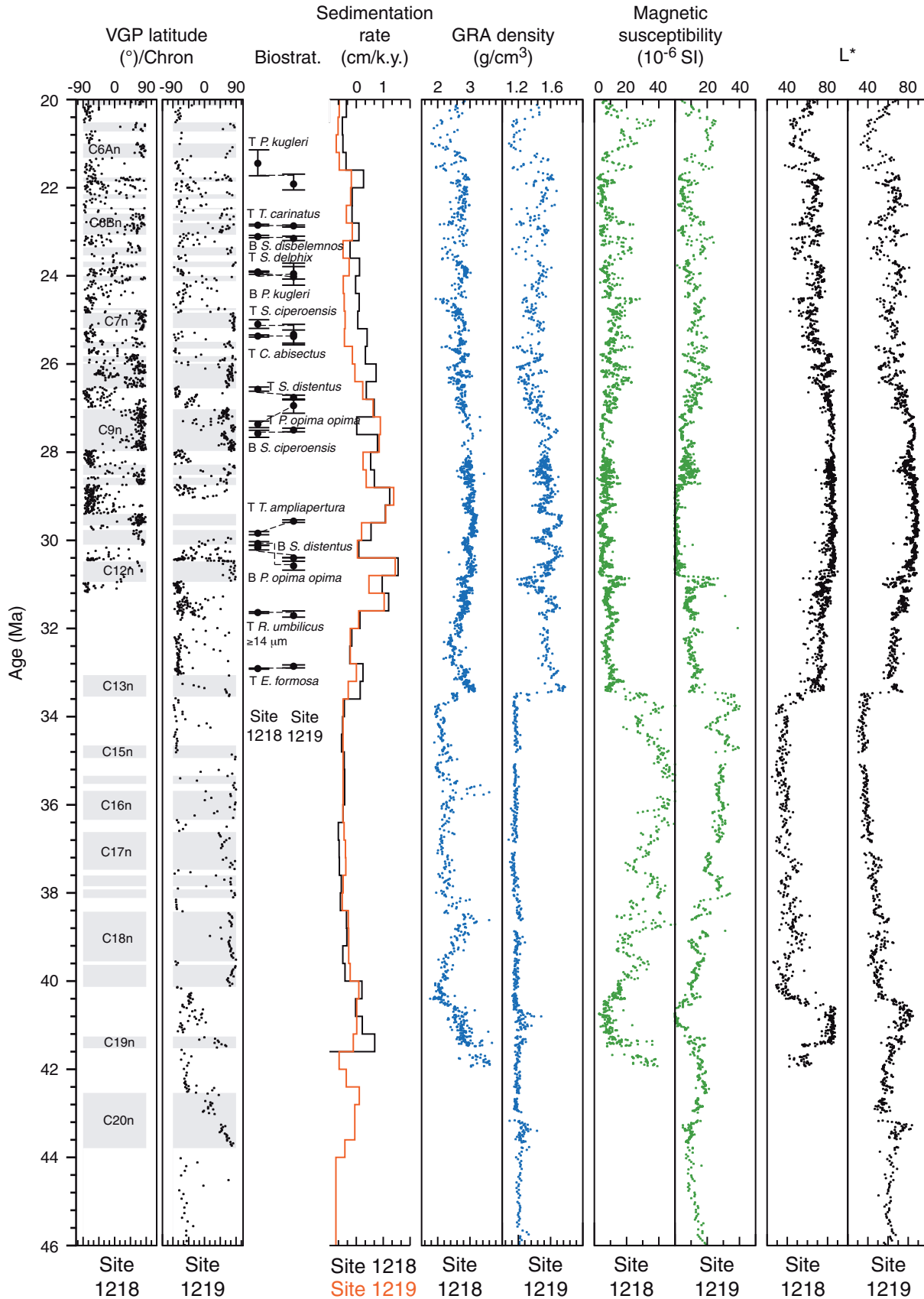
Figure F10. Model of early Eocene equatorial upwelling from Huber (2002), showing global land-sea distribution and annual average upwelling into thermocline (56 Ma sites, fixed-hotspot paleopositions). Red = regions of vigorous upwelling, green to blue = regions of weak upwelling, white = areas of average downwelling. Current streamlines at ~100 m ocean depth are shown for the Pacific Ocean. All map views are projected on a Mollweide projection. Upwelling region in eastern Pacific was broader than that of the modern region, primarily because of secondary upwelling centers on edges of region.
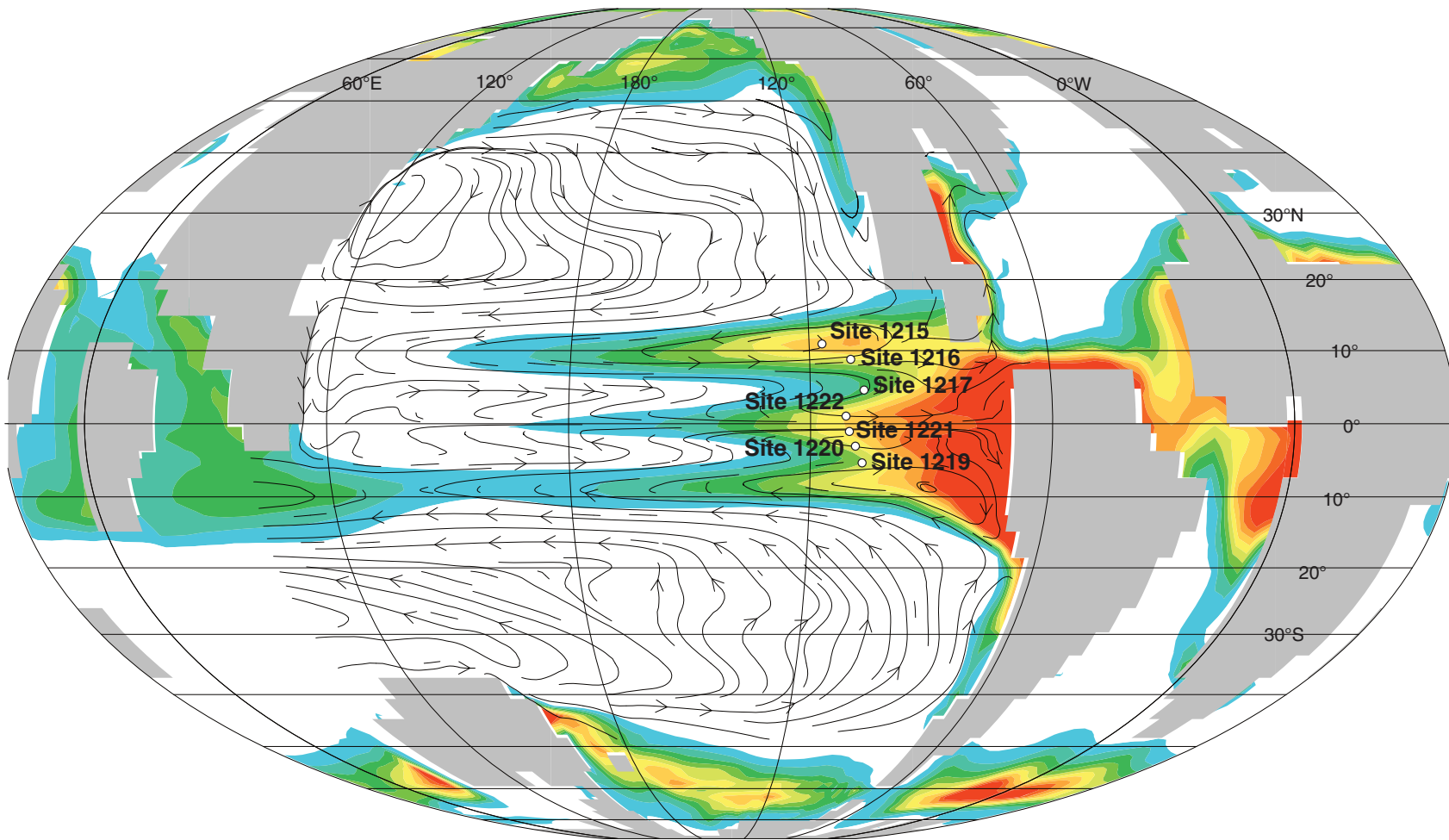
Figure F11. Average sedimentation rate for the interval 40–46 Ma, given in m/m.y. (after Moore et al., 2004). DSDP and ODP site positions are backtracked to their estimated position at 43 Ma. Site locations are colored according to sediment type for the time interval: blue = carbonate, green = siliceous-carbonate, red = siliceous, brown = clay. Contours are at 1, 5, and 10 m/m.y. Red dashed line = approximate geographic paleoequator based on the sediment archive, with a notable difference compared to the fixed-hotspot based rotation. Two regions of relatively high accumulation occur on both sides of the paleoequator in addition to the primary upwelling center.
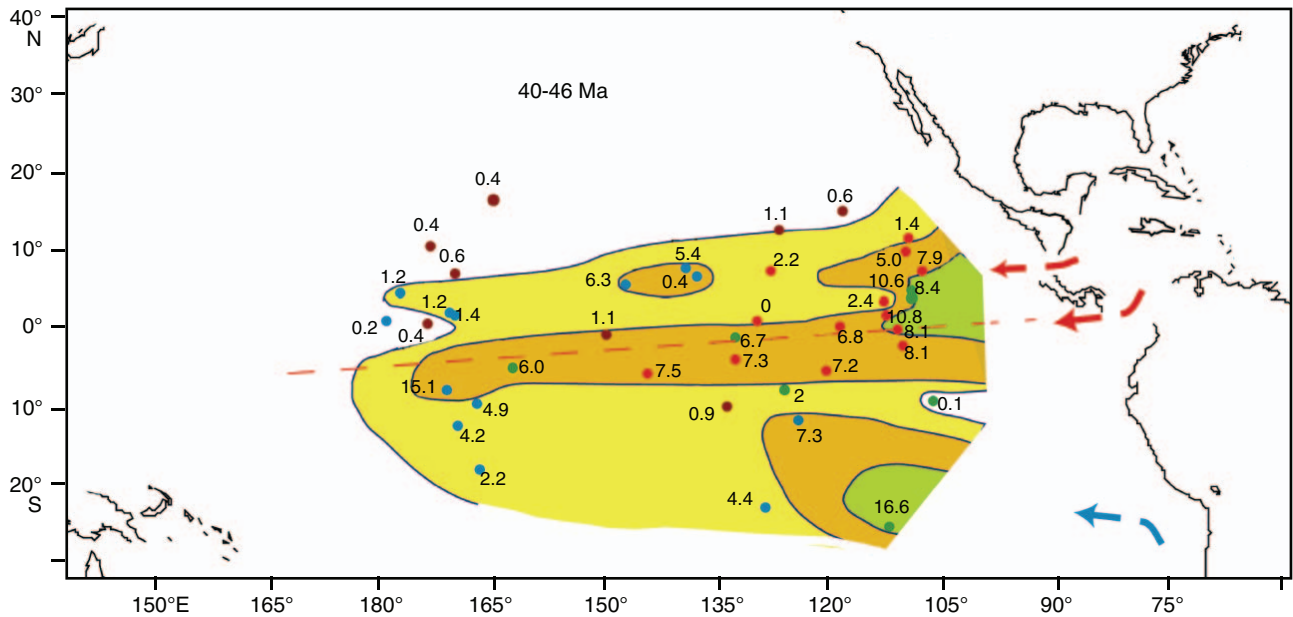
Figure F12. Stratigraphic summary plots, PEAT Sites U1331–U1338 and ODP Site 1218. Green = Eocene, blue = Oligocene, yellow = Miocene, pink = Pliocene–Pleistocene.
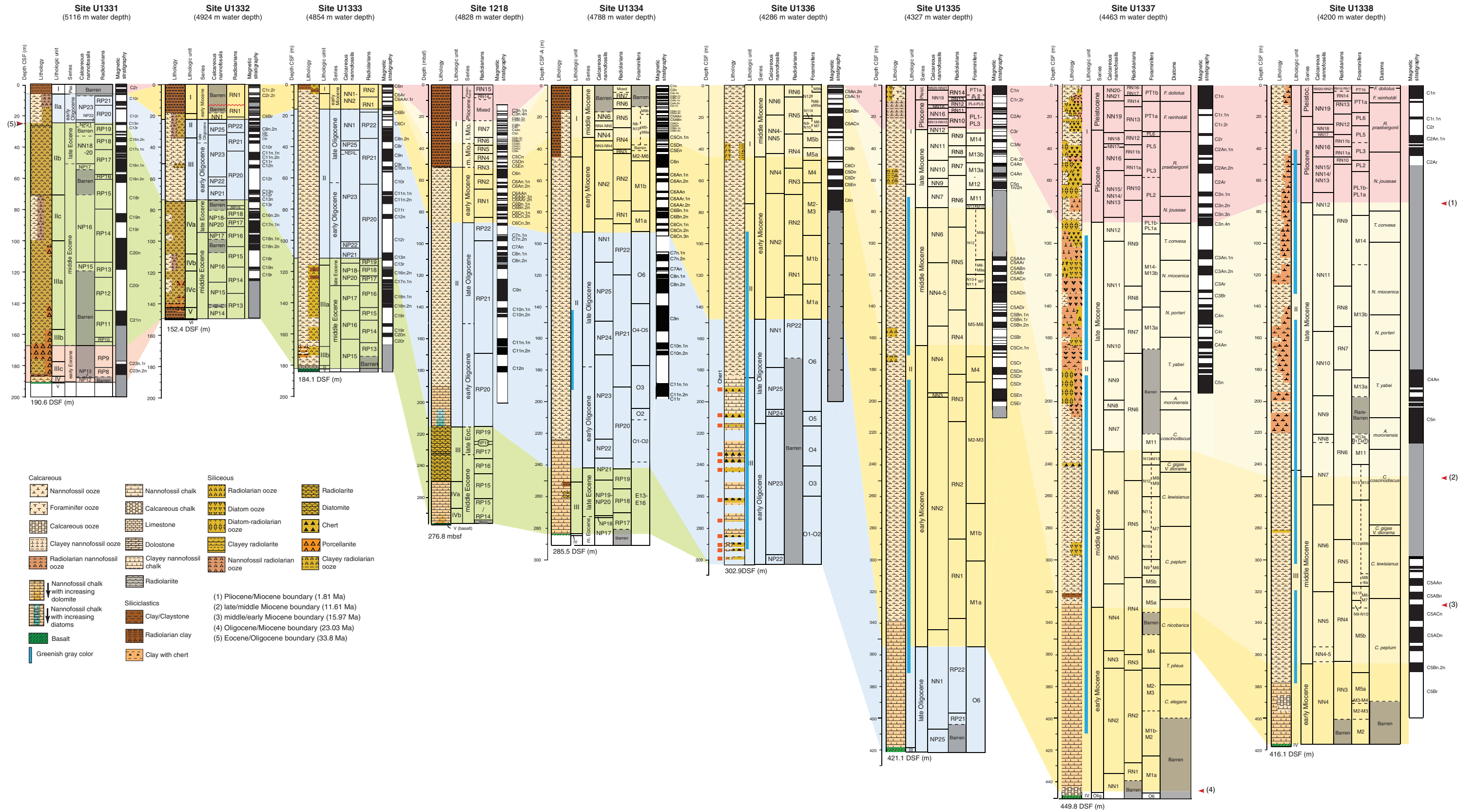
Figure F13. CaCO$_3$ and carbonate mass accumulation rates from Expedition 320/321 and selected ODP Leg 199 sites (1218 and 1220) (Lyle, Wilson, Janecek, et al., 2002). **A.** Weight percentages from shipboard analysis of samples from all Expedition 320/321 drill sites plotted vs. shipboard PEAT age model for each site and reconstructed paleodepth (see Fig. **F3**). Bubble area is proportional to CaCO$_3$ wt% measured. Events marked are the Eocene–Oligocene transition (E/O) (e.g., Coxall et al., 2005) and carbonate accumulation events (CAE) of Lyle et al. (2005). Dashed gray line = previous reconstructions of equatorial CCD during the Cenozoic (Lyle, 2003; Rea and Lyle, 2005), solid gray line = revised tentative reconstruction based on new data. **B.** As in A, with carbonate mass accumulation rates (CAR) for each site. Calculation uses linear sedimentation rates and dry bulk densities determined on board. Sedimentation rates calculated from data tables (see "Stratigraphic correlation and composite section" in each site chapter) adjusted CCSF depth scales by dividing by the growth factor for each site to convert thicknesses back into in situ sediment thickness. **C.** As in B, plotting carbonate mass accumulation rates (CAR) as a function of age and site paleolatitude, reconstructed using stage poles from Koppers et al. (2001). Note that although the equatorial upwelling zone does result in elevated accumulation rates, the disappearance of carbonate for most sites is primarily a function of paleodepth. (**Figure shown on next page.**)

**Figure F13 (continued).** (Caption shown on previous page.)
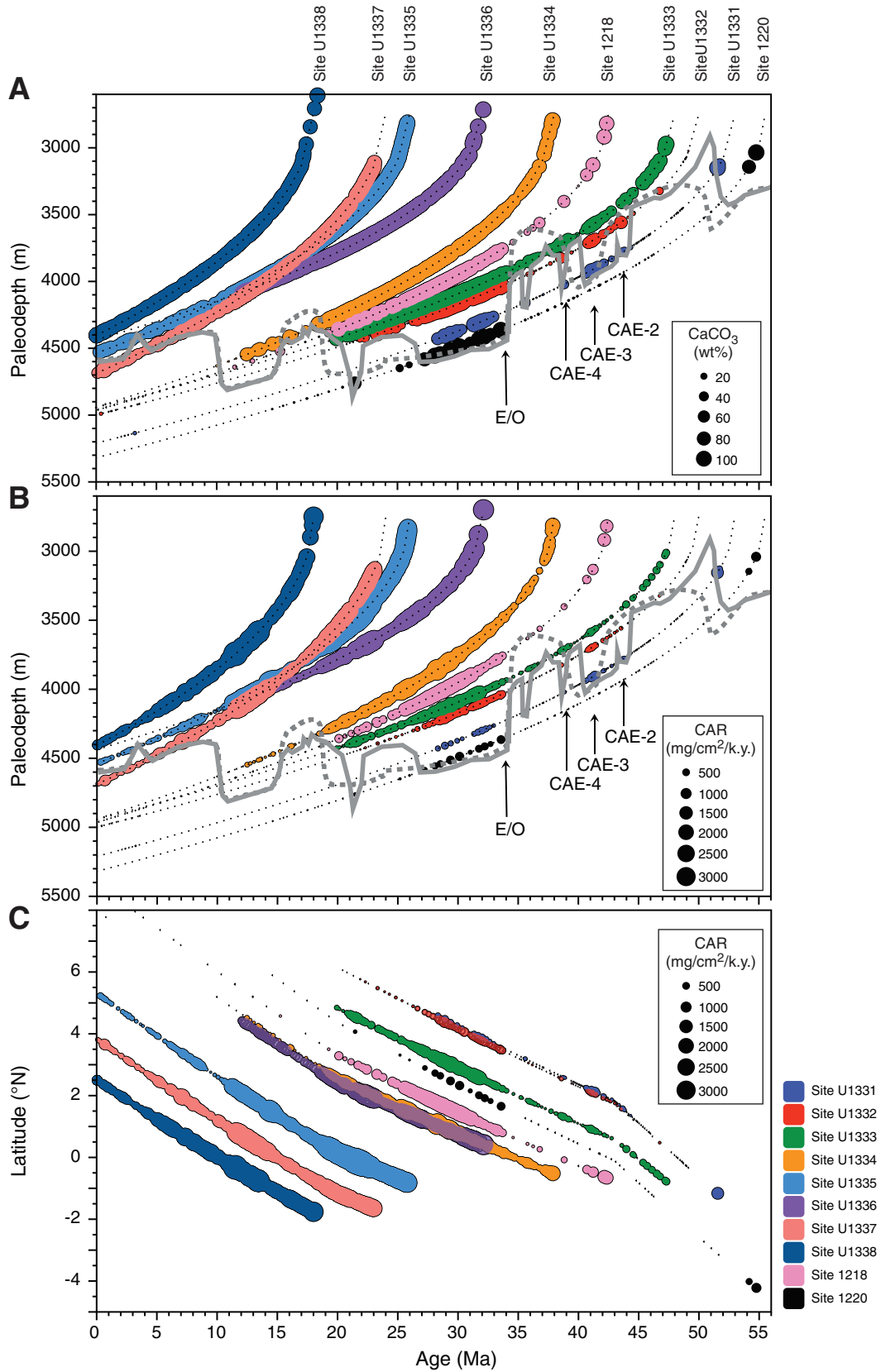
Figure F14. Summary of sedimentation rates derived from age-depth models at each PEAT (Expedition 320/321) site plotted vs. corrected core composite depth.
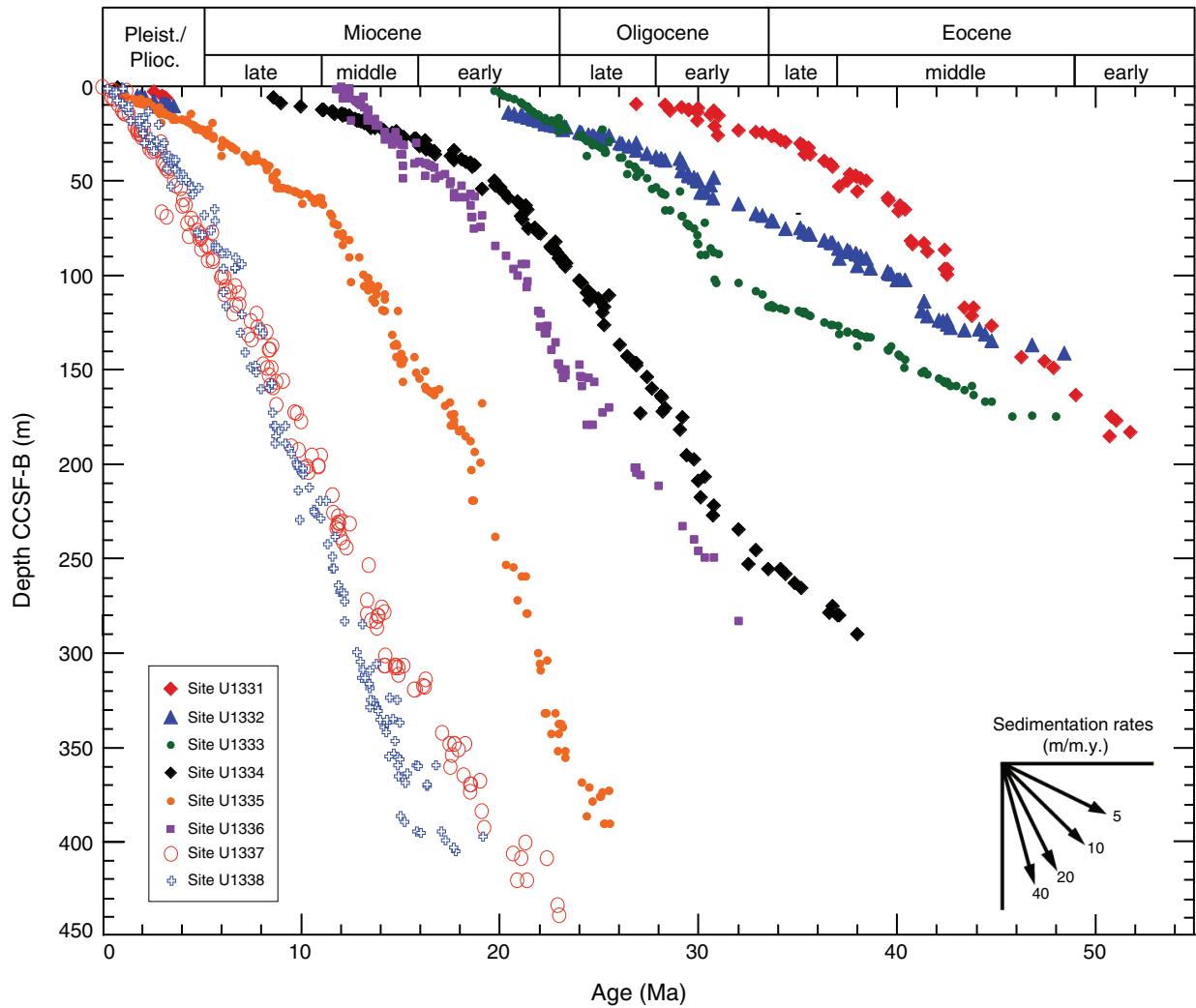
Figure F15. Expedition 320/321 Sites U1331–U1338 and select ODP sites plotted against the PEAT timescale. Sites are plotted approximately ordered by site longitude and basement age. Estimated crustal ages are shown underneath each stratigraphic column. Carbonate accumulation events (CAE) appear as defined by Lyle et al. (2005). MECO = Middle Eocene Climatic Optimum.
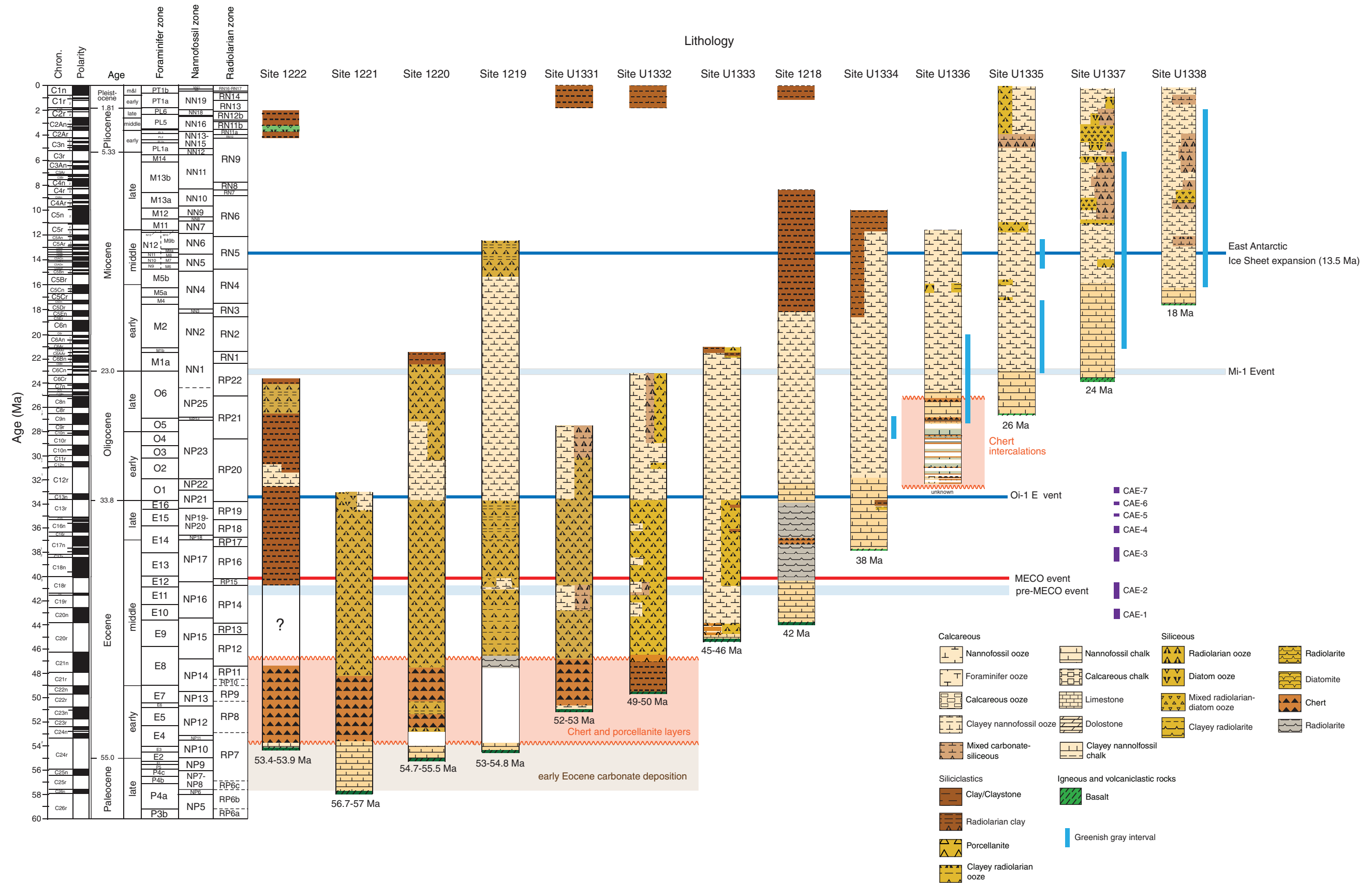
Figure F16. Calcium carbonate concentrations and total organic carbon (TOC) contents, Sites U1336–1338. TOC contents determined by acidification method.
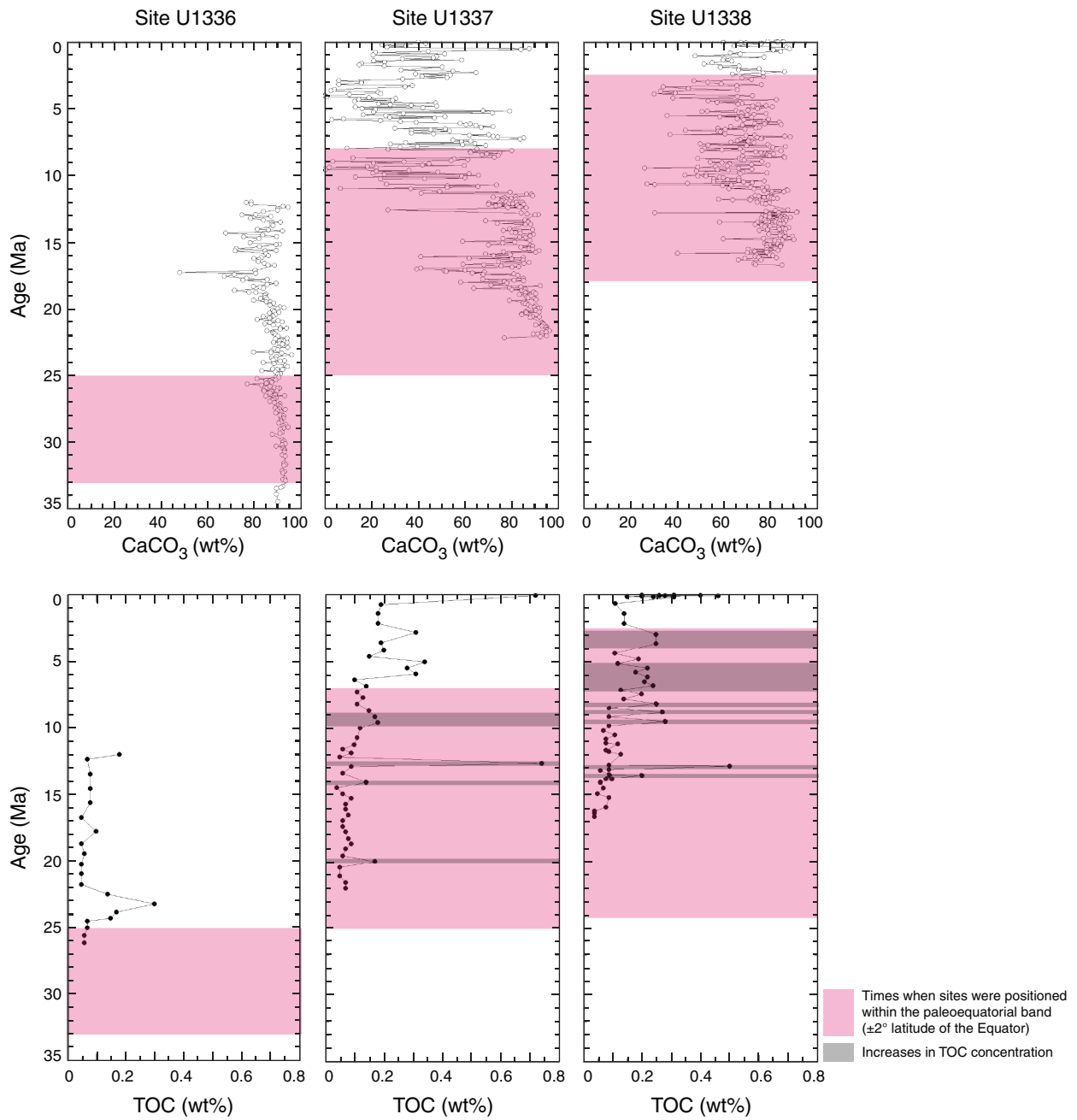
Figure F17. Planktonic foraminifer abundance and benthic/planktonic foraminifer ratios, Sites U1337 and U1338. Red line = average values. Light blue shading = low-carbonate (dissolution) interval ("carbonate crash") (Lyle et al., 1995). Downcore variations in planktonic vs. benthic foraminifers reflect intervals of dissolution during the Pleistocene to early Miocene. Benthic foraminifers are more resistant to dissolution than most planktonic foraminifers (PF).
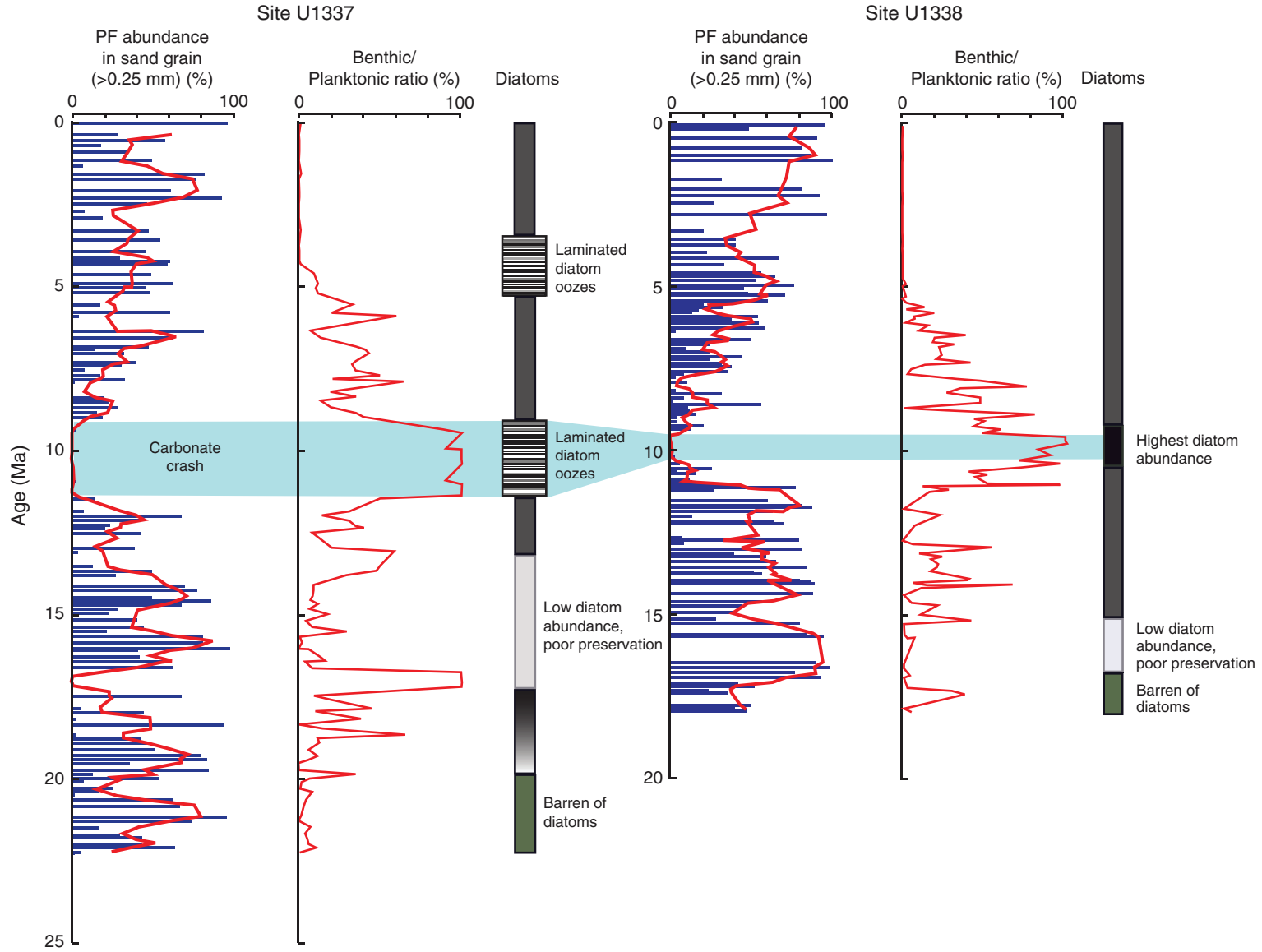
Figure F18. Carbonate content vs. preservation and abundance of calcareous microfossil groups. Blue shading = wt% CaCO₃, blue line = nannofossil preservation, purple crosses = abundance of coccolith taxon *Helicosphaera* (all from Hole A). Red shading = semiquantitative assessment of planktonic foraminifer abundance (percent of planktonics vs. other grains), red line = planktonic foraminifer preservation, orange line = benthic foraminifer preservation (all with compiled data from Holes A, B, and C). Preservation: G = good, M = medium, P = poor. Core composite images are from Hole A. **A.** Site U1332. (**Continued on next page.**)
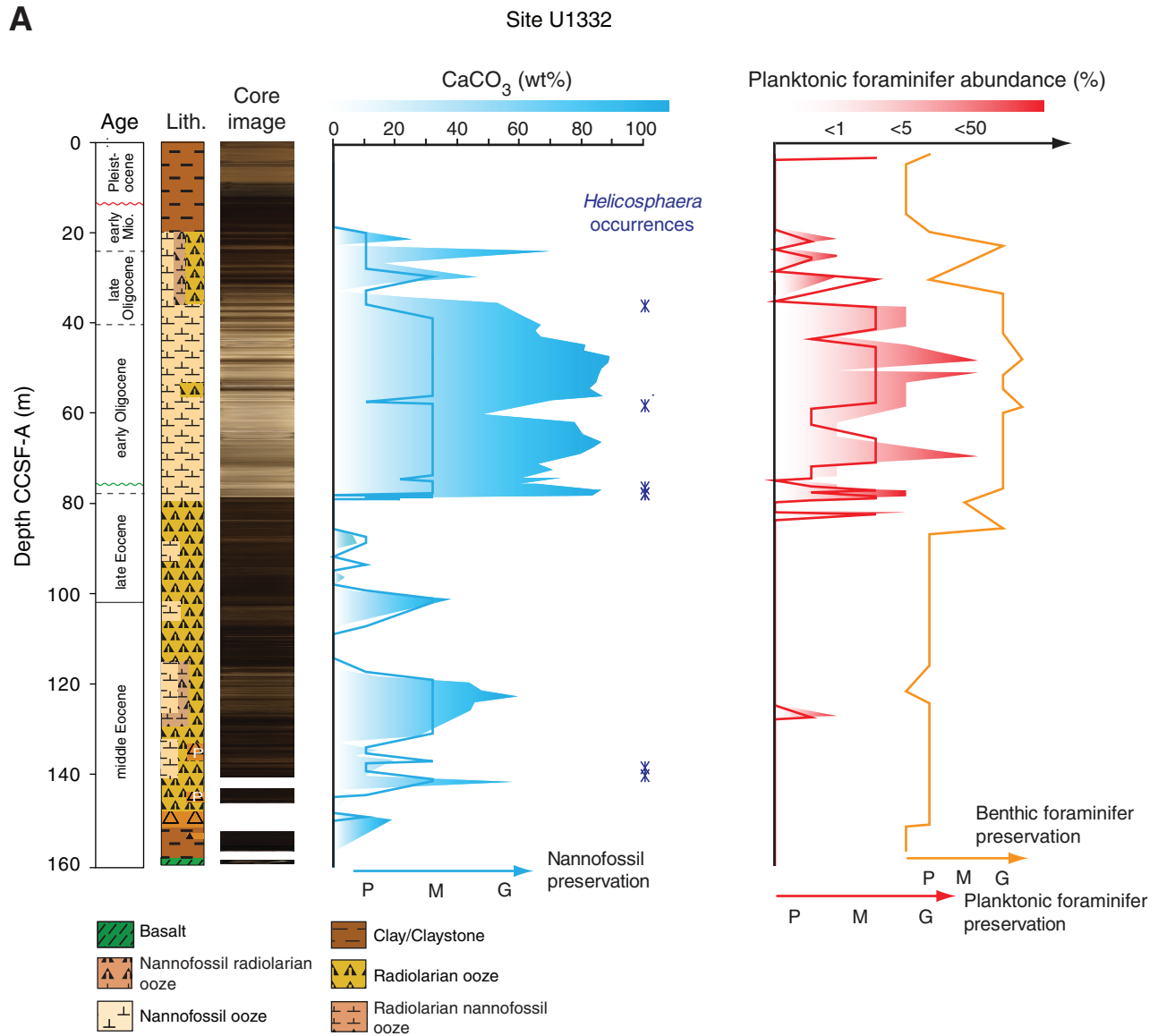
Figure F18 (continued). B. Site U1334.
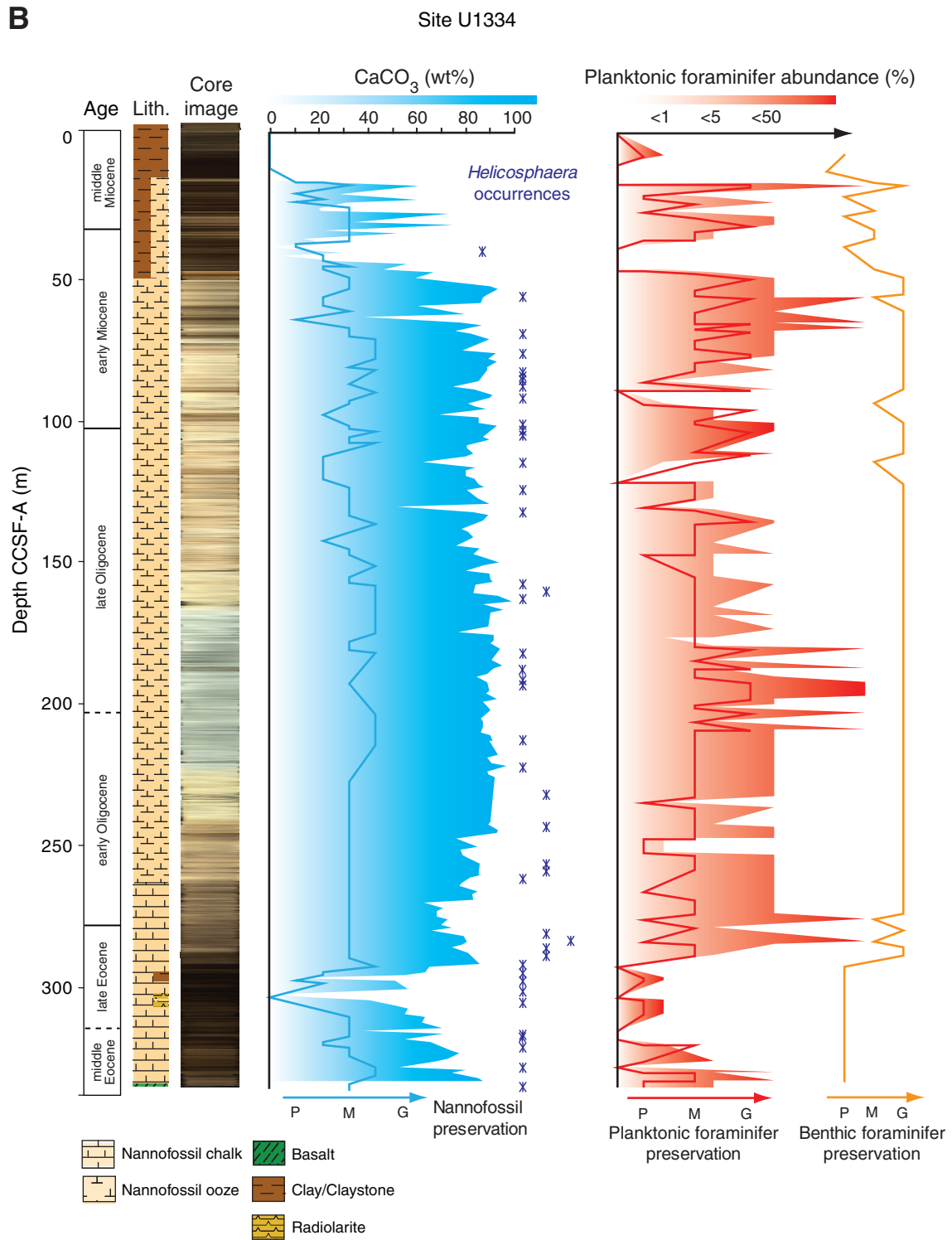
Figure F19. Planktonic foraminifer assemblage variations, Holes U1337A and U1338A. Correlation lines based on biochronologic data.
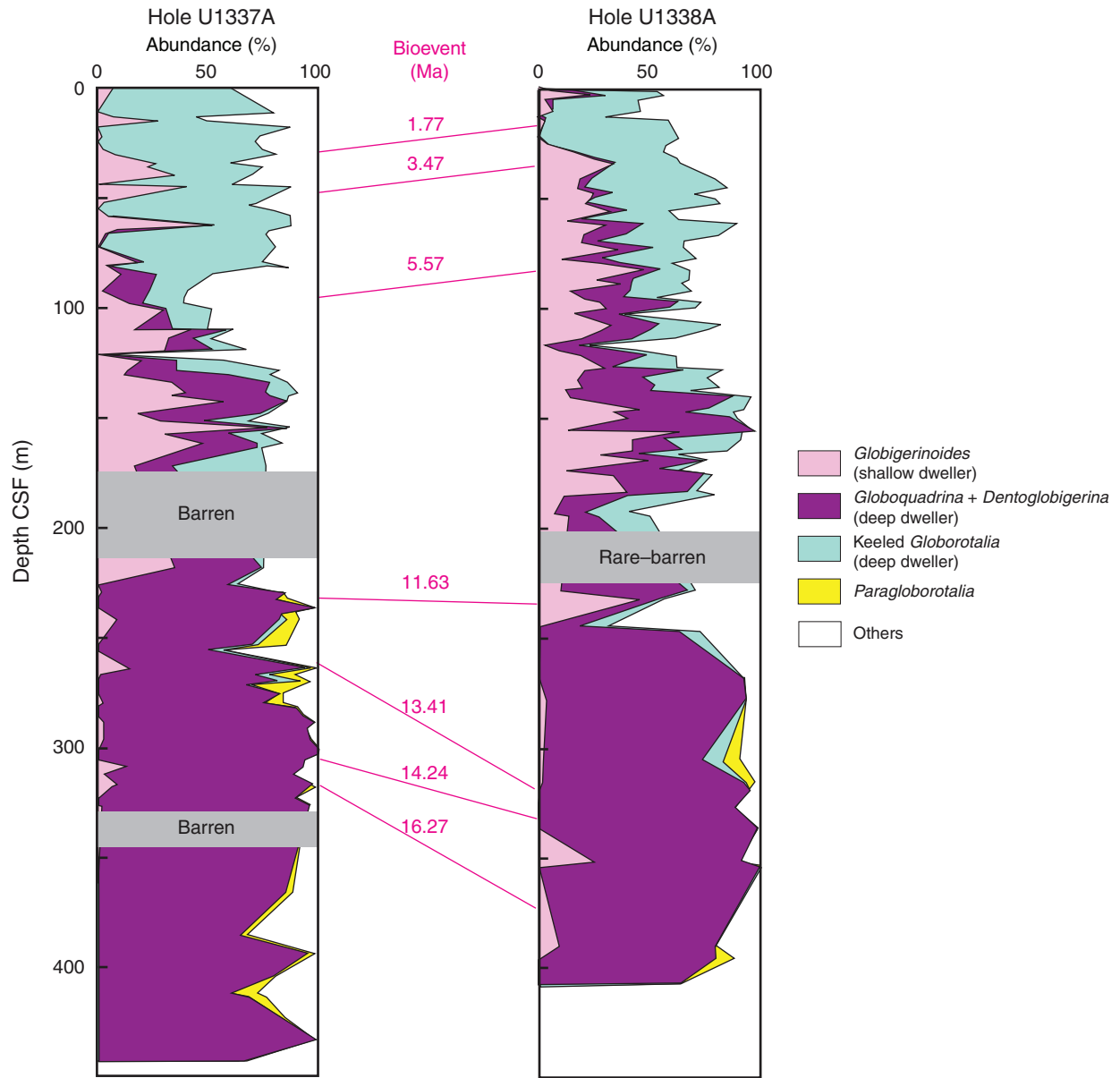
Figure F20. Line scan image compilation of basement basalt fragments recovered during Expedition 320, with overlying sedimentary section.
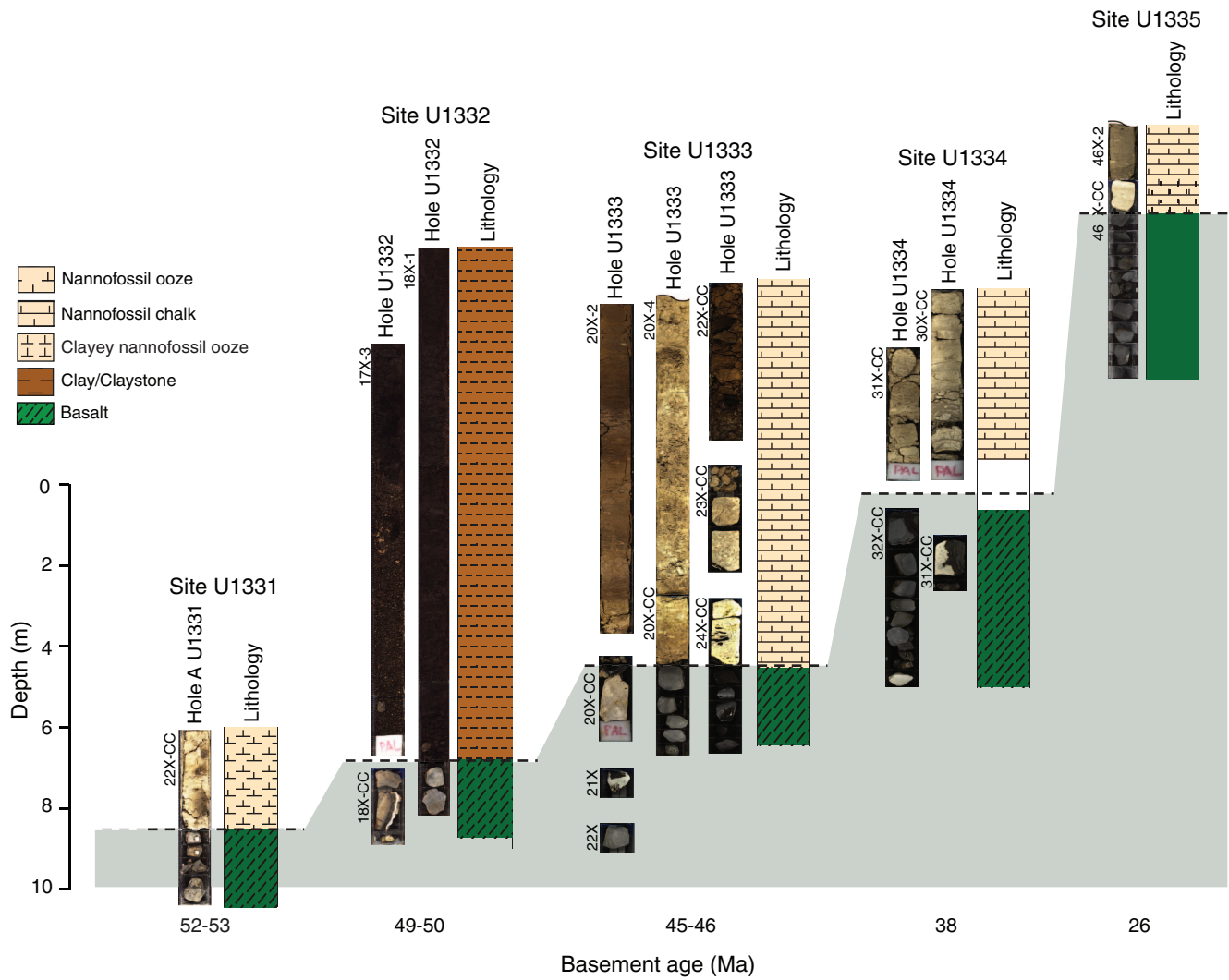
Figure F21. Stratigraphic compilation of diatom abundance in sediments from Expedition 320/321 and ODP Site 1218. Data for the Expedition 320/321 sites are from shipboard analysis. Data from Site 1218 are from Steiger (2006).
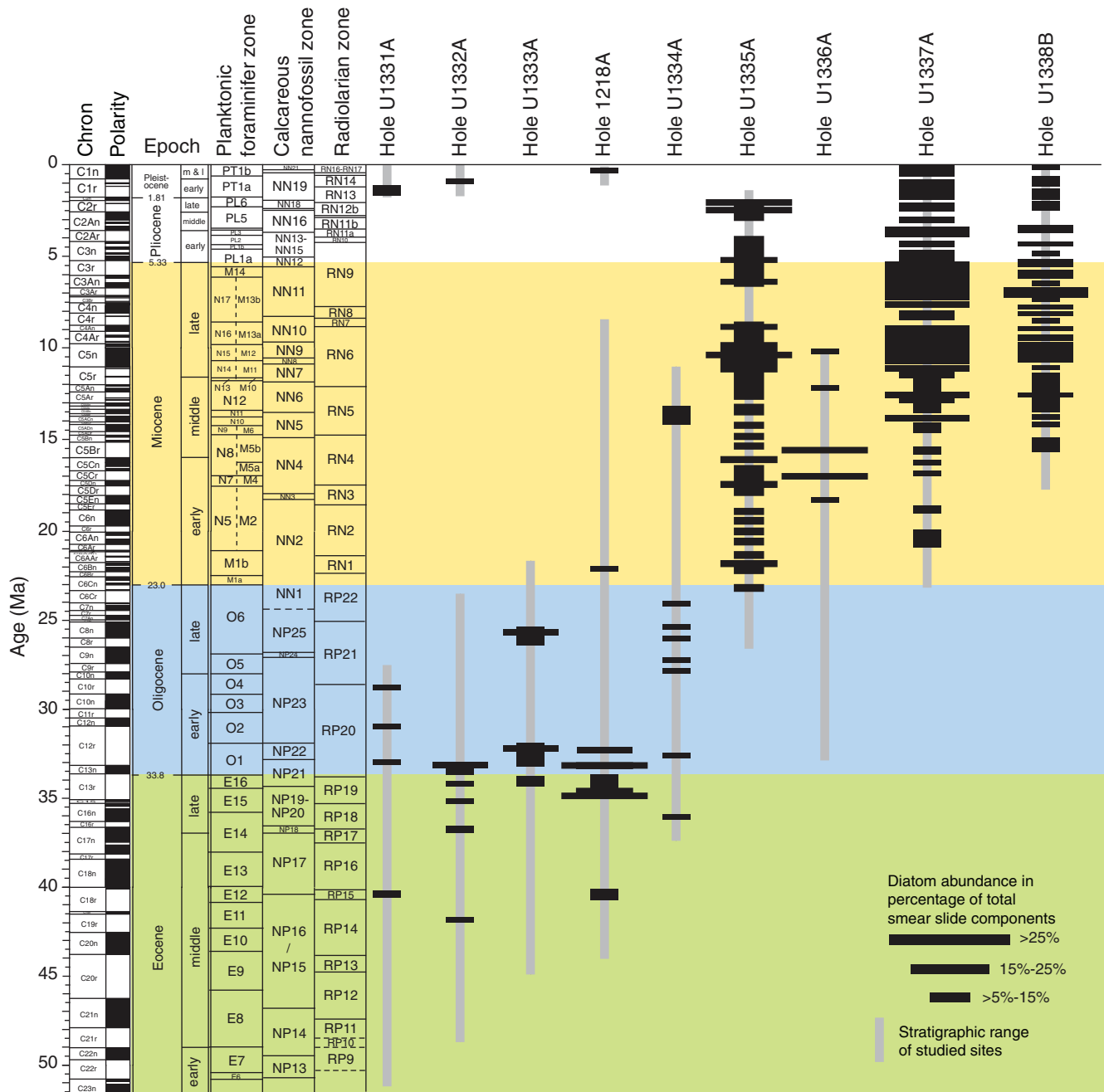
Figure F22. A. Line scan image of diatom mat (Section 321-U1337C-6H-2). **B.** Transmitted light microscope photograph of smear slide of *Thalassiothrix* diatom mat.
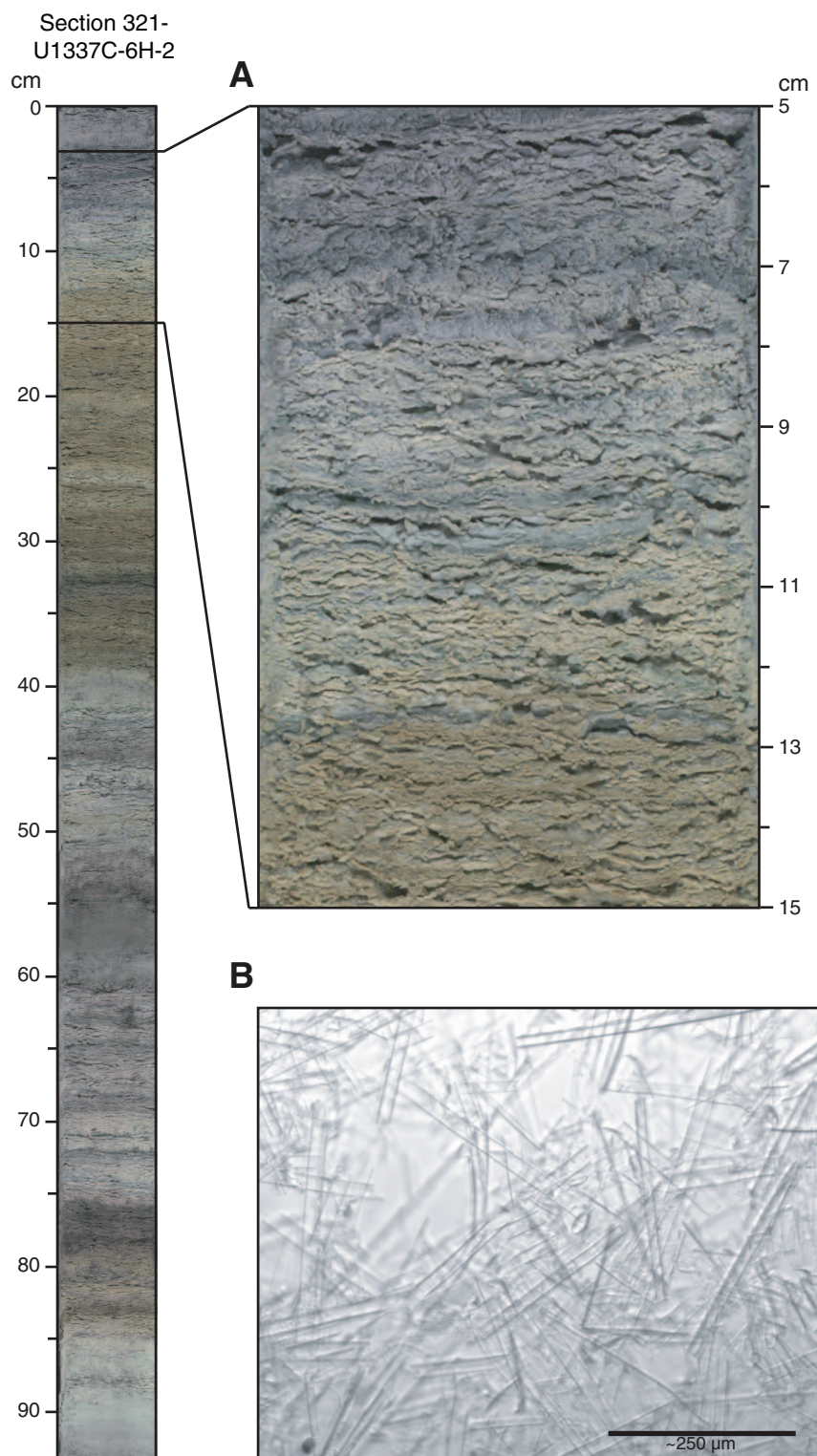
Figure F23. Summary of occurrence vs. age of recovered intervals of diatom mats and diatom-rich sediments, Expedition 321 Sites U1336–U1338; ODP Sites 844, 847, and 849–851; and DSDP Site 572.
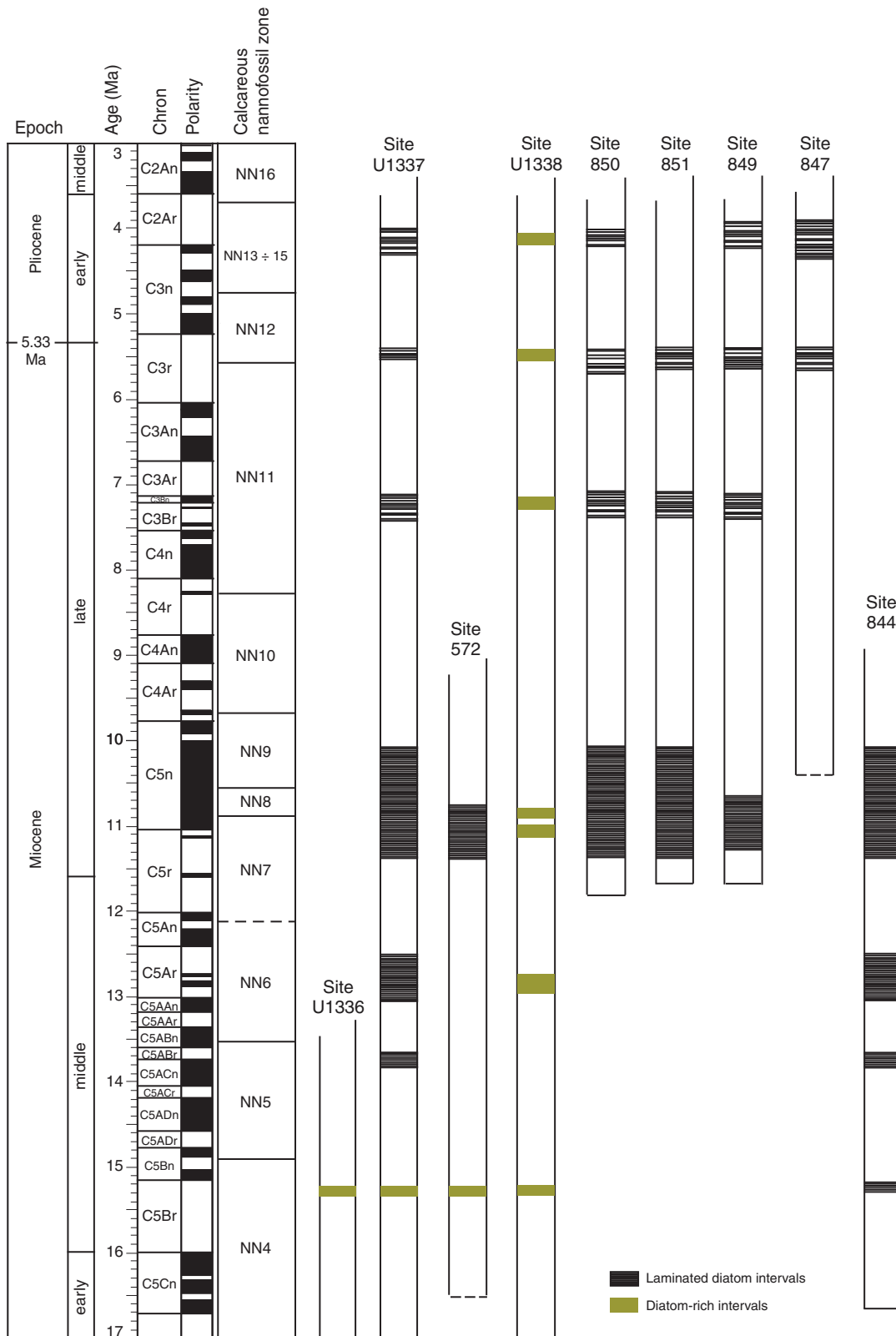
Figure F24. Downhole variation of paleomagnetic declination (green) and magnetostratigraphic interpretations, Site U1331–U1336. Red lines = possible geomagnetic excursions.
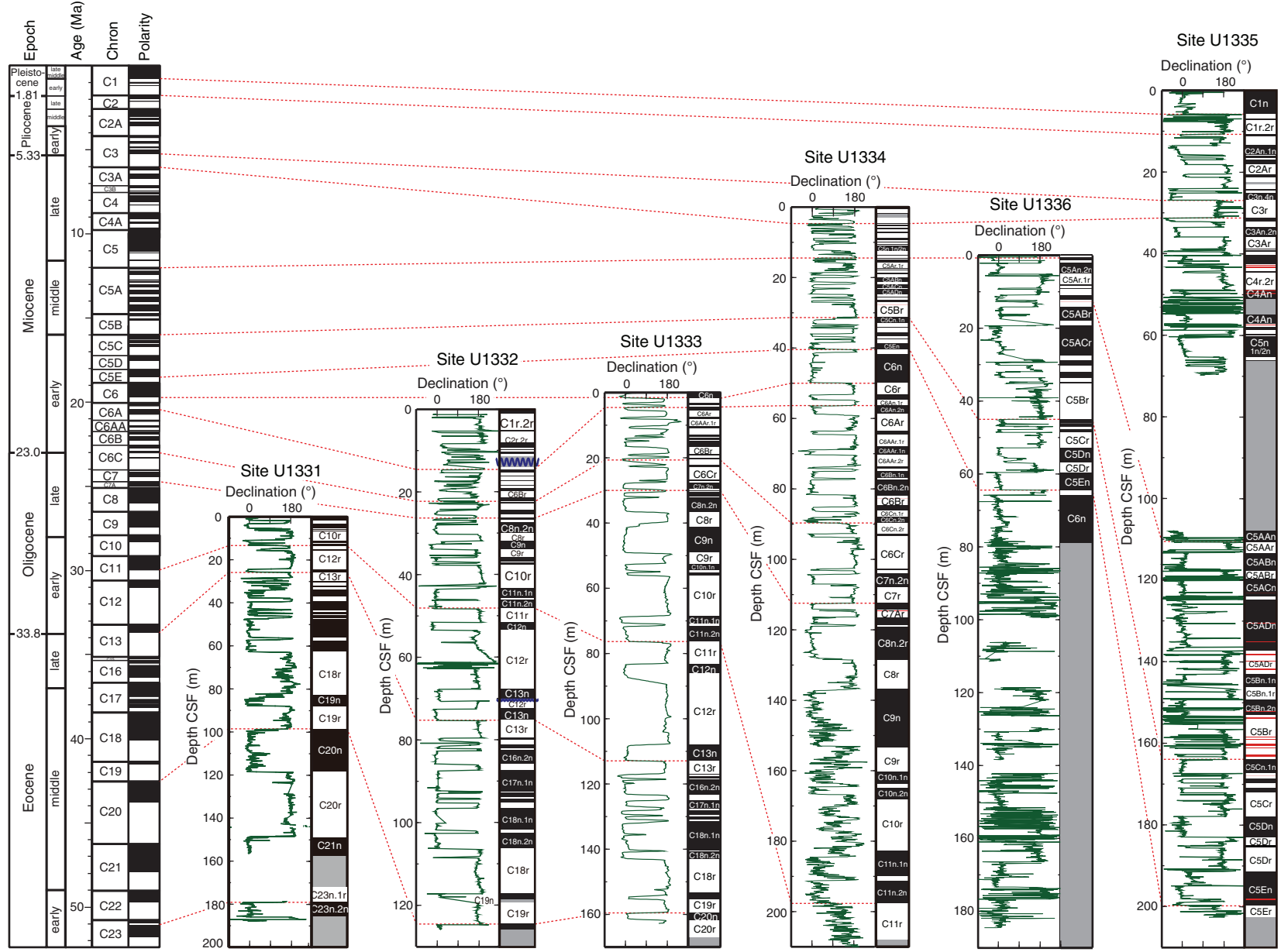
Figure F25. Downhole variation of paleomagnetic declination (green) and magnetostratigraphic interpretations, Sites U1334–U1338. Red lines = possible geomagnetic excursions.
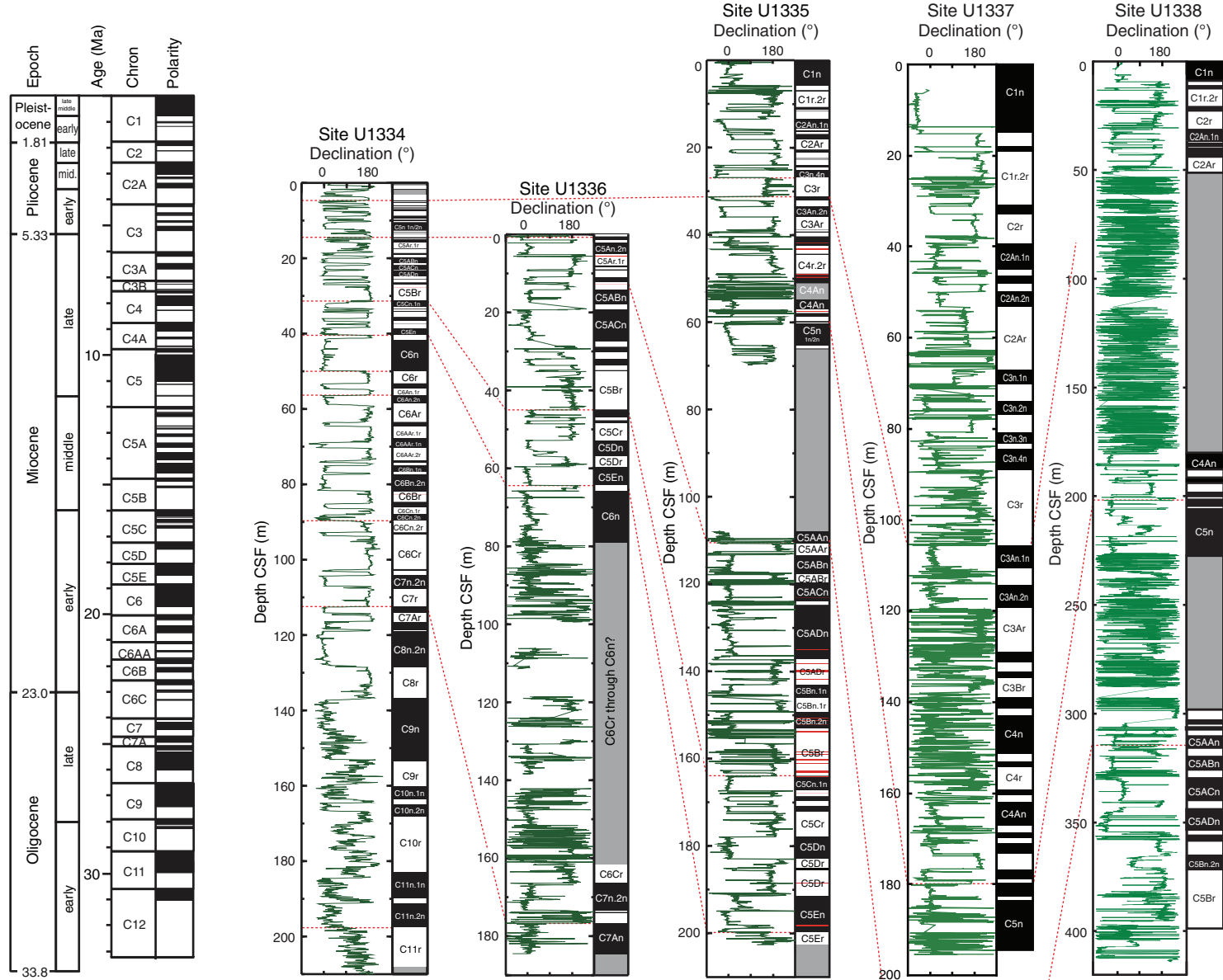
Figure F26. Coherence of sediment properties between widely separated drill sites from ODP Leg 199 and Expedition 320 in the equatorial Pacific is very high, allowing correlation of sediment properties over hundreds of kilometers. ODP Site 1220 and Expedition 320 Sites U1331 and U1332 are compared from 45 to 30 Ma. VGP = virtual geomagnetic pole. GRA density = gamma ray attenuation density (estimated on board).
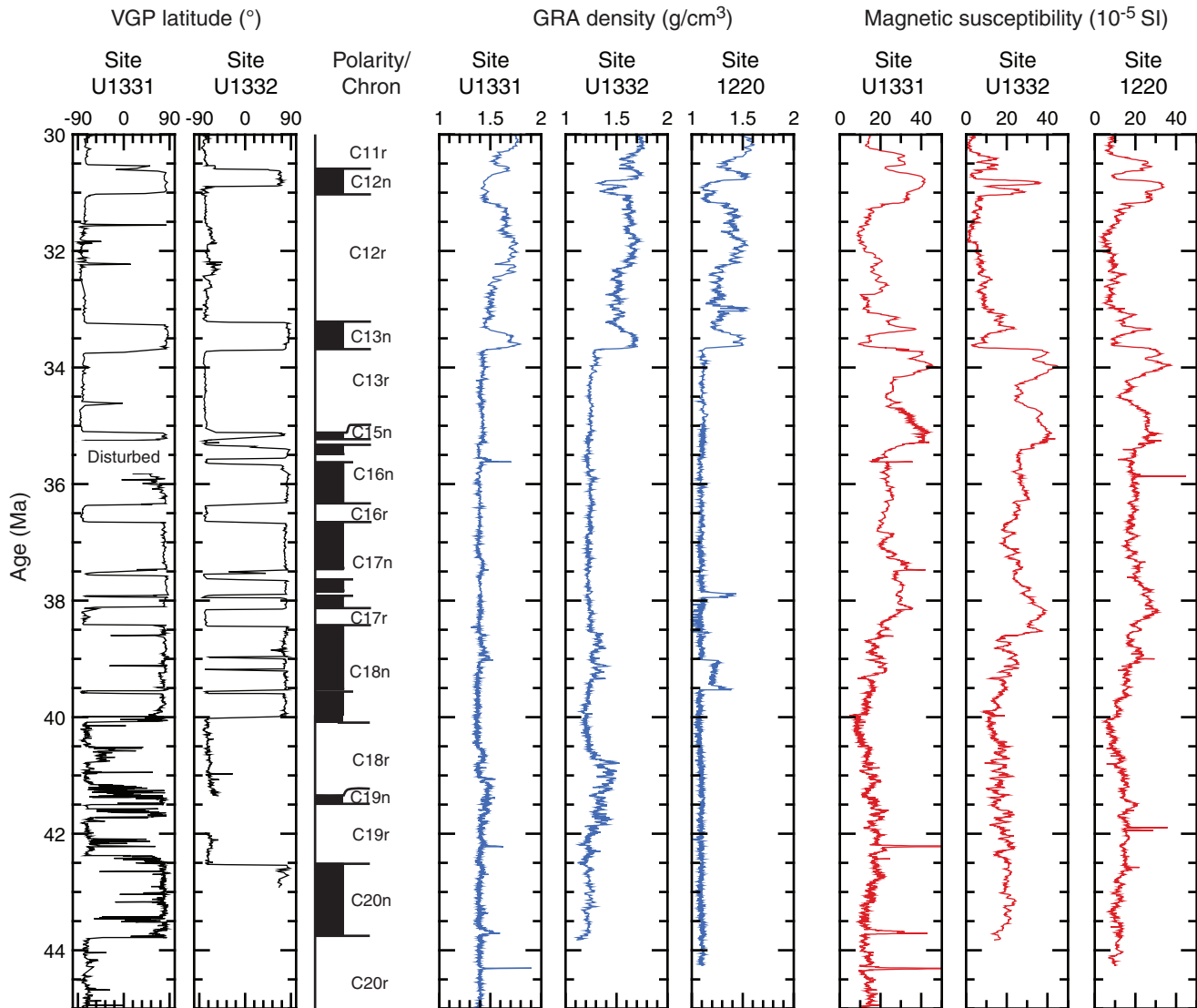
Figure F27. Coherence of sediment properties between widely separated drill sites from ODP Leg 199 and Expedition 320 in the equatorial Pacific is very high, allowing correlation of sediment properties over hundreds of kilometers. ODP Site 1218 and Expedition 320 Sites U1333 and U1334 are compared from 35 to 20 Ma. VGP = virtual geomagnetic pole. GRA density = gamma ray attenuation density (estimated on board).
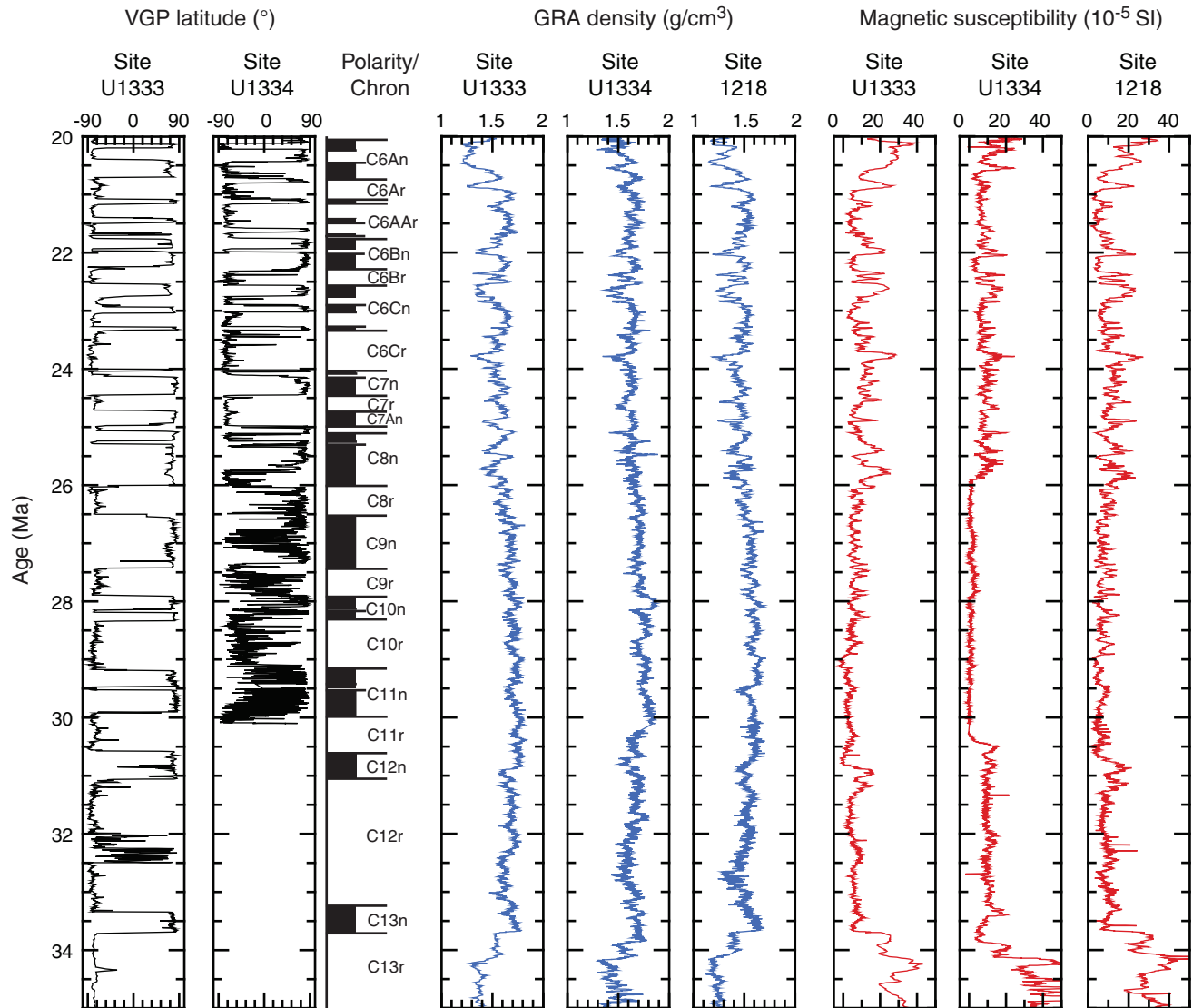
Figure F28. High-resolution bulk density downhole logs from Holes U1337A (black) and U1338B (red) with depth scales shifted and stretched to match the different sedimentation rates at the two sites. Blue = nannofossil events and respective ages. Pa Rp = paracme *Reticulofenestra pseudoumbilicus*. Dh = *Discoaster hamatus*. Cm = *Coccolithus miopelagicus*. Dk = *Discoaster kugleri*. Sh = *Sphenolithus heteromorphus*. Dd = *Disocaster deflandrei*. Depths of nannofossil events are core depths below seafloor and may differ from wireline log matched depth below seafloor (WMSF) by several meters.
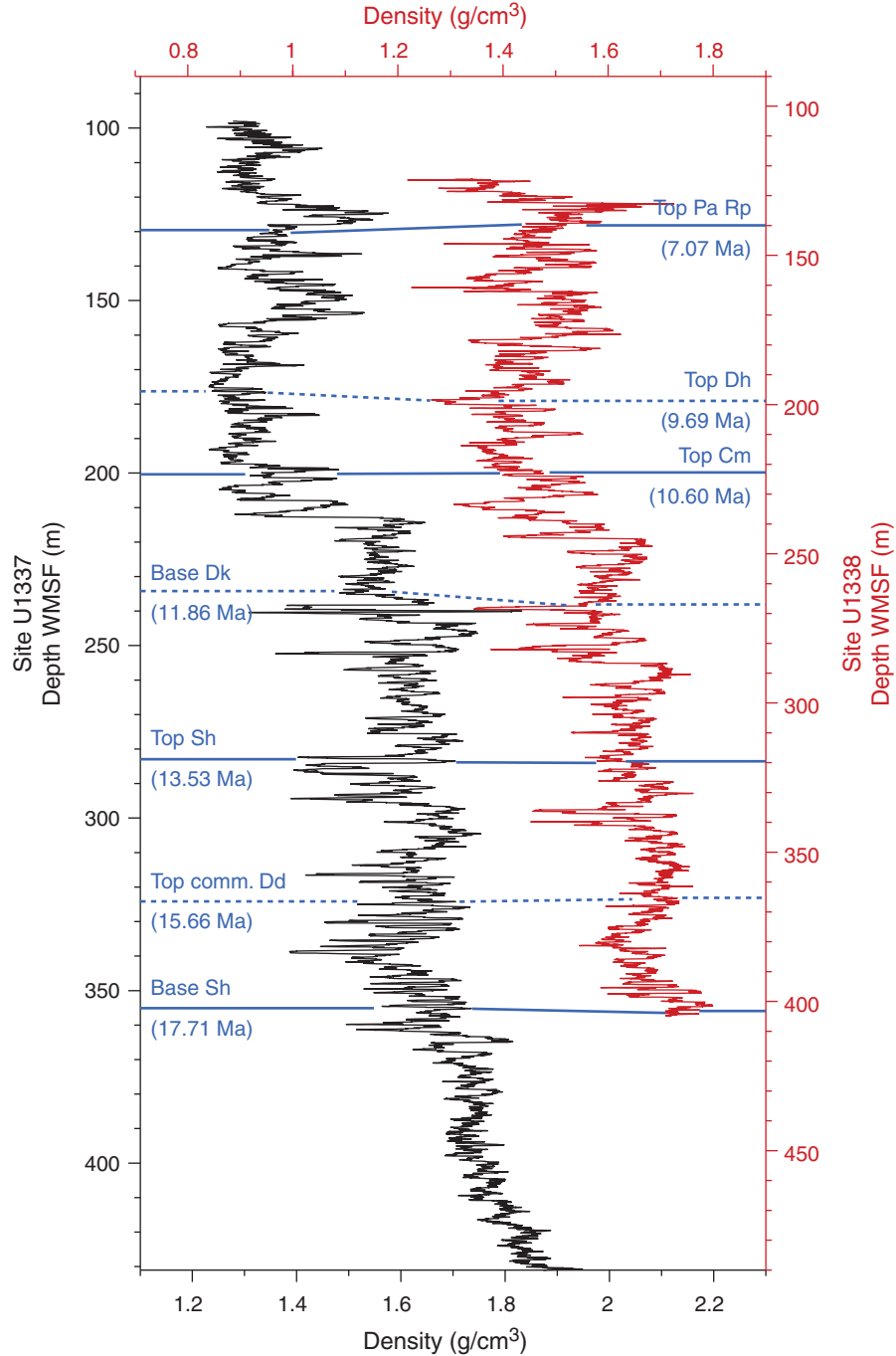
Figure F29. Indicative gamma ray attenuation (GRA) bulk density megasplice constructed from a stack of Leg 138 equatorial Sites 849–851. Sites 849 and 851 were correlated to Site 850 using the Analyseries program (Paillard et al., 1996) and biostratigraphic datums to check the similarity in character of the curves. These records were stacked and averaged (three-point smooth), forming the Site 850 composite record. Site 844 was also correlated to the lower part of the Site 850 composite and appended to the bottom of the record in order to extend its range back to the middle Miocene. Expedition 320 Site U1335 (black curve) was correlated to the bottom of this composite record, again using biostratigraphic datums, to check the similarity in character of the two records near the join. This exercise was repeated to join Site U1335 to the Site 1218 record (green curve). Because the base of Site U1335 is several hundred meters below the seafloor, its compacted density was substantially offset from the Site 1218 values. A density offset value of 0.44 was added to all density values of the Site 1218 record. Near the Eocene/Oligocene boundary, the Site 1218 density record was correlated to that of Site 1334 (the site with the highest carbonate content) with an added density offset of 0.22 (purple curve). This completes the megasplice density record back to the top of the middle Eocene.
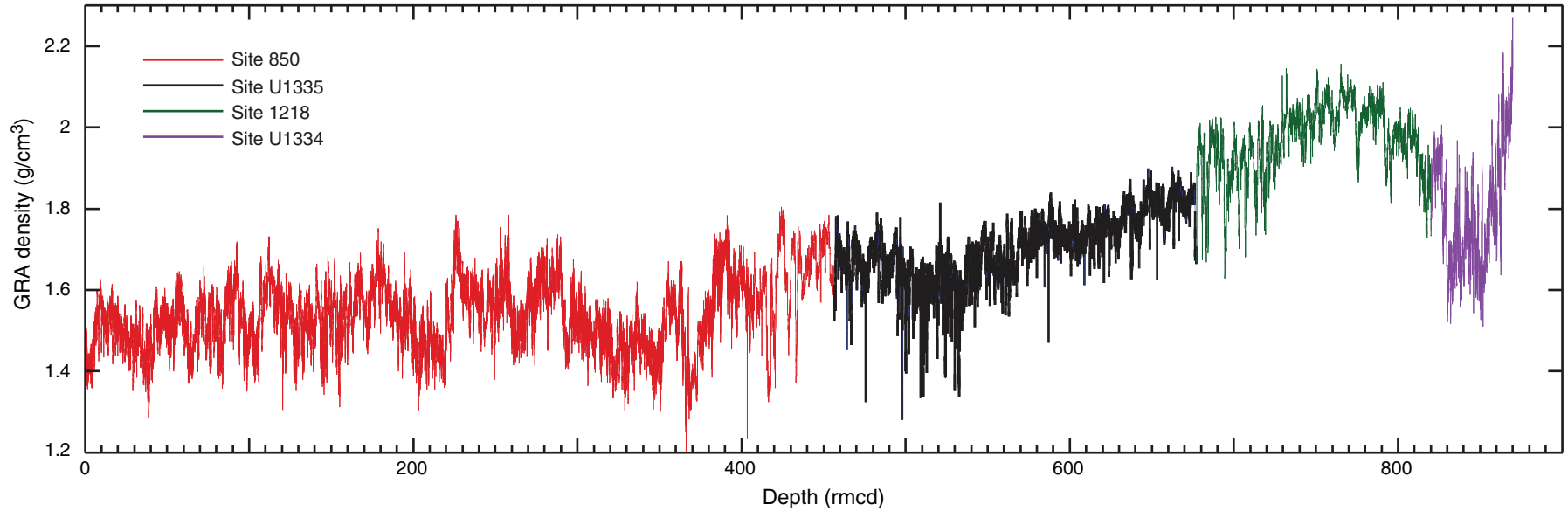
Figure F30. Summary of sedimentation rates derived from age-depth models at each Expedition 320 site.
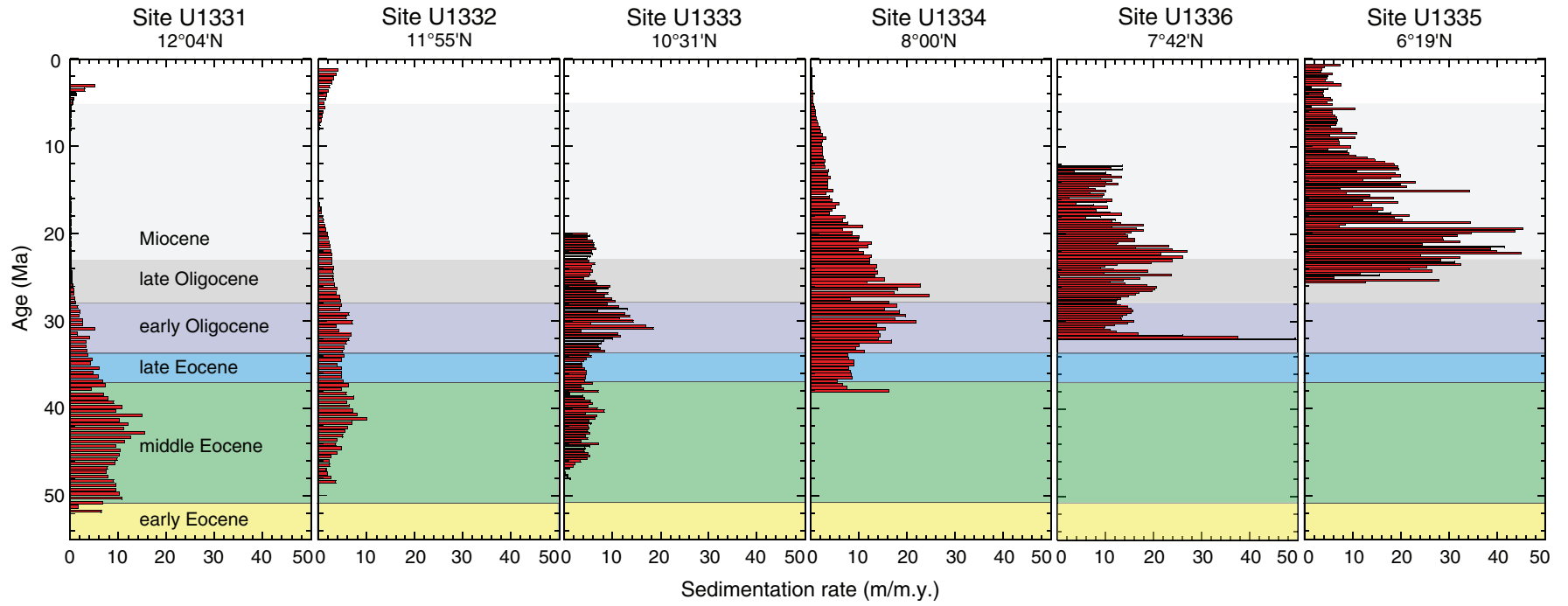
Figure F31. Line scan images of the Middle Eocene Climatic Optimum (MECO) event, Holes U1333A–U1331C.
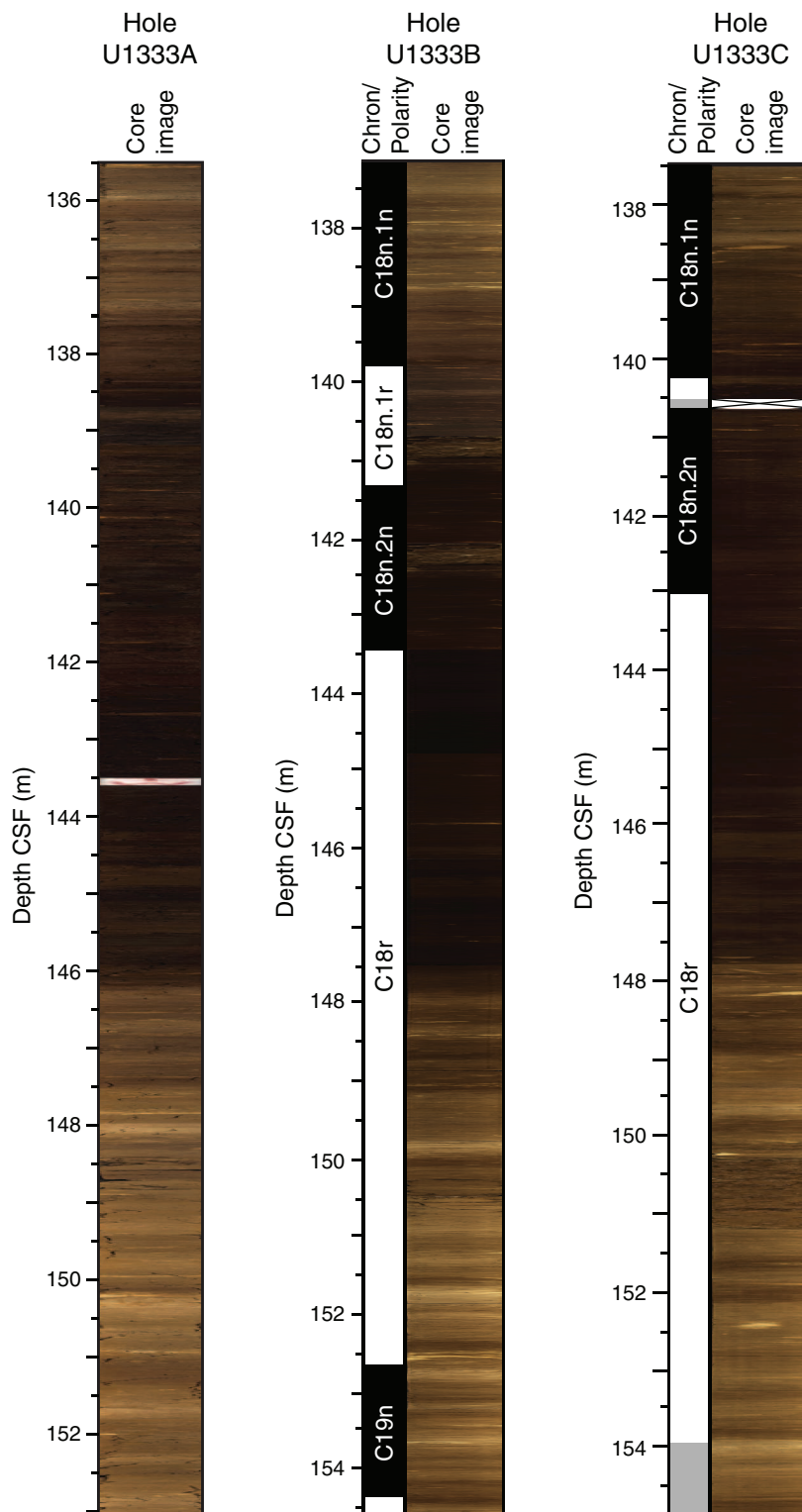
Figure F32. Line scan image compilation of depth transect across Eocene–Oligocene transition captured by Expedition 320 Sites U1331–U1334. Dashed line approximates position of the Eocene/Oligocene boundary, as refined by Pearson et al. (2008).
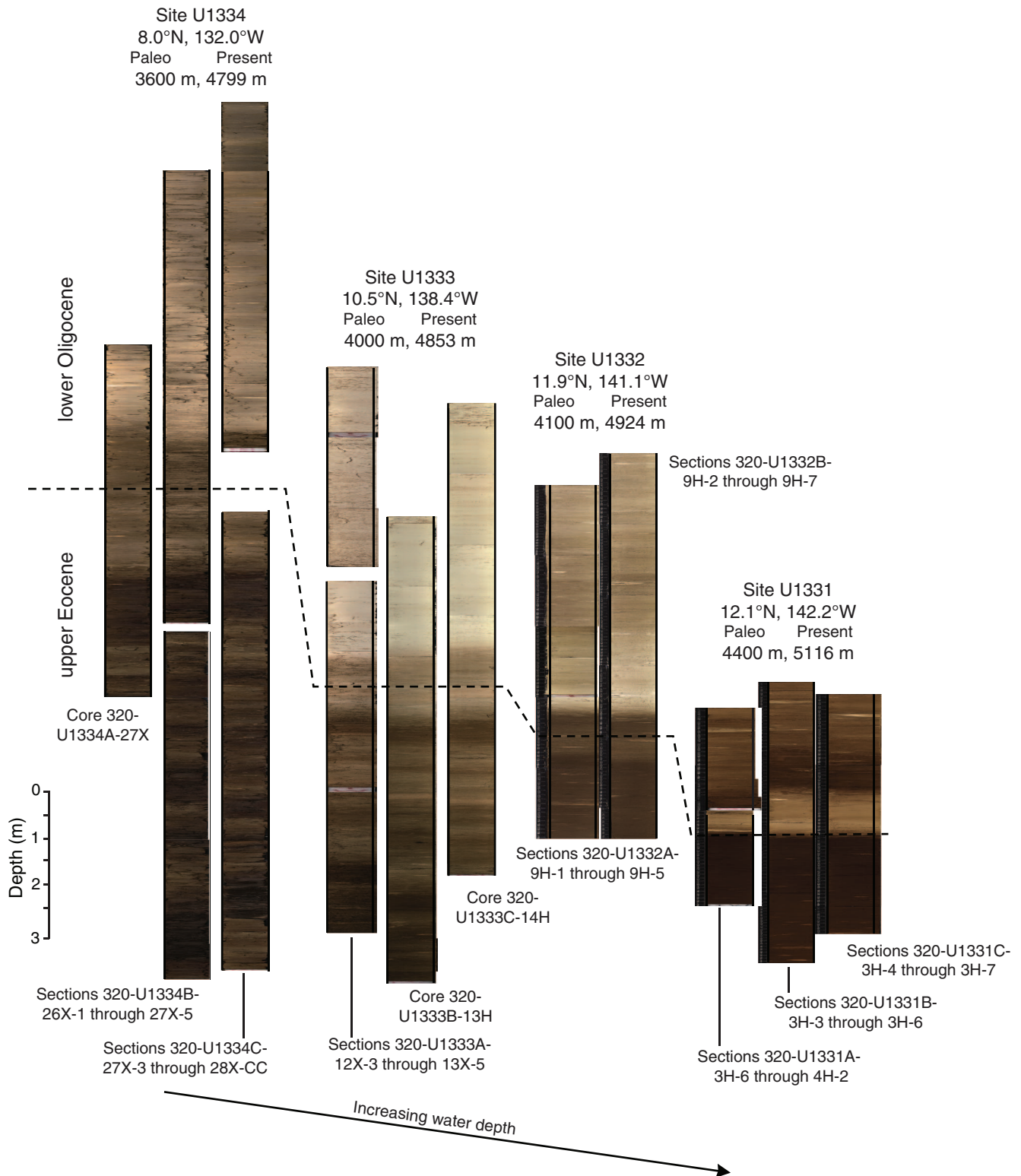
Figure F33. Line scan images of Eocene–Oligocene transition. **A.** Hole U1334A. **B.** Hole U1334B. **C.** Hole U1334C. Images were manipulated by applying a shadow-highlight adjustment to the whole image for better visual inspection of the darker strata. Nonmanipulated images are shown in Figure **F12** in the "Site U1334" chapter. L* = reflectance value of sediment as defined in the LAB color model.
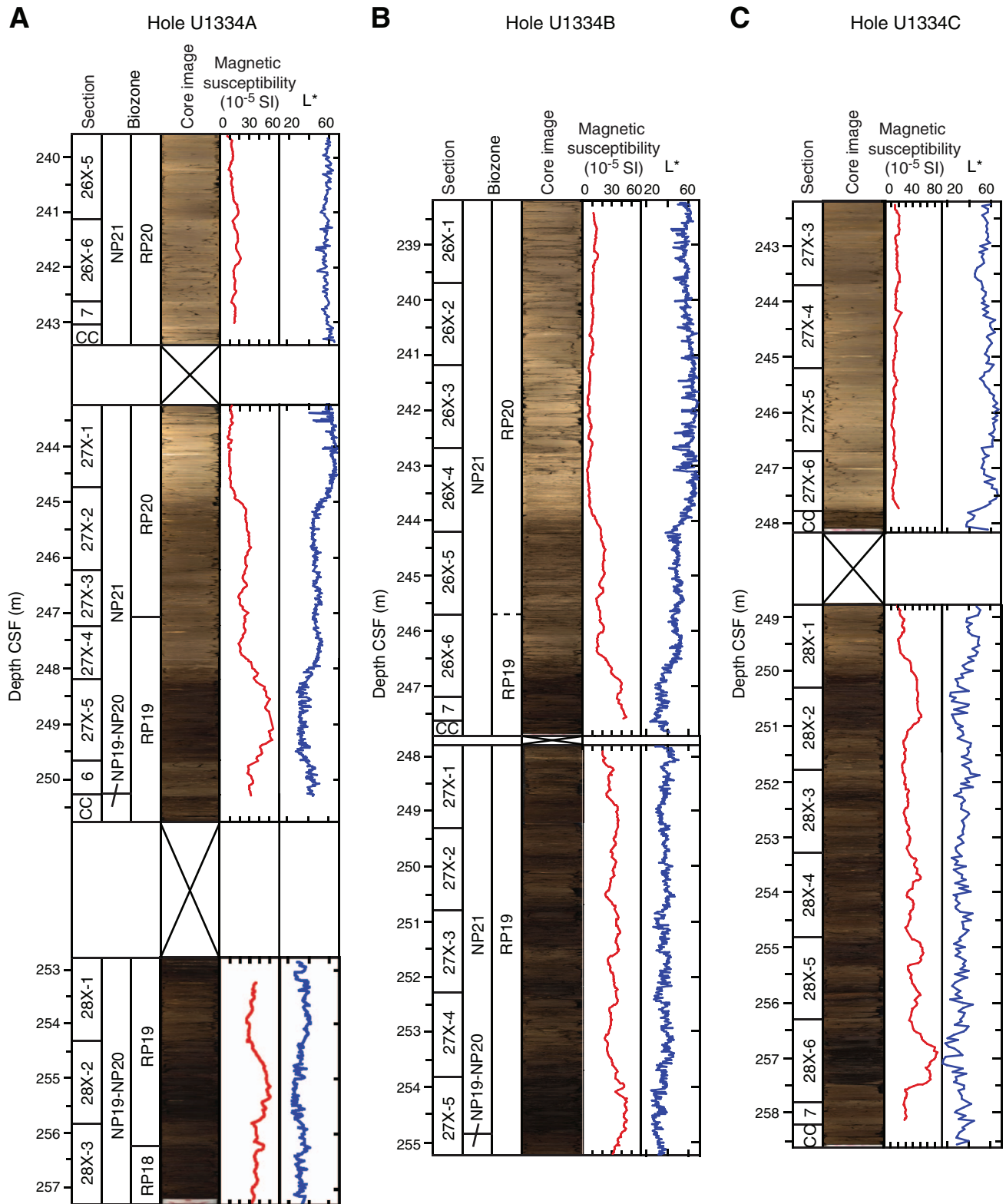
Figure F34. Magnetic susceptibility for each hole drilled at Site U1333. Depths are adjusted in overlapping hole intervals to match CCSF-A. Solid black circle = first appearance of Eocene species, solid black arrowhead = last appearance of Eocene species, open red circle = first appearance of Oligocene species, open red arrowheads = last appearances of Oligocene species. T = top, B = bottom.
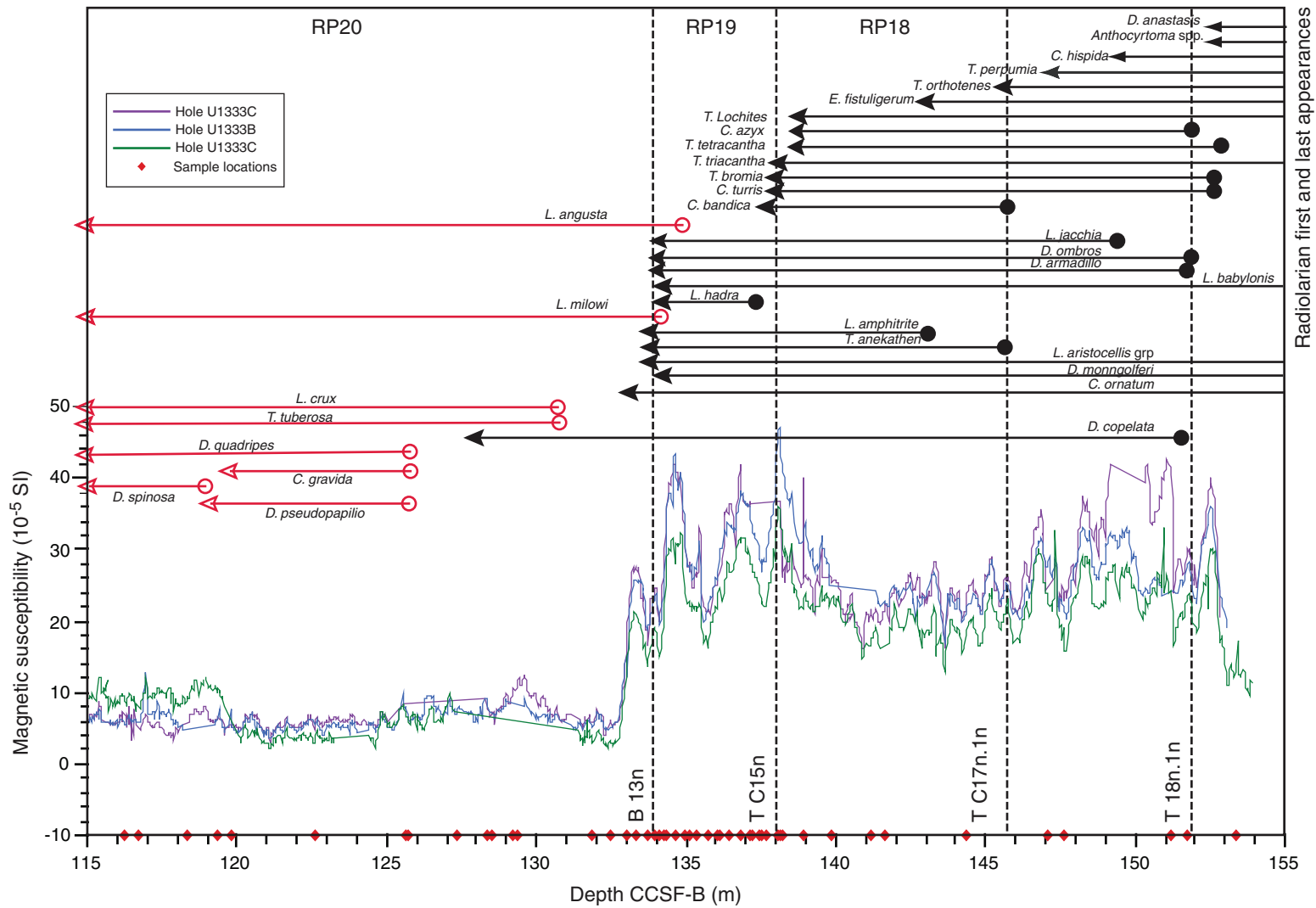
Figure F35. Correlation of magnetic susceptibility records from ODP Site 1218 and Expedition 320 Sites U1334 and U1333 for the upper Eocene and lower Oligocene. Solid and dashed vertical lines = positions of magnetic chron boundaries, solid green and dashed red lines = points of proposed correlation, green stars = species datums used in correlation. T = top, B = bottom.
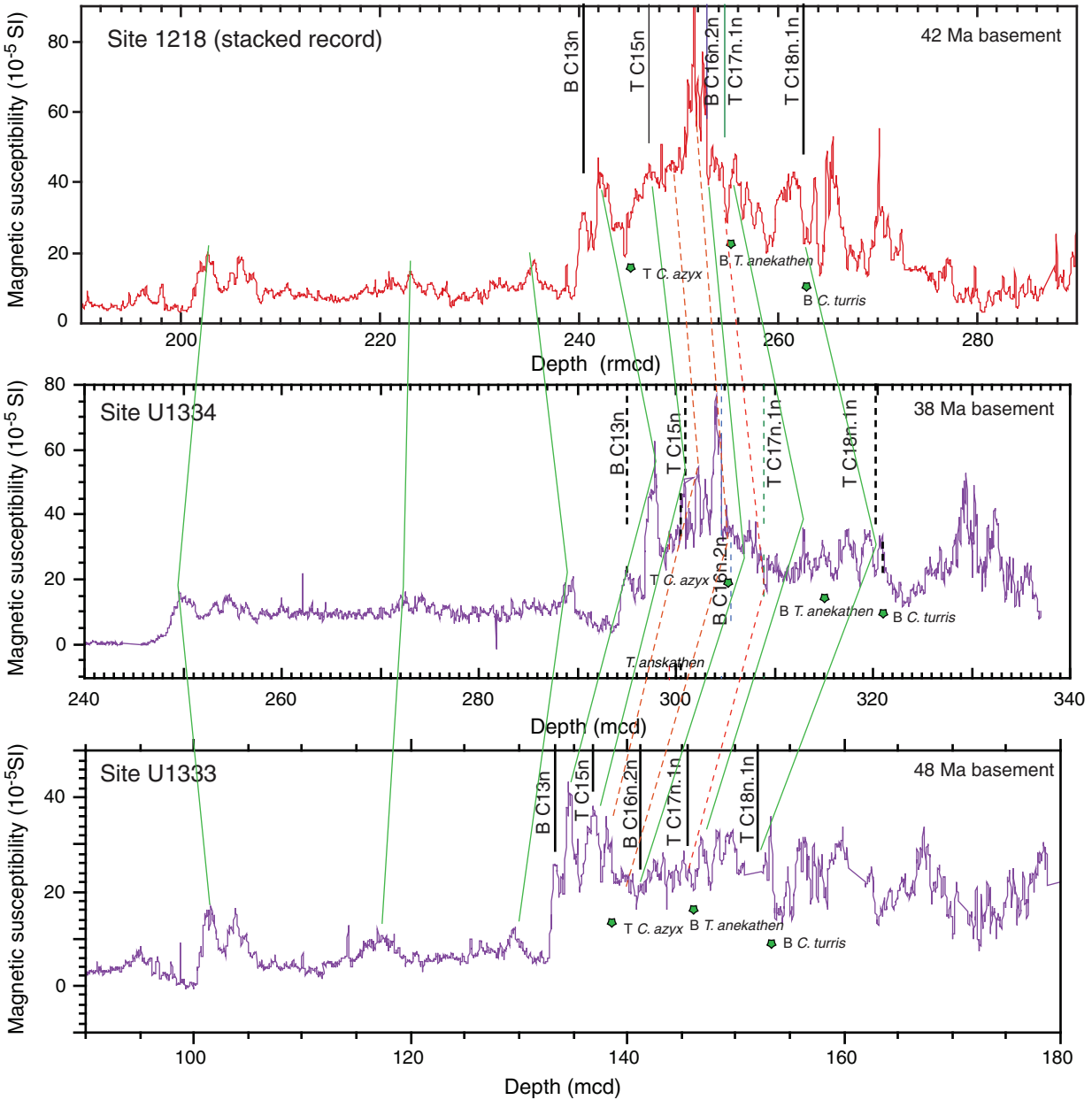
Figure F36. Magnetic susceptibility records for ODP Sites 1218–1220 and Expedition 320 Site U1333 for the upper Eocene. Site 1219 and 1220 depths have been adjusted to match the record of Site 1218. Note that the general character of the record from Site U1333 (located on 48 Ma crust) is more similar to records from Sites 1219 and 1220 (located on 56 Ma crust) than to that of Site 1218 (located on 42 Ma crust).
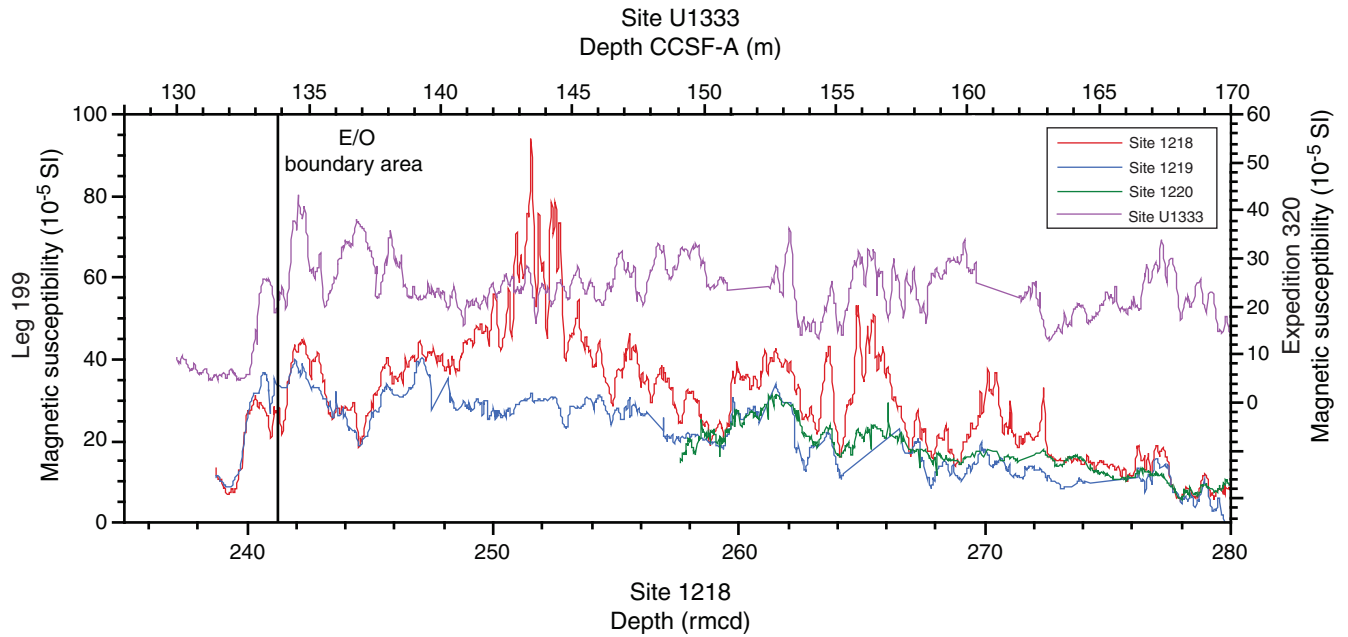
Figure F37. Lowermost Oligocene through upper middle Eocene magnetic susceptibility records, Sites U1331–U1334. Radiolarian datums in this section guide the correlation (red lines) of these records. All records plotted using approximately the same depth scale. Oligocene section is expanded as we move southward toward the early Oligocene paleoequator (Site U1334); Eocene section is expanded at the northern Sites (U1331 and U1332) that are closer to the middle Eocene paleoequator. However, the northern sites have the most condensed Eocene/Oligocene boundary interval. The two-step transition from the Eocene to the Oligocene is most pronounced at Sites U1333 and U1334. T = top, B = bottom.
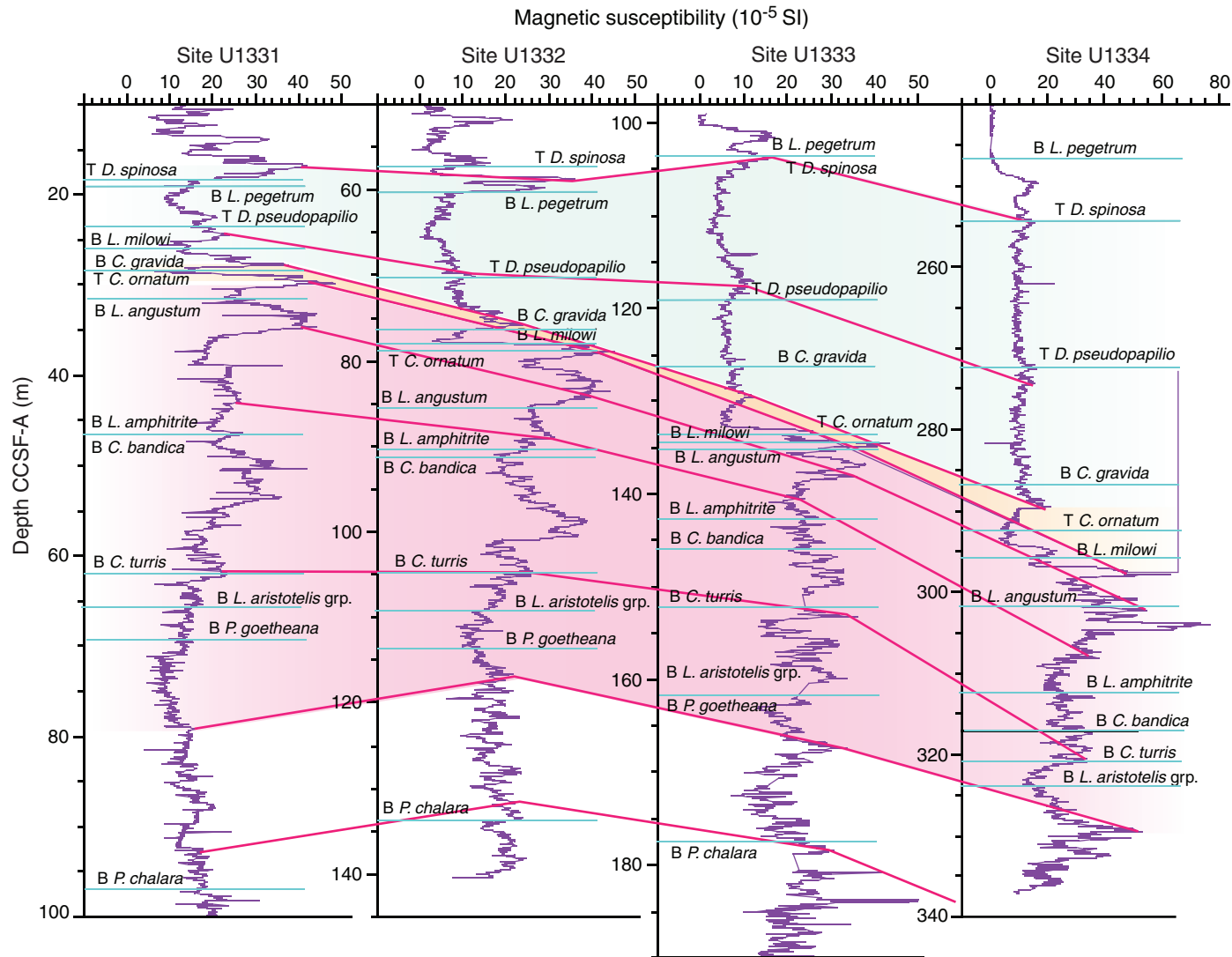
Figure F38. Composite line scan images of cores taken from the Oligocene–Miocene transition, Sites U1332–U1334 and U1336. The Oligocene/Miocene (O/M) boundary is defined by the M1a/O6 planktonic foraminifer zone boundary, here approximated at the base of the C6Cn.2n Chron at Sites U1332–U1334 and at the lower middle part between the *S. delphix* biozone and the first occurrence (FO) depth of *P. kugleri* at Site U1336, taking account of sedimentation rate and light–dark color alternation pattern. Paleo-water depths estimated at 23 Ma. Note that an O/M boundary was also recovered at Site U1335. However, biostratigraphic control is only available for Hole 1335A where the utility of the core section images is limited by the effect of the core splitting process. These sediments are too consolidated for use of a cheese wire and too soft for use of a saw to cut whole-round core sections. Physical property data did not yet allow correlation between Holes U1335A and U1335B in these intervals. Chron is listed on the left for Sites U1332–U1334. LO = last occurrence.
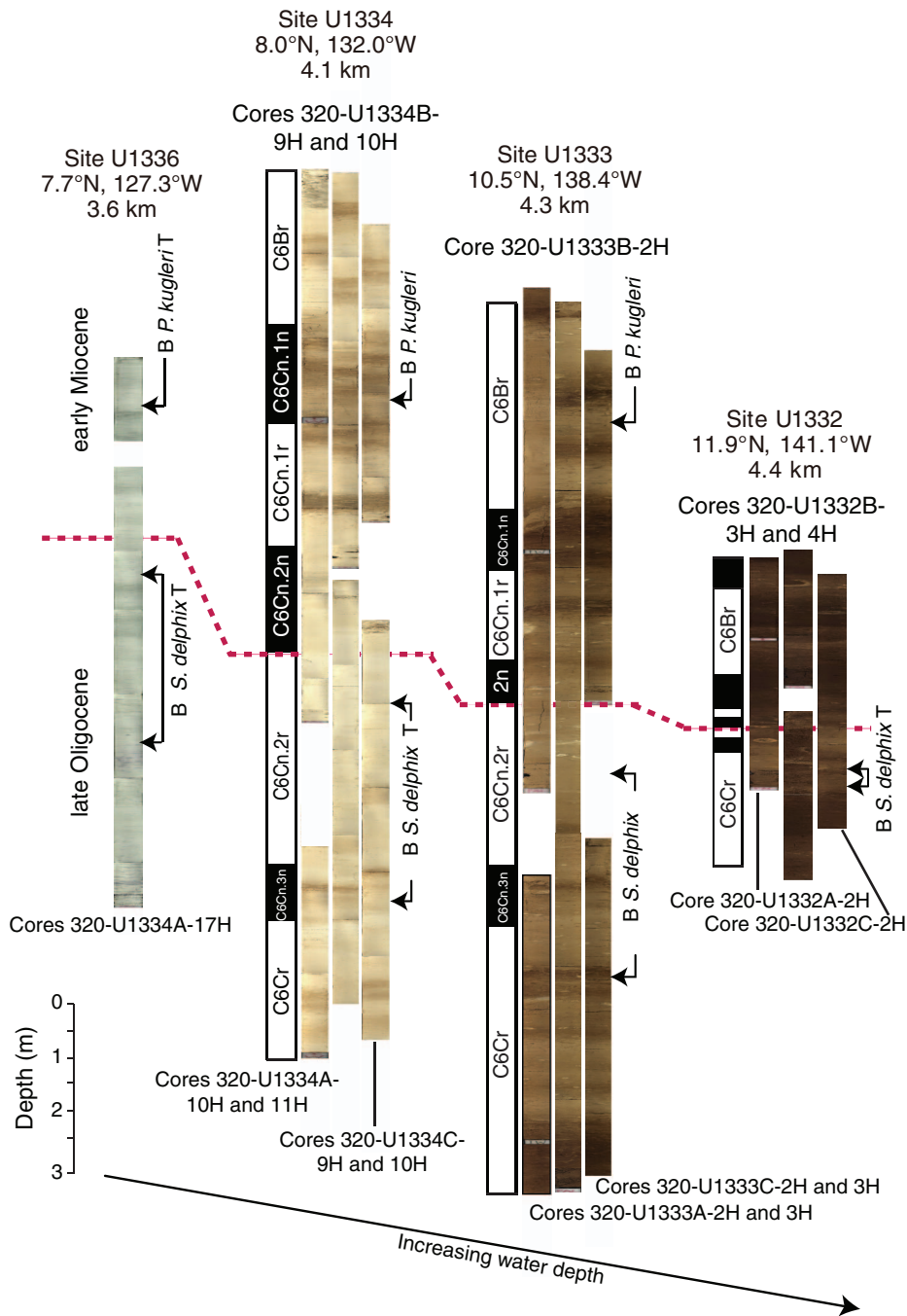
Figure F39. Sediment color and interstitial water chemistry change summaries. **A.** Site summaries. **B.** Sediment color changes superimposed on site backtrack curves as interpreted from visual core descriptions.
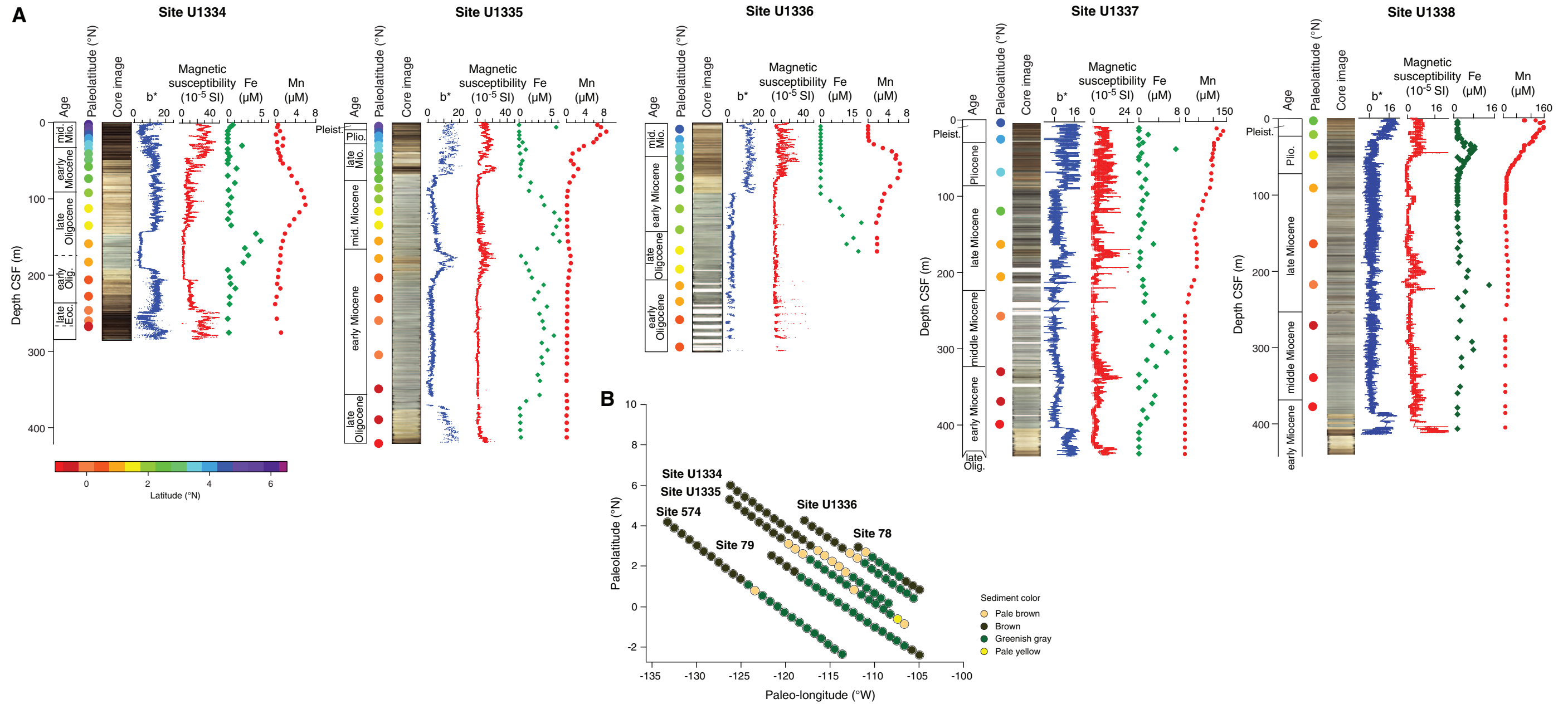
Figure F40. Calcium carbonate (CaCO₃) concentrations in sediments, Holes U1331A, U1332A, U1333A, U1334A, U1335A, and U1336A.
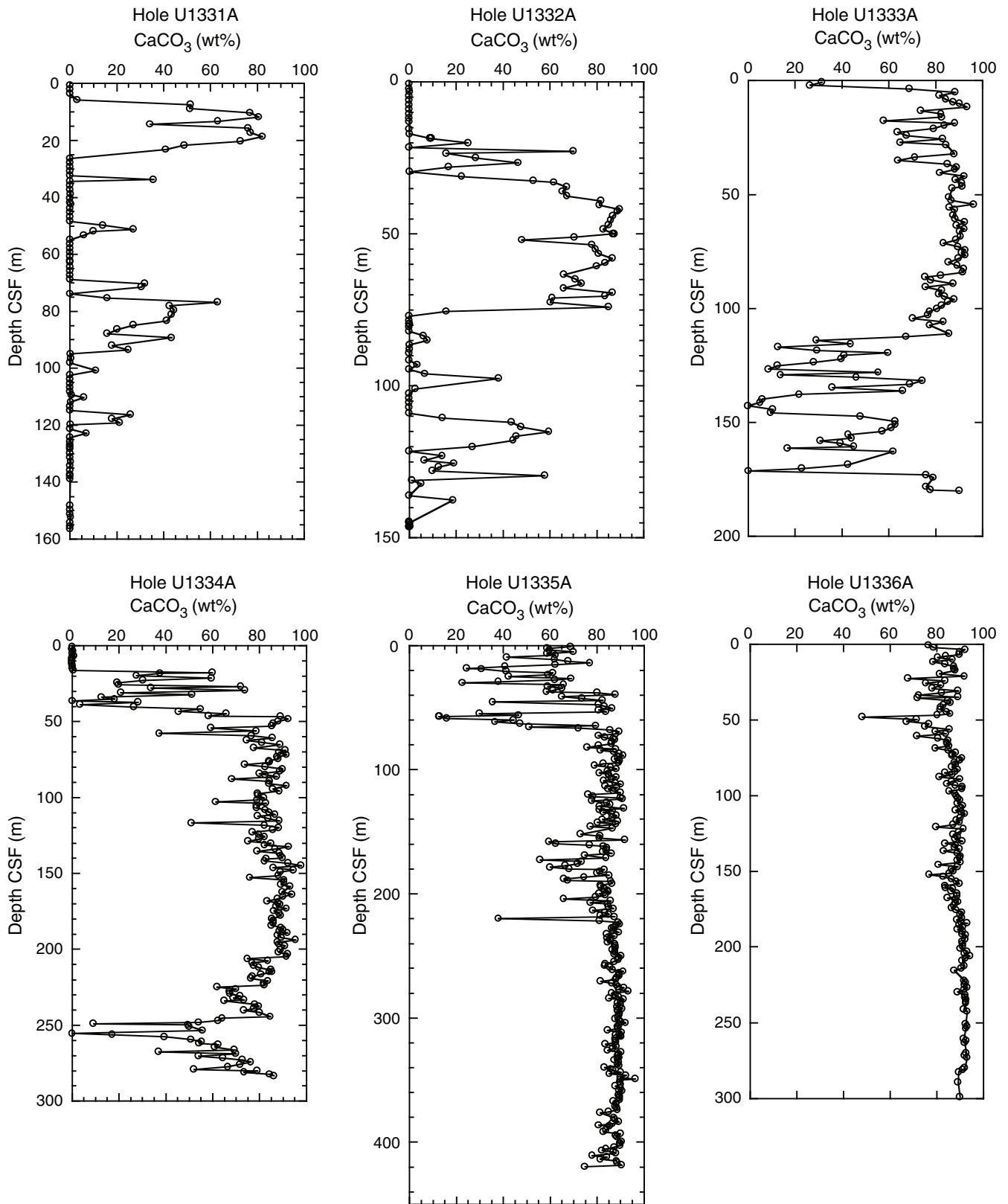
Figure F41. Total organic carbon (TOC) content in sediments determined by acidification method, Holes U1331A, U1332A, U1333A, U1334A, and U1335A.
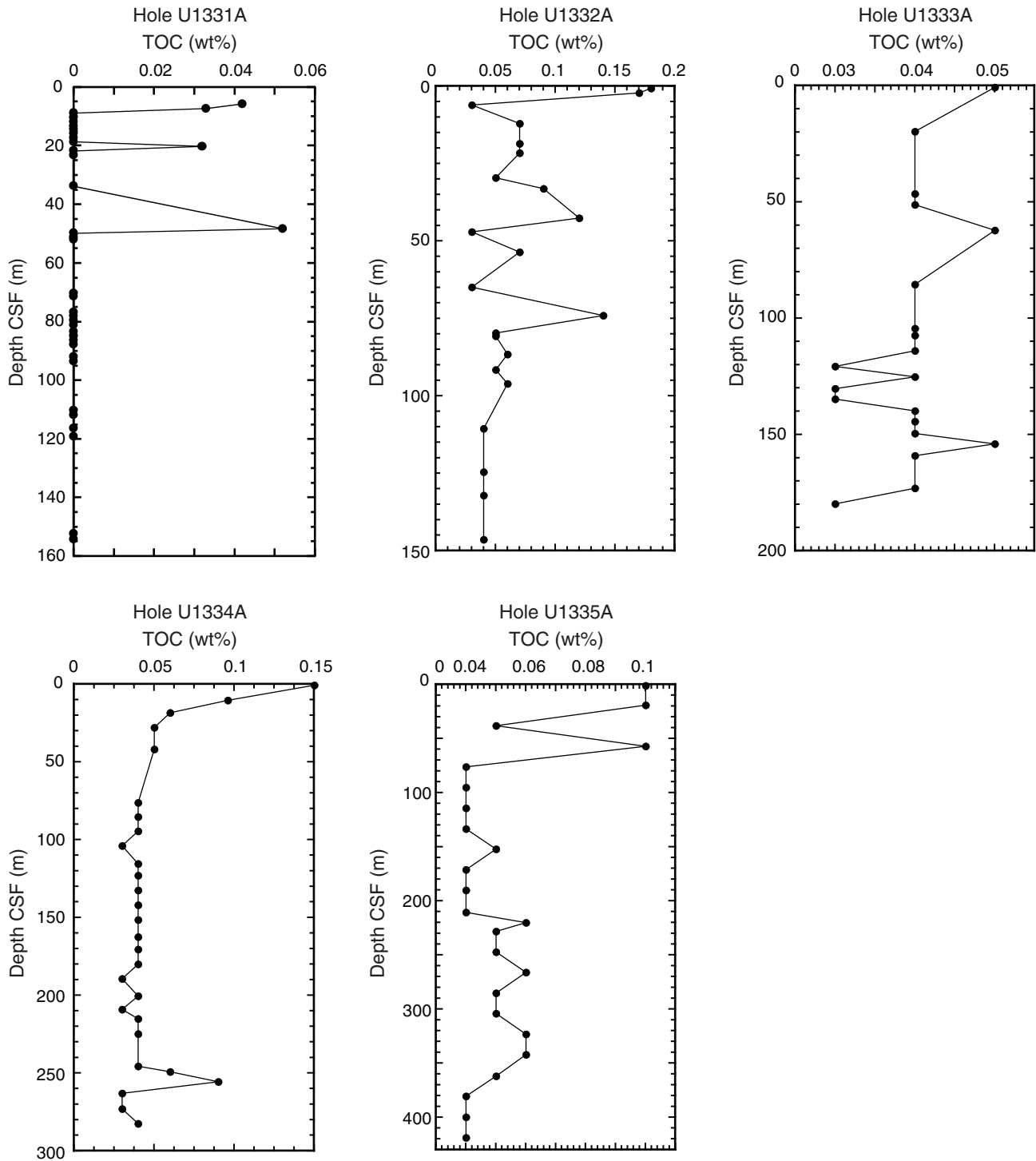
Figure F42. Depth profiles of dissolved strontium concentrations in interstitial waters, Sites U1331–U1338.
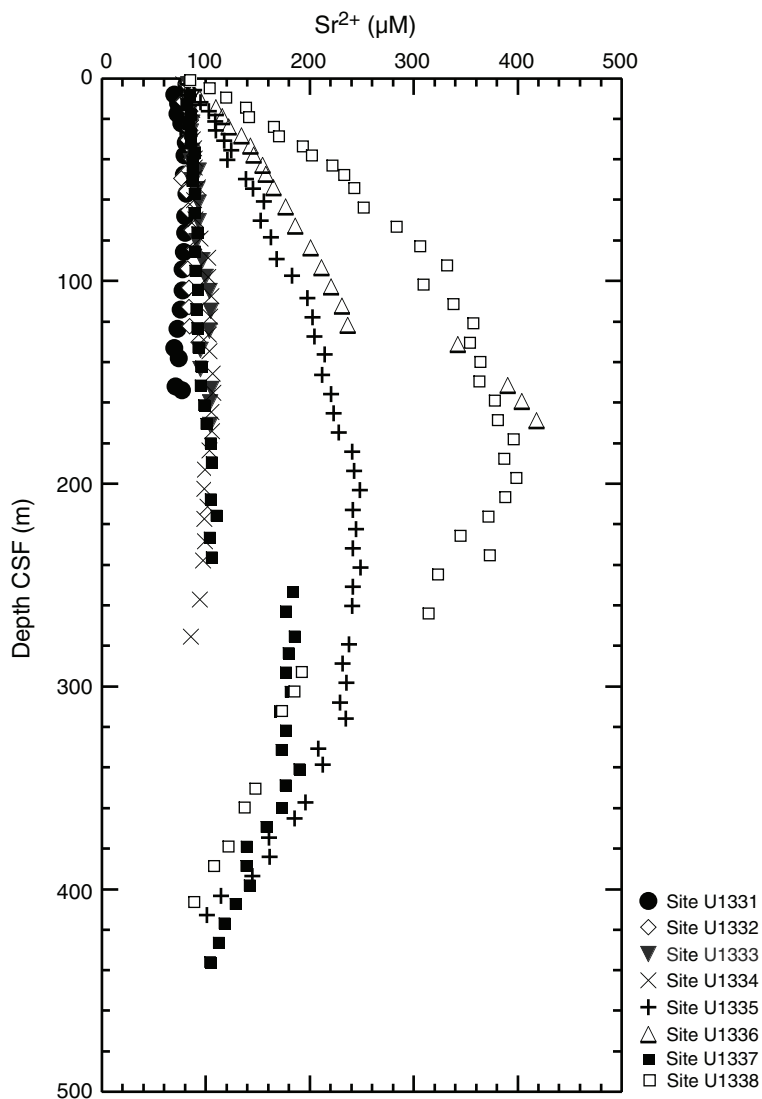
Figure F43. Depth profiles of dissolved lithium in interstitial waters, Sites U1331–U1338.
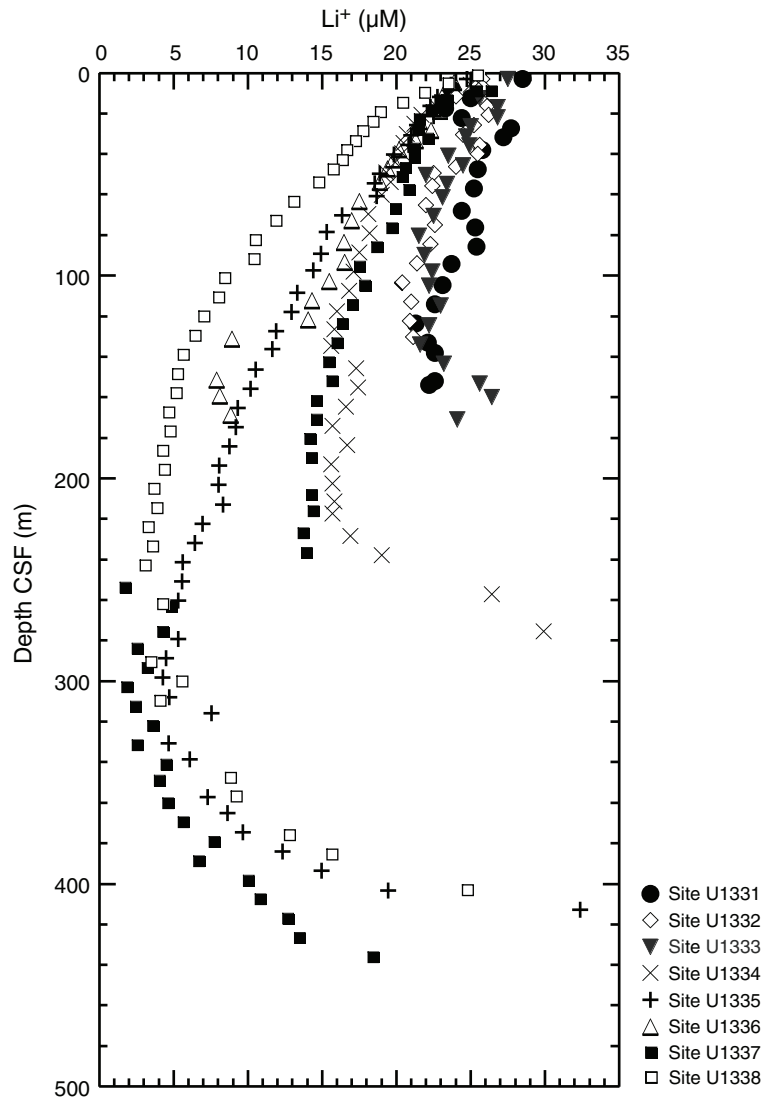
Figure F44. Correlation between seismic reflection records from DSDP Site 574, Site U1337 seismic imaging, and logging data from Hole U1337A. MAD = moisture and density, p1 = uplog pass 1, p2 = uplog pass 2, IMPH = medium induction phasor-processed resistivity, SFLU = spherically focused resistivity, VSP = vertical seismic profile, WMSF = wireline log matched depth below seafloor.
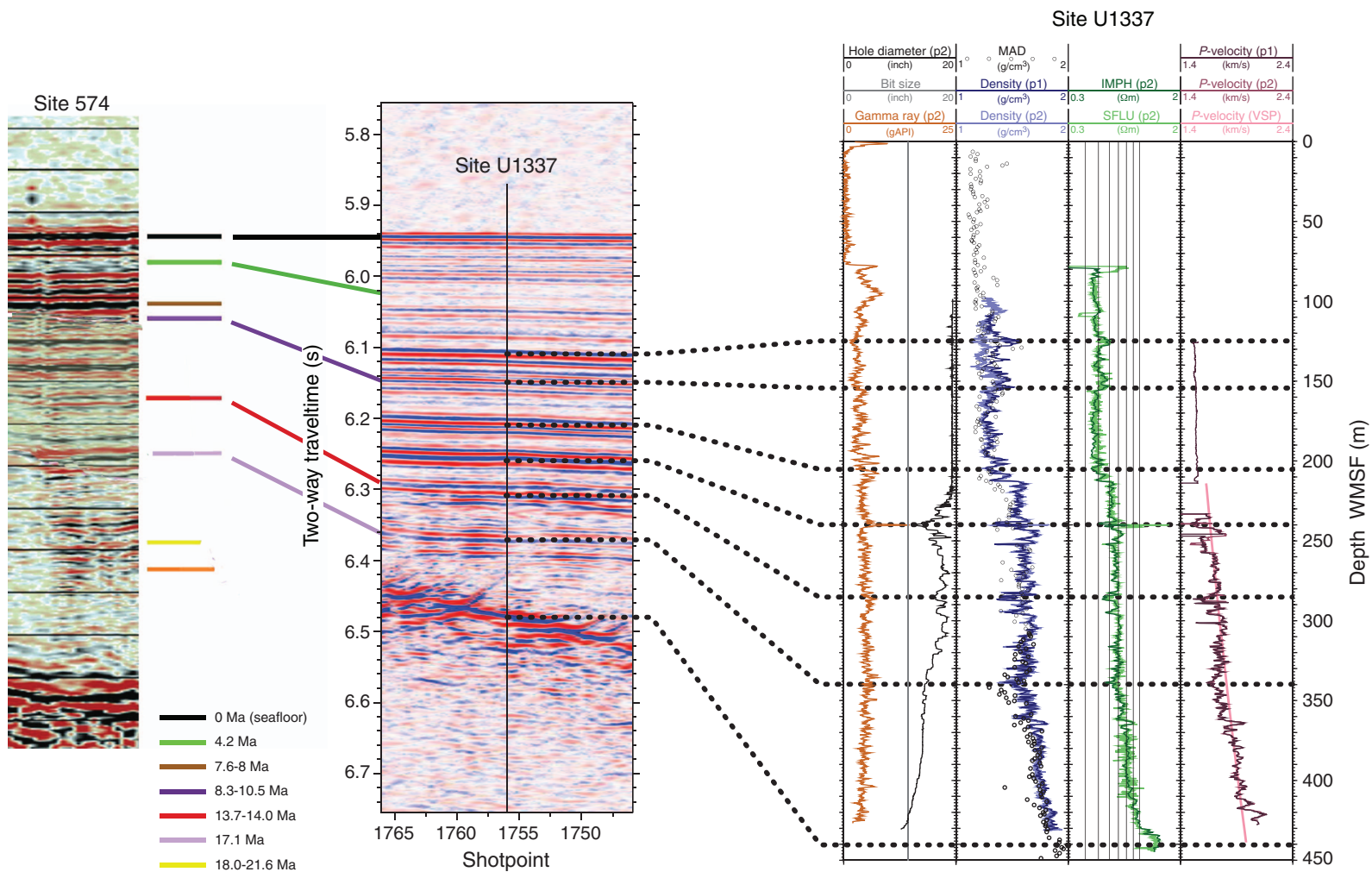
Figure F45. Synthetic seismogram for Site U1331, using core- and downhole log–derived bulk density estimates.
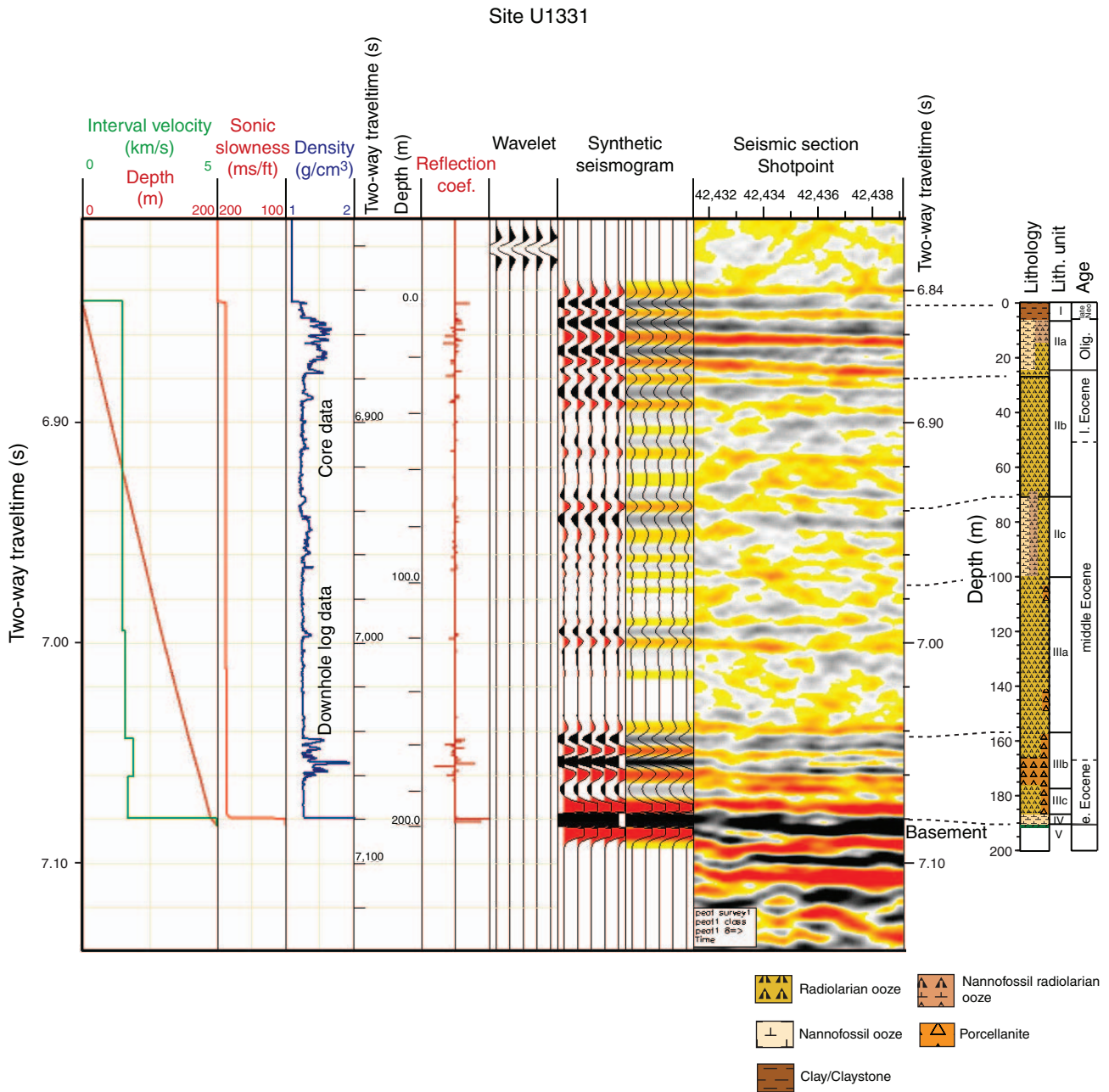
Figure F46. Occurrences of chert and porcellanite at Sites U1331–U1333 and U1336, together with previous ODP Leg 199 sites (1218–1222) (Shipboard Scientific Party, 2004).
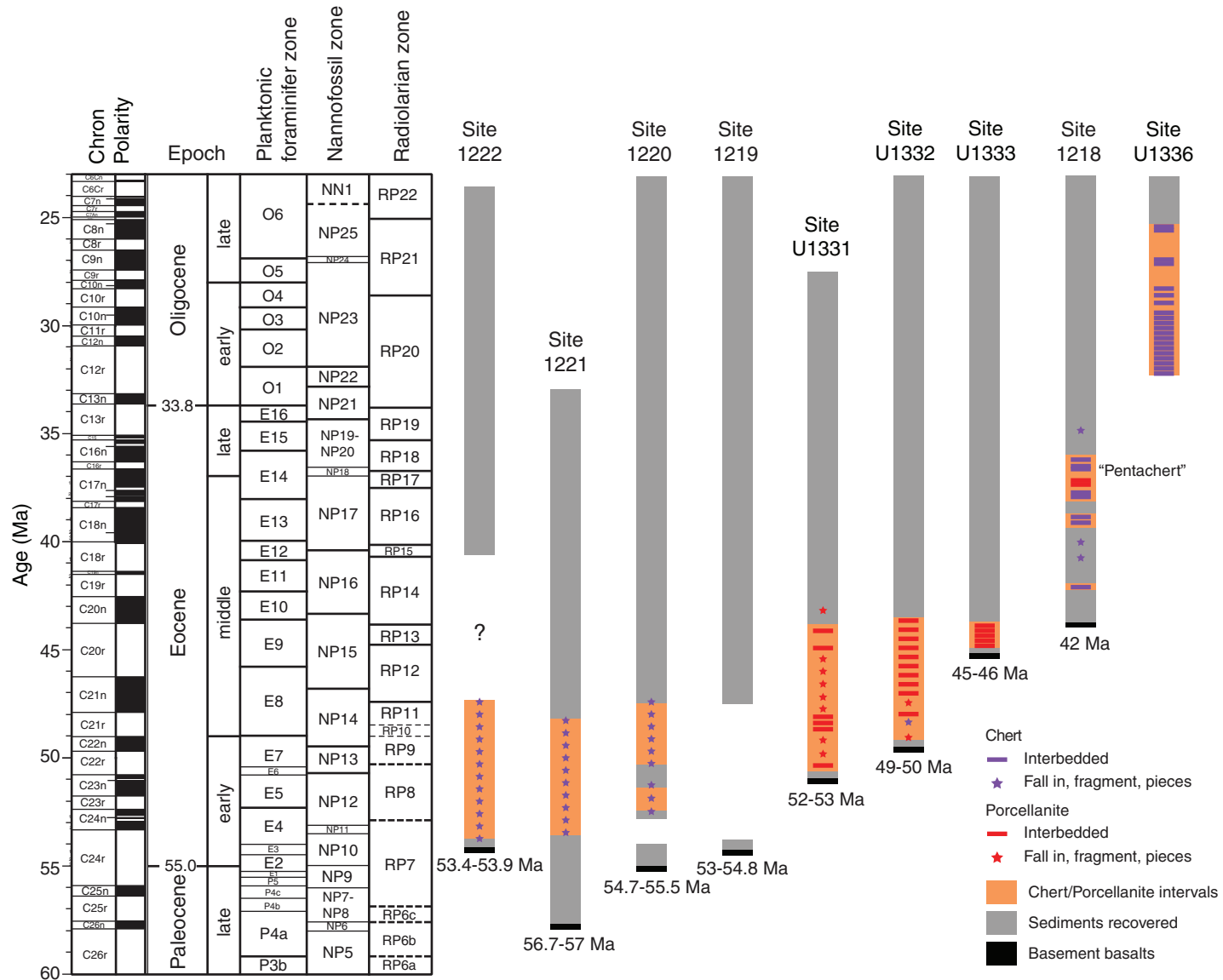
Figure F47. Formation MicroScanner (FMS) and downhole log curves highlighting the location of a thin "baby chert" layer at Sites U1337 (A, B, and C) and U1338 (D). **A.** Total gamma ray measured by Hostile Environment Gamma Ray Sonde (triple combination tool string). **B.** Bulk density measured by Hostile Environment Litho-Density Sonde. **C, D.** FMS four-pad downhole resistivity images. Depth interval of baby chert layer in A and B is slightly offset (~0.4 m) from the FMS image (C). WMSF = wireline log matched depth below seafloor. Depth scale on left is for Hole U1337A (A, B, and C). Depth scale on right is for Hole U1338B (D).
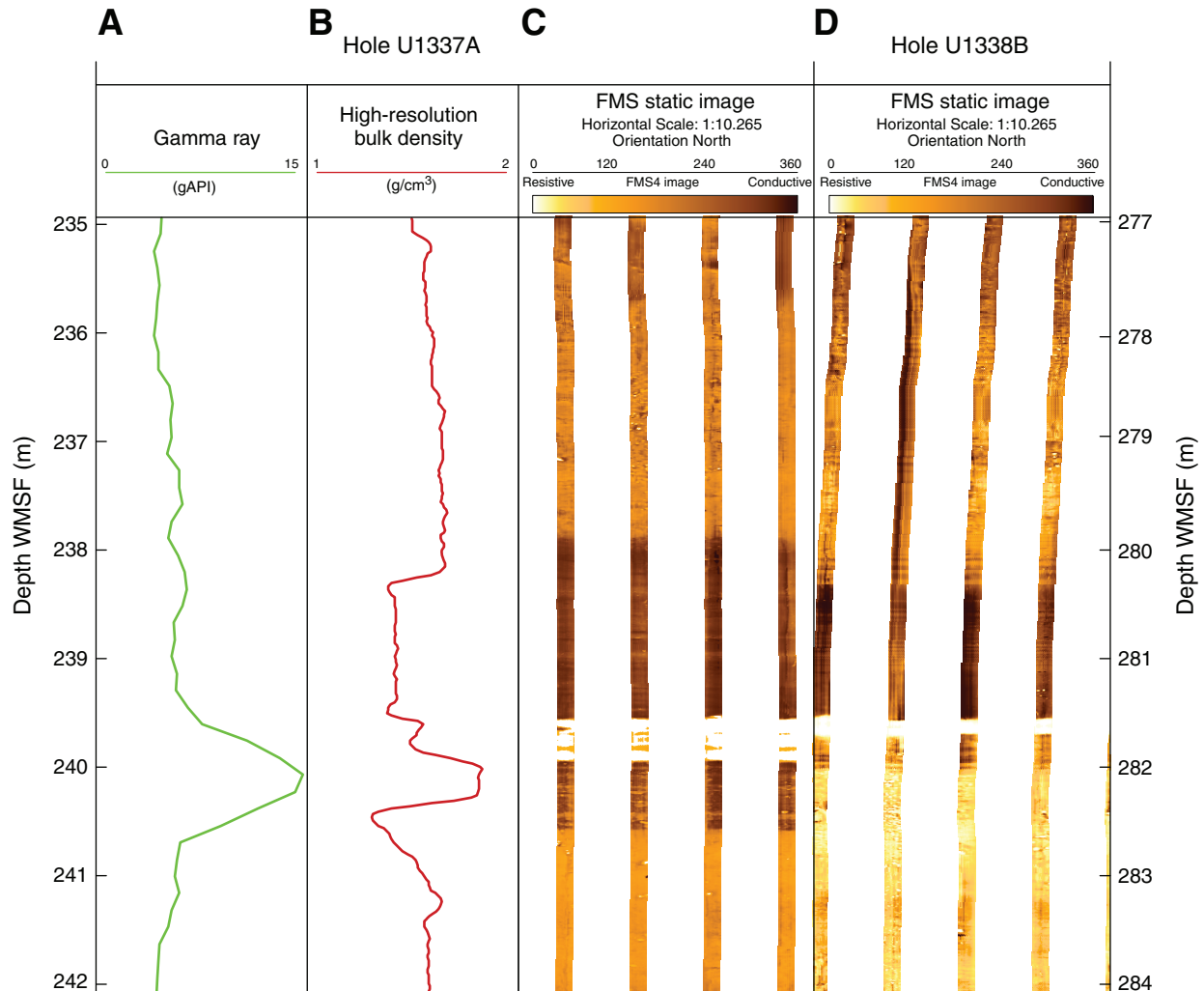
Figure F48. Compilation of geothermal heat flow measurements obtained during Expedition 320 and previous measurements.

Figure F49. Lithologic summary of Sites U1331 and U1335 indicating the frequency and thickness of gravity flows (turbidites). At Site U1335, planktonic foraminifer Zone O6 is informally divided into an upper and lower part using the base of *Paragloborotalia pseudokugleri.* Detailed descriptions of lithology are given in **"Site summaries."** See the **"Methods"** chapter for definition of the biozones.

Figure F50. Comparison of XCB vs. APC drilling recovery in roughly equivalent intervals, Site U1338.
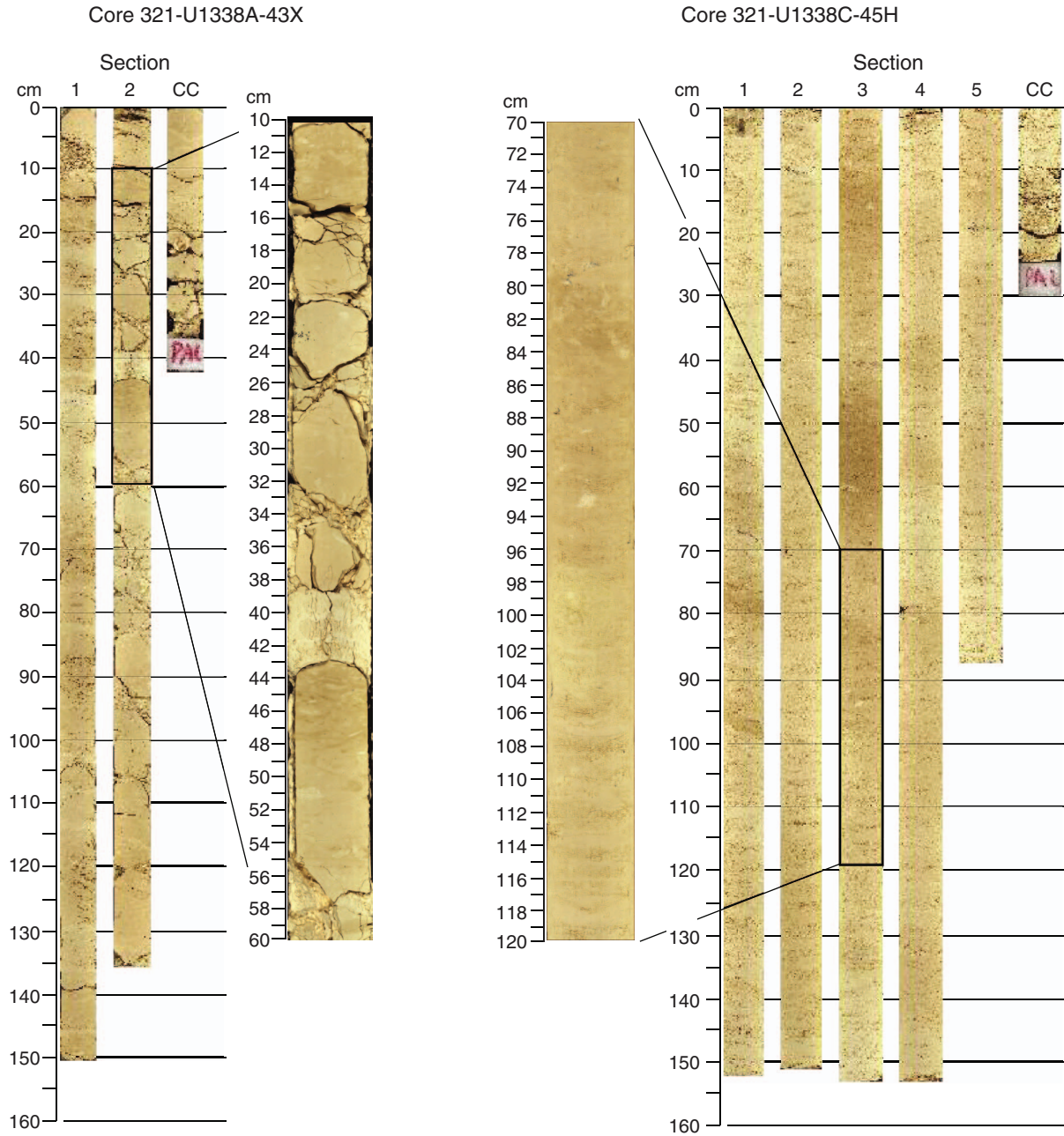
Figure F51. Digital line scan images, Site U1337. Red lines = base of a splice interval (tie point), yellow lines = top of the next splice interval (tie point). Images were depth registered by Roy Wilkens using IGOR-Pro software.
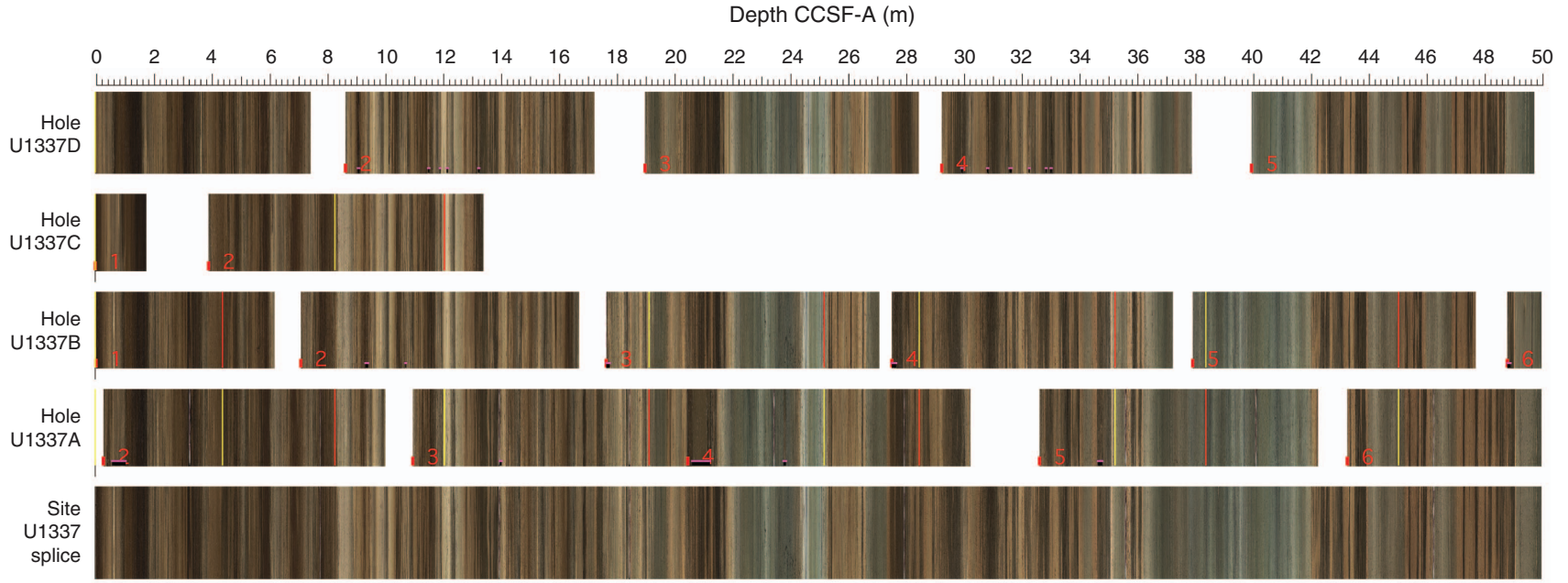
Figure F52. Depth vs. natural gamma radiation (NGR), Sites U1331–U1338.
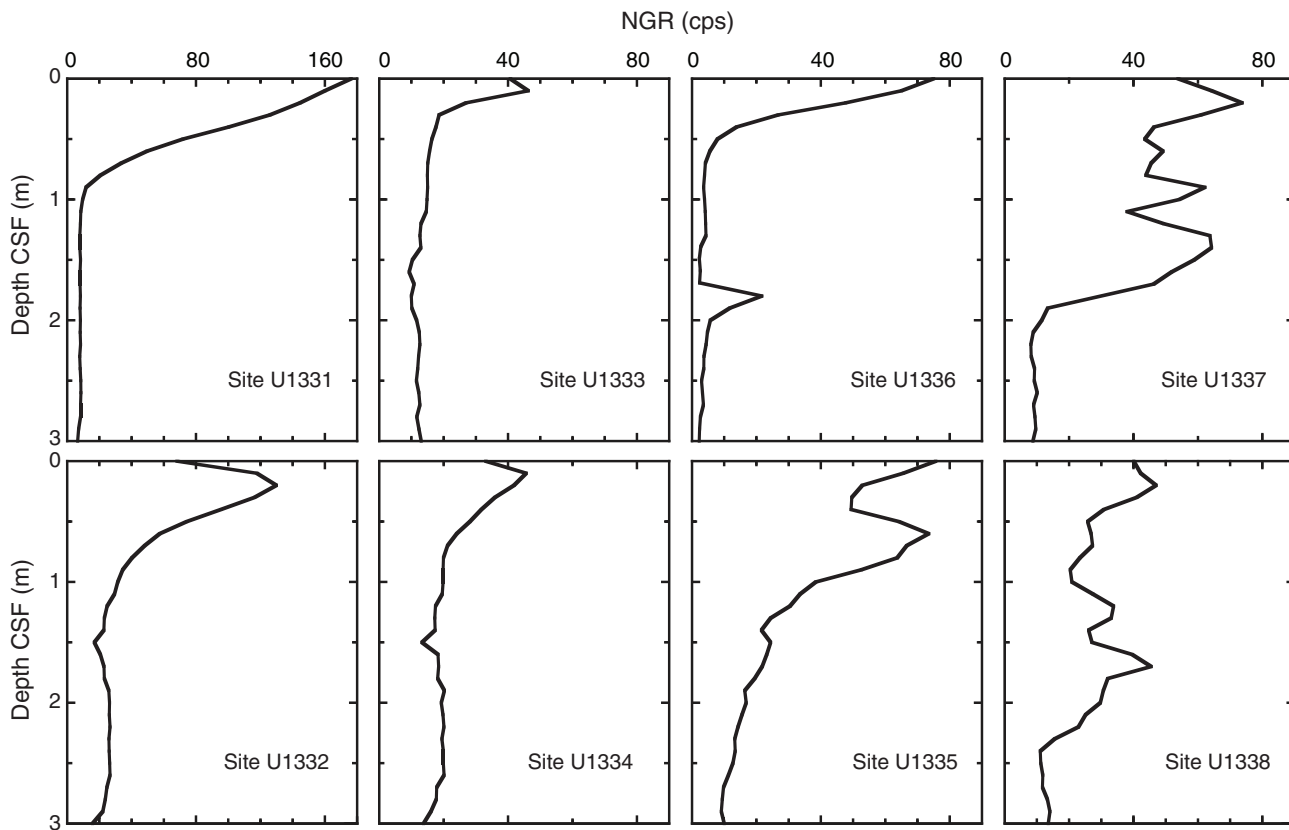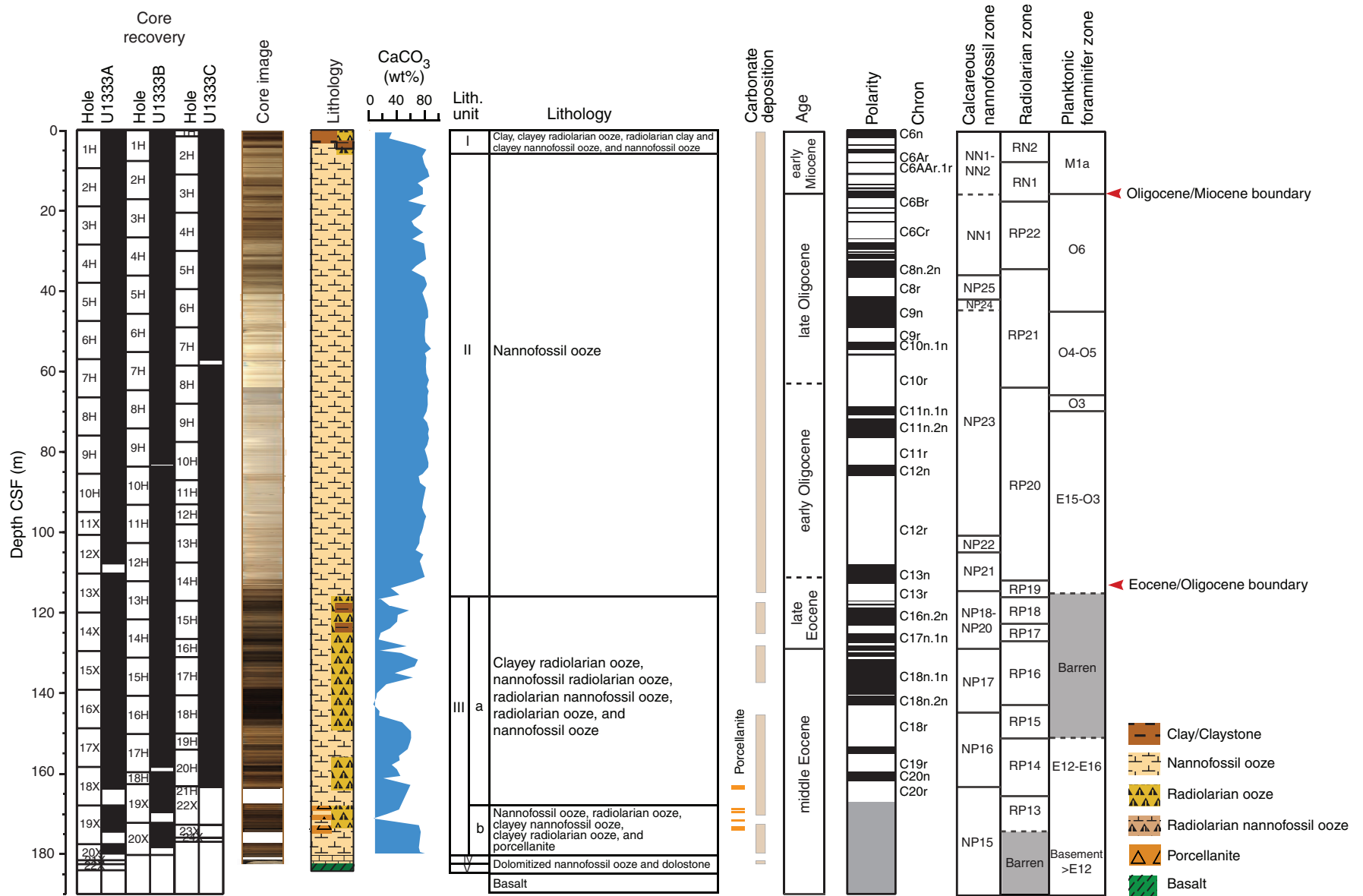
Figure F53. A. ETOPO1 (Amante and Eakins, 2008) bathymetric overview map of Site U1331 and PEAT drilling locations, with previous ODP and DSDP sites. **B.** Swath map bathymetry for Site U1331 region from the AMAT-03 site survey. Black labels = seismic shotpoints, white labels = bathymetric contours. Orange line = seismic Line PEAT1C-sl-8 (see Fig. **F2** in the "Site U1331" chapter). F.Z. = fracture zone.
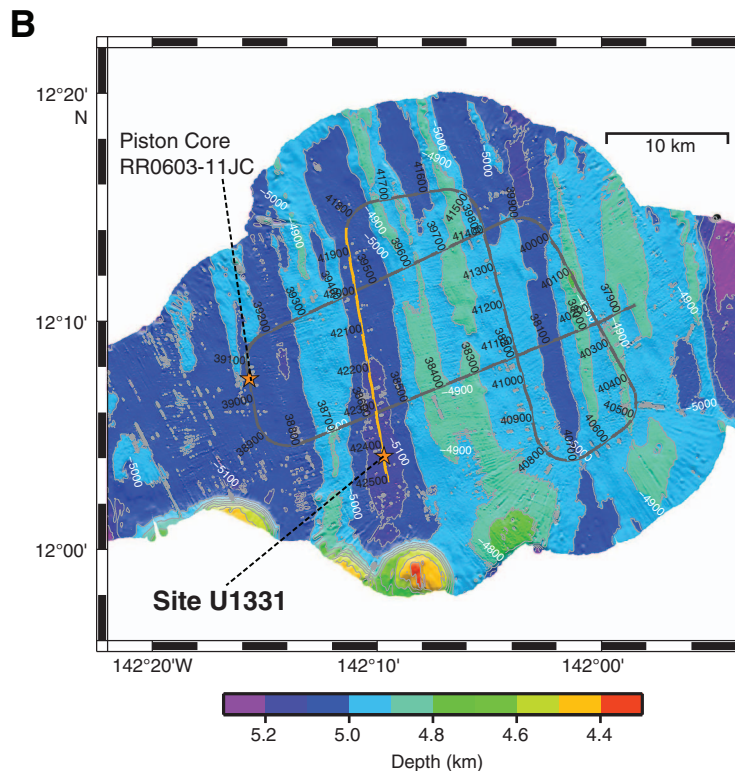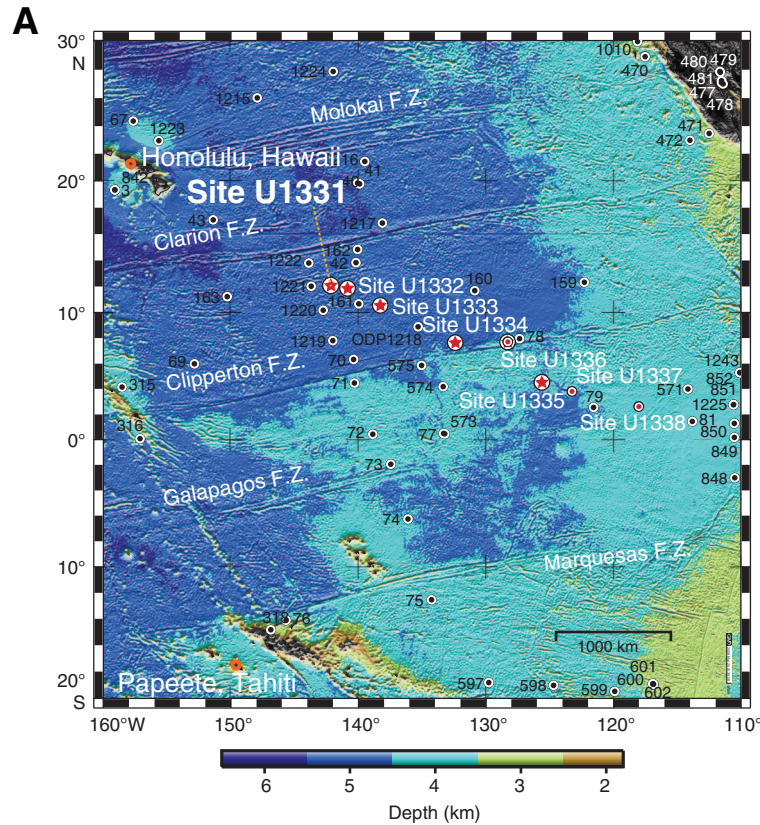
Figure F54. Site U1331 summary.
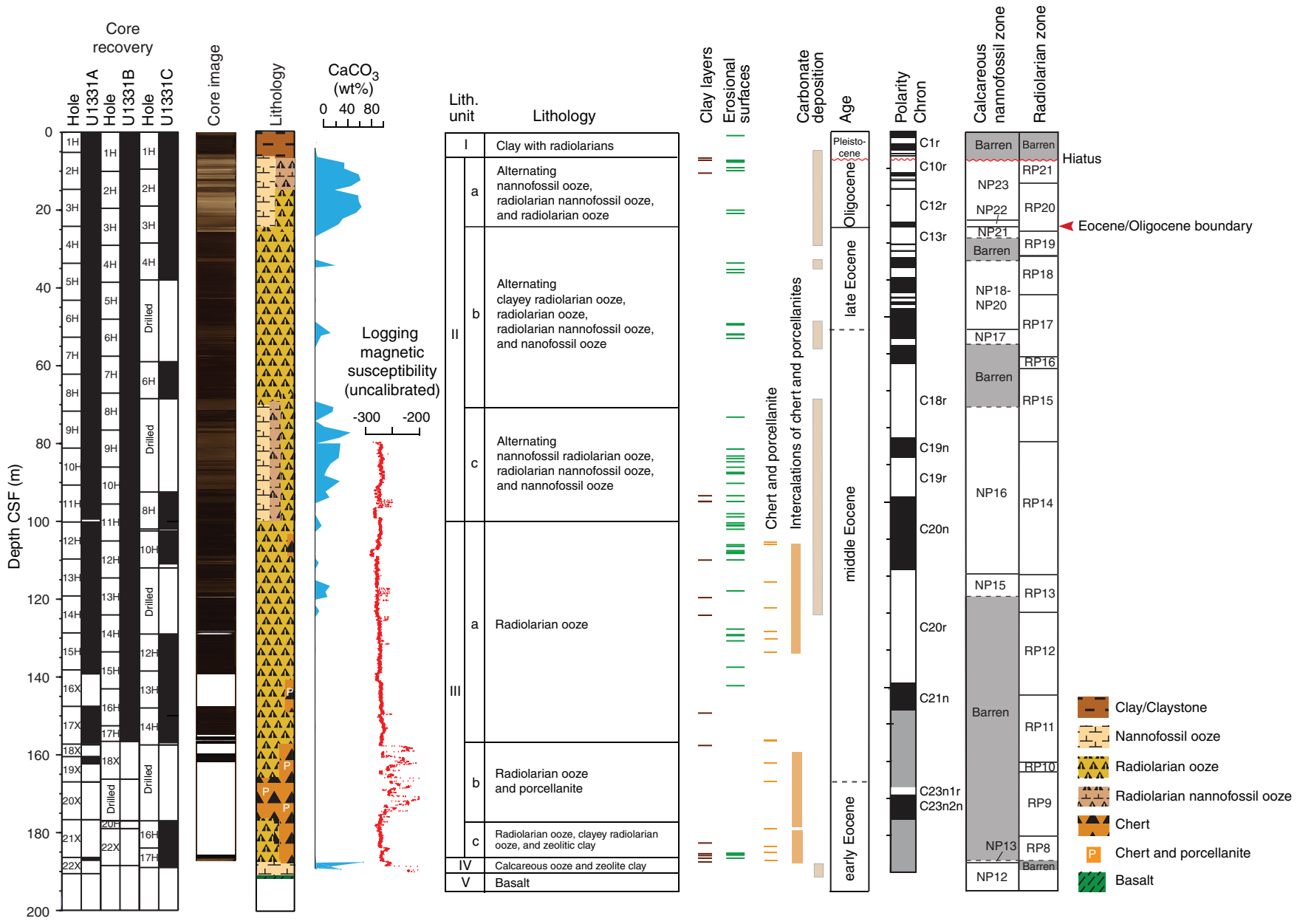
Figure F55. Lithologic summary, Site U1331. L* = reflectance value of sediment as defined in the LAB color model. See the **"Methods"** chapter for biozone definitions.
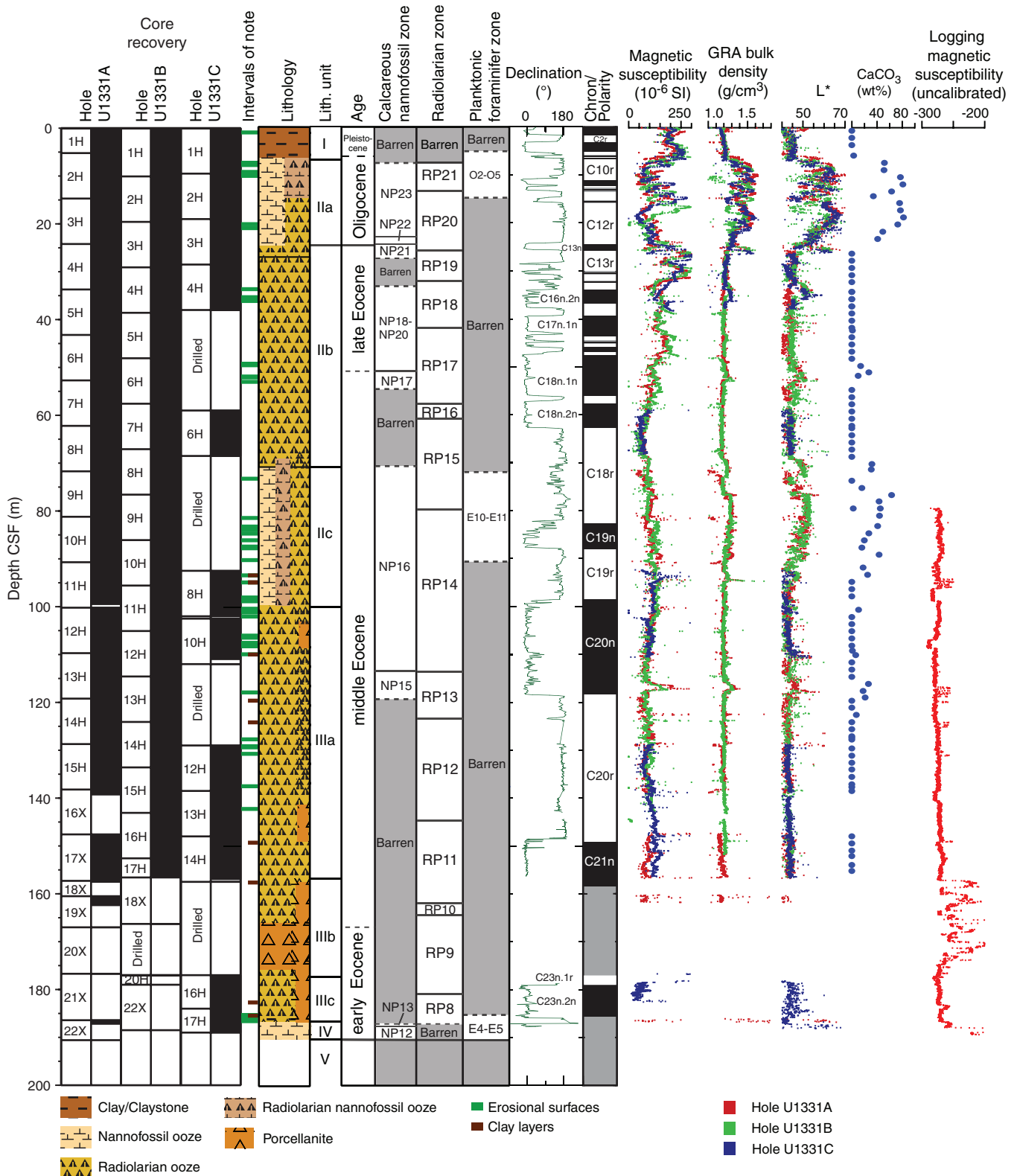
Figure F56. A. ETOPO1 (Amante and Eakins, 2008) bathymetric overview map of Site U1332 and PEAT drilling locations, with previous ODP and DSDP sites. **B.** Swath map bathymetry for Site U1332 region from the AMAT-03 site survey. Black labels = seismic shotpoints, white labels = bathymetric contours. Yellow line = north–south trending survey line for Site U1332. F.Z. = fracture zone.
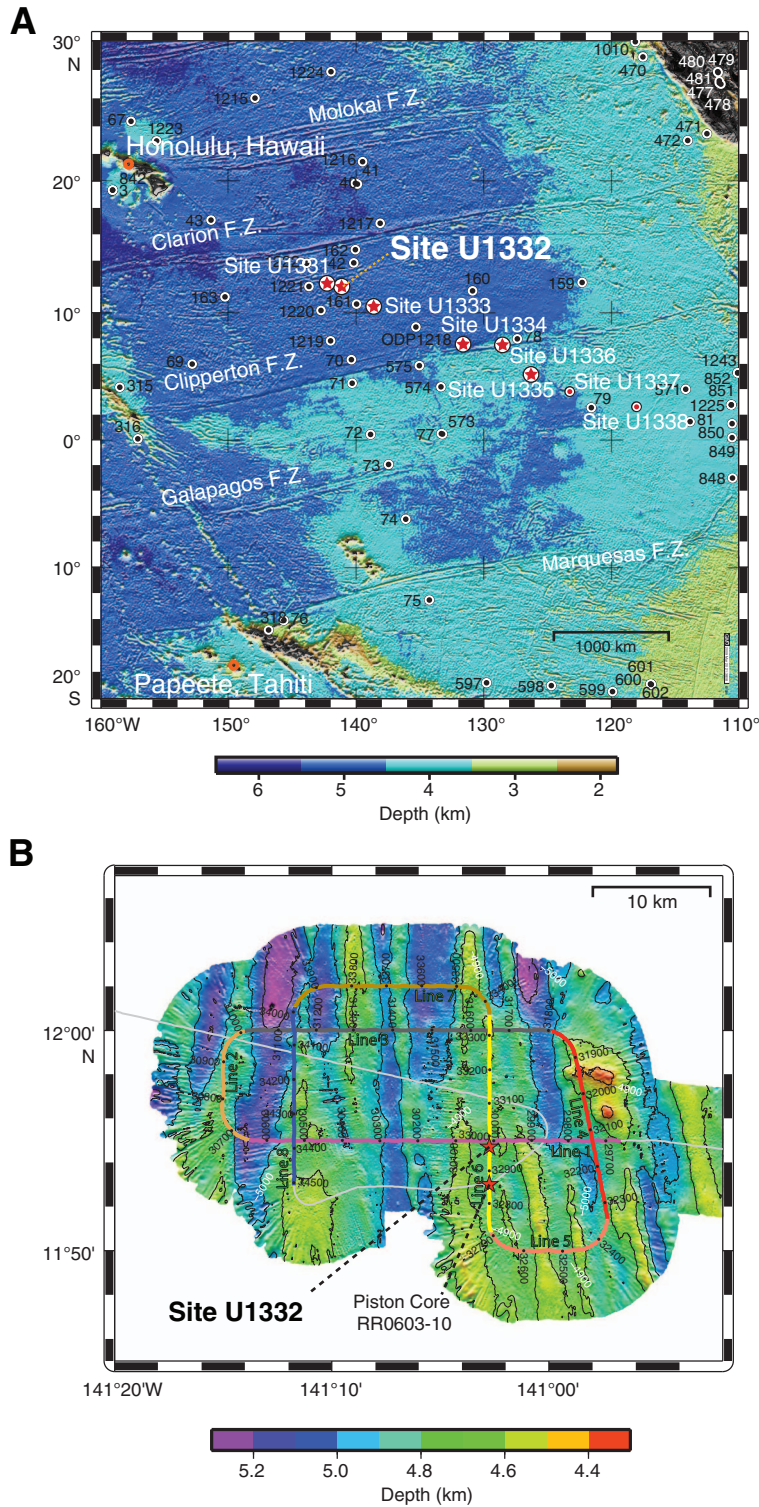
Figure F57. Lithologic summary, Site U1332. A +5 m adjustment is added to the downhole logging magnetic susceptibility depths to convert from WMSF to CSF. L* = reflectance value of sediment as defined in the LAB color model. Chron/Polarity: green wavy line = slump, red wavy line = hiatus.
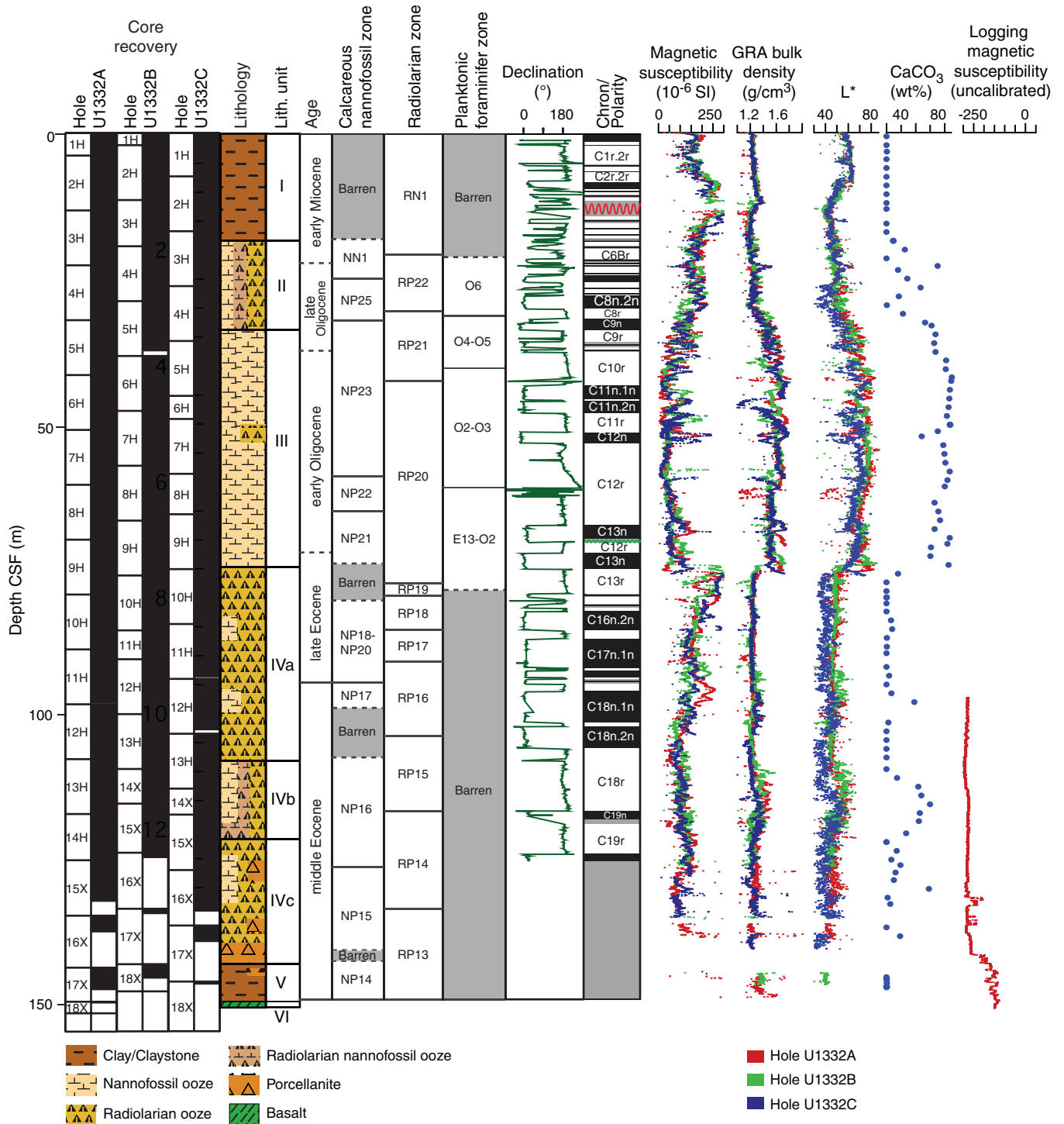
Figure F58. Site U1332 summary.
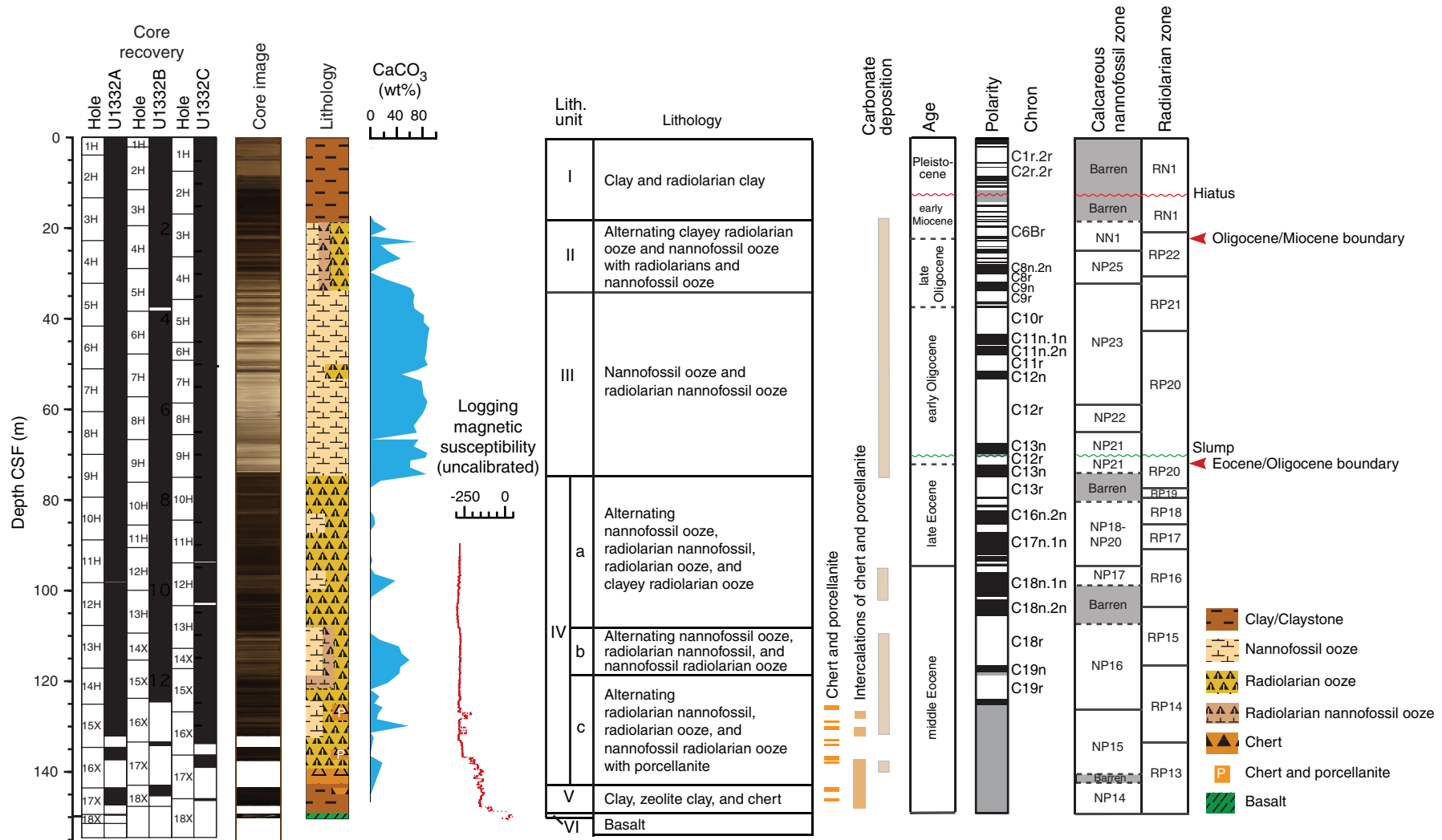
Figure F59. A. ETOPO1 (Amante and Eakins, 2008) bathymetric overview map of Site U1333 and PEAT drilling locations, with previous ODP and DSDP sites. **B.** Swath map bathymetry for Site U1333 region from the AMAT-03 site survey. Black labels = seismic shotpoints, white labels = bathymetric contours. White line = part of the seismic reflection profile across Site U1333 (see Fig. F2 in the "Site U1333" chapter). F.Z. = fracture zone.
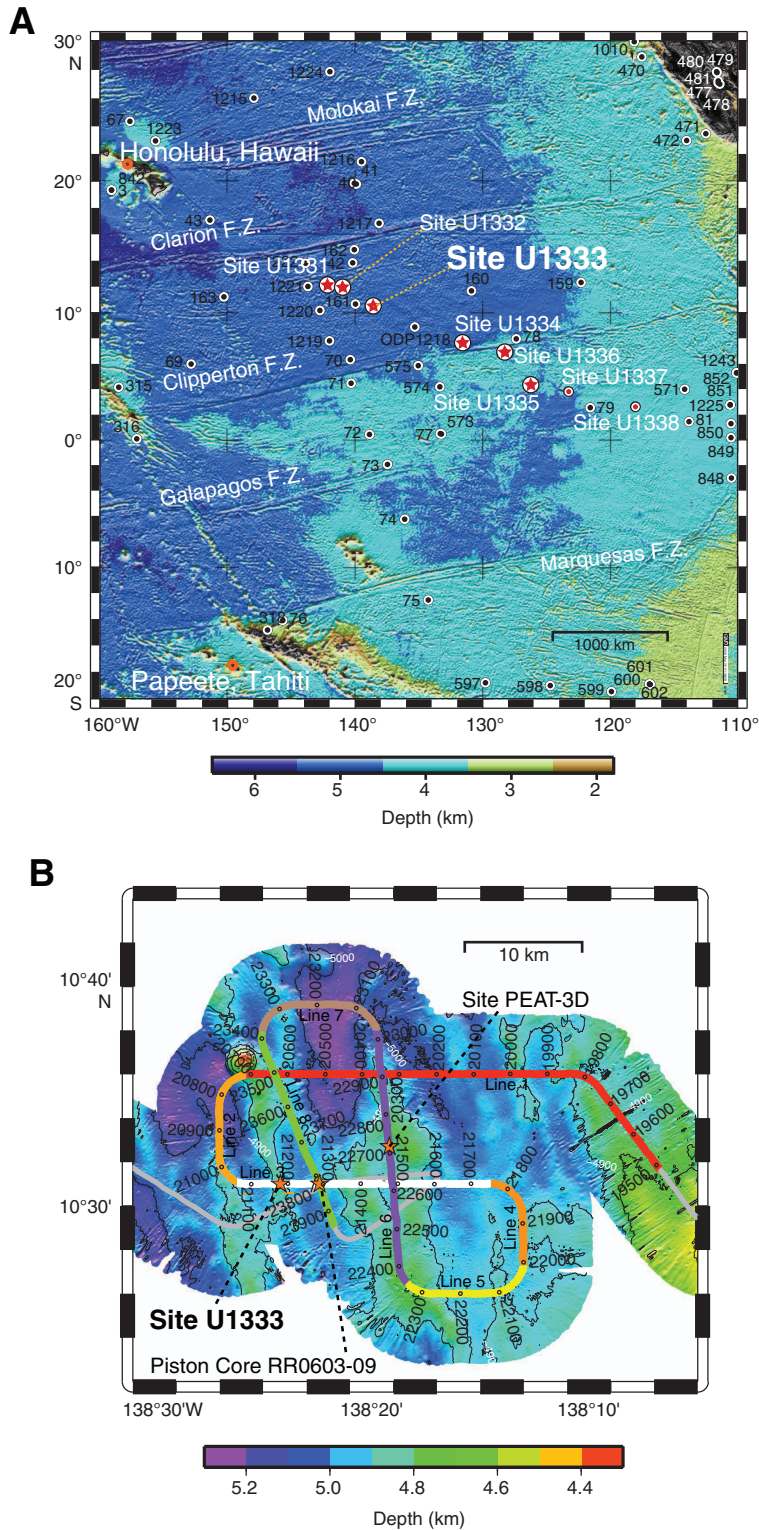
Figure F60. Site U1333 summary. At Site U1333, planktonic foraminifer Zones O3 and O6 are informally divided into an upper and lower part using the top of *Subbotina angiporoides* and base of *Paragloborotalia pseudokugleri,* respectively.

Figure F61. Site U1333 lithologic summary. At Site U1333, planktonic foraminifer Zones O3 and O6 are informally divided into an upper and lower part using the top of *Subbotina angiporoides* and base of *Paragloborotalia pseudokugleri,* respectively. L* = lightness reflectance value of sediment as defined in the LAB color model.
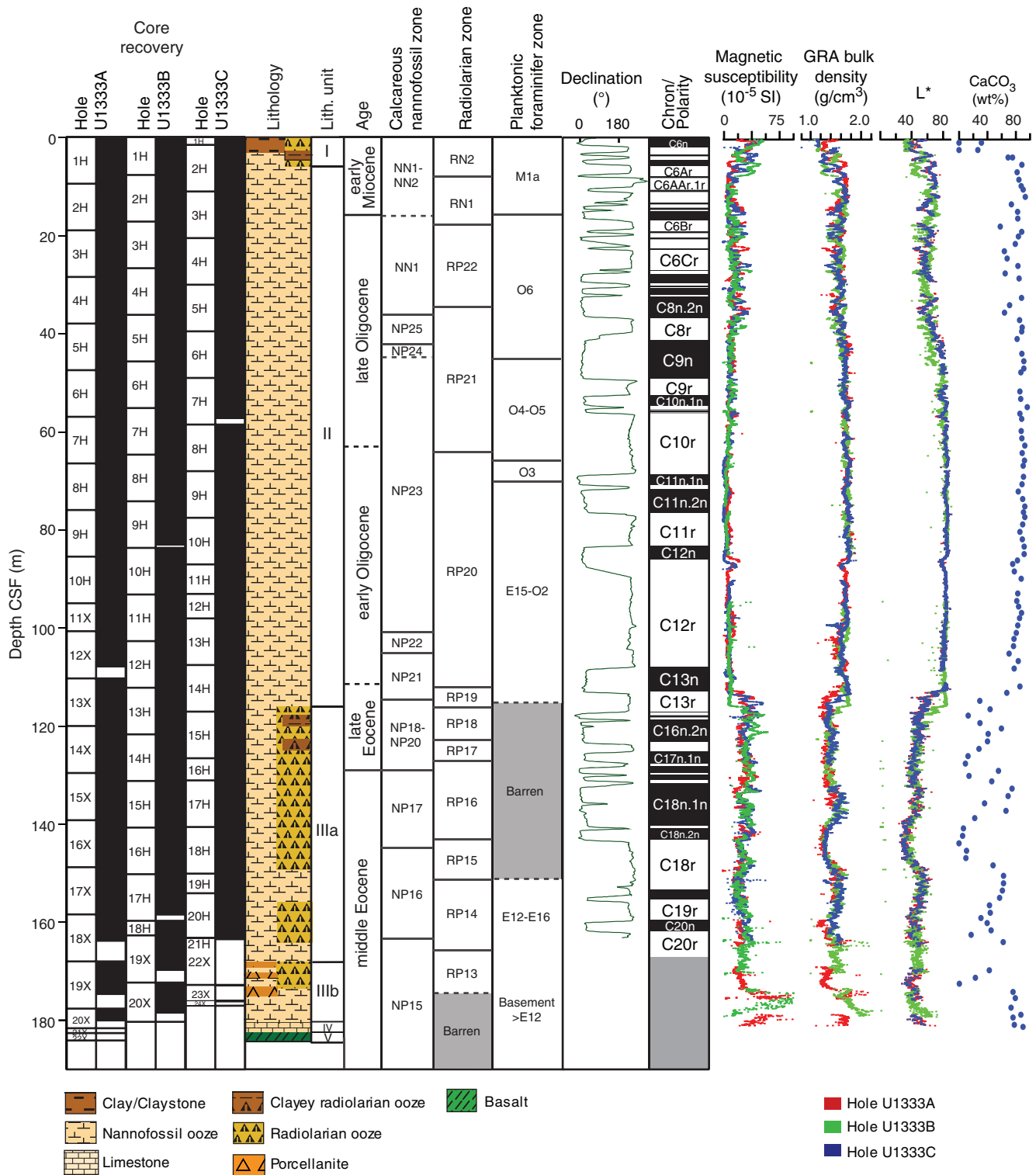
Figure F62. A. ETOPO1 (Amante and Eakins, 2008) bathymetric overview map of Site U1334 and PEAT drilling locations, with previous ODP and DSDP sites. **B.** Swath map bathymetry for Site U1334 region from the AMAT-03 site survey. Black labels = seismic shotpoints, white labels = bathymetric contours. White line = survey Line 1, purple line = survey Line 6. F.Z. = fracture zone.
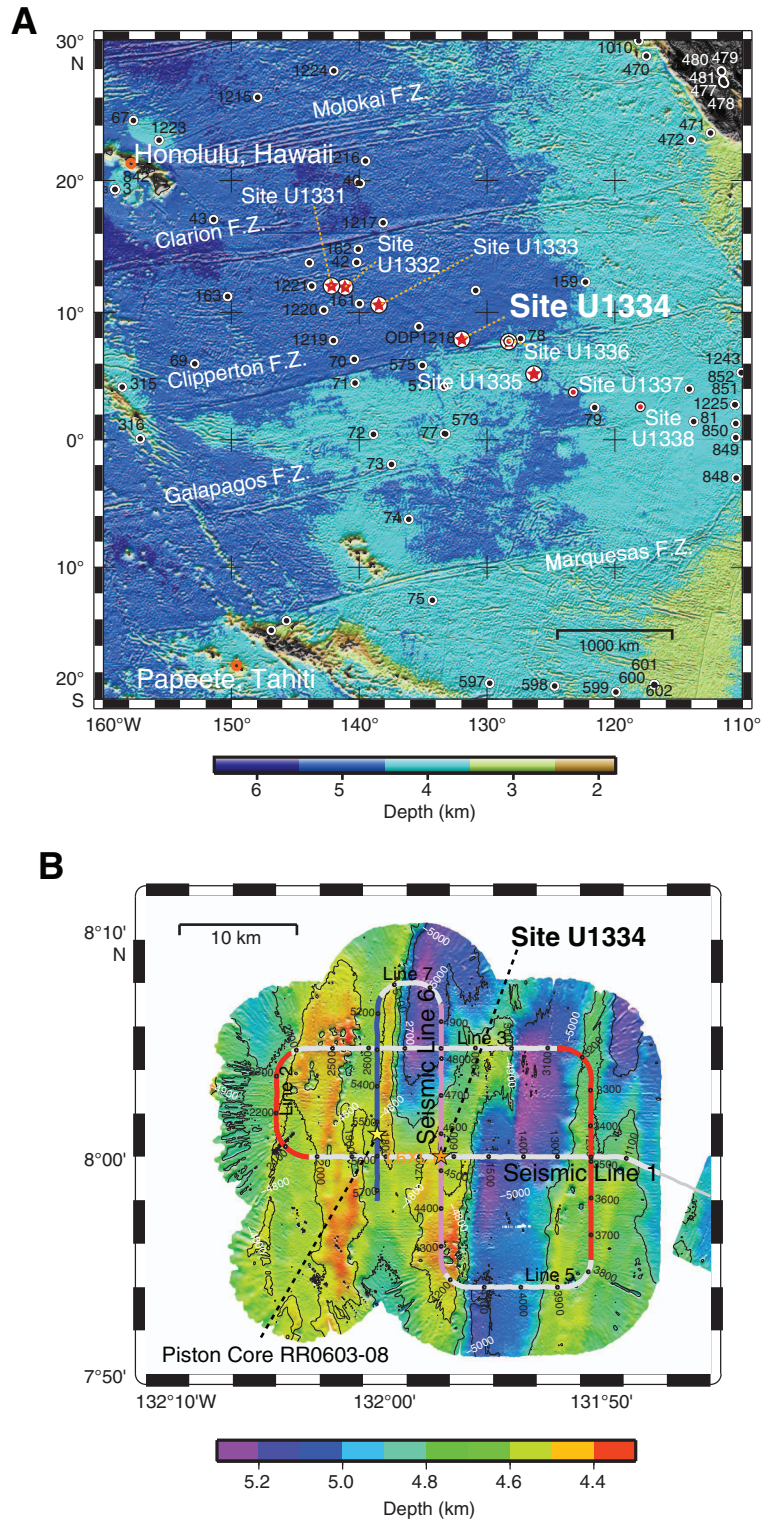
Figure F63. Site U1334 summary. At Site U1334, planktonic foraminifer Zones O2, O3, and O6 are informally divided into an upper and lower part using the base of *Paragloborotalia opima* and top of *Subbotina angiporoides* and the base of *Paragloborotalia pseudokugleri,* respectively.
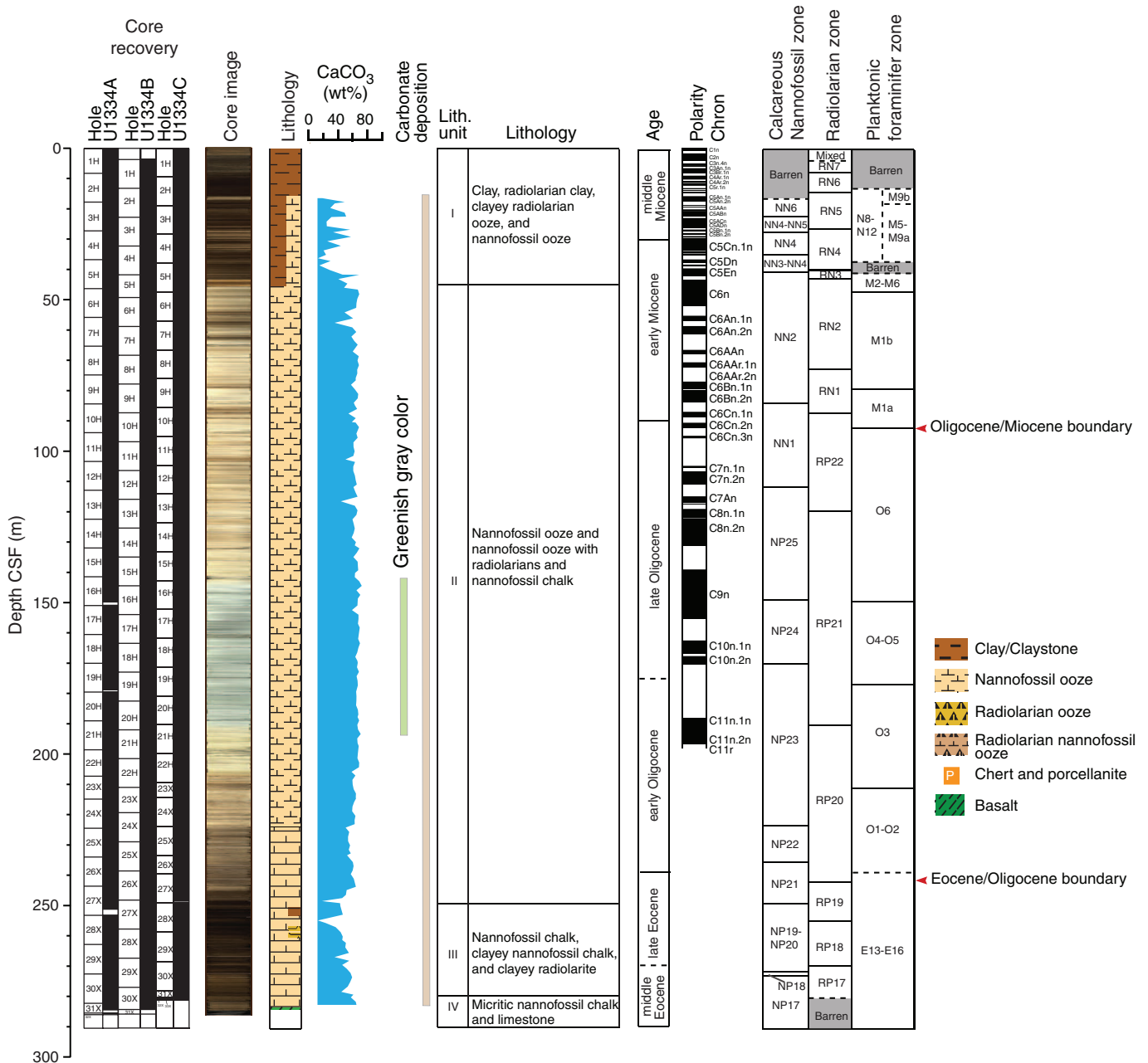
Figure F64. Lithologic summary, Site U1334. L*, b* = reflectance value of sediment as defined in the LAB color model.
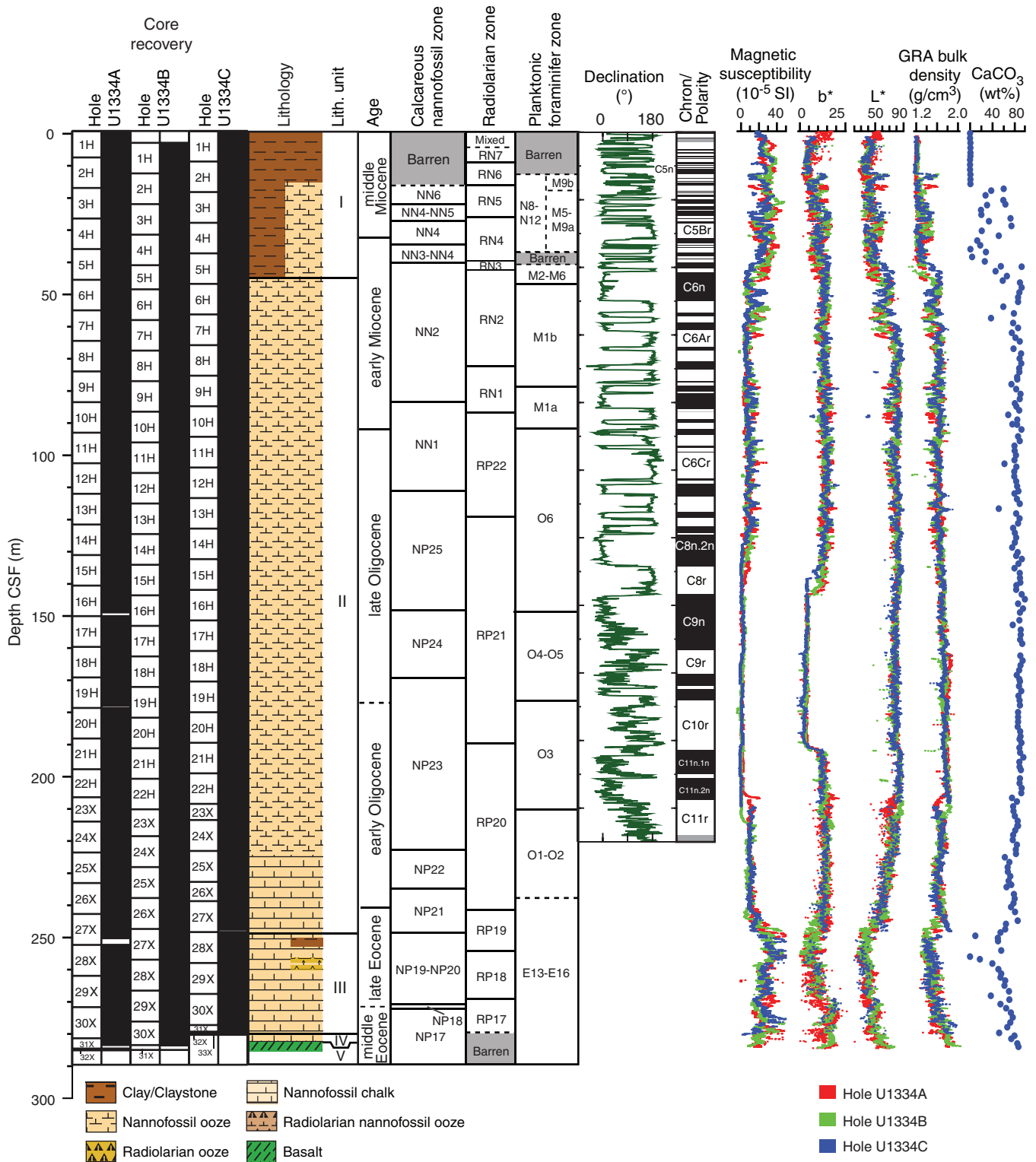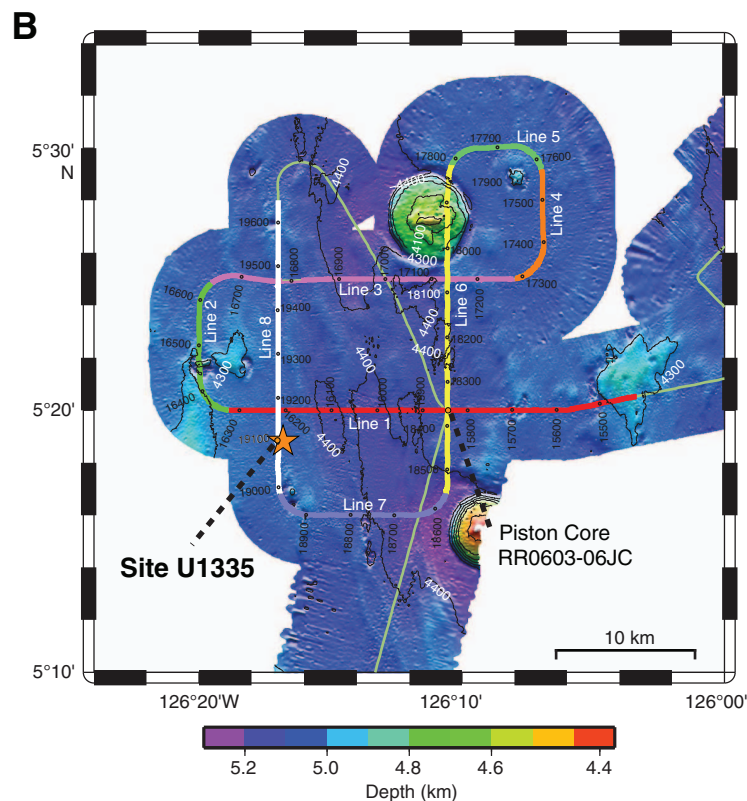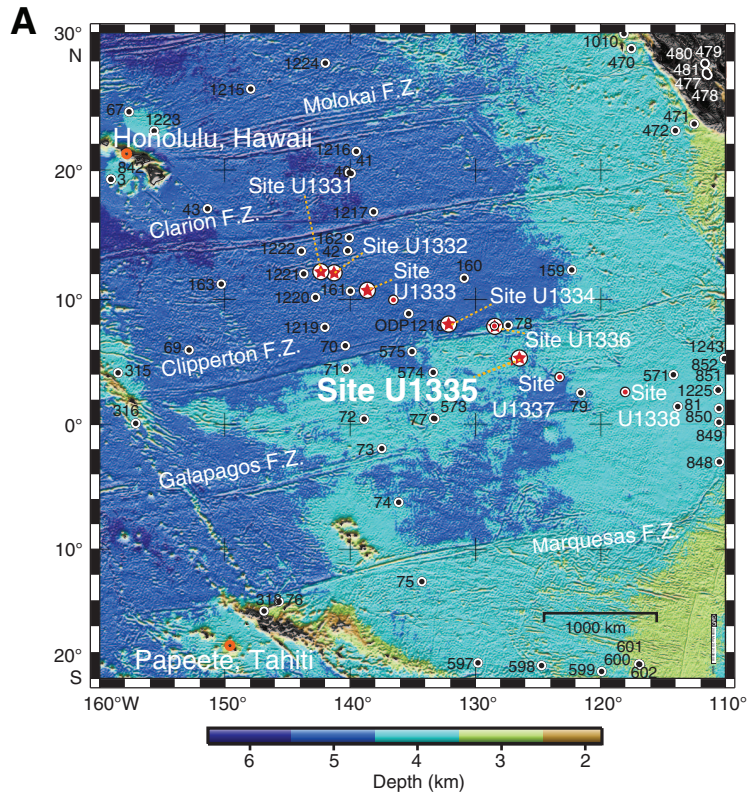
Figure F65. Calcium carbonate ($CaCO_3$), total carbon (TC), inorganic carbon (IC), and total organic carbon (TOC) determined by normal and acidification methods in sediments from Hole U1334A. (See **"Lithostratig-raphy"** in the "Site U1334" chapter for information on unit boundaries.)
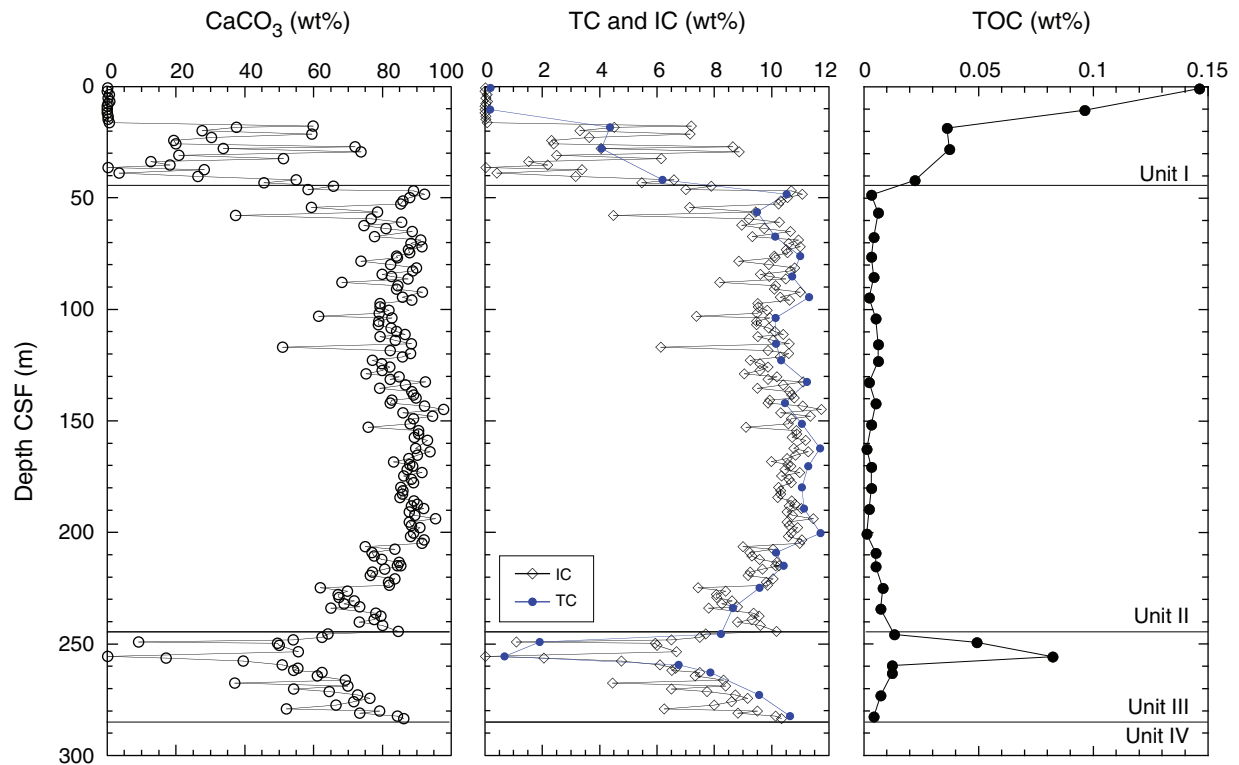
Figure F66. Color reflectance and magnetic susceptibility, Hole U1334A. Line scan images from Cores 320-U1334A-15H through 16H and 21H through 23X highlight observed color changes. L*, a*, b* = reflectance value of sediment as defined in the LAB color model.]
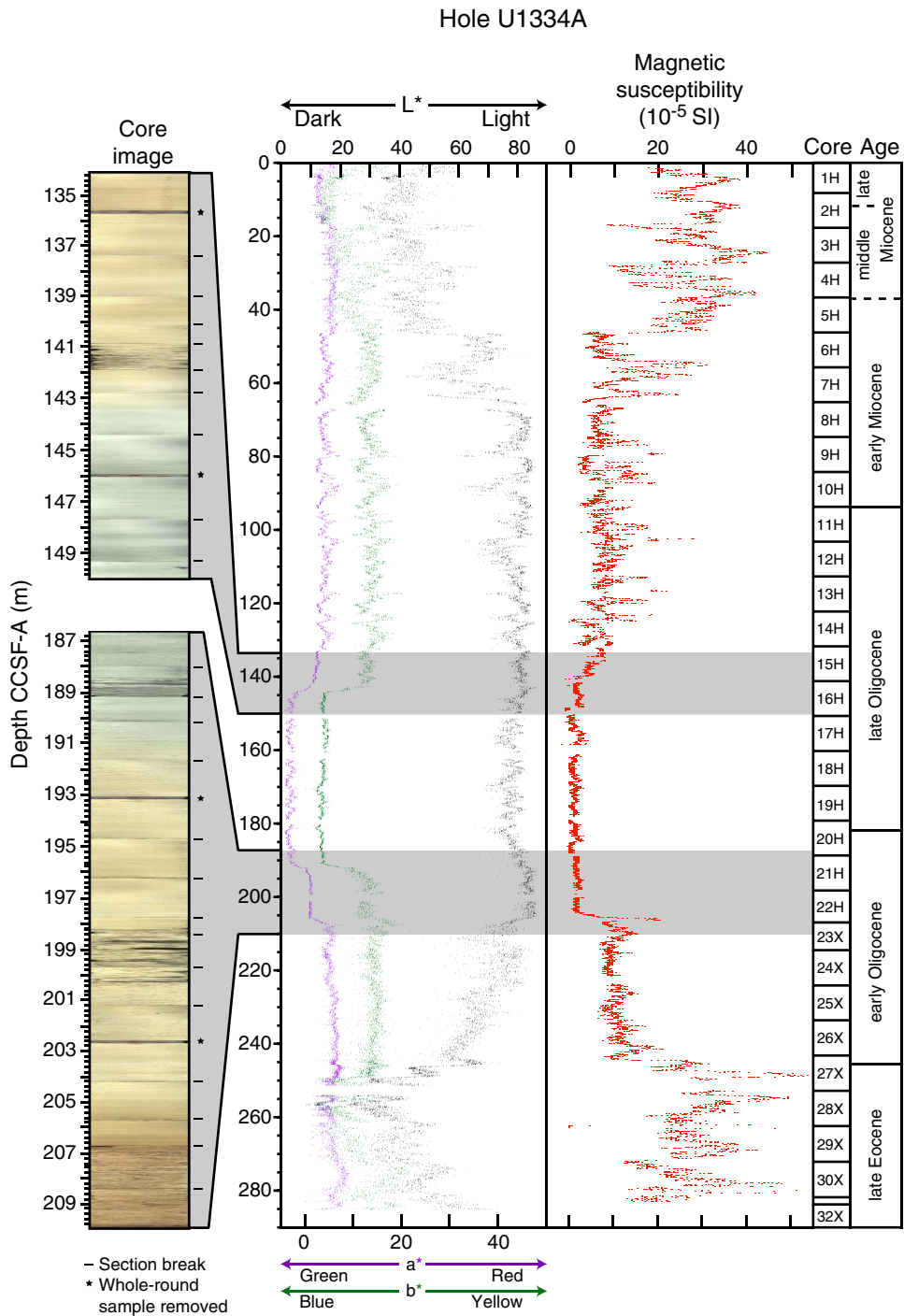
Figure F67. A. ETOPO1 (Amante and Eakins, 2008) bathymetric overview map of Site U1335 and PEAT drilling locations, with previous ODP and DSDP sites. **B.** Swath map bathymetry for Site U1335 region from the AMAT-03 site survey. Black labels = seismic shotpoints, white labels = bathymetric contours. White line = survey Line 8 (see Fig. **F2** in the "Site U1335" chapter). F.Z. = fracture zone.

Figure F68. Site U1335 summary. At Site U1335, planktonic foraminifer Zone O6 is informally divided into an upper and lower part using the base of *Paragloborotalia pseudokugleri.*
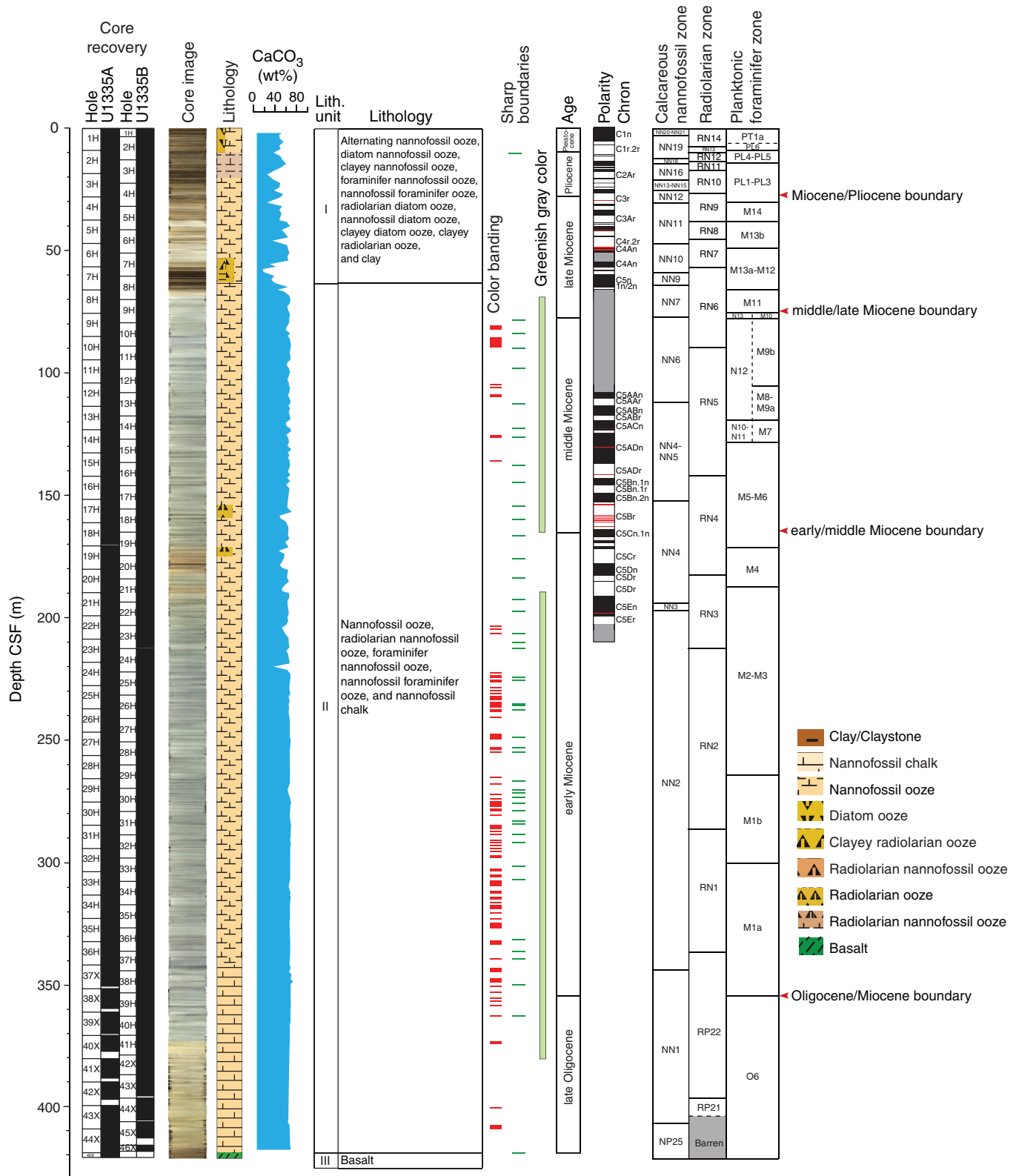
Figure F69. Lithologic summary, Site U1335. Magnetic stratigraphy data based on Hole U1335B. Geomagnetic polarity: red interval = possible geomagnetic excursions (cryptochron), gray interval = undetermined interval. L*, b* = reflectance value of sediment as defined in the LAB color model.
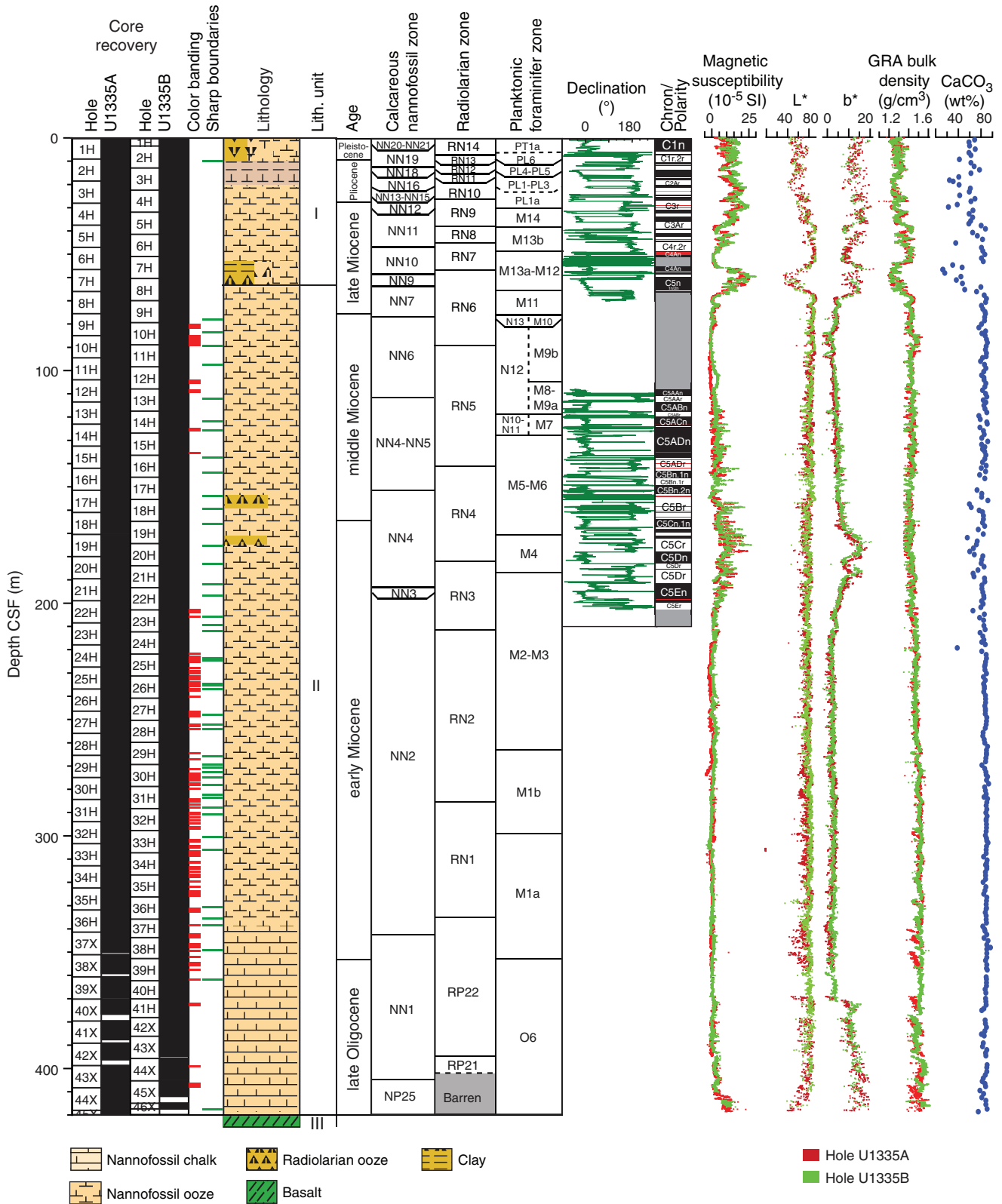
Figure F70. Calcium carbonate ($CaCO_3$), total carbon (TC), inorganic carbon (IC), and total organic carbon (TOC) determined by normal and acidification methods in sediments from Hole U1335A. (See **"Lithostratig-raphy"** in the "Site U1335" chapter for information on unit boundaries.)
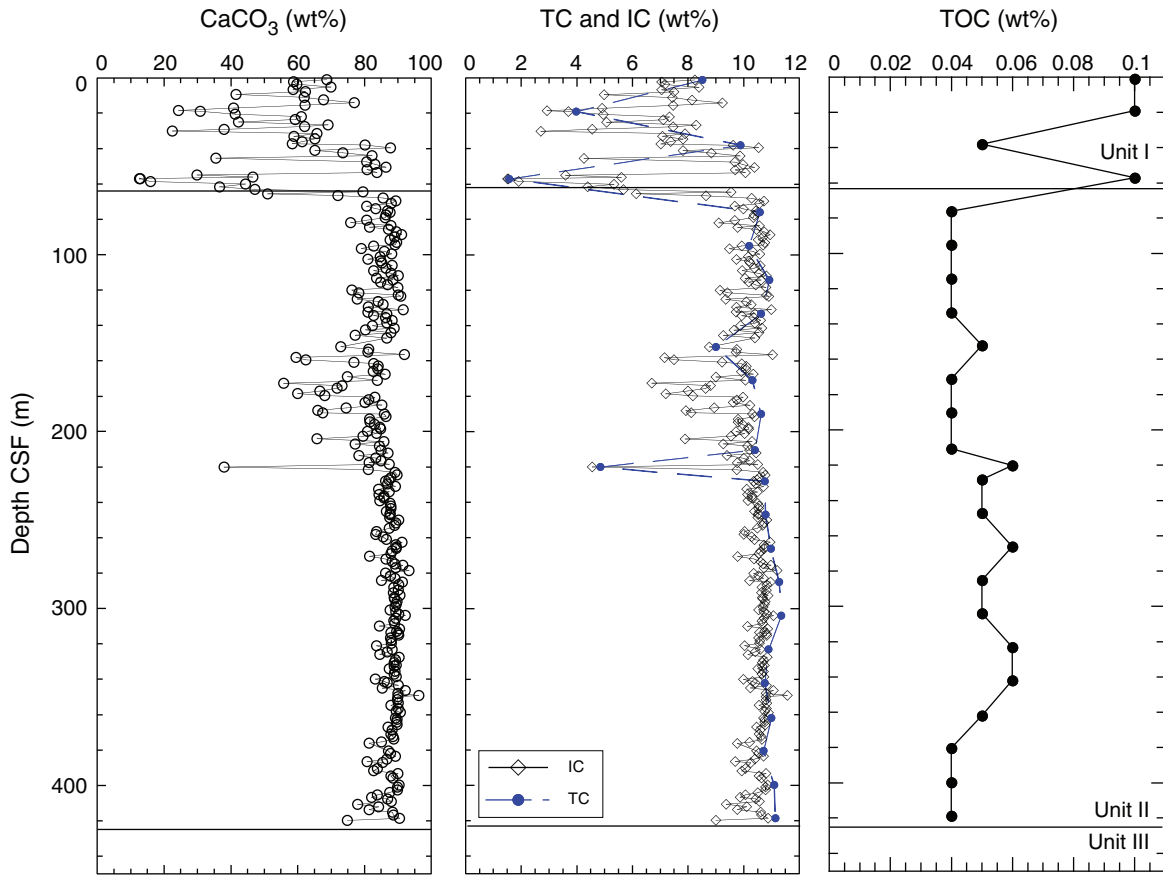
Figure F71. Color reflectance and magnetic susceptibility, Hole U1335A. Line scan images from Cores 320-U1335A-7H through 8H, 18H through 22H, and 39X through 45X highlight observed color changes. L*, a*, b* = reflectance value of sediment as defined in the LAB color model.
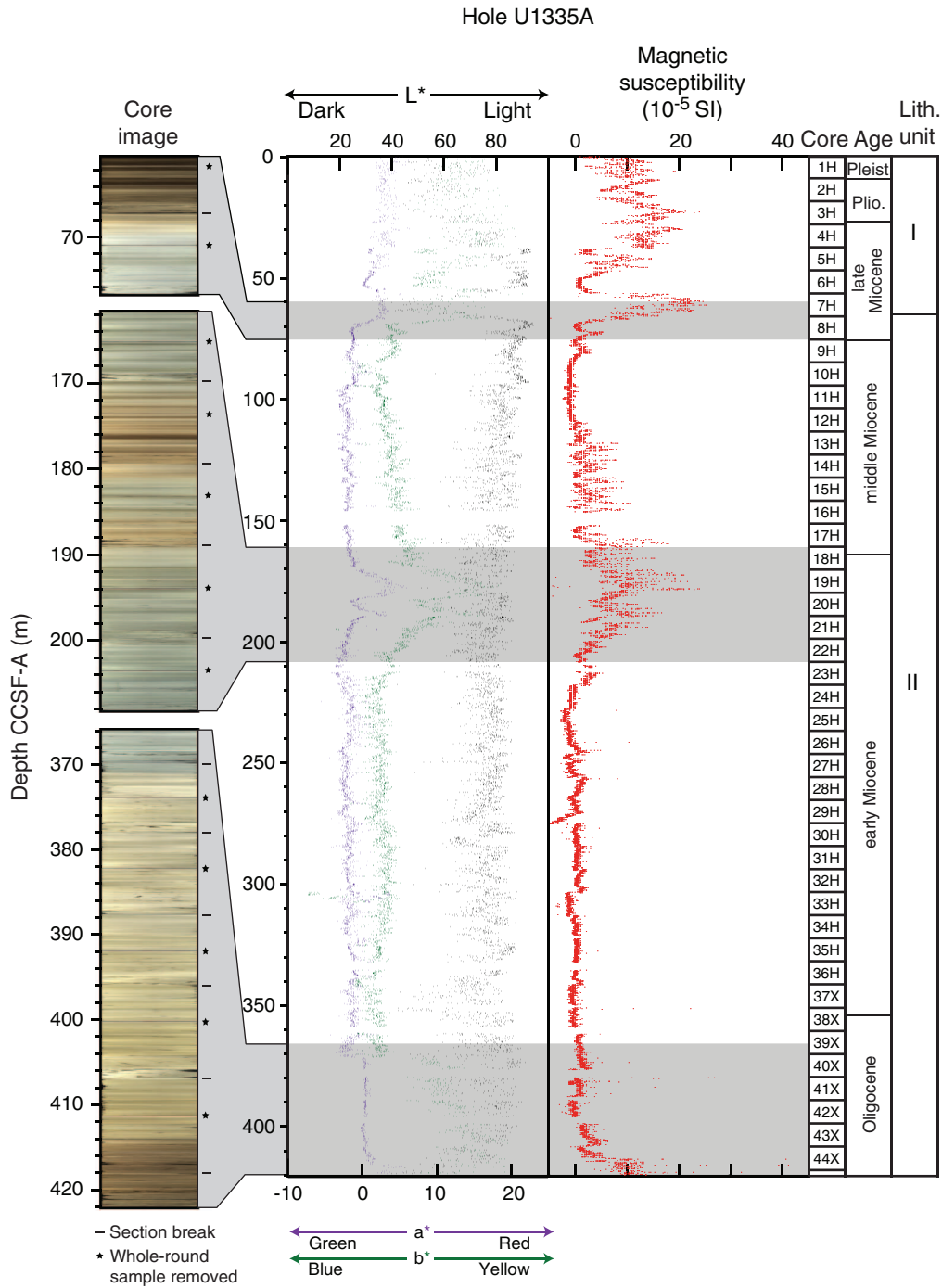
Figure F72. Summary of magnetic susceptibility and paleomagnetic results for Hole U1335B. Declinations are shown in sample coordinates (not reoriented to geographical coordinates).
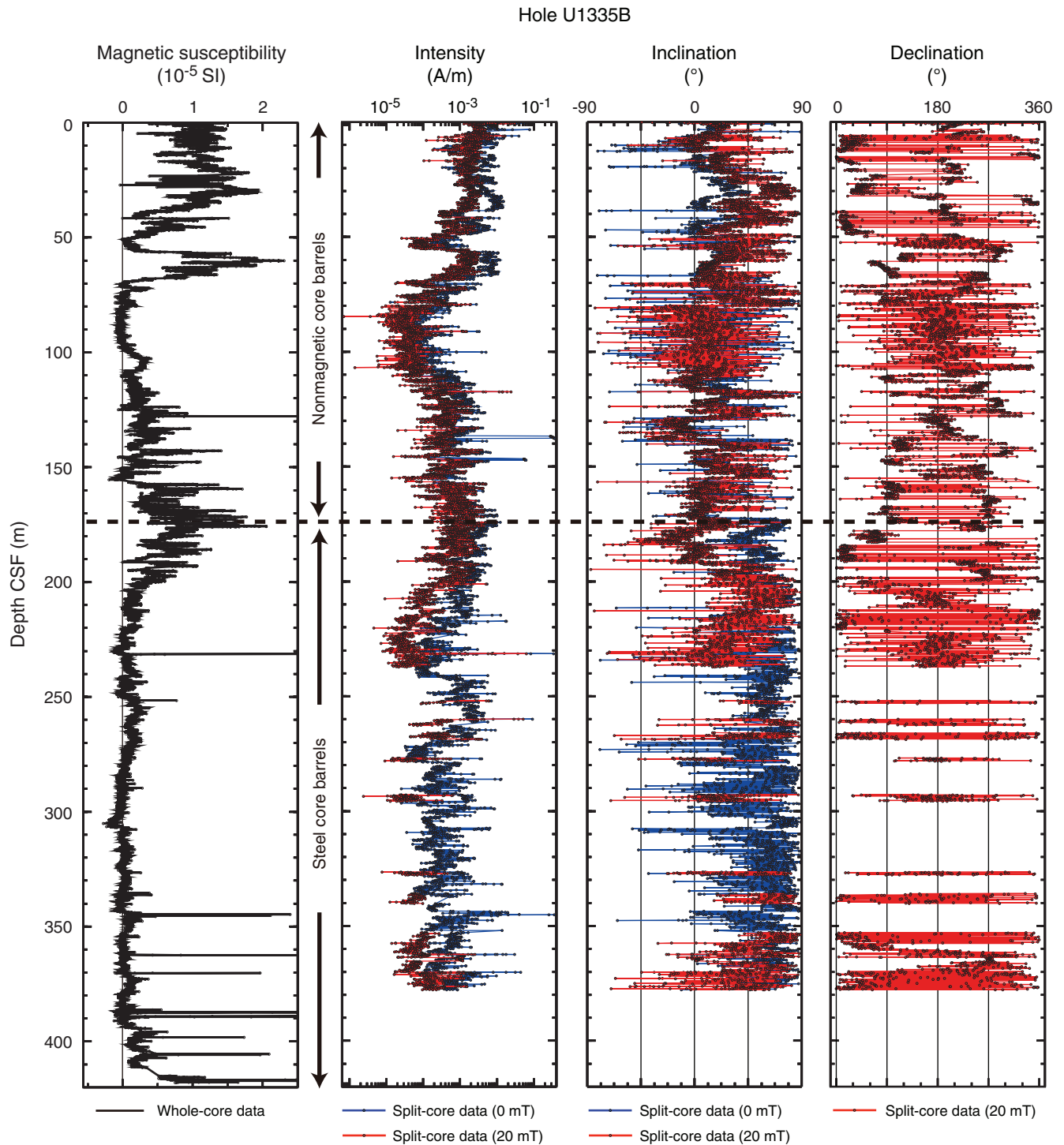
Figure F73. A. ETOPO1 (Amante and Eakins, 2008) bathymetric overview map of Site U1336 and PEAT drilling locations with previous ODP and DSDP sites. F.Z. = fracture zone. **B.** Swath bathymetry from AMAT-03 site survey, Site U1336 region. White line = survey Line 6.

Figure F74. Site U1336 summary.
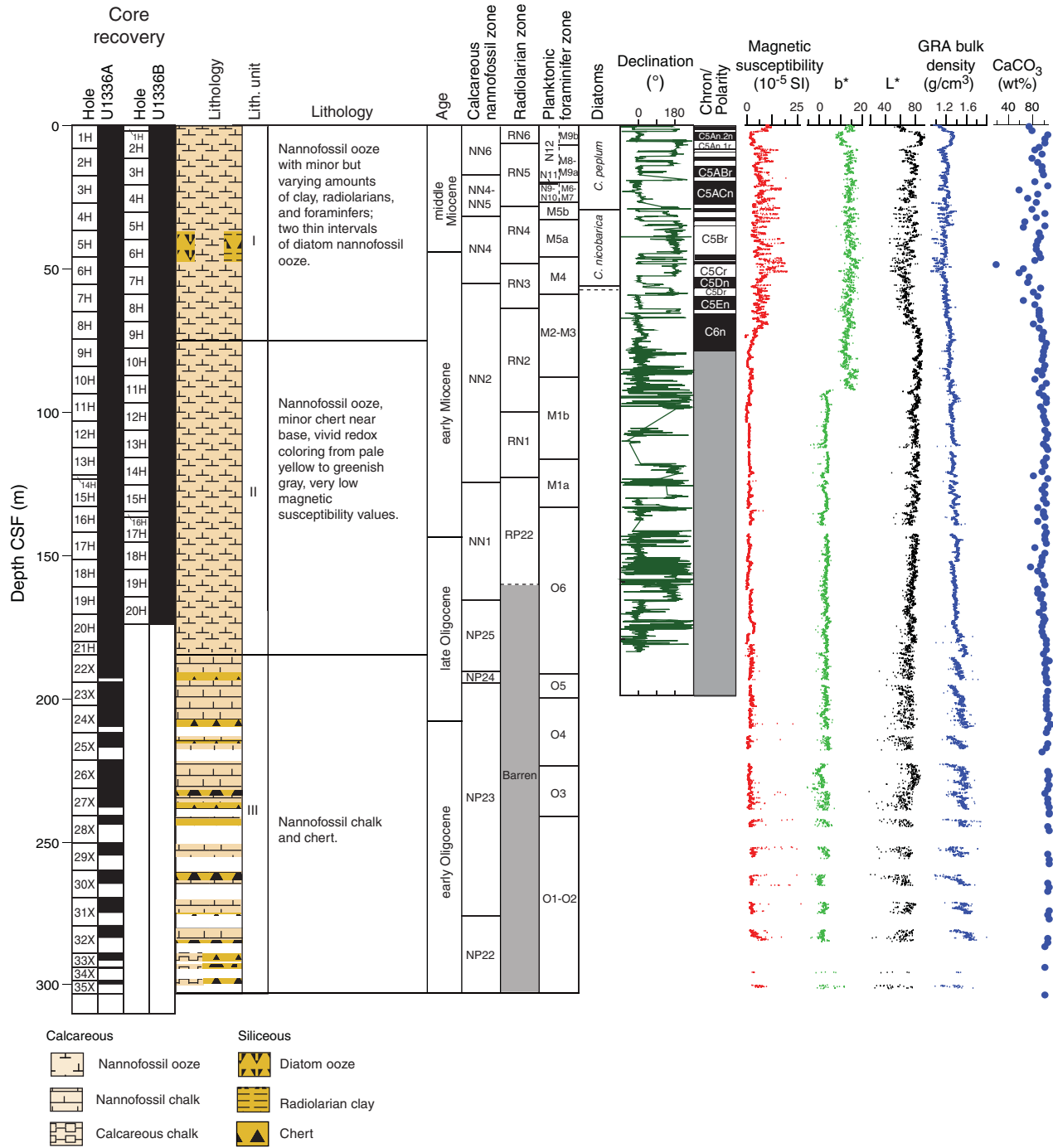
Figure F75. A. Site U1337 and PEAT program drill sites. F.Z. = fracture zone. **B.** Swath bathymetry from AMAT-03 site survey, Site U1337 region.
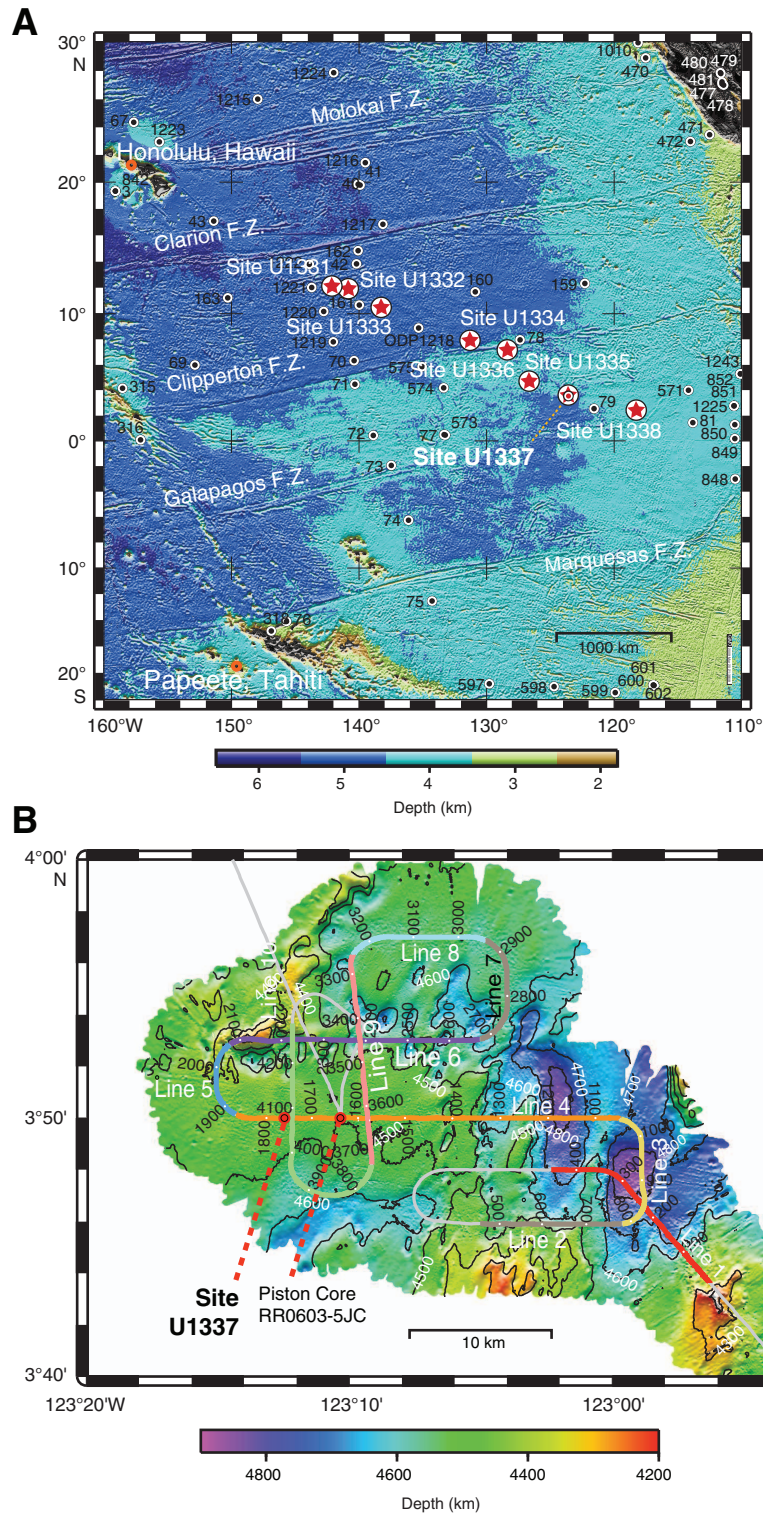
Figure F76. Site U1337 summary. Light green circles = CaCO₃ contents from Hole U1337B. Diatom mat intervals are from Hole U1337D. Core depth below seafloor for Holes U1337D and U1337B were converted to core depth below seafloor for Hole U1337A. Magnetic stratigraphy represents a spliced record from all holes and is plotted relative to corrected core composite depth below seafloor.

Figure F77. Downhole log measurement summary, Hole U1337A. p1 = uplog Pass 1, p2 = uplog Pass 2, MAD = moisture and density, IMPH = medium induction phasor-processed resistivity, SFLU = spherically focused resistivity, VSP = vertical seismic profile.
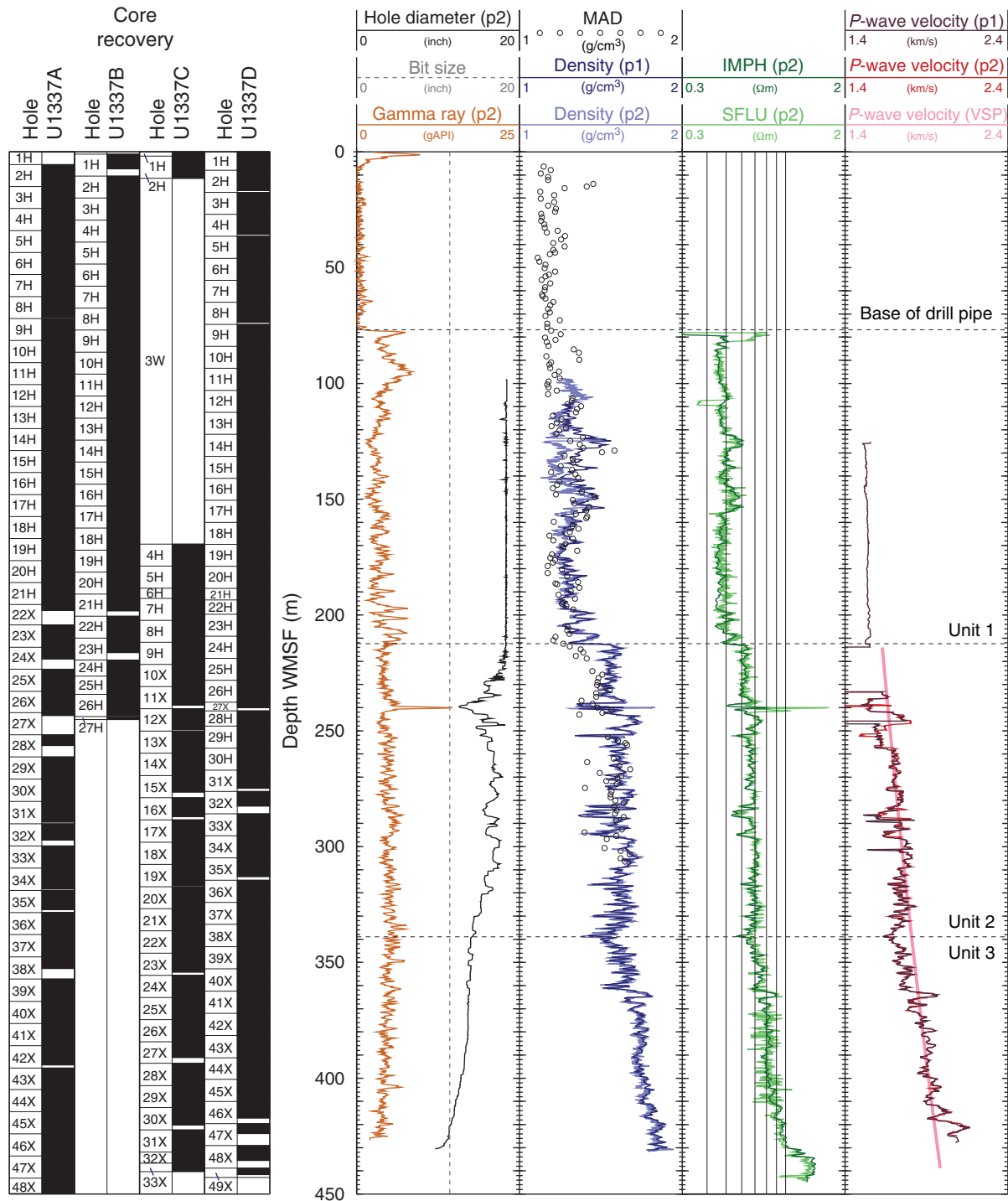
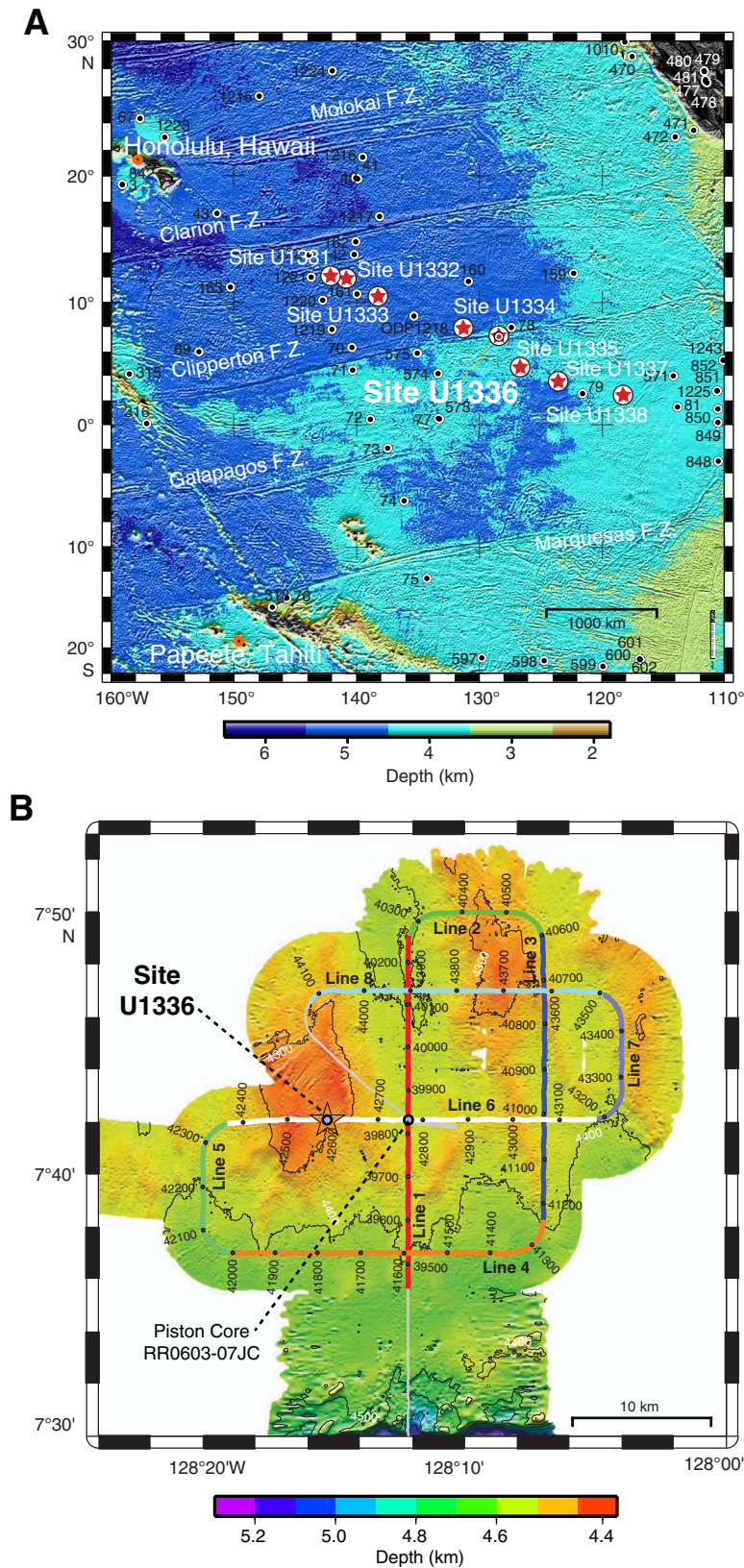**Figure F78. A.** Site U1338 and PEAT program drill sites. F.Z. = fracture zone. **B.** Swath bathymetry from AMAT-03 site survey, Site U1338 region.
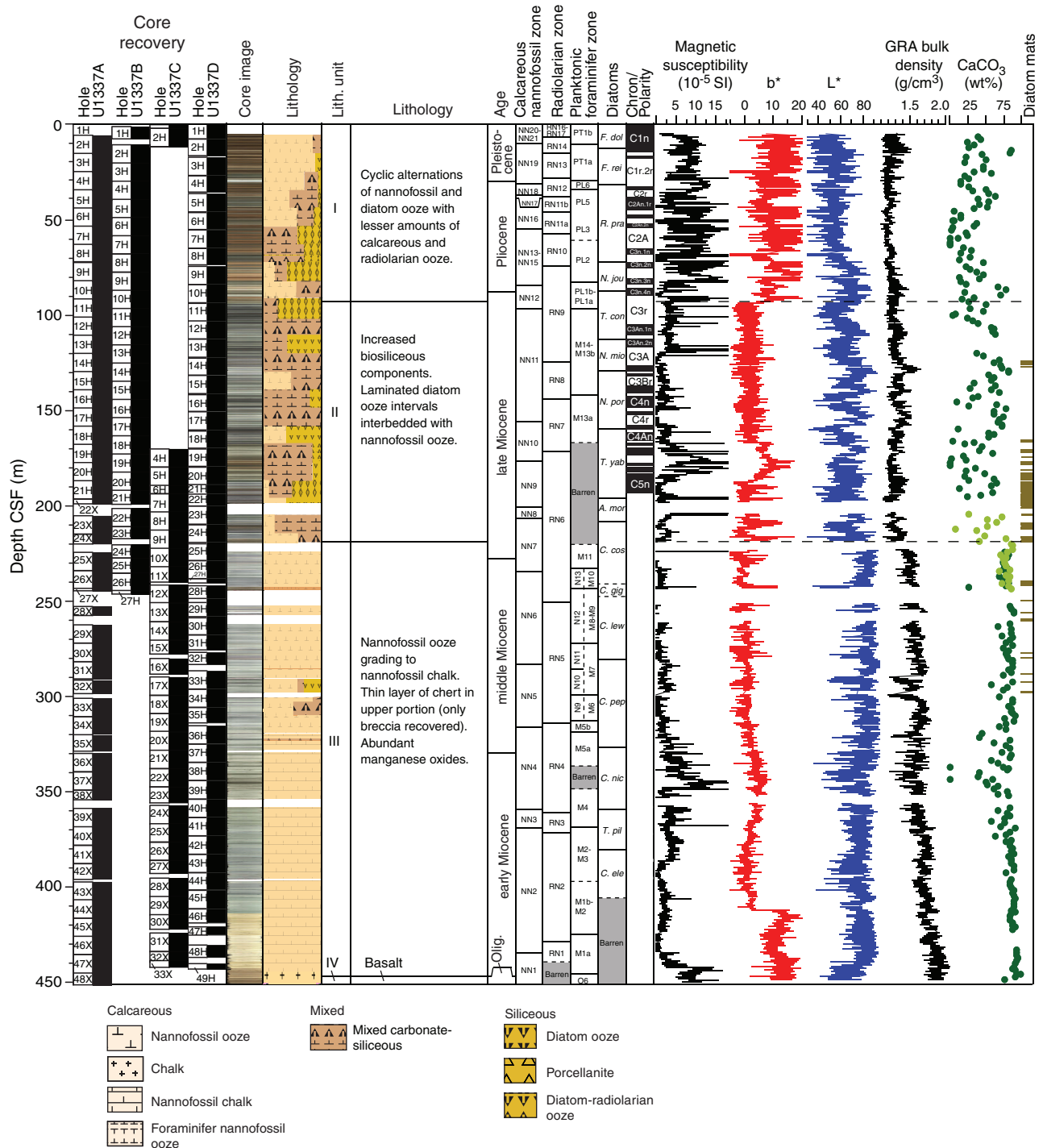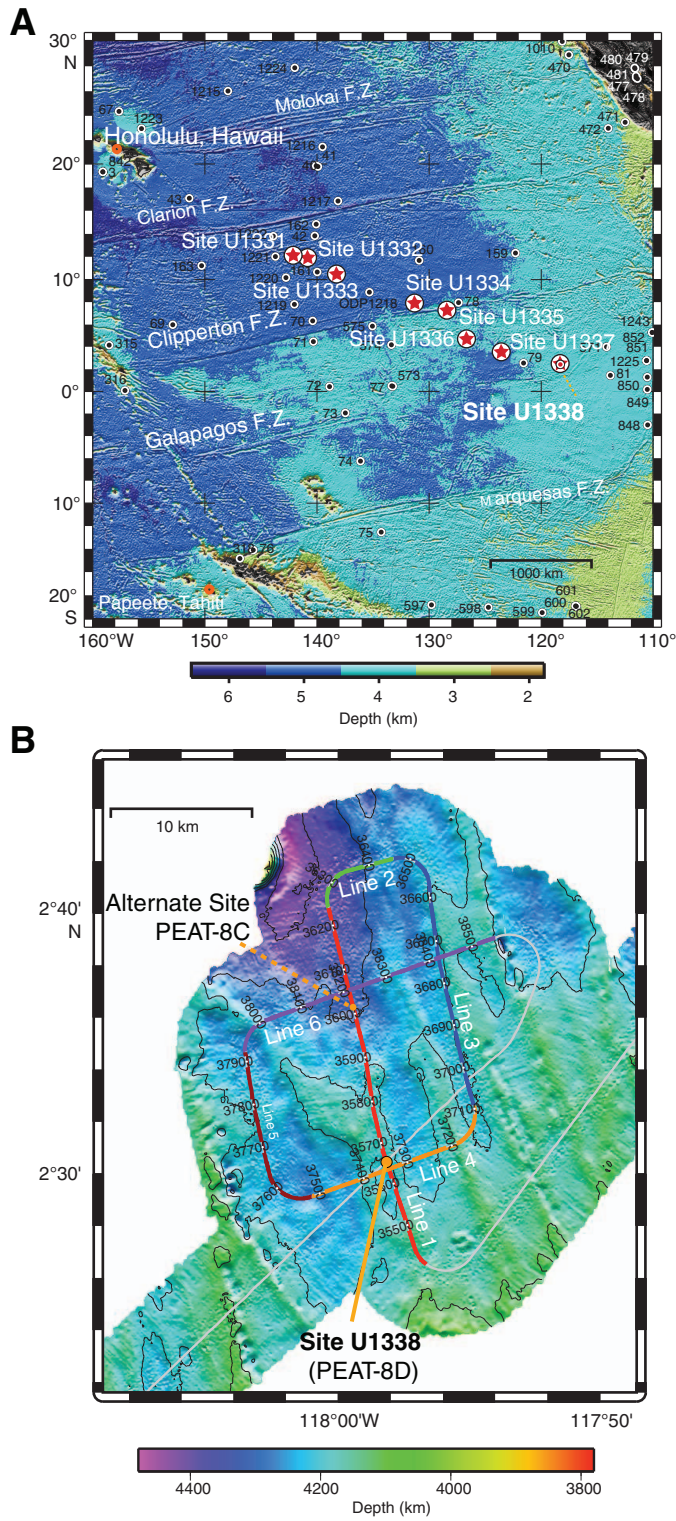
Figure F79. Site U1338 summary. Biostratigraphic zones and CaCO$_3$ contents mainly based on Hole U1338A. Light green circles = CaCO$_3$ contents from Hole U1338B. Core depth below seafloor for CaCO$_3$ samples from Hole U1338A were converted to core depth below seafloor from Hole U1338B. Magnetostratigraphy represents a spliced record from all holes and is plotted relative to corrected core composite depth below seafloor.

Figure F80. Downhole log measurement summary, Hole U1338B. TC = triple combo, MAD = moisture and density, IMPH = medium induction phasor-processed resistivity, SFLU = spherically focused resistivity, VSP = vertical seismic profile.

Table T1. Expedition 320 coring summary. (**See table note.**)

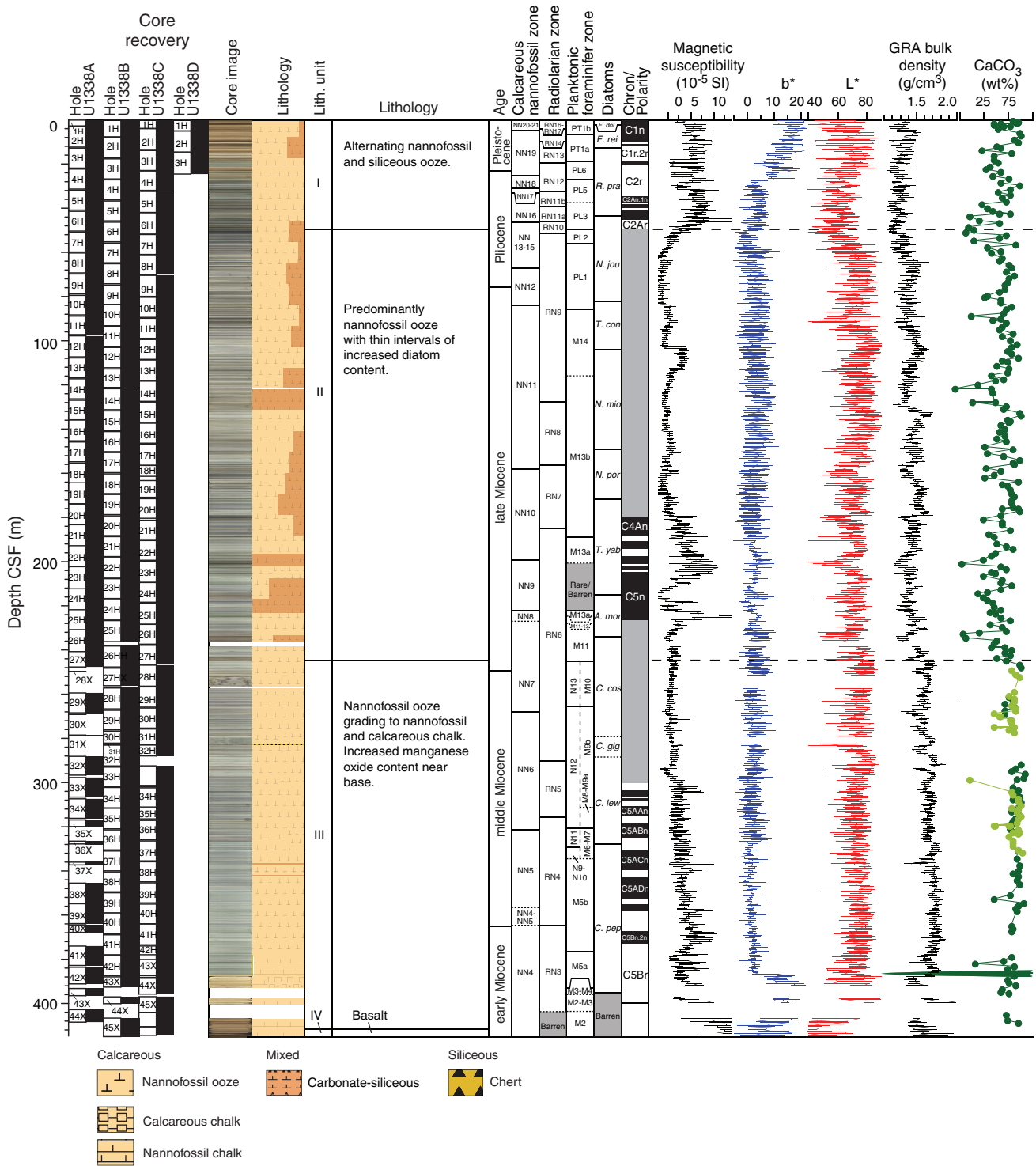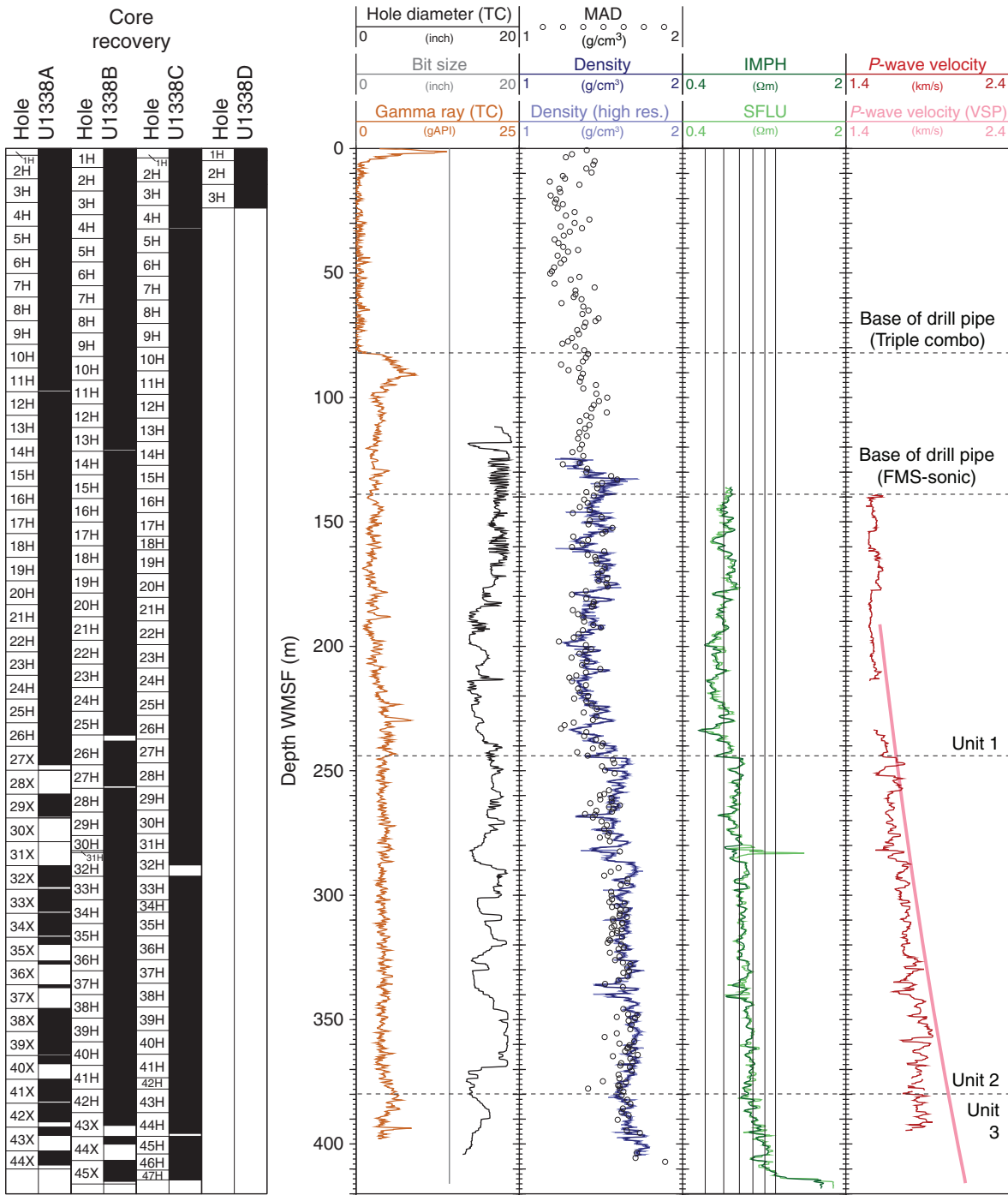| Hole	Latitude	Longitude	Seafloor depth DRF (m)	Water depth (m)	Cores (N)	Cored (m)	Recovered (m)	Recovered (%)	Drilled (m)	Total penetration (m)	Total depth DRF (m)	Total depth (mbsl)	Time on hole (h)	Time on hole (days)
U1331A	12°04.0884′N	142°09.6961′W	5127.3	5116.2	22	190.6	155.08	81.4	0.0	190.6	5317.9	5306.8	80.83	3.4
U1331B	12°04.0877′N	142°09.7085′W	5127.4	5116.3	20	175.8	163.03	92.7	12.7	188.5	5315.9	5304.8	38.00	1.6
U1331C	12°04.0892′N	142°09.7201′W	5128.0	5113.9	12	107.0	109.54	102.4	82.0	189.0	5317.0	5304.8	54.67	2.3
		Site U1331 totals:			54	473.4	427.65	90.3	94.7	568.1	NA		173.50	7.2
U1332A	11°54.7095′N	141°02.7428′W	4935.1	4923.9	18	152.4	145.61	95.5	0.0	152.4	5087.5	5076.3	89.25	3.7
U1332B	11°54.7209′N	141°02.7427′W	4936.9	4925.7	18	148.6	140.31	94.4	0.0	148.6	5085.5	5078.3	38.50	1.6
U1332C	11°54.7366′N	141°02.7422′W	4934.0	4922.8	18	155.5	148.06	95.2	0.0	155.5	5089.5	5078.3	45.00	1.9
		Site U1332 totals:			54	456.5	433.98	95.1	0.0	456.5	NA		172.75	7.2
U1333A	10° 30.9953′N	138°25.1728′W	4865.0	4853.7	22	184.1	176.25	95.7	0.0	184.1	5049.1	5037.8	45.92	1.9
U1333B	10° 30.9960′N	138°25.1597′W	4861.8	4850.5	20	180.3	178.36	98.9	0.0	180.3	5042.1	5030.3	30.83	1.3
U1333B	10° 30.9958′N	138°25.1459′W	4865.1	4853.8	24	177.0	177.04	100.0	0.0	177.0	5042.1	5030.8	47.50	2.0
		Site U1333 totals:			66	541.4	531.65	98.2	0.0	541.4	NA		124.25	5.2
U1334A	07°59.9980′N	131°58.3937′W	4799.3	4789.9	32	285.5	288.80	101.2	0.0	285.5	5084.8	5073.4	57.58	2.4
U1334B	07°59.9979′N	131°58.4071′W	4799.3	4787.9	31	281.7	294.59	104.6	0.0	281.7	5081.0	5073.3	44.83	1.9
U1334C	07°59.9979′N	131°58.4219′W	4801.0	4789.6	33	280.7	285.87	101.8	0.0	280.7	5081.7	5073.3	75.33	3.1
		Site U1334 totals:			96	847.9	869.26	102.5	0.0	847.9	NA		177.75	7.4
U1335A	05°18.7341′N	126°16.9949′W	4339.0	4327.5	45	421.1	422.08	100.2	0.0	421.1	4760.1	4748.6	72.92	3.0
U1335B	05°18.7362′N	126°17.0088′W	4343.4	4328.1	46	417.5	428.70	102.7	0.0	417.5	4760.9	4745.6	76.33	3.2
		Site U1335 totals:			91	838.6	850.78	101.5	0.0	838.6	NA		149.25	6.2
U1336A	07°42.0735′N	128°15.2526′W	4296.9	4285.3	35	302.9	259.12	85.5	0.0	302.9	4599.8	4588.2	60.25	2.5
U1336B	07°42.0599′N	128°15.2526′W	4298.1	4286.5	20	173.6	179.59	103.5	0.0	173.6	4471.7	4460.4	33.25	1.4
		Site U1336 totals:			55	476.5	438.71	92.0	0.0	476.5	NA		93.50	3.9
		Expedition 320 totals:			416	3634.3	3552.03	97.7	94.7	3729.0	NA		891.00	37.1

Note: NA = not applicable.

Table T2. Expedition 321 coring summary. (**See table note.**)

Hole	Latitude	Longitude	Seafloor depth DRF (m)	Water depth (m)	Cores (*N*)	Cored (m)	Recovered (m)	Recovered (%)	Drilled (m)	Total penetration (m)	Total depth DRF (m)	Total depth (mbsl)	Time on hole (h)	Time on hole (days)
U1337A	3°50.0065′N	123°12.3558′W	4472.0	4460.9	48	449.8	420.11	93.40	0.0	449.8	4921.8	4910.7	141.75	5.9
U1337B	3°50.0067′N	123°12.3621′W	4472.0	4461.0	28	250.9	242.65	96.71	1.0	251.9	4723.9	4712.9	61.25	2.6
U1337C	3°50.0067′N	123°12.3755′W	4478.6	4467.5	32	282.3	273.72	96.96	158.0	440.3	4918.9	4907.8	63.25	2.6
U1337D	3°50.0067′N	123°12.3858′W	4476.5	4465.4	49	442.9	431.97	97.53	0.0	442.9	4919.4	4908.3	74.50	3.1
Site U1337 totals:					157	1425.9	1368.45	95.97	159.0	1584.9	NA		340.75	14.2
U1338A	2°30.4685′N	117°58.1623′W	4210.8	4199.6	44	410.0	345.96	84.38	0.0	410.0	4620.8	4609.6	67.75	2.8
U1338B	2°30.4692′N	117°58.1736′W	4209.9	4198.6	45	413.6	417.18	100.87	2.5	416.1	4626.0	4614.7	118.00	4.9
U1338C	2°30.4687′N	117°58.1842′W	4212.7	4201.4	47	414.4	432.48	104.36	0.0	414.4	4627.1	4615.8	75.25	3.1
U1338D	2°30.4689′N	117°58.1948′W	4212.6	4201.3	3	23.9	24.79	103.72	0.0	23.9	4236.5	4225.2	14.25	0.6
Site U1338 totals:					139	1261.9	1220.41	96.71	2.5	1264.4	NA		275.25	11.5
Expedition 321 totals:					296	2687.8	2588.86	96.32	161.5	2849.3	NA		616.00	25.7

Note: NA = not applicable.

Table T3. Radiolarian zones present in Expedition 320 sites. (**See table note.**)

Radiolarian zone	Site					
	U1331	U1332	U1333	U1334	U1335	U1336
RN16						
RN15						
RN14					X	
RN13					X	
RN12					X	
RN11					X	
RN10					X	
RN9					X	
RN8					X	
RN7				X	X	
RN6				X	X	X
RN5				X	X	X
RN4				X	X	X
RN3				X	X	X
RN2			X	X	X	X
RN1		X	X	X	X	X
RP22		X	X	X	X	X
RP21	X	X	X	X	X	
RP20	X	X	X	X		
RP19	X	X	X	X		
RP18	X	X	X	X		
RP17	X	X	X			
RP16	X	X	X			
RP15	X	X	X			
RP14	X	X	X			
RP13	X	X	X			
RP12	X					
RP11	X					
RP10	X					
RP9						
RP8						
Total thickness (m):	189	151	182	285	420	298
Thickness of SFZ (m):	15.5	16	12	7	8	128

Note: SFZ = silica-free zone.